The application of a Distributed Activation Energy based model to the gasification and combustion of coal and biomass char blends

Patience Moyo

A dissertation submitted to the Faculty of Engineering and the Built Environment, University of the Witwatersrand, Johannesburg, in fulfillment of the requirements for the degree of Master of Science in Engineering.

Johannesburg 2013

Declaration

I declare that this dissertation is my own unaided work, unless otherwise stated and acknowledged. It is being submitted for the degree of Master of Science in Engineering to the University of the Witwatersrand, Johannesburg. It has not been submitted before for any degree or examination to any other university.

Signed: ..... on this ..... day of....., year .....

Abstract

Thermo-gravimetric analysis was carried out on a vitrinite-rich coal (VC), highveld grass (HG) and pine wood (PW) chars, and coal-biomass char blends of each. The analysis was carried out on combustion and gasification tests using air and CO_2 respectively. The blends were modeled by the application of a distributed activation energy (DAE) based model. The DAE based model is a modification of an algorithm developed by Scott et al. for the pyrolysis of complex fuels obeying linear kinetics (Scott et al., 2006). The modified DAE model was able to derive the activation energy, E, the grouped pre-exponential factor, A, and the number of reactions occurring in the thermal conversion process. Furthermore, the mass fraction associated with each unique reaction was obtained. The ability to determine multiple reactions distinguishes the DAE based model as a unique and robust method for kinetics determination.

The first order and the random pore reaction models (RPM) were applied to describe the reaction profiles. The conversion of all the coal and biomass blends were successfully modeled using the RPM to high accuracy. During combustion, E's and A's in the range of 180-255kJ/mol and 5.34E+8 to 2.80E+15 $s^{-1}m^{-1}$ were determined for the PW char. E's and A's in the range of 125-138kJ/mol and 5.38E+4 to 3.94E+5 $s^{-1}m^{-1}$ were determined for the rest of the chars and blends during combustion. For gasification, E's and A's in the range of 222 -304kJ/mol and 5.36E+5 to 3.96E+9 $s^{-1}m^{-1}$ were determined for all the chars and blends. The structural parameters (φ) obtained lie in the range of 8.3 to 18.9. The φ determined during combustion were sufficient for modeling the same material during gasification. Multiple reactions were identified for most of the chars during both gasification and combustion.

Kinetic analysis showed that PW char was the most reactive char, followed by the HG and VC chars respectively. For the 50:50 heat input ratio coal-biomass blends during combustion, synergetic behavior and a decrease in E was observed.

Acknowledgements

Heartfelt gratitude is extended to the following individuals for their contribution to this study.

- My husband, for the unconditional encouragement and moral support throughout this work.
- My Supervisors, Prof. N. Wagner and Dr S. Kauchali, for their guidance, funding and expert supervision throughout this research.
- Thinesh Vittee for the research suggestions, and Fadeela Saloojee and Qasim Fakir who began the research study in this area.
- The Coal and Carbon Research group members for their encouragement. A special mention to Nthabiseng Maledi for her advice and assistance during the study.
- Lastly and most of all, God, who made all things possible.

Table of Contents

List of figures

List of Tables

Nomenclature

a − Dimensionless constant (-)

A_o – Pre-exponential factor (s^{-1})

A – Grouped pre-exponential factor ($s^{-1}m^{-1}$)

b −Dimensionless constant (-)

C_g −Concentration of gaseous reactant ($mol.m^{-3}$)

E – Activation energy ($J.mol^{-1}$)

E_c– Corrected activation energy ($J.mol^{-1}$)

f – Fraction of material (-)

h −Shape factor dependent on the grain geometry (-)

L_0 −Initial segment length per unit volume (m^{-2})

$M_v(t)$ −Total mass of volatile matterat time t, (kg)

$M(t)$ – Total mass remaining at time t, (kg)

M_0– Initial sample mass (kg)

r-Instantaneous char reactivity ($mol.s^{-1}.K^{-1}$)

R – Ideal gas constant ($kJ.mol^{-1}K^{-1}$)

R^2-Coefficient of linear correlation (-)

S_0- Initial surface area per unit volume (m^{-1})

T – Temperature (K)

T_0 – Initial temperature (K)

u − Dummy variable

w – Inert mass (kg)

X – Fractional conversion (-)

x_0-Initial char mass fraction (-)

x_{ash}- Mass fraction of the ash contained in the char (-)

x-Mass fraction of char at a given time during conversion (-)

y_i −Experimentally determined dependent variable (-)

$\hat{y}_i$ −Model predicted dependent variable (-)

$\bar{y}_i$ −Mean of experimentaly determined dependent variables (-)

z −Coal energy input fraction (-)

τ-lumped shrinking core reaction rate dependant parameter (s)

Subscript

i – indicates reaction number, or component number

v – indicates property of volatile matter

0 – indicates initial state

Greek Letters

β – Heating rate ($K.s^{-1}$)

φ – Structural parameter (-)

Ψ - $\exp\left[-A(E)\int_0^t \exp((-E)/RT)dt\right]$ (reaction function) (-)

$\in_0$ – Initial material porosity (-)

Abbreviations

DAE- Distributed activation energy

DAEM- Distributed activation energy model

RPM- Random pore reaction model

SCM-Shrinking core reaction model

TGA-Thermo-gravimetric Analyzer

CV- Calorific Value

Al – Elemental Aluminium

C- Elemental Carbon

Ca- Elemental Calcium

CO_2 - Carbon Dioxide gas

Fe- Elemental Iron

K- Elemental Potassium

Mg- Elemental Magnesium

Mn- Elemental Manganese

N- Elemental Nitrogen

N_2- Nitrogen gas

Na- Elemental Sodium

O- Elemental Oxygen

S- Elemental Sulphur

Si- Elemental Silicon

1. INTRODUCTION

Over the years, coal has proven stability in both cost and supply, leading to the fuel gaining renewed interest as an energy source (Irfan et al., 2011). However, due to coal's high carbon to hydrogen ratio, carbon dioxide emission and control is a major concern for its current and future use. Combustion and gasification are the two main processes used to convert the chemical energy content in coal. Henrich et al. (1999) notes that even though char combustion and gasification are old and well known processes, the complex heterogeneous reaction mechanisms are not reliably understood. A precise knowledge of the intrinsic kinetic characteristics of the gasification and combustion processes is essential for understanding and modeling gasification and combustion at industrial scale, so as to develop an efficient and economically competitive clean process (Mani et al., 2011; Vamvuka et al., 2011; Fermoso et al., 2010; Huang et al., 2010; Gil et al., 2010(a); Kuo-Chao et al., 2009; Fermoso et al., 2008; Roberts and Harris, 2007; Ochoa et al., 2001; Dutta and Wen, 1977). The optimization of coal conversion processes not only leads to a significant reduction in carbon dioxide emissions, but an extension of the coal resource lifetimes as well (Saloojee, 2011).

Coal combustion may be described as a series of sequential events, beginning with drying, followed by devolatilization, homogeneous oxidation of volatile matters and heterogeneous oxidation of solid char, and finally, the burning out of char (Kuo-Chao et al., 2009). Volatile combustion occurs very fast such that the overall combustion rate is controlled by the relatively slow char combustion process (Sadhukhan et al., 2008; Kastanaki and Vamvuka, 2006). Gasification is the more efficient technology for coal utilization as it has a high carbon conversion and hence contributes to the reduction of air pollutant emissions (Higman and van der Burgt, 2008; Zhu et al., 2008; Liu and Niksa, 2004). Many researchers agree that the char gasification reaction rate is one of the most significant factors controlling the overall performance of either coal or biomass during gasification (Lahijani et al., 2012; Fermoso et al., 2010; Gil et al., 2010(b); Roberts et al., 2010). Integrated gasification combined-cycle (IGCC) processes are arguably the cleanest, most efficient means of producing electricity from coal (Wagner et al., 2008; Zou et al., 2007; Liu et al., 2004). From the provided information it is clear

that the determination of intrinsic kinetics of gasification and combustion of coal and biomass is a crucial area of study for the optimization of energy systems.

Co-firing of coal with CO_2 neutral energy sources like biomass, offers the advantage of a reduction in greenhouse gas emissions (Fermoso et al., 2009), and is also suggested to have a positive impact on the emission of other pollutants like SO_2 and NO_x (Senneca, 2007). Kastanaki and Vamvuka (2006) also mention that the co-utilization of the two fuel types in existing coal fired utilities may not only yield environmental benefits, but technical and economic benefits as well. Co-firing in this context is defined as the combined use of coal with another fuel. With the endorsements of mandatory targets by the European Council and Kyoto Protocol, for the use of renewable sources and the controlling of CO_2 emissions, the interest in biomass continues to rise (European Commission, 2009). The use of biomass in the gasification process has also proven catalytic effects (Mitsuoka et al., 2011; Hernández et al., 2010; Zhu et al., 2008). According to Biagini et al. (2002), existing coal power plants may be used for biomass co-firing with very few modifications. However, minor modifications may be required for the implementation of biomass co-firing in existing coal units. It is an important prerequisite to accommodate the nature of the thermal behavior of biomass materials in the modifications. This aspect highlights the need for a fundamental understanding of the thermal properties and reaction kinetics involved in the conversion processes (Kastanaki and Vamvuka, 2006; Senneca, 2007). Chimica and Federico (n.d.) as well as Kastanaki and Vamvuka (2006) also highlight that very few comparison studies of coal and biomass blends exist in literature.

The main purpose of modeling chemical reactions is to obtain the kinetic triplet of the reaction, and use it to reproduce the progression of the reaction under typical industrial operating conditions. The kinetic triplet consists of the reaction model function,$(f(x))$, where x is conversion, the activation energy of the conversion reaction, (E), and the grouped pre-exponential factor,(A). An advanced iso-conversion method is applied to thermo-analytical data obtained from the gasification and combustion of coal and biomass char blends in this research. This method was modified from an algorithm developed by Scott et al. (2006(a)). The algorithm was intended for the determination of kinetics for a complex fuel dissociating under numerous parallel first order reactions. Saloojee (2011) identified that the evaluation of E using the

algorithm is model independent. Vittee (2012) extended the use of this algorithm to fuels dissociating according to the random pore reaction model (RPM). The adaptations have been suited to both non-isothermal and isothermal conditions, and have proven apparent success in the modeling of coal char combustion and gasification. From this work, it was shown that the algorithm can actually be adapted to any known reaction model, under which a compound is assumed to be dissociating according to numerous parallel reactions.

The motivation of this research focuses on further validation of the modified model with experimental data. The model was applied on coal and biomass blends during gasification and combustion. The models which best describe the dissociation of the biomass and the blends formed are unknown, and an attempt to determine these with the use of the algorithm was executed in this study. Upon determination of these, the modeling of these processes was then carried out using the algorithm. Thought-provoking discussions are expected to arise from the variations in the intrinsic reaction kinetics and the presence or absence of synergy between the two fuels during conversion. This study is highly beneficial to most industries planning on undertaking biomass co-firing in the near future. For example, according to Koko (2012), Eskom plans on co-firing up to 10% biomass by energy input on their coal fired units. As stated above, the efficient modeling, design and control of these processes is highly dependent on the knowledge of the reaction kinetics taking place. The model has been applied on the analysis of gasification and combustion kinetics under both non-isothermal and isothermal conditions.

2. LITERATURE REVIEW

This section outlines the background study of the proposed research. The types of models for kinetics determination are discussed, along with the actual char reaction models to be applied. The section includes a description of the Distributed Activation Energy (DAE) based model, as well as a consideration of the biomass types and blend ratios to be used in the study. The aim and objectives are also presented.

2.1. Methods of Kinetics determination

Char reactions have been studied from as early as 1948 (Irfan et al., 2011;Turkdogan et al., 1968). Bos et al. (1997) carried out an assessment of the issues related to kinetics determination and application in the European industry. The outcome of the assessment showed that kinetic parameters are obtained mainly for use in three major areas, that is: process development, process optimization and; catalyst development. The overall aim in kinetics determination is to obtain the intrinsic kinetics of the particular substance reacting. Intrinsic kinetics are the reaction kinetic parameters which are not influenced by the transport processes occurring during the reaction (Hurt and Calo, 2001).They are determined when the observations are only affected by chemical kinetics at the active sites (Thybaut and Marin, n.d.). All transport phenomena must therefore be eliminated from the reaction kinetics in order to determine the intrinsic kinetics of a reaction (Bos et al., 1997). Various methods have been proposed and explored over the years with varying degrees of success. In general, the methods of kinetic parameter determination may be classified into model dependent methods (Non iso-conversion methods), and Iso-conversion methods. The dependence and independence in this context refers to the reaction model function.

2.2. Model dependent methods/Non iso-convension methods

It has already been shown that experimental data can be fitted to produce kinetic parameters by the application of various reaction mechanisms (Starink, 2003). Model dependent methods are based on different mathematical functions, which describe the dissociation profile. These methods assume a particular reaction model/mechanism and use this assumption to evaluate the

remaining members of the kinetic triplet. When a suitable function has been selected, the dissociation profiles are evaluated depending on the derived model parameters (Dash et al., 2010). For example, for coal char gasification, most model dependent methods are based on the Langmuir-Hinshelwood model. The Langmuir-Hinshelwood reaction model has been established for the description of the intrinsic kinetics of gasification at low and high pressure operation, and has been successfully used for CO_2 gasification (Irfan et al., 2011). However, Irfan et al. (2011) further notes that the Langmuir-Hinshelwood model poses difficulty in the evaluation of the large number of adsorption and kinetic parameters from experimental results when multiple gases are present. According to Ioannou (2009), model dependent methods are less reliable than model free methods due to the use of the various kinetic models with different dependence on the representative function of the actual reaction mechanism, according to the 'index' of the reaction.

2.3. Iso-conversion methods

Vyazovkin (1997) declares that the extraction of the parameters independent of the reaction model is the best way to obtain more reliable kinetics. Iso-conversional methods are often unwisely termed 'model-free methods' (Brown and Gallagher, 2008), and can be grouped into two main groups: the integral and the differential iso-conversion methods. Iso-conversion methods estimate the value of E in relation to the varying extents of conversion (x), independent of the reaction model. Vyazovkin (1997) notes that the sole dependence of E on conversion is adequate for the reliable prediction of the reaction kinetics of a given process over a wide temperature region. Starink (2003), on the other hand, states that these methods are the most reliable for the determination of E, for thermally activated reactions. According to Brown and Gallagher (2008), the iso-conversion approach has been adopted by a number of major manufacturers of thermal equipment. The authors also state the application of the concept to a wide variety of processes with great success. Iso-conversional methods are convenient methods to identify complex reactions due to the variation in the relative contribution of single steps to the overall reaction rate (Sis, 2009). Tiwari and Deo (2012) note that the applicability of iso-conversion models to the decomposition of a complex fuel is excellent.

As observed by Vittee (2012), the derivation of all iso-conversion methods according to Starink (2003), is based on the simplified assumption that the conversion rate during a reaction is the

product of two functions, one dependent on temperature and the other dependent on the actual conversion (fraction transformed).This is demonstrated by Equation [2-1].

$$\frac{dx}{dt} = f(x)k(T) \qquad [2\text{-}1]$$

The temperature dependent function generally assumes Arrhenius dependency (Starink, 2003).

$$k = A_o e^{-E/RT} \qquad [2\text{-}2]$$

In this expression, E, is the activation energy (kJ/mol), A_o is the pre-exponential factor (s^{-1}), R is the universal gas constant (8.314 J/ (mol K)) and T is the reaction temperature (K).

Iso-conversion methods can be grouped into two groups: the integral iso-conversion methods and the rate/differential iso-conversion methods. Substituting the two equations and taking logarithms, leads to a linear form of the expression:

$$\ln\left(\frac{dx}{dt}\right) = -\frac{E}{RT} - \ln\big(f(x)\big) \qquad [2\text{-}3]$$

Which translates to Equation [2-4] at a constant heating rate (β).

$$\ln\left(\frac{dx}{dT}\beta\right) = -\frac{E}{RT} - \ln\big(f(x)\big) \qquad [2\text{-}4]$$

E is then evaluated from the slope of the plots of $\ln\left(\frac{dx}{dt}\beta\right)$ against $(\frac{1}{T})$, (Starink, 2003). This approach illustrates the differential iso-conversion method. These methods make no use of mathematical approximations to the temperature integral (Starink, 2003). They instead use a determination of the reaction rate at an equivalent stage of the reaction at different heating rates as by Equation [2-4]. The Friedman-Ozawa method (Friedman, 1964, and Ozawa, 1986) is an example of a differential iso-conversion method as cited by Srivastava et al. (2010).

Another way of manipulating Equations [2-1] and [2-2] is by substitution and integration instead of directly taking logarithms. This leads to the expression:

$$\int_0^x \frac{dx}{f(x)} = \frac{A}{\beta}\int_{T_o}^{T} e^{\frac{-E}{RT}}\,dT = \frac{A}{\beta}\int_u^{\infty} \frac{e^{-u}}{u^2}\,du \qquad [2\text{-}5]$$

Where $u = \frac{-E}{RT}$, and the integral term $\int_u^\infty \frac{e^{-u}}{u^2}$, is generally known as the temperature integral (Starink, 2003). Various approximations to the integral term have been suggested and assumed in literature (Starink, 2003). The methods which use these various approximations are known as the integral iso-conversion methods (Rotaru and Goêa, 2009).

Furthermore, numerical integration of the temperature integral may be carried out for higher precision (Vyazovkin, 1997). Starink (2003) concludes that highly accurate integral iso-conversion methods exist upon the use of highly accurate approximations to the temperature integral.

Friedman (1965) and Li-Tang (1997; 1999(a); 1999(b)) applied conversion rate data (differential methods), and showed these to be the worst of the iso-conversion methods, even though they do not assume any approximations (Rotaru and Goêa, 2009). According to Starink (2003), in cases where there is some uncertainty over baselines of the thermal analysis data, or the accuracy of the determination of the conversion rates is limited, integral methods will often be more accurate than the differential methods. Starink (2003) further concludes, from the comparative study of the two methods, that the integral methods are generally more accurate than the differential methods.

Since the iso-conversion methods evaluate (E) for the reaction independent of the reaction model, various methods must further be applied to determine the rest of the kinetic triplet. The various iso-conversion methods are usually followed by discrimination procedures, such as the Invariant kinetic parameters method, and the Masters plot method for identifying the true conversion function of each linear non-isothermal process. Another example is the Perez-Maqueda et al. (2002) criterion, a heating-rate independence criterion for establishing the entire kinetic triplet of a process (Rotaru & Goêa, 2009). Vyazovkin (2008) discusses the compensation effect method of evaluating A from the obtained E. This compensation effect is brought about by the mutual compensating correlation of E and A. The relationship can be presented in the form of a linear equation, upon the evaluation of E and A, the reaction model can then be numerically reconstructed. Note that this method is only applicable to single step conversions where the E evaluated does not show systematic variation with x (Vyazovkin, 2008). For heterogeneous fuels like coal and biomass, which are multiple step processes, a different approach must be taken. In this study, the method applied evaluates E model independently, as an iso-conversion method.

Upon the evaluation of the E, a reaction model is assumed, and used to evaluate the corresponding A. A third step is then carried out to identify if the evaluated kinetic triplet is real. This is carried out by inverting the overall model equation to calculate the actual mass fraction reacting under the obtained triplet in the conversion system. A detailed presentation of the method is given in Section 2.4.

2.4. Char Reaction models

Numerous reaction models have been proposed for the description of the dissociation profiles obtained during char conversion. From Section 2.3 above, it is important to discuss the actual reaction model functions applicable to char conversion. Typical reaction models for gas solid reactions are: the RPM, the shrinking core model (SCM), as well as the homogenous/first order reaction model. De Micco et al. (2012) gives an overall kinetic expression applicable to char conversion:

$$r = \frac{dx}{dt} = k(T)G(C_g)f(x) \qquad [2\text{-}6]$$

Here, r is the instantaneous char reactivity, $G(C_g)$ is a parameter related to the concentration of the gaseous reactant,$f(x)$ is the reaction model which is a function of conversion, whilst $K(T)$ is a function of temperature. Lahijani et al. (2012) explains that, given the gas pressure is held constant, the function reduces to Equation [2-7];

$$r = \frac{dx}{dt} = k(T)f(x) \qquad [2\text{-}7]$$

The three reaction models applied in this work are briefly discussed in the subsequent subsections.

2.4.1. First order reaction model

The first order reaction model is frequently used in most thermo-gravimetric studies (Gil et al., 2010(a)).This model is also referred to as the homogenous or volume reaction model (Seo et al., 2010). It was based on the assumption that the reaction takes place homogenously throughout the char particle (Seo et al., 2010), it is described by the function;

$$f(x) = 1 - x \qquad [2\text{-}8]$$

The Distributed activation energy model (DAEM), is based on this reaction model which is assumed to apply in devolatization. Gil et al. 2010(a) upon studying the combustion of coal and pine sawdust conclude that the first order reaction model is the most effective mechanism for the description of the first stages of biomass oxidation and coal combustion.

2.4.2. The RPM

The RPM is the most widely used in the modeling of char gasification (Rafsanjani and Jamshidi, 2008). It is developed based on a pore size distribution with randomly interconnected/overlapping set of cylindrical pores (Abanades, 2009; Rafsanjani and Jamshidi, 2008).The model, according to Bhatia and Vartak (1996), found extensive application in the interpretation of gas-solid reaction rate data. Bhatia and Vartak (1996) attribute its success to the fact that the model is able to adequately represent the rate maximum with increase in conversion without the use of the arbitrary adjustable additional parameters. This capability is brought about by the overlapping pore concept on which the model is based. This concept appears to adequately describe the competitive mechanisms of surface area increase and loss related to pore growth and intersection, respectively as the reaction proceeds (Bhatia and Vartak, 1996). The RPM expression is provided by these authors as presented by Equation [2-9],

$$f(x) = \frac{S_o}{1-\epsilon_o}(1-x).\sqrt{1-\varphi \ln(1-x)} \qquad [2\text{-}9]$$

Where the structural parameter φ is described as

$$\varphi = \frac{4\pi L_o(1-\epsilon_o)}{{S_o}^2} \qquad [2\text{-}10]$$

S_o is the initial area per unit volume, $\epsilon_o$is the initial porosity of the material whilst L_o is the initial pore segment length per unit volume. On substituting into Equation [2-9],

$$r = \frac{dx}{dt} = A_0 \exp(-\frac{E}{RT}).\frac{S_o}{1-\epsilon_o}(1-x).\sqrt{1-\varphi \ln(1-x)} \qquad [2\text{-}11]$$

From this expression, A_0 is grouped into a constant, renamed the grouped pre-exponential factor (A);

$$A = \frac{A_o S_0}{1 - \epsilon_o} \quad [2\text{-}12]$$

Providing an overall expression;

$$r = \frac{dx}{dt} = A \exp(-\frac{E}{RT})\,(1 - x).\sqrt{1 - \varphi \ln(1 - x)} \quad [2\text{-}13]$$

As discussed by Vittee (2012), the structural parameter may be evaluated by experimental evaluations of S_o , ϵ_o and L_o. Su and Perlmutter (1985) report that there is good agreement in the value of the parameter when calculating it experimentally and when it is mathematically evaluated (i.e. using regression analysis). Vittee (2012), Everson et al. (2006), and Bhatia and Vartak (1996) conclude that the mathematical evaluation of the parameter is most suitable as it avoids lengthy experimental procedures and improves the reliability and accuracy of the kinetics obtained. According to Sadhukhan et al. (2010), the RPM is the most widely accepted of structural models for the prediction of the development of pore surface area during gasification and combustion of porous coal char.

2.4.3. The shrinking core model (SCM)

Seo et al. (2010) states that the SCM is based on the assumption that the reaction initially occurs at the char's external surface and gradually moves inside. Szekely and Evans (1970) assumed the existence of an assembly of uniform nonporous grains and that the reaction takes place on the surface of these grains. The space between the grains constitutes the porous network (Lu, 1994). According to Lu (1994), the shrinking core behavior applies to each of those grains during the reaction. The actual reaction model expression in the chemical reaction controlled regime is given by Lu (1994) as:

$$f(x) = \frac{S_o(1 - x)^h}{(1 - \epsilon_o)} \quad [2\text{-}14]$$

Here, S_o is the initial surface area per unit volume and ϵ_o is the initial porosity. h is defined as a shape factor dependent on the grain geometry (for spheres h =2/3, cylinders h=1/2, flat plates $h = 0$). However, Lu (1994) notes that the same parameter is defined as the reaction order in other work, for example, Ishida and Wen (1971). Lu (1994) further explains that the model

predicts a monotonically decreasing reaction rate and surface area since the surface area of each grain is receding during the reaction. The author highlights that for gas solid reactions with pore volume growth, the solid surface area increases as the reaction proceeds; this leads to a corresponding increase in the reaction rate. However, as the reaction proceeds, the micro pores begin to coalesce into larger macro pores and meso pores, hence reducing the surface area and reaction rate. The model therefore presents a shortcoming for reactions with pore volume growth as it does not consider the structural changes explained (Saloojee, 2011; Sadhukhan et al., 2010; Lu, 1994). However, a number of authors have successfully applied the SCM in char conversion reactions. Everson et al. (2006) showed that the SCM is applicable for the gasification of pulverized coal-chars from inertinite-rich coal discharges which are rich in carbon.

Bhat et al. (2001) applied the reaction model to the CO_2 gasification of rice husk char. Umeki et al. (2010) applied the model to large wood chars successfully, whilst Kwon et al. (1988) applied it to coal char-CO_2 reaction, to name a few. It is acknowledged that the SCM is most commonly used for the modeling of the combustion conversion process. However, work by previous MSc researchers in the area (Saloojee, 2011), have shown unsuccessful results on application of the SCM to combustion data. The RPM and first order reaction models were therefore applied in the current study.

2.5. The DAE based model

The algorithm developed by Scott et al. (2006(a)) is based on the DAEM. Coal, was first treated as a mixture of a large number of species decomposing by parallel first order reactions, by Pitt (1962). The DAEM makes use of this description, and further assumes that the complexity of the fuel is such that a continuous distribution of E's exists for a discretized number of arbitrary reactions. This allows a function of E, and time, to define the mass of volatile material with E's between the initial activation energy (E_0) and the activation energy at some point in time(E_t) (Fakir, 2011; Scott et al., 2006(a)). The assumption leads to the formation of a double exponential term, which acts over a narrow range of E's and changes as time progresses (Please et al., 2003). According to Please et al. (2003), this term is the main source of numerical difficulty on application of the DAEM. Scott et al. (2006(a)) describes this term as given by Equations [2-15] and [2-20]. According to Scott et al. (2006(a)), the DAEM assumes that the material being modeled is so complex such that a continuous distribution of activation energies is

assumed where the mass of volatile material with activation energies between E and $E + dE$, at a given time t is $m(E,t)dE$. Therefore the total mass of volatile matter, $M_v(t)$ is described by:

$$M_v(t) = \int_0^\infty m(E,t)dE \qquad [2\text{-}15]$$

Now, an assumption is made that the material in interval E to $E + dE$ decomposes according to the first order reaction model, with a pre exponential factor $A(E)$.

$$\frac{dm(E,t)}{dt} = -A(E)\exp\left(\frac{-E}{RT}\right) m(E,t) \qquad [2\text{-}16]$$

Therefore

$$m(E,t) = m_0(E)\exp\left[-A(E)\int_0^t \exp\left(-\frac{E}{RT}\right) dt\right] \qquad [2\text{-}17]$$

Where $m_0(E)$ is the initial mass of volatile material decomposing with activation energy in the interval E to $E + dE$. Considering Equation [2-1], Equation [2-17] may be written as:

$$m(E,t) = m_0(E)\exp\left[\int_{x_0}^{x} \frac{\partial x}{f(x)}\right] \qquad [2\text{-}18]$$

The quantity $m(E,t)$ cannot be measured in practice; only the total amounts, $M_v(t)$, or the total rates of decomposition can be measured (Scott et al. 2006(a)). Therefore, integrating over all energies yields:

$$\frac{M_v(t)}{M_{v0}} = \frac{M_{v0-}V(t)}{M_{v0}} = \int_0^\infty g(E) \times \exp\left[-A(E)\int_0^\tau \exp(-E/RT)\, dt\right] dE \qquad [2\text{-}19]$$

Where

$$\Psi(E,t) = \exp\left[-A(E)\int_0^\tau \exp(-E/RT)\, dt\right] \qquad [2\text{-}20]$$

Here, $M_v(t)$ is the total mass of volatile matter. M_{vo} is the initial value of $M_v(t)$, $V(t)$ is the yield of volatiles, whereas $g(E)$ is the underlying initial distribution of E's which characterizes the material. $g(E)$ may be evaluated from:

$$g(E) = \frac{m_0(E)}{\int_0^\infty m_o(E)dE} \qquad [2\text{-}21]$$

Please et al. (2003) outlines a number of numerical approximations to the evaluation of Equation [2-19]. Numerous approximations have been suggested to give a closed form of the double integral term. An approximate closed form of the model can be obtained by assuming that as conversion proceeds, the functional groups with the lowest E's (i.e. weakest bonds), dissociate

first, as demonstrated by Rostami et al. (2004).The distribution of E's was first discretized by Braun and Burnham (1987). This was carried out by assuming a finite set of discrete first order reactions in the place of the continuous distribution of E's. Scott (2006(a)) further proposed an algorithm based on this discretization. This algorithm will be referred to as Scott's algorithm.

2.5.1. Scott's Algorithm

The algorithm is designed for the kinetics determination of a material decomposing subject to numerous parallel first order reactions. For such a material:

$$\frac{M(t)}{M_0} = w + \sum_{All\ reactions,i} f_{i,0} exp\left[-A_i \int_0^{\tau} exp(-E_i/RT(t))dt\right] = w + \sum_{All\ reactions,i} f_{i,0} exp\left[\int_{x_0}^{x} \frac{\partial x}{f(x)}\right] \quad [2\text{-}22]$$

In this case $M(t)$ is the sample mass of initial value M_0 containing a fraction w of inert material. $f_{i,0}$ is the initial mass fraction of M_0 which decomposes with activation energy, E_i and pre-exponential factor, A_i. The aim is to find the$f_{i,0}$, A_i and E_i of each reaction using the experimentally measured sample mass. From the above expression, it must be noted that instead of the continuous fractional density function ($g(E)$), as in the DAEM (which is the discrete analogue), f is used to denote an actual fraction of material with specified A and E. Instead of a continuous underlying distribution of E's, Scott et al. (2006(a)) assumes a range of mass components fractions characterized by f, reacting at each assumed parallel reaction. By assuming the range of mass component fractions in the char, the heterogeneity of the reacting compound is catered for (Kastanaki and Vamvuka, 2006). It is also assumed that a reaction is dominating at a unique conversion when a constant heating rate is applied. Hence, the algorithm is to be applied to thermo-gravimetric experiments carried out at two or more different, but constant, heating rates.

The Equation [2-22] above becomes a linear matrix problem if the reactions are known together with each value of E and A. The mass of solid fuel remaining at a time is the sum of the masses of each of the components remaining. The equation may then be written in a matrix format such that for any set of times $(t_1, t_2, t_3 \ldots)$ the remaining mass of fuel $M(t)$ is given by Equation [2-23].

$$\frac{1}{M_0}\begin{bmatrix} M(t_0) \\ M(t_1) \\ M(t_2) \\ \vdots \\ \vdots \end{bmatrix} = \begin{bmatrix} \Psi_1(t_0) & \Psi_2(t_0) & \dots & \Psi_n(t_0) & 1 \\ \Psi_1(t_1) & \Psi_2(t_1) & \dots & \Psi_n(t_1) & 1 \\ \Psi_1(t_2) & \Psi_2(t_2) & \dots & \Psi_n(t_2) & 1 \\ \vdots & \vdots & \vdots & \vdots & \vdots \\ \vdots & \vdots & \vdots & \vdots & \vdots \end{bmatrix} \times \begin{bmatrix} f_{1,0} \\ f_{2,0} \\ f_{3,0} \\ \vdots \\ w \end{bmatrix} \qquad [2\text{-}23]$$

Such that $M = \Psi f$

Given $\frac{dT}{dt} = \beta$ then:

$$\Psi_i(t) = \Psi_i(T) = exp\left[-\frac{A_i}{\beta}\int_{T_0}^{T} \exp(-E_i/RT(t))dT\right] = exp\int_{x_0}^{x}\frac{\partial x}{f(x)} \qquad [2\text{-}24]$$

$f_{i,0}$ is then evaluated by solving the matrix equation. A set of reactions must first be generated each with their unique sets of E's and A's. Assuming at a given conversion there is a single reaction dominating, the fraction of initial mass remaining for the *i*th component is given by Equation [2-25].

$$f_i(T) = f_{i,0} exp\left[-A_i\int_0^{\tau}\exp(-E_i/RT)dt\right] = f_{i,0}\,\Psi_i(T) \qquad [2\text{-}25]$$

It was shown in Scott et al. (2006(a)):

$$\Psi_i(\beta_1, T_1) = \Psi_i(\beta_2, T_2) \qquad [2\text{-}26]$$

Where

$$\ln\ \Psi_i = \frac{A_i}{\beta}\left[T_0 \exp\left(\frac{-E_i}{RT_0}\right) - \frac{E_i}{R}\int_{E/RT_0}^{\infty}\frac{exp(-u)}{u}du - T\ exp\left(\frac{-E_i}{RT}\right) + \frac{E_i}{R}\int_{E_i/RT}^{\infty}\frac{exp(-u)}{u}du\right] \qquad [2\text{-}27]$$

Taking natural logarithms and substituting the Ψ_i expressions:

$$\frac{1}{\beta_1}\left[T_0 \exp\left(\frac{-E_i}{RT_0}\right) - \frac{E_i}{R}\int_{E/RT_0}^{\infty}\frac{exp(-u)}{u}du - T_1\ exp\left(\frac{-E_i}{RT_1}\right) + \frac{E_i}{R}\int_{E_i/RT_1}^{\infty}\frac{exp(-u)}{u}du\right] = \frac{1}{\beta_2}\left[T_0 \exp\left(\frac{-E_i}{RT_0}\right) - \frac{E_i}{R}\int_{E/RT_0}^{\infty}\frac{exp(-u)}{u}du - T_2\ exp\left(\frac{-E_i}{RT_2}\right) + \frac{E_i}{R}\int_{E_i/RT_2}^{\infty}\frac{exp(-u)}{u}du\right] \qquad [2\text{-}28]$$

Solving this nonlinear equation for E_i, gives the exact value of E given the solid fuel is made up several components when one reaction dominates the overall mass loss at the conversion of interest (Scott et al., 2006(a)).According to Ozawa (1992), pp.160,'The conversion at the maximum rate of conversion is constant and independent of the heating rate in the case of linear heating, and if the rate constant follows the Arrhenius law'. It is then assumed that the dominating reaction is at a conversion corresponding to the maximum rate of decomposition for a single first order reaction when the material is heated at a constant rate. This is at the point when:

$$\frac{d}{dt}\left(\frac{df_i}{dt}\right) = \frac{d}{dt}\left\{f_{i,0}A_i exp(-E_i/RT) \times exp\left[-A_i \int_0^t \exp(-E_i/RT)\, dt\right]\right\} = 0 \qquad [2\text{-}29]$$

For a first order conversion this value relates to the value of

$$\Psi_{imax} = e^{-1} \approx 0.368$$

A_i, can then be calculated from the Equation [2-30]:

$$\begin{aligned} \ln\ \Psi_{imax} &= -1 \\ &= \frac{A_i}{\beta_1}\left[T_0 \exp\left(\frac{-E_i}{RT_0}\right)\right. \\ &\left. - \frac{E_i}{R}\int_{E/RT_0}^{\infty} \frac{exp(-u)}{u}\, du - T_1\, exp\left(\frac{-E_i}{RT_1}\right) + \frac{E_i}{R}\int_{E_i/RT_1}^{\infty} \frac{exp(-u)}{u}\, du\right] \end{aligned} \qquad [2\text{-}30]$$

Upon obtaining all the values of A_i, the matrix is then inverted to obtain discrete values of E_i and $A_i$of the active reactions, together with the mass fractions of the components ($f_{i,o}$) dissociating according to these reactions. Non zero values of ($f_{i,o}$), are generated by the inversion for all non-spurious reactions from the n candidate reactions assumed.

The main difference between the algorithm and the DAEM lies in the evaluation of the double exponential term (Ψ). This term (Ψ), is integrated over an infinite range of E's using the DAEM, whilst Scott (2006(a)) evaluates it over a temperature range. The integration of the term over the range of E's is the main source of numerical difficulties when using the DAEM. Saloojee (2011) discusses some of the challenges faced in the application of the DAEM for non-isothermal systems. The double integral obtained will need to be evaluated for each temperature without the

possibility of estimating the error of integration before the calculation in order to minimize it. Scott et al. (2006(a)) also declares that the application of the DAEM proves difficult even when the kinetic parameters are fully specified. The advantage of Scott's algorithm is that a large number of reactions can be specified arbitrarily to cover the conversion range. However, the inversion of the matrix inherently reduces the number of reactions to the ones' required to sufficiently model the system. The final number of reactions does not have to be pre-specified as traditional DAE techniques require.

2.5.2. The modified DAE based model

As stated in Section 1, the model can evaluate the E's of complex compounds dissociating according to different reaction models. The second stage of the model, involving the evaluation of A, is however, dependent on the particular reaction model/mechanism. The suitable conversion, upon which the rate of dissociation is maximum, is dependent on the reaction model best describing the particular process. During pyrolysis, first order dissociation is observed; hence the value of the conversion applied to obtain Ψ is obtained using the first order reaction function. According to Vittee (2012), for a compound decomposing according to the SCM, the corresponding maximum rate of decomposition is as expressed by Equation [2-31].

$$\frac{d}{dT}\left(\frac{dx}{dT}\right) = \frac{d}{dT}\left[\left(\frac{A_i}{\beta} exp\left(\frac{-E}{RT}\right)\right)(1-x)^{2/3}\right] = 0 \qquad [2\text{-}31]$$

And for the RPM Equation [2-32] applies;

$$\frac{d}{dT}\left(\frac{dx}{dT}\right) = \frac{d}{dT}\left[\left(\frac{A_i}{\beta} exp\left(\frac{-E}{RT}\right)\right)(1-x)\sqrt{1-\varphi \ln(1-x)}\right] = 0 \qquad [2\text{-}32]$$

The above expressions [2-31] and [2-32], may be solved graphically or analytically. Vittee (2012) showed that the analytical evaluation of the x_{max} is a more accurate method, as compared to the graphical method. However, provided the second derivative of the expression cannot be explicitly found, and the x_{max} value cannot be determined from the analytical expression, there is a need to apply the graphical method. Here, the above expressions are manipulated and used to generate reaction data. The numerical derivatives would then be used to determine the conversion value at maximum decomposition. From the first derivative graph, the maximum

point along the graph corresponds to the zero point of the second derivative, as shown by Figure 2-1. The Ψ term's relation to x for each model must also be evaluated in order to calculate the Ψ matrix. These can be analytically evaluated, and are given in Table 2-1.

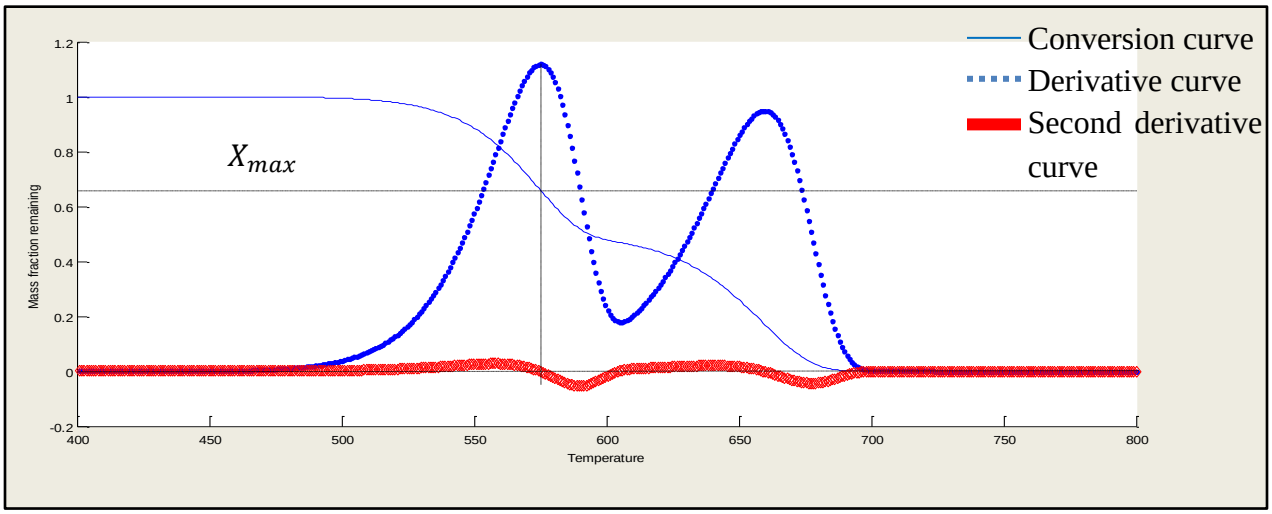

Figure 2-1: Determination of the Xmax value.

Table 2-1:Terms for the evaluation of xmax (Vittee, 2012)

Model	$\int_0^x \frac{dx}{f(x)} = g(x)$	x_{max}	**Ln** $\Psi_{max} = g(x_{max})$	**Ln** Ψ_{max}
First order	$ln(1-x)$	0.6321	$\ln(1-x_{max})$	-1
RPM	$\frac{2}{\varphi}\left(\sqrt{1-\varphi\ln(1-x)}-1\right)$	0.6502	$\frac{2}{\varphi}\left(\sqrt{1-\varphi\ln(1-x_{max})}-1\right)$	-0.8801

When the matrix [2-23] is calculated, the Isqnonneg algorithm in Mat lab is then applied onto the matrix for the inversion and generation of the vector f. A summary of the procedure for adapting the DAE based model to various reaction mechanisms is given by Figure 2-2.

Step 1

Collect Mass loss vs. Temperature data for at least two different constant heating rates (by experimentation or simulation)

Step 2

Select n values of conversion. These are the number of equally spaced points over the range at which E and A for each component i will be evaluated.

Step 3

Propose a reaction model (Or use of the reaction model used for the simulation) and find the value of the conversion at which the reaction i reaches a maximum rate of decomposition. Find the corresponding value of Ψ_i from the model dependent equivalent of the $ln\,\Psi_i$ expression.

Step 4

Using the expanded form of the equation:

$$\Psi_i(\beta_1, T_1) = \Psi_i(\beta_2, T_2)$$

Find E values for each candidate reaction/component i.This is model independent.

Step 5

The value found in step three influences the pre exponential factor. Using this value and the known E_i solve the following equation forA_i.

$$\ln\ \Psi_i = \frac{A_i}{\beta_1}\left[T_0 \exp\left(\frac{-E_i}{RT_0}\right) - \frac{E_i}{R}\int_{E/RT_0}^{\infty} \frac{exp(-u)}{u}\,du - T_1\, exp\left(\frac{-E_i}{RT_1}\right) + \frac{E_i}{R}\int_{E_i/RT_1}^{\infty} \frac{exp(-u)}{u}\,du\right]$$

Step 6

Using the n set of reactions each with now specified E_i and A_i values, find each reaction's initial mass fraction $f_{i,0}$ using matrix inversion on $M = \Psi f$

The equation used to find each element of $f_{i,0}$ must be model-dependent.Non-zero mass fractions corresponding to E_i and A_i values found for each reaction indicate the values to be used.

Figure 2-2: General Procedure for the adaptation of the DAE based algorithm to various reaction mechanisms (Vittee 2012).

A similar procedure is followed on application of the model to isothermal conditions. Here, two temperatures are used instead of heating rates and the integral is evaluated by integration over time.

2.6. Intrinsic kinetics

According to Le Manquais et al. (2009), a wide variety of operating temperatures, heating rates and particle sizes have been studied using thermo-gravimetry. Le Manquais et al. (2009) highlights that the variation of these parameters, together with incomplete understanding of the fundamental interactions taking place, has led many a times to the absence of the true kinetic control. Hurt and Calo (2001) also acknowledge the extensive literature on kinetics, particularly of the CO_2 reaction, without a universal consensus on the magnitude of E and the global orders. This they also attribute to the variation in experimental techniques. Kim et al. (2011) argues that kinetic models can only be discriminated if their experimental data is obtained under similar experimental characteristics.

As mentioned in Section 2.1 the intrinsic kinetics of a reaction are independent of the effects of transport phenomena taking place during the reaction. Lahijani et al. (2012) confirms the findings of other researchers, that temperature is the most influential parameter in controlling the conversion reaction rate. This is because the various regimes taking place during a reaction can be distinguished by the temperature ranges for given particle sizes. Therefore within these temperature ranges, the effects of transport phenomena vary, hence defining the reaction zone/regime for a particular particle size range. At low conversion temperatures and small particle sizes (Williams et al., 2001), the rate of reaction is controlled by the chemical reaction taking place; this regime is known as the kinetic/chemically controlled regime (regime I) (Lahijani et al., 2012). As the temperature/particle size increases, the controlling factor becomes the pore diffusion mechanisms occurring during the conversion. This regime is known as the diffusion regime, (regime II), where E is lower than in the kinetic controlled regime (Lahijani et al., 2012). With further increase in temperature the external diffusion limitation (regime III) is experienced (Charpenay et al., 1992). Williams et al. (2001) describes regime III as occurring at high temperatures where bulk mass transfer limitations are controlling or where the particles are large.

The current study is aimed at evaluating the intrinsic kinetics of the conversion processes under the chemical reaction controlled regime. This allows the elimination of the uncertainty of parameter extraction through transport models (Roberts and Harris, 2007; Hurt and Calo, 2001). Reactivity data in the chemical regime serves as a reliable basis for crude extrapolations into the transport controlled regimes at higher temperatures and faster rates (Roberts and Harris, 2007; Henrich et al., 1999). Through observation of the bed mass, particle size, and conversion temperature in thermo-gravimetric, transport limitations can be eliminated (Hurt and Calo, 2001). The reaction may then be assumed to be in regime I. It could also be assumed that the effects of pressure, char type and temperature on the intrinsic reactivity may be obtained and used to predict the apparent char reactivity at higher temperatures by use of the effectiveness factor and the intrinsic reactivity (Liu et al., 2000).

Kinetic data extracted from regime II has been described as less clear and leading to poor precision in kinetics (Hurt and Calo, 2001). Hurt and Calo (2001) further explain that the intrinsic values within this regime are normally extracted with the use of transport models and/or classic Thiele mapping relations. The Thiele modulus is used to calculate the reaction rate as a function of the intrinsic rate by use of correlations and char properties (Charpenay et al., 1992). Hurt and Calo (2001) amongst other reasons attributed the poor precision to the need for detailed and assumption-laden heat and transport models to extract the intrinsic parameters. Also mentioned as a source of inaccuracy is the Thiele relation itself:

$$n_{observed} = \frac{n+1}{2} \qquad [2\text{-}33]$$

The relation narrows down the range of possible intrinsic orders from 0-1,to 0.5 to 1 in regime II, with corresponding loss of resolution.

A number of authors have defined the kinetic controlled regime under various conditions for varying conversion processes and sample types. Naming a few, for combustion, Irfan et al. (2011), Sima-Ella et al. (2005) and Hurt and Calo (2001) describe the regime I, as evaluated

below 900K, and regime II as referring to all data extracted above 1100K. Hurt and Calo (2001) and Irfan et al. (2011) studied coal chars, whilst Sima-Ella et al. (2005) studied activated carbon char. Kastanaki and Vamvuka (2006) carried out combustion tests using thermo-gravimetry. The authors used a mass range of 3-7 mg, under heating rates of 10K/min from 298K to 1123K to ensure kinetic control. The low sample mass was to ensure a thin char layer without temperature and oxygen concentration gradients. Kastanaki and Vamvuka (2006) selected the slow heating rates to ensure the absence of deviations of sample temperature with respect to the selected temperature value. Fisher et al. (2012) carried out an isothermal kinetic study on gasification and combustion of biomass chars, (torrefied and raw willow) in O_2 and steam respectively. Fisher et al. (2012) specified experimental operations of 1023K-1173K, a particle size of below 50μm and a sample mass of less than or equal to 5 mg to obtain the intrinsic kinetics regime.

For the char $-CO_2$ reaction, Khalil et al. (2009) studied pine and birch charcoals. For the exclusion of heat transfer problems, Khalil et al. (2009) used sample masses in the range of 1-2 mg and heating rates of between 5 and 20K/min. Ahn et al. (2001) made use of a temperature range of 1173K-1273K to attain the regime I for Indonesian coal char. Mani et al. (2011) define the chemical reaction controlled regime as occurring at temperatures below 1273K, whilst studying wheat straw char gasification by CO_2. Lahijani et al. (2012) studied the isothermal gasification of oil palm shell char, and identified an intrinsic regime below 1173K. Yuan et al. (2011) established a transition to regime II at temperatures between 1123 K - 1273K, when studying the gasification of rice straw char, china leaves char, and pine sawdust char. Henrich et al. (1999) states that with a particle size of $50 \pm 10\mu m$, char conversion remains in the chemical regime for total burnout times of approximately 10^3 seconds or more, under isothermal conditions. This author studied the gasification and combustion of municipal waste, electronic scrap, wood and straw.

Arrhenius plots have been used by various authors to determine the regime in which a reaction is taking place (Lahijani et al., 2012; Kim et al., 2011; Mani et al., 2011; Qi et al., 2011; Yuan et al., 2011; Roberts et al., 2010; Hurt and Calo, 2001). Lahijani et al. (2012) and Mani et al. (2011) explain that the Arrhenius plots of ln k vs. 1/T (for isothermal conversion), may describe independent lines of different E's. In such a case, the lower E obtained at higher temperatures

corresponds to the pore diffusion controlled regime (regime II) (Lahijani et al., 2012; Mani et al., 2011; Hurt and Calo, 2001). Whereas the higher E at lower temperatures correspond to regime I. Ahn et al. (2001) explains that the reason why the apparent E is lower at high temperature than at lower temperature is due to the pore diffusion resistance of reactant gas into char increases as the temperature increases. Kim et al. (2011) noted that the extent of the transition between the two regimes is dependent on the particle size, the higher the particle size, the greater the deviation. This method was applied in the current study, along with the literature guidelines outlined, to ensure that the experimental conditions applied, describe the chemically controlled regime.

2.7. Combustion

The char-O_2 reaction in most cases takes place on the external surface of the char particle and is controlled by ash layer diffusion (Irfan et al., 2011). As temperature and particle size increase, the reaction tends to proceed towards the gas film diffusion controlled regime. However, the reaction proceeds towards the regime I, and takes place uniformly throughout the internal pore surfaces of the particles if temperature and /or particle size substantially decreases (Irfan et al., 2011).According to Irfan et al. (2011), combustion is chemical reaction controlled for pulverized combustors where the particle size is below 50μm. For particle sizes above 100μm, the reaction is diffusion dominated.

The global reaction of the char oxygen reaction is as defined by Equation [2-34], below.

$$C + O_2 \xrightarrow{\Delta H=-392.9kj/mol} CO/CO_2 \qquad [2\text{-}34]$$

Sima-Ella et al. (2005), along with Smith and Tyler (1972) and Walker et al. (1967), describe the air oxidation of chars as a global one step kinetic reaction model. Chimica and Federico (n.d.) however suggests that the conversion takes place according to a multi-step process.

2.8. Gasification

In this study gasification of the fuels was carried out in CO_2 atmosphere. As noted by Vittee (2012) and Irfan et al. (2011) the reaction in carbon dioxide is similar to that in steam. However, it is relatively slower, easier to measure and hence more suitable for studying the char reactivities of various fuels (Irfan et al., 2011). The reaction between char and carbon dioxide is known as the Boudouard Reaction and is expressed by Equation [2-35],

2.9. Biomass Co-firing

Increasing the fraction of renewable and sustainable energy in the national energy supply is one of the means of mitigating the potential global environmental impacts of fossil fuels used for power generation and other energy supplies (Baxter and Koppejan, 200). Biomass in this context is defined as organic matter produced as a result of photosynthesis. Kuo-Chao et al. (2009) states that direct combustion is the simplest, most common and successful thermo-chemical process for energy conversion from biomass. The authors also mention that the decomposition kinetics of a variety of biomass feedstock is very crucial for the understanding of the chemical behavior of the complicated fuels.

According to Hernández et al. (2010), the higher reactivity of the biomass is associated with the higher volatile content and higher porosity of the formed char. Hernández et al. (2010) however, also noted some findings on implications of synergy between biomass and coal char, especially at low fuel/air ratios and low reaction temperatures, which might be attributed to the content and composition of the blend ash (especially due to the catalytic effect of Ca and K from the biomass ash, and the Fe, Ni, and Zn contents of the coal-coke ash). Lahijani et al. (2012), Kim et al. (2011), Mitsuoka et al. (2011), Zhu et al. (2008), Miura (1989) and Chimica and Federico (n.d.) conclude that the catalytic effect of inorganic constituents present in some biomass types is one of the major factors which control reactivity during coal gasification. Chimica and Federico (n.d.) also suggest catalytic effects of alkali metals in oxidation reactions. The authors go on to conclude that water- or acid-soluble minerals have a higher influence on char reactivity than the surface area does. Bockelie et al. (n.d.) states that the use of potassium (K) and other alkali metals to catalyse coal gasification is well established. It is also noted that Capucine Dupont et al. (2011) identified that the gasification reaction rate for woody biomasses correlates with the ratio of K /Si, confirming the catalytic effect of the K and reflecting an inhibiting effect of Si. Spiro et al. (1983) mentions the importance of alkali carbonates as excellent catalysts in the strength order of Cs > K> Na> Li.

So, it can then be suggested that biomass also plays the role of being a potential source of inexpensive catalysts in the co-processing of coal and biomass. An experimental study carried out by Hernández et al. (2010) showed that an increase in biomass content in co-gasification of biomass and a coal-coke mixture in the fuel blend upgrades the producer gas quality and improves the cold gas efficiency. The co-firing of biomass has been demonstrated successfully in

over 150 installations worldwide for most fuel combinations and boiler/unit types. Most of these (about a hundred) are in Europe, whilst about 40 commercial demonstrations were carried out in the United States and the rest mainly in Australia (Davidson et al., 2007; Fernando, 2005).

When considering biomass co-firing there is need to take into account the physical and chemical characteristics of biomass compared to coal (Sadhukhan et al., 2008; Senneca, 2007; Klose and Wolki, 2005).Chemical composition variations amongst biomass fuels are much greater than those observed amongst coals. All biomasses have more O_2 and H_2 and less carbon than coal (Senneca, 2007). Wornat et al. (1996) studied the combustion reactivities of woody and herbaceous biomass and noted that biomass char particles burn over a much wider temperature range of 450K, whilst coal char tends to burn within a 150K temperature range. The author adds to this observation that the biomass char particles span the entire range of theoretical limits 'from the slowest burning inert particles to the fastest burning diffusion controlled particles', under conditions simulating pulverized pine and switch grass biomass chars burn at rates comparable to those of high volatile bituminous coals (Wornat et al., 1996).With conversion, the reactivity tends to decrease; Wornat et al. (1996) and Chimica and Federico (n.d.) attribute this to preferential depletion of the more reactive carbon and the physical and chemical transformations of the inorganic constituents that render them catalytically inactive. Wornat et al. (1996) concludes that the irregular morphologies of the biomass chars and their wide range of burning rates are most likely to make a detailed kinetic analysis quite difficult.

2.9.1. Operational drawbacks in biomass co-firing

Co-firing may be applied directly or indirectly in industry. Direct co-firing involves the firing of coal and biomass in the same combustor or gasifier, whilst in indirect co-firing the combustion and gasification of biomass occurs in a separate unit. Several technical issues tend to arise during direct co-firing, as the biomass constituents enter the coal unit. The drawbacks to biomass co-firing can include fuel preparation, handling and storage, milling and feeding problems, different combustion behavior, possible decreases in overall efficiency, deposit formation (slagging and fouling), poor carbon burn out, agglomeration, corrosion and/or erosion, and impacts on ash utilization and marketing. The degree of these difficulties depends on the quality and percentage of biomass in the fuel blend, type of combustion and/or gasification used the co-firing configuration of the system, and properties of coal. The importance of the problems rises however with increased biomass/coal ratios, and when low quality biomass is used as a feedstock, especially in direct co-firing systems without dedicated biomass infrastructure (Maciejewska et al., 2006; Baxter and Koppejan, 2004: Fernando, 2005) .

2.9.2. Biomass and blend range selection

A broad combination of fuels, such as residues, energy crops, herbaceous and woody biomasses have been co-fired in various boiler units amongst the various trials carried out globally. The range of biomass and wastes that have been co-fired included biomass pellets, waste wood, paper sludge, cocoa shells, chicken litter, sewage sludge, wood pellets, meat and bone meal, refuse derived fuel and olive kernels. In the UK, dry imported fuels such as wood pellets and dry solid residues from olive oil and palm oil production have been co-fired on a fully commercial basis (Fernando, 2005). When pre-blending the biomass with the coal and processing the blended fuel through the existing coal handling and firing system, a maximum co-firing ratio of 10% biomass on a thermal basis should be adhered to in order to ensure modest impacts on the unit operations (Livingston, 2012; Fernando, 2005). Though herbaceous biomass have been co-fired in several plants worldwide, their higher inorganic matter content results in higher chance of slagging and fouling during combustion (Fernando, 2005). However, for gasification, providing the K in the biomass avoids the need for expensive, proprietary catalysts that increase the cost of the gas produced (Bockelie et al., n.d.). Replacing the expensive potassium based catalysts by use of biomass as the alkali metal source is a much more economical solution. The two main criteria, which have been used for the choice of biomass in this study, are the availability of biomass in

South Africa as well as the biomass composition. The biomass composition in terms of the ash content, S and N_2 content relates to the properties of the biomass as briefly explained in Section 3.5.1.

2.9.3. Biomass availability in South Africa

The selection of the biomass type was based mainly on a national study on the availability of biomass resources reported by the Department of Minarals and Energy (2004) as well as a report by Marbek Resource Consultants Ltd. (2007) for the Ethekwini municipality. Two major types of biomass are available in South Africa: wood residues and bagasse from the sugar industry. There are various sources of wood residues in the country, according to the report; the various biomass yields from the sources are as shown in Table 2-2.

Table 2-2: Biomass availability in South Africa (DME, 2004)

Wood residue type/source	Biomass tonnage(millions/per annum)	Percentage
Commercial plantations	3.1	11%
Indigenous Woodlands	15.5	57%
Alien Vegetation	6.6	22%
Deciduous Offcuts	0.23	0.8%
Sawmills	1.57	5.7%
Pulp Mills	1	3.6%
Total yield	27.4	100%

Two companies, Sappi and Mondi, own all the sawmills in South Africa. Hog waste is produced at the mills using softwood pulp. This is a mixture of the mill waste and the bark stripped off the logs. In 2003, a total biomass waste of about 2, 95 million tons was produced with a composition of 55% wood chips, 28% sawdust and 17% bark (Marbek Resource Consultants Ltd., 2007). Table 2-3 gives a breakdown of the energy value of all sawmill waste in the country, according to the Department of Minerals and Energy in 2004.

Table 2-3: Energy value of sawmill waste in South Africa (DME 2004)

Waste type	Mass(1000t)	Moisture %	Ash %	Net Calorific Value (MJ/t)	% Fibre
Chips	1622	40	0.8	10 316	59.20
Dust	826	40	0.5	10 611	59.50
Bark	501	40	2.0	10 135	58.00
Total	2948	40	0.92	10 368	59.08

From this report, it is said that the volume of waste remaining in the forests is about thrice the total waste used or discarded in all mills, and as such is potentially a large renewable energy resource. However, no other information is provided on this type of waste.

Sugar cane residue in the form of bagasse and tops and trash is a source of biomass. Bagasse is the residue that remains after the sugar cane is milled, whilst tops and trash are the material left behind after harvesting; these are usually burnt in the fields (Rich, 2007). Rich (2007) estimates an annual production of 11.47 million tons of bagasse. However, according to the Department of Minerals and Energy in 2004, bagasse is not normally available for other uses of energy conversion. This is mainly because the material is exported for use in the production of paper, board, furfural etc., whilst some of it is used for steam generation for the primary sugar mill. Some of the bagasse is used for electricity generation mainly for the sugar industry itself with very little of it exported to the grid.

According to the Biomass Corporation (2008), Bamboo is a renewable energy source that is fast growing in popularity due to its exceptional properties. It is said to be the fastest growing plant with the highest carbon dioxide uptake. The plant shoots are a food source whilst the wood has a greater tensile strength than steel. Bamboo contains very little sulphur and has a relatively high calorific value which goes up to 26.80 MJ/kg when torrefied. Bamboo has shown adaption to the dryer conditions of Eastern Cape. The Eastern Cape Development Corporation has embarked on pilot projects for bamboo production.11 hectares of land were dedicated for bamboo farming in 2011, with the first harvest expected in 2013 (The Biomass Corporation, 2008).

It must be noted that the only herbaceous type of biomass accounted for is bagasse. This bagasse, as mentioned earlier, is not normally available for energy conversion. A fairly abundant source of herbaceous biomass is highveld grass which unaided, grows all around the country. Its main challenge lies in the low calorific values and high bulk densities. As one of the only significant herbaceous biomass sources, it is considered as a renewable energy source in South Africa.

2.9.4. Biomass composition

The composition of biomass is of great importance for its selection for co-firing in various coal fired units. The constituents of the biomass tend to cause various operational drawbacks as detailed in Section 2.9.1. During combustion, fouling leads to a reduction in heat transfer and overall efficiency. It also leads to damage to the combustion chamber when large particles break off (Miles et al., 1993). Miles et al. (1993) measures the biomass slagging potential as a function of the alkali content in the biomass ash, as shown in Table 2-4.

Table 2-4: Alkali content and slagging potential of various biofuels (Miles et al., 1993)

Fuel	Btu/lb. (dry)	Ash %	Total Alkali			Relative slagging
			% in Ash	lb./ton	lb./MMus	
WOOD						**Minimal Slagging**
Pine Chips	8 550	0,70%	3,00%	0,4	0,07	**0.4 lb./MMBtu** ↓
White Oak	8 165	0,40%	31,80%	2,3	0,14	
Hybrid Poplar	8 178	1,90%	19,80%	7,5	0,46	
Urban Wood Waste	8 174	6,00%	6,20%	7,4	0,46	**Probable Slagging** ↓
Tree Trimmings	8 144	3,60%	16,50%	11,9	0,73	
GRASSES						**Certain slagging** ↓
Switch Grass	7 741	10,10%	15,10%	30,5	1,97	
Wheat Straw-average	7 978	5,10%	31,50%	32,1	2,00	
Wheat Straw-hi alkali	7 167	11,00%	36,40%	80,0	5,59	
Rice Straw	6 486	18,70%	13,30%	49,7	3,80	
Bagasse – washed	8 229	1,70%	12,30%	4,2	0,25	

It is can be seen from the information presented that the most representative choice of biomass would a woody biomass as well as a herbaceous biomass source. Highveld grass was used as a source of herbaceous biomass, whilst pine dust was used as the woody biomass representative. The high alkali content in the herbaceous biomass gives the opportunity to evaluate its effect in gasification. The pine dust represents a major source of biomass waste from the country's sawmills and paper industry, and is more appealing to the combustion process as it has minimal slagging abilities.

2.10. Thermo-gravimetric analysis

Thermo-gravimetric analysis has been widely applied in kinetic studies of thermal conversion of complex fuels (gasification, combustion and pyrolysis), with the associated temporal weight change profiles being used to extract kinetic information and to validate gasification models

(Lahijani et al., 2012; Qi et al: Rotliwala and Parikh, 2011; Otero et al., 2008; Scott et al. 2006(b); Duz et al., 2005; Arenillas et al., 2004;1999). Thermo-gravimetry provides one of the most convenient and widely used methods for analyzing the kinetics of gas–solid reactions, as well as distinguishing between competing models. A thermo-gravimetric analyzer (TGA) is used to measure the temperature variation of the sample mass and its rate of change. Weight loss as a function of temperature reflects the conversion of gas products yielded in the various stages of the thermal decomposition. A suitable model may then be used to interpret the resulting variation of sample with time and its derivative and obtain the kinetic parameters of the thermal events (Fermoso et al., 2010; Gil et al., 2010(a); Feng and Bhatia, 2002). It can then be concluded that thermo-gravimetric analysis is a useful, simple and fast tool for studying the thermal behavior, reactivity and kinetics parameters of carbonaceous materials (Gil et al., 2010(a); Fermoso et al., 2008; Arenillas et al., 2004; 1999).

2.11. Study aim and objectives

The overall aim of this research study is to determine the intrinsic reaction kinetics of gasification and combustion of biomass and coal chars under non-isothermal and isothermal conditions. The objectives are outlined below.

2.11.1. Objectives

The objectives of the study are as follows:

• To validate the modified DAE based model by application to combustion and gasification thermo-analytical data. This objective is fulfilled by the evaluation of the model predicted kinetics to the actual experimental data obtained. This is carried out by using the obtained kinetics to simulate or predict the reaction progression. The simulated curve is then compared to the experimentally obtained conversion curve. Two statistical error evaluation methods were used for the evaluation, these are outlined on Section 4.2.

• To identify the suitable reaction models for biomass and biomass-coal char blends in gasification and combustion. Various reaction models can be compared by use of different DAE model adaptations. The DAE based model has been successfully adapted to the RPM and first order reaction models (Scott et al. 2006(a); Vittee , 2012). Application of these two adaptations to the model was carried out on the obtained thermo-analytical data. Additional adaptations will

be applied if these two reaction models cannot accurately describe the conversion profiles of the biomass materials.

• To investigate the effect of the presence of biomass on coal char combustion and gasification using the DAE based model. The behavior of the biomass under the two different conversion environments was determined by the model. The kinetics from the coal-biomass char blends conversion were then used for comparison with pure components to identify any changes.

• To analyze the reaction kinetics of non-isothermal combustion and gasification. For the pure coal sample, both isothermal and non-isothermal conversions are experimentally studied for gasification. The kinetics of these conversions under the differing temperature programs were compared to fulfill this objective.

These objectives were addressed by the application of the methodology presented in Chapter 3 of this study.

2.1. Conclusion

A woody and herbaceous biomass, pine chips and highveld grass, have been selected for blending with coal during gasification and combustion using thermo-gravimetry. The blends under the named conversion processes are utilised for an intrinsic kinetic study by the application of an iso-conversional DAE based model. The RPM and first order reaction models are used in conjunction with the DAE based model. Efforts are applied to ensure that the experiment conditions describe the chemical reaction regime. Upon application, the model determines E, A and the f_o of each reaction taking place. An outline of the aims and objectives of the study has also been presented in this chapter.

3. RESEARCH METHODOLOGY

This chapter serves to provide a sequential breakdown of the events and experimental work carried out during this research. A detailed description of the experimental work is provided. As a continuation to the work done by Vittee (2012), the methodology involves model evaluation by simulation in order to observe the model's accuracy with respect to simulated data. Physical experimentation follows after this stage. This was broken down into two stages:

- The preliminary stage, involving the identification and optimization of the experimental runs towards the chemical reaction controlled regime and;
- The second stage involves the final experimentation work which is broken down into sample characterization and thermo-gravimetric analysis.

Finally, model application and data analysis was carried out to conclude the study.

3.1. Research method 1: Model evaluation by simulation

The development of the simulations and the DAE based model were carried out using Math works' Matlab software package. Following the evaluation by Scott et al. (2006(a)), the Matlab code developed by previous MSc researchers (Fakir, 2012; Vittee, 2012, Saloojee, 2011), must be tested by application on simulated data. Fakir (2012) and Saloojee (2011) successfully wrote the Matlab code to carry out the calculations from Scott's algorithm. Scott's algorithm may be referred to as the DAE based model adapted to first order reaction model dissociation. Vittee (2012) successfully adapted this coded algorithm to materials dissociating according to the RPM. In this study, the two sets of code are used for kinetics determination. Before using these codes, there is need to ensure the absence of errors and to validate whether the model is capable of kinetics determination as described in Section 2.5. A conversion vs. temperature curve is simulated using a known kinetic triplet. The simulated data is then fed into the DAE based model, which determines a kinetic triplet. The model determined kinetic triplet is then compared to the initial triplet used to simulate the data, and the indication of the model accuracy. All coding used in this work is provided and explained in Appendix A.

3.2. Research method 2: Experimentation Methods

3.2.1. Sample material

3.2.1.1. Coal

A vitrinite-rich coal sample obtained from density fractionation of a South African coal was used in this study. The sample was pulverised to -75 µmetres in a pulveriser. This coal type was selected because of its high reactivity, which relates to shorter high temperature exposure times of the equipment during the isothermal runs.

3.2.1.2. Biomass

Highveld grass obtained from South Africa's road sides in Annlin (Pretoria) was oven dried overnight at 70 ^{0}C and pulverised to -75µm. Pine wood blocks obtained from the University of Witwatersrand's School of Chemical and Metallurgical Engineering workshop was used for the study. The blocks were also pulverised and reduced to a -75µm size.

3.2.1.3. Gases

High purity N_2 gas, technical standard air and high purity CO_2 gas was used for the thermo-gravimetric analyses.

3.2.2. Equipment

The following equipment was used to carry out experimental procedures.

- A high temperature TGA (TA instruments TGA) for all the combustion and gasification tests.
- A low temperature TGA (The Perkin Elmer TGA) for proximate analysis.
- A Dry Cal Bomb Calorimeter for calorific value determination.
- A PANalytical Empyrean diffractometer with PIXcel detector and fixed slits with Fe filtered Co-Kα radiation for X-Ray diffraction (XRD) analysis.
- A Leco CHN Truspec and a Leco SC 632 for ultimate analysis.
- Perkin Elmer ICP-OES for the inductively coupled plasma optical emission spectrometry (ICP-OES).
- A Leica DM 4500P reflected light microscope for petrography.

The thermo-gravimetric equipment is discussed further.

3.2.2.1. The Perkin Elmer TGA

The Perkin Elmer series STA 600 displayed on Figure 3-1 was used for the proximate analysis of the samples. The TGA can be utilized up to a maximum working temperature of 900^0C. On this TGA a separate cooling unit is attached for temperature control.

Figure 3-1: Perkin Elmer TGA

3.2.2.2. The SDT Q600 TGA

The use of a TA instruments SDT-Q600 high-temperature TGA, displayed on Figures 3-2 and 3-3, was employed as the backbone of experimental study in this research.

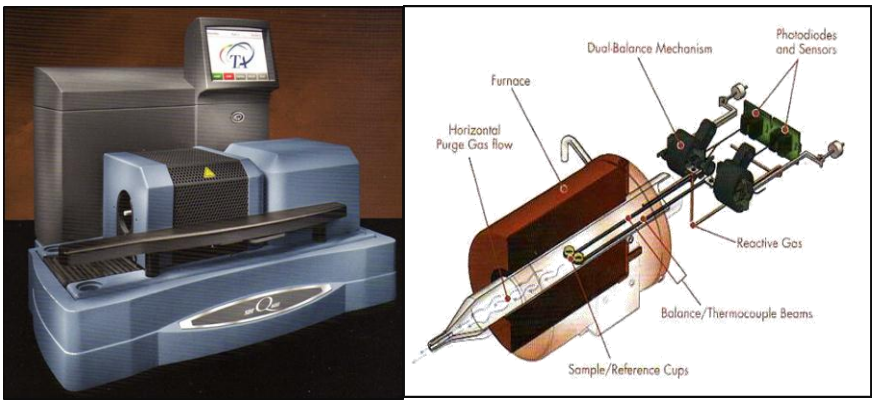

Figure 3-2: TA instruments TGA

Figure 3-3: TA instruments TGA furnace

The equipment has a balance sensitivity of 0.1µg and a differential thermal analysis (DTA) sensitivity of 0.001℃. This unit consists of a furnace capable of operating up to 1500℃. The internal set up of the equipment is shown in Figure 3-3.From the diagram, the two balance beams are equipped with in-built thermocouples. According to the supplier's recommendations, it is not advisable to allow CO_2 gas to through the TGA's in-built mass controllers. A separate add on flow controller was therefore built and attached to the reactive gas port of the unit. This add-on system gives access of CO_2 and pure O_2 gas to the furnace's reactive gas port. According to Vittee (2012), this mass flow controller together with a gas switching accessory (GSA) unit was designed and incorporated into the standard TGA configuration.

The TGA records and outputs the mass against time or temperature data through its software package, Universal analysis. It must be noted that the raw data provided may be used to generate the derivative data curve for use in the algorithm determination of x_{max}.

3.2.3. Research method 2.1: Preliminary Experimentation

As outlined in the Chapter 2, the present study is comparative, and hence there is need to identify an optimum and constant environment in which to carry out the physical experimentation. There are three different reaction zones in which the conversion reactions may take place as detailed in Section 2.6. With the aim of determining intrinsic kinetics in the chemical reaction zone, preliminary experimental work is essential to establish the boundaries of the environment for the materials under study. From the vast range of literature available on obtaining the chemical reaction controlled regime during conversion, the variations in findings show that these conditions may slightly vary with the particular material under observation. There is therefore a need to optimize the particle size, sample mass and heating rates, as well as temperature ranges to be used. It must also be noted that combustion is a highly exothermic reaction (ΔH).This may cause temperature or heating rate fluctuations as the reaction proceeds towards its maximum. Hence, measures must be taken to optimize the dependent parameters to minimize the fluctuations.

This stage of the methodology involves optimisation of the material conversion processes in the Thermo-gravimetric analyser (TGA) to ensure chemical reaction controlled regime dominance over the overall reaction. This involved particle size, particle mass, heating rate, and temperature optimisation.

3.2.4. Research method 2.2: Experimentation

This stage involves the final experimental work, inclusive of sample characterisation as well as the actual thermo-gravimetric experimentation for model application. Data analysis and model application follows thereafter. This stage involves the application of the validated DAE based model, to the experimental data obtained. Universal analysis software from TA instruments was used to read and analyse the thermo-analytical data obtained from the TGA before it was manipulated by the DAE based model. This code was used to carry out the algorithm calculations as outlined in Section 2.5.

3.2.5. Characterisation Analysis

Characterization analysis was carried out on the samples as presented in the following subsections. The characterization includes calorific value determination, proximate analysis, ultimate analysis, petrography and rank determination, particle size distribution analysis and mineralogical assay. Ultimate analysis and mineralogical assay was carried out in an external laboratory.

3.2.5.1. Calorific Value Determination

There is a need to determine the calorific value of the parent samples in order to blend them appropriately. The calorific values of the samples under study were determined by the use of a Dry Cal bomb calorimeter. Bomb calorimetry is used for the determination of the total amount of heat produced from completely burning one unit mass or volume of fuel under high pressure oxygen atmosphere. The Dry Cal Calorimeter system makes use of a dry bomb comprising a thermally conductive heat sink, into which the temperature sensors are cast, shrunk onto the stainless steel combustion vessel. The samples were loaded onto a crucible and placed on a sample holder in the bomb. Filtered O_2 gas was charged to a pressure of 2 500 KPa with the use of a valvepin. The bomb was then lowered into the calorimeter to commence the analysis. Water from a thermostatically controlled tank circulated the calorimeter's walls using a jacket circulation system. This provided a controlled temperature environment around the bomb during the determination. The calorimeter measured the heat energy produced per unit mass in burning the loaded sample in the bomb.

3.2.5.2. Particle size distribution analysis

A Malvern Mastersizer 2000 was used for the analysis of the particle size distribution of the samples. The Malvern Mastersizer is a manual wet sample dispersion unit. Distilled water was used as the dispersant. The samples were gradually added onto the dispersant; a homogenized suspension of the sample was then produced and maintained by continuous agitation of the mixture. The suspension of the particles in the measurement zone allowed the determination of the particle sizes using the Mastersizer 2000 software. This provides a more detailed breakdown down of the sizes of the particles contained in the sample.

3.2.5.3. Proximate analysis

This involves the assay of the ash, volatile matter, moisture and fixed carbon. The analysis determines these parameters by heating the material under specific conditions. Each of these parameters has an effect on the conversion behavior of the fuels under study. The analysis was carried out on the pure samples and the coal-biomass blend samples. A Perkin Elmer TGA was utilized for this purpose. The experiments involved the drying and devolatization in N_2 atmosphere, followed by combustion in an O_2 atmosphere. The sample was equilibrated at ambient temperature (30^0C) and heated at 30^0C/min to 700^0C. At this point the gas switches over from N_2 to O_2 to allow combustion up to a final temperature of 900^0C

The drying step is considered to be within the 30^0C to 110^0C points in time. The devolatization is measured as the weight loss between the 110^0C mark and the 700^0C mark, whereas the combustion step is evaluated as the weight change between the 700^0C mark and the 900^0C mark .The remaining residue is considered to be the total ash content

3.2.5.4. Ultimate analysis

This is the absolute measurement of the elemental composition of a substance. The elements to be determined are Carbon (C), Hydrogen (H), Nitrogen (N), Sulphur (S), and Oxygen (O) by difference. The determination of the C, H and N was carried out using the Leco CHN Truspec. The samples were analyzed at 950^0C using O_2 for combustion and the carrier gas. The ASTM D5373 standard was used.

3.2.5.5. Mineralogical Assay

XRD Analysis

XRD analysis is an X-ray scattering technique used to identify the material crystal structure and chemical composition. A qualitative and quantitative XRD analysis was carried out on the coal and biomass samples and blends. The sample material was prepared for XRD analysis using a back loading preparation method. The samples were analyzed with a PANalytical Empyrean diffractometer with PIXcel detector and fixed slits with Fe filtered Co-Kα radiation. The phases were identified using X'Pert High score plus software. The analysis identifies the mineral group contained in the sample.

ICP-OES Analysis

The method of analysis is used in the determination of non-mineral organics in liquid solutions. This is a quantitative analysis of the chemical ash composition of a substance. The samples were analyzed by UIS Analytical services. A Perkin Elmer Optima 5300 DV was used to determine the oxides of major elements for each material ash (815 °C), including SiO_2, Al_2O_3, CaO, K_2O, Na_2O, Fe_2O_3, MnO, MgO, TiO_2, BaO and P_2O_5. The material ash samples were prepared by Lithium tetraborate fusion in a platinum crucible and leached in diluted Hydrochloric acid to get the sample into solution. The solution was then analysed by ICP-OES to determine the percentage of the total oxides in the ash. This procedure was carried out on each of the pure samples and their coal-biomass blends. The analysis provided information on the possible catalysis by alkali metal components.

3.2.5.6. Petrographic Analyses and Rank Determination

These analyses were carried on the coal sample in order to quantify and identify the coal's maceral contents and rank. The rank determination was carried out by measuring the coal particles' reflectance. The sample was prepared into petrographic blocks as follows:

Clean sample cups lined with a thin layer of Vaseline were filled halfway with coal. A mixture of 1 part of hardener to 7 parts of epoxy resin was then added and mixed uniformly with the coal into a thick paste. The sample is then labeled and the remaining resin mixture poured over the label. Twelve hours of drying was then allowed for the sample to harden into a petrography block. At this point the sample was then removed from the sample cups and polished using a Struers Tegraforce Polisher.

The petrographic analysis was carried out by Professor N. Wagner at the University of the Witwatersrand, Johannesburg. A Leica DM 4500P reflected light microscope was used for the analysis. The maceral group and reflectance analysis were carried out according to the ISO 7404 standard.

3.2.6. Thermo-gravimetric analysis

This is a technique which monitors the mass of a substance as a function of temperature and /or time as the substance is subjected to a controlled temperature program in a controlled atmosphere. Char formation was carried out by exposing the samples to high temperatures (up to 1373 K) under an inert atmosphere (high purity N_2 gas) in the TA instruments Q600 TGA. After

char formation, the chars were exposed to a constant heating rate in a CO_2 environment during a non-isothermal gasification experiment, a constant temperature is applied for isothermal conditions. For combustion, the chars are exposed to an air environment at a constant heating rate or temperature. Three heating rates were applied for each sample to allow a variation in the sets of two heating rates used for kinetics determination, as detailed in Table 3-1.

Table 3-1: Experimentation matrix

Sample blend	**Characterisation analysis**	**Process**	**Non-Isothermal conditions**		
High vitrinite coal	-Calorific value determination -Proximate Analysis -Ultimate analysis -Mineralogical assay	Gasification	B1 K/min in CO_2	B2 K/min in CO_2	B3 K/min in CO_2
		Combustion	B1 K/min in Air	B2 K/min in Air	B3 K/min in Air
Biomass 1	- Calorific value determination -Proximate Analysis -Ultimate analysis -Mineralogical assay	Gasification	B1 K/min in CO_2	B2 K/min in CO_2	B3 K/min in CO_2
		Combustion	B1 K/min in Air	B2 K/min in Air	B3 K/min in Air
Biomass 2	- Calorific value determination -Proximate Analysis -Ultimate analysis -Mineralogical assay	Gasification	B1 K/min in CO_2	B2 K/min in CO_2	B3 K/min in CO_2
		Combustion	B1 K/min in Air	B2 K/min in Air	B3 K/min in Air
90:10 (Coal/ biomass2)	-Proximate Analysis -Ultimate analysis -Mineralogical assay	Gasification	B1 K/min in CO_2	B2 K/min in CO_2	B3 K/min in CO_2
		Combustion	B1 K/min in Air	B2 K/min in Air	B3 K/min in Air
90:10 (Coal/ biomass 1)	-Proximate Analysis -Ultimate analysis -Mineralogical assay	Gasification	B1 K/min in CO_2	B2 K/min in CO_2	B3 K/min in CO_2
		Combustion	B1 K/min in Air	B2 K/min in Air	B3 K/min in Air
Additional blends					
50:50 (Coal/ biomass1)		Combustion	B1 K/min in Air	B2 K/min in Air	B3 K/min in Air
50:50(Coal /biomass2)		Combustion	B1 K/min in Air	B2 K/min in Air	B3 K/min in Air

The isothermal runs were only carried out on the pure coal sample during gasification. The aim for these runs is to identify whether it was possible to model non-isothermal reactions using kinetics obtained from isothermal reaction runs. And these were carried out as presented in Table 3-2.

Table 3-2: Isothermal experiments

Isothermal conditions		
T1 ^{0}C in CO_2	T2 ^{0}C in CO_2	T3 ^{0}C in CO_2

The TGA sequences employed for the combustion and gasification tests are outlined in Appendix B.

3.3. Modelling

This stage involves the application of the validated DAE based model to the experimental data obtained. Universal analysis software from TA instruments was used to read and analyse the thermo-analytical data obtained from the TGA before it is manipulated by the DAE based model. The DAE based model, which is coded into Mathworks's Mat lab® software, was used to carry out the algorithm calculations as detailed in Section 2.5.

3.4. Conclusion

The structure of the research has been presented in this chapter. The research methods were broken down into the format by which they were carried out. The investigation commences with the model validation by simulation and preliminary analysis. These were followed by characterisation and thermo-gravimetric results and analysis. The successful completion of these steps implied the fulfilment of the aims and objectives of the study.

4. MODEL EVALUATION BY SIMULATION

As outlined in Section 2.5.2, Vittee (2012) presented a complete adaptation of the RPM to the algorithm developed by Scott et al. (2006(a)). Some of the important steps carried out during the DAE based model application are discussed in the sections that follow. As explained in Section 2.4.3, the first order and RPM reaction models will be considered.

4.1. Data collection via simulation

TGA data can be simulated via various ODE solvers and the use of a semi-analytical method. Vittee (2012) used two ODE solvers, ODE45 and ODE15s for simulation of kinetic data of the same kinetic triplet. The author applied Scott's algorithm to the simulated data and showed the variance in accuracy for the different solvers. According to Vittee (2012), the semi-analytical method of data simulation is most suitable and accurate as proven by the successful application of Scott's algorithm.

4.1.1. The semi analytical method of data simulation

This method involves the derivation of a solution for the mass fraction remaining. Equation [2-1] may be presented as shown below:

$$\frac{dx}{dt} = A\, e^{-E/RT} \cdot f(x) \qquad [2\text{-}1]$$

Separating variables and integrating:

$$\int_0^x \frac{dx}{f(x)} = \int_{T_o}^{T} A e^{-E/RT} dt \qquad [4\text{-}1]$$

The right hand term (the temperature integral) of the above expression has no analytical solution, and must be numerically evaluated, hence the name semi-analytical. An in-built numerical integration function in Mat Lab is applied to solve the integral in this study. The function approximates the integral using recursive adaptive Simpson quadrature. The left hand side can however be analytically evaluated, and the mass fraction remaining$(1 - x)$ is solved for. A

matrix of$(1-x)$ is then generated, with the number of columns varying as per number of specified reactions. Multiplication of the mass fraction remaining during each reaction by the specified fractional components$(f_{i,o})$ normalizes the respective reactions to their specified initial masses (Vittee 2012). This method of data simulation was used in this study.

4.2. Statistical methods for analysing the quality of fit

The model accuracy was measured using two methods: the correlation coefficient (Vittee, 2012), also known as the R^2 statistic, and the root mean square value of the differences between the simulation and the experimental plot (Sima-Ella et al., 2005). The simulation in this case is obtained by the use of the kinetics determined by the DAE based model for the particular conversion. The two parameters are obtained by the application of regression analysis on the experimental data and the simulated curve. The correlation coefficient is defined by the Equation [4-2] (Vittee, 2012; Draper and Smith, 1981).

$$R^2 = 1 - \frac{\sum(y_i - \hat{y}_i)^2}{\sum(y_i - \bar{y})^2} \qquad [4\text{-}2]$$

Here, $\hat{y}_i$ is the model predicted dependant variable, y_i is the experimentaly determined dependant variable and $\bar{y}$ is the mean of the experimental values. The root mean square (RMS), error value is defined as

$$RMS = \sqrt{\frac{1}{i}\sum(y_i - \hat{y}_i)^2} \qquad [4\text{-}3]$$

On application of the model, the kinetics are determined by the use of conversion data from two different heating rates. The conversion data from the third heating rate is normally used for evaluation of the quality of fit (Vittee 2012). This is carried out by using the kinetics determined by the first two heating rates to predict the reaction progression at the third heating rate. The two methods of evaluating the quality of fit in this study were not only applied on the heating rate being predicted, but instead, the quality of fit was evaluated for all three heating rate conversion data. The average values of these were then given out by the model. This allowed an evaluation of the determined kinetics based on its suitability for predicting the reaction progression, not only at one heating rate, but at three different heating rates.

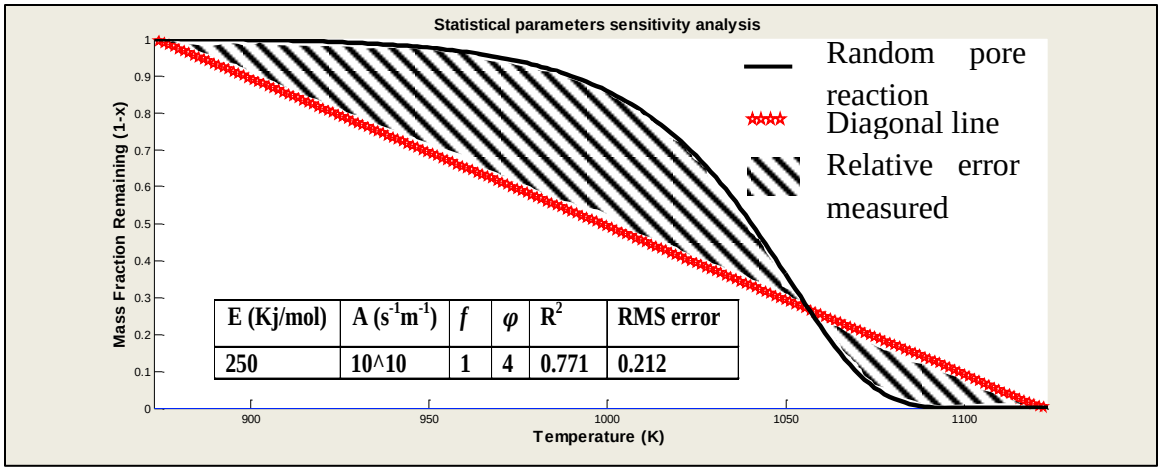

Figure 4-1: Statistical parameters for a diagonal line through an RPM conversion

The statistical parameters were measured for a straight diagonal line through the conversion of a given random pore reaction. The specified kinetic triplet for the random pore reaction and the statistical parameter results are displayed on Figure 4-1. The R^2 statistic for the diagonal is reported as 0.771 and the RMS error value is reported as 0.212. In this study, an accuracy of 0.0100 and 0.999, RMS error value and R^2 statistic respectively will be considered of high accuracy. Clearly, a perfectly accurate plot must give an R^2 value as close to 1 as possible, and a RMS error value as close to 0 as possible. The RMS value obtained when comparing the diagonal line to the random pore reaction represents an increase in the relative error greater than 2000% from the value being considered of high accuracy in the current study. The R^2 value obtained when the diagonal line is compared to the random pore reaction conversion represents an increase in the relative error of only 129% from the value of 0.999. Even though the R^2 statistic is an important tool for evaluating the quality of the fits obtained, it is less sensitive to changes in the relative errors as compared to the RMS error values. The use of both parameters will therefore be employed in this study.

4.2.1. RPM DAE based model evaluation

At this stage a set of kinetics is specified to simulate typical conversion vs. temperature data. The simulated data is fed onto the DAE based model for kinetics determination. The DAE based model determined kinetics are then compared to the initial specified kinetics and the percentage error is then evaluated. Not only does this process evaluate the model accuracy, it ensures the

elimination of errors in the coding. The code has also been tested on simulated data for multiple reactions, these are not discussed here.

Table 4-1: Model evaluation by simulation (RPM)

	E (kJ/mol)	A ($s^{-1}m^{-1}$)	f_o	φ	R^2	RMS
Specified Kinetics	200	1.0E+12	1.00	4	0.99999	0.0011
Model determined kinetics	199.85	1.02E+10	0.998	4.1366		
Relative Error	0.07%	2%	0.2%	3%		

The relative errors for all the kinetic parameters are desirably low. As observed in Table 4-1, the overall fit accuracy is maintained at an excellent value of R^2= 0.99999 and RMS=0.0011. It can then be concluded that no errors in the coding exist.

4.2.2. First order DAE based model evaluation

A similar analysis is carried out for the first order DAE based model. Table 4-2 displays the outcome obtained.

Table 4-2: Model evaluation by simulation (First order)

	E (kJ/mol)	A (sec^{-1})	f_o	R^2	RMS
Specified Kinetics	200	10E+10	1.00	1	5.76e-006
Model determined kinetics	199.99	9.98E+09	1.00004		
Relative Error	0.0%	0.2%	0.0%		

The results displayed show almost exact replicability of the simulated curve by the DAE based model. The quality of the fit is measured at a remarkable R^2 value of 1 and a corresponding RMS value of 5.76e-006. The DAE based first order model has therefore been successfully validated and it can be concluded that no coding errors exist. The code is working successfully as described in Section 2.5.2.

4.3. Conclusion

The semi analytical method described in this chapter is used in the study for simulation of conversion data. The two statistical parameters, the correlation coefficient and the root mean square value, were used for the assessment of the quality of the fits obtained. The two models have been successfully validated by simulation and it is concluded that no coding errors exist. The model is ready for application on experimental data. The preliminary analysis follows in Chapter 5.

5. PRELIMINARY EXPERIMENTAL ANALYSIS

5.1. Introduction

This chapter presents the preliminary experimental results obtained. The preliminary experimental analysis was carried out on samples that were pulverised and sieved to a particle size of -75 µm. At this stage, only non-isothermal thermo-gravimetric analyses were carried out on virgin samples to identify the chemical reaction controlled regime for the combustion reaction. The conversion vs. temperature plots for the preliminary combustion tests were obtained at different heating rates: 12K/min, 15K/min and 20K/min following Vittee (2012). The analysis was carried out by allowing the char samples to undergo the non-isothermal temperature environments at the different constant heating rates in an air atmosphere. The first stage of this analysis involves char formation in the TGA. All the samples were pyrolysed in the SDT Q600 TGA in N_2 atmosphere. The samples were heated at a constant heating rate of 20K/min up to 1250^0C. When this temperature was reached, the samples were cooled to 700^0C and held at this temperature to ensure the release of all the volatile matter. It must be noted that even though the results from char production via TGA may not be directly applicable to industrial facilities, char samples are easy to obtain and are very useful for comparison purposes (Kastanaki and Vamvuka, 2006).

After the char is formed, the actual conversion then proceeds after cooling and equilibration. Char sample masses beginning at about 8mg were used at this stage. The mass and particle size were lowered accordingly in order to attain the chemical reaction controlled regime. The Arrhenius plot method was used to identify the presence of a single or multiple regimes as detailed in Section 2.2. This method is outlined in the following subsection.

5.2. The Arrhenius plot method

The method involves the linearization of the kinetic equation, expressed by Equation [2-1]

$$\frac{dx}{dt} = A\, e^{-E/RT} \cdot f(x) \qquad [2\text{-}1]$$

5.2.1. Non –Isothermal Analysis

During non-isothermal analysis, a constant heating rate β is assumed. Equation [2-1] translates to Equation [5-1];

$$\frac{dx}{dT} = \frac{A}{\beta}\, e^{-E/RT} \cdot f(x) \qquad [5\text{-}1]$$

Taking logarithms of both sides' results in the direct Arrhenius plot method equation which was applied at this stage.

$$\ln\left[\frac{dx}{dT} \cdot \left(\frac{1}{f(x)}\right)\right] = \ln\left(\frac{A}{\beta}\right) - \frac{E}{RT} \qquad [5\text{-}2]$$

For the first order reaction model, the equation breaks down to:

$$\ln\left[\frac{dx}{dT} \cdot \left(\frac{1}{1-x}\right)\right] = \ln\left(\frac{A}{\beta}\right) - \frac{E}{RT} \qquad [5\text{-}3]$$

And for the RPM, the equation becomes:

$$\ln\left[\frac{dx}{dT} \cdot \left(\frac{1}{(1-x).\sqrt{1-\varphi\ln(1-x)}}\right)\right] = \ln\left(\frac{A}{\beta}\right) - \frac{E}{RT} \qquad [5\text{-}4]$$

Because the value of φ is uknown, the equation may be expressed as (Vittee, 2012):

$$\ln\left[\frac{dx}{dT} \cdot \left(\frac{1}{(1-x)}\right)\right] = \ln G(x) - \frac{E}{RT} \qquad [5\text{-}5]$$

In this case

$$G(x) = \frac{A}{\beta} \cdot \sqrt{1-\varphi\ln(1-x)} \qquad [5\text{-}6]$$

It is noted that Equations [5-3] and [5-5] define the same slope. However, the slopes defined by these equations is not identical to the one defined by the use of Equation [5-4]. Equation [5-5] is much simpler to use and most preferred as it does not require a known structural parameter and defines the same slope for RPM behavior as that defined for first order reaction model behavior. However, a plot of $ln\left[\frac{dx}{dT}\frac{\beta}{(1-x)}\right]$ versus $\frac{1}{T}$ as implied by Equation [5-5] assumes that $\ln G(x)$ is a

constant. This assumption may only be considered if the variations in $\ln G(x)$ have negligible effect on the slope of the equation. Since φ is uknown, there is need to evaluate Equation [5-4] at the different values of φ within the range considered in this study. This is to ensure that there are no major deviations in the slope described by Equation [5-5] and Equation [5-4]. Figure 5-1 demonstrates and evaluates the differences in the slopes obtained from Equations [5-4] and [5-5].

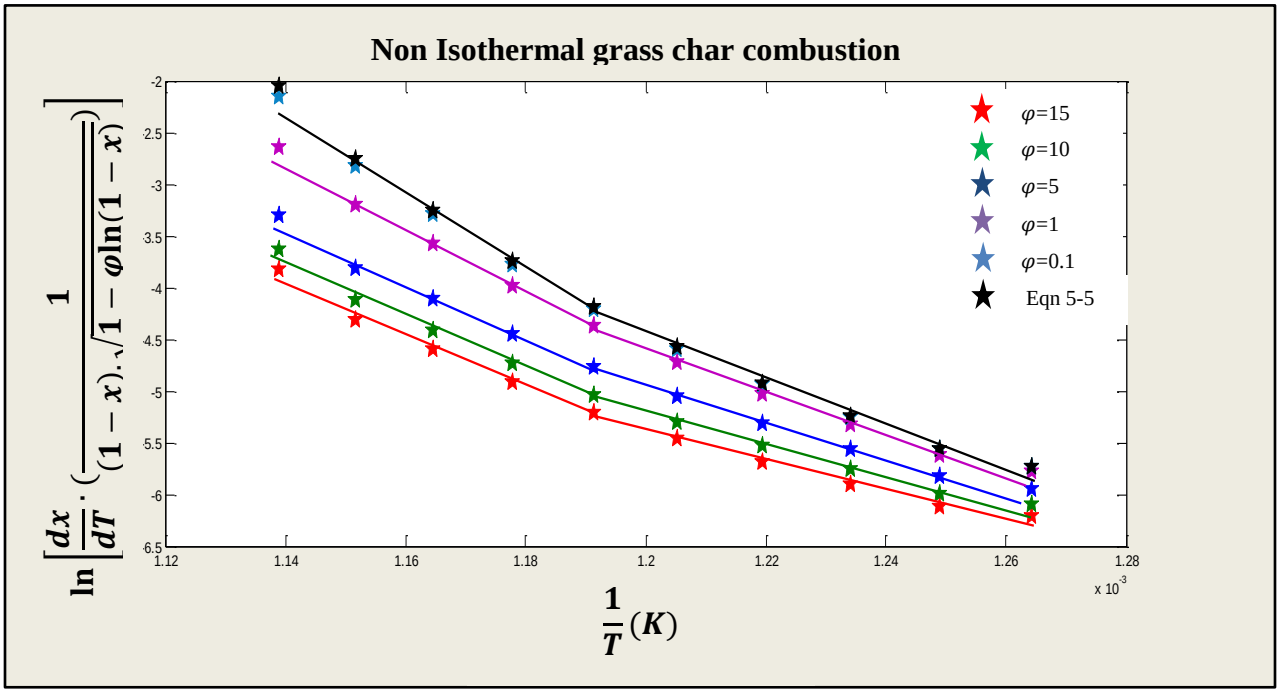

Figure 5-1 Application of Equation [5-4] at varying values of phi

On Figure 5-1 similar slopes are observed for both Equations [5-5] and [5-4] throughout a range of structural values (φ). The result therefore qualifies the use of Equation [5-5] for the identification of single or multiple regimes as the reaction progresses. The method can therefore be applied on the data even though the φ is uknown. The Equations [5-5] and [5-3] have been shown to adequately represent both first order and RPM behaviour. Since it is desirable to have a single Arrhenius plot for the identification of the diffusion regimes, a plot of $\ln\left[\frac{dx}{dT}\cdot\left(\frac{1}{(1-x)}\right)\right]$ against $\frac{1}{T}$ has been proven suitable for this purpose and will be applied.

5.2.2. Isothermal analysis

For isothermal analysis, integration of Equation [2-1] yields

$$\int \frac{dx}{f(x)} = \int A\, e^{-E/RT} dt \qquad [5\text{-}6]$$

This breaks down to Equation [5-7];

$$\ln(1-x) = kt \qquad [5\text{-}7]$$

Where $k = A\, e^{-E/RT}$. A plot of $\ln(1-x)$ against time therefore yields a straight line with a gradient of –k. The Arrhenius plot is then constructed by the linearization of the k. This results in Equation [5-8];

$$\ln k = \ln A - \frac{E}{RT} \qquad [5\text{-}8]$$

The Arrhenius plots carried out in this study were calculated from the conversion values in the range of 0.1-0.9 (Lahijani et al., 2012). Arrhenius plots for the three different samples are displayed on Figure 5-2. The graphs display two sets of Arrhenius plots, at a higher mass and particle size (-75µm), whereas the other plot is at a lower mass and particle size (-53µm). The sample masses are displayed on the Figure 5-2.

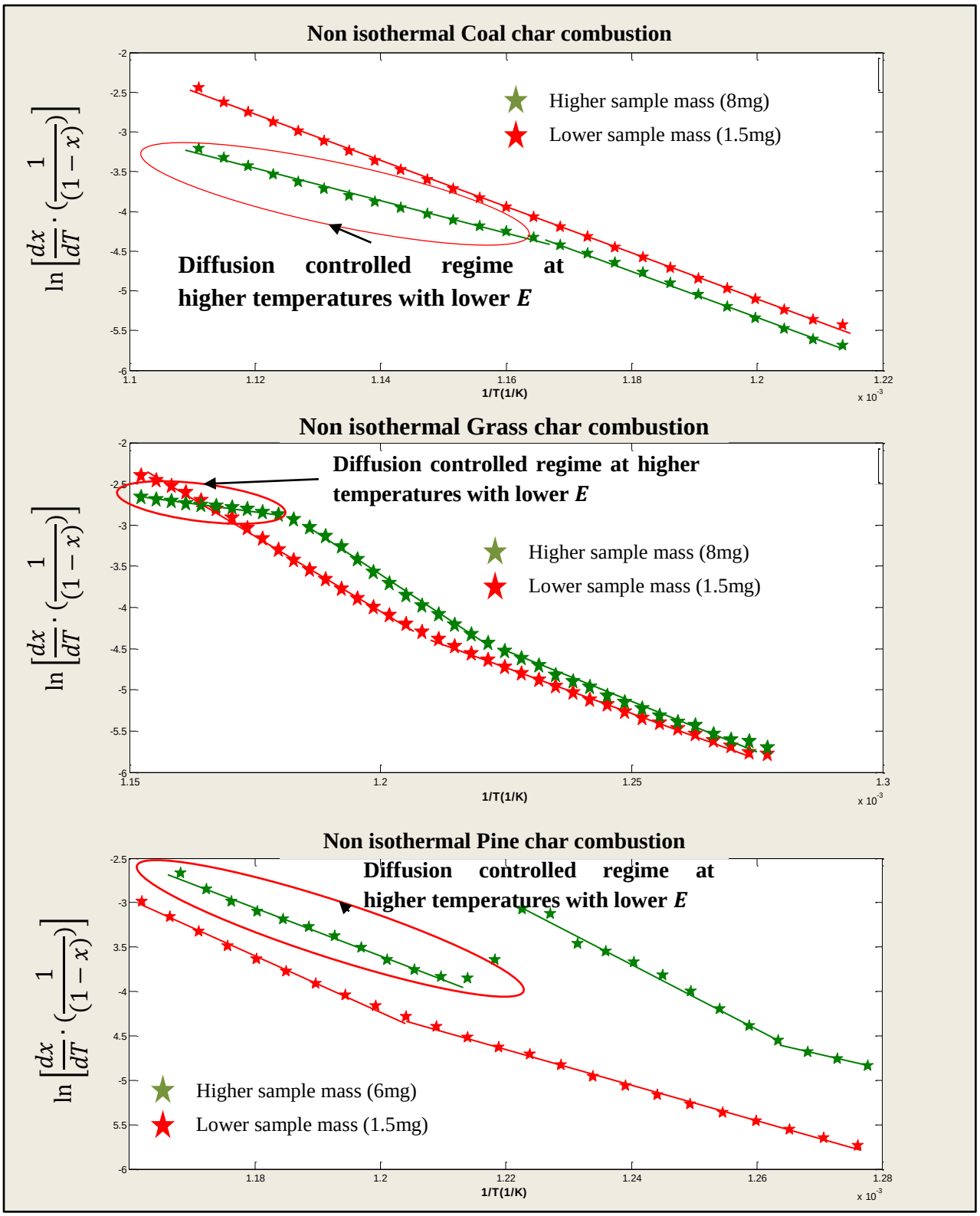

Figure 5-2: Combustion Arrhenius plots at different sample masses.

When using higher sample masses, a decrease in the slope of the graphs is observed at higher temperatures. The decrease in slope demonstrates a second reaction of lower E. This reaction is assumed to describe the pore diffusion controlled regime as detailed in Section 2.6. Clearly, with decrease in sample mass and particle size from about 8mg down to 1.5mg and -75µm to -53µm, the reaction is maintained in the chemical reaction controlled regime. This is observed by the absence of a lower activation energy as the reaction progresses at higher temperatures.

It must be noted however, that for the two biomass materials, two slopes are observed before a decrease in E is observed. A distinct transition range is observed for pine char combustion where a negative slope is observed before the diffusion regime dominates. The first change in the slope of the Arrhenius plot, however does not in this case define the deviation from the chemical reaction controlled regime to the pore diffusion regime. As detailed in Section 2.6, when the chemical reaction controlled regime proceeds into the pore diffusion controlled regime, a decrease in E is observed with increase in temperature. In such a case the lower E obtained at higher temperatures corresponds to the pore diffusion controlled regime (regime II) (Lahijani et al., 2012; Mani et al., 2011; Hurt and Calo, 2001), whereas the higher E at lower temperatures correspond to the chemical reaction controlled regime. In the case of the biomass material chars, an increase in E is observed with increase in temperature before a lower E is finally observed at even higher temperatures as the reaction progresses. Clearly the arrhenius plot suggests that the chemical reaction controlled regime of the biomass chars consists of two different reactions. A possibility exists that there are two different char components which react in accordance with the assumption that the lower E components react first followed by the higher E components. However, an alternative explanation to the difference in gradients during this phase may imply the non conformity of the material conversion to the Arrhenius law, this is beyond the scope of this study. The focus of the use of the Arrhenius plots in this study is plainly to ensure the absence of the diffusion controlled regime during the conversions being studied.

This same method was applied to the gasification data to ensure the reaction is maintained in the chemical reaction controlled regime. The gasification thermo-gravimetric analysis was then carried out using the sample mass and particle size determined during the preliminary analysis.

5.3. Gas flow rate

The reactive and purge gas pressures were maintained at atmospheric pressure. The gas flow rates were varied from 45-70ml/min and no changes were observed. The final flow rate used during the analysis was 70ml/min.

5.4. Heating rate variations

Khawam and Flanagan (2005) declare that experimental thermo-gravimetric curves are generally expected to produce more errors in the iso-conversional kinetic analysis. These errors Khawam and Flanagan (2005) partly attributes to the variation in the actual heating rates from the programmed values due to the self-heating and cooling effects of the TGA. Furthermore, (Vyazovkin, 1997) notes that "the inaccurate determination of heating rates affects all calculation methods in solid state kinetic analyses". The two arguments give reason to a detailed analysis in the heating rate variations occurring during the reactions. The combustion reaction between carbon and oxygen is an exothermic reaction with a high enthalpy of reaction (-392.9 kJ/mol).The gasification reaction on the other hand, is endothermic and has a lower enthalpy of reaction (159.7 kJ/mol). The combustion reaction is therefore more likely to inhibit heating rate deviations during the reaction.

For the same sample, program heating rate and varying masses, the actual heating rate variation plots are presented on Figure 5-3. In this study, the actual heating rate values are determined at each point by reading both the temperature versus time during the reaction. The derivative of the two variables then provides the heating rates at each point during the conversion.

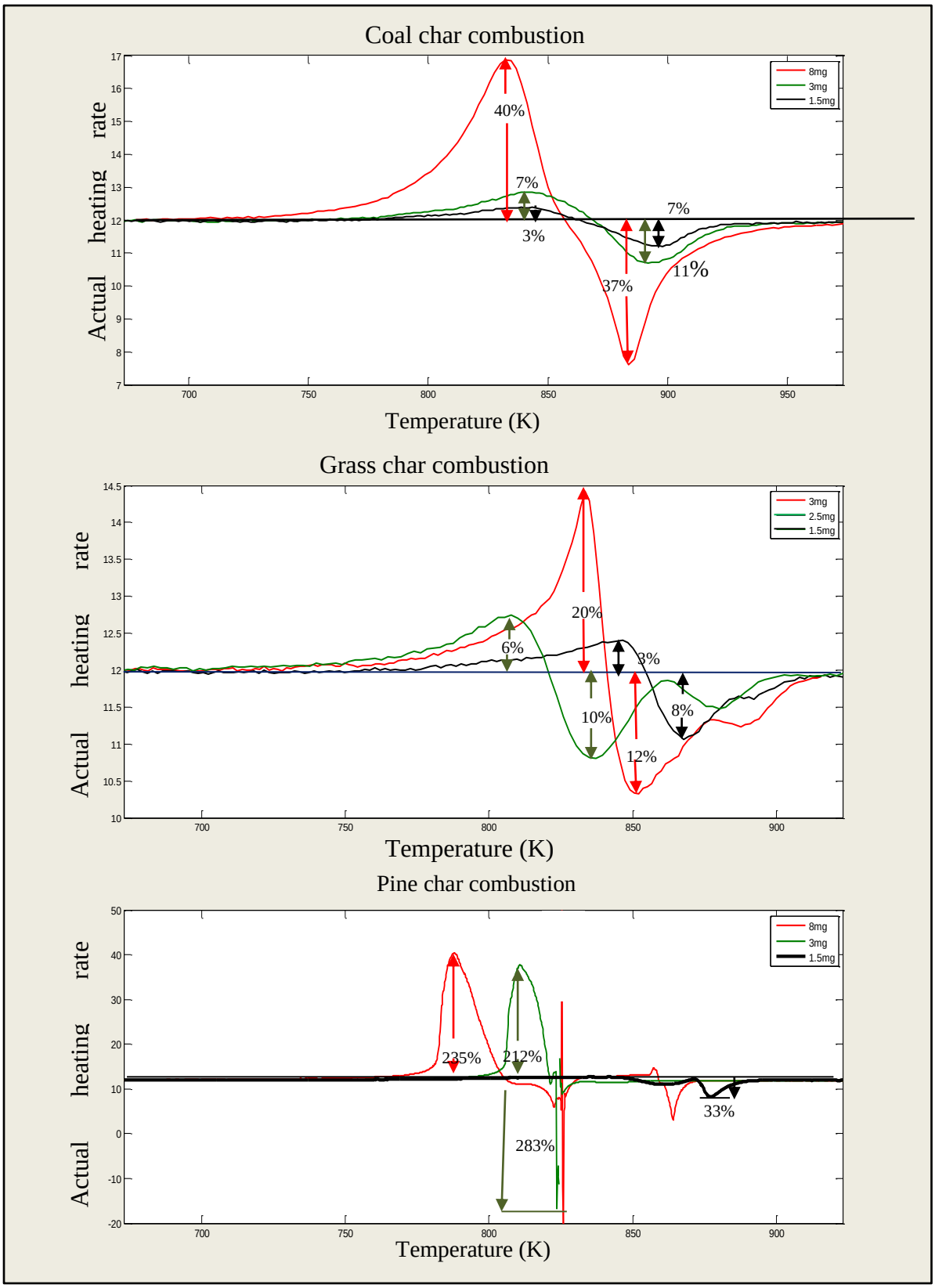

Figure 5-3: Heating rate deviations with varying mass

From Figure 5-3, it is clear that the actual heating rate tends to deviate from the program heating rate more with the increase in mass. For coal char combustion, the duration of the disturbances also seems to reduce with decrease in the sample mass. For pine char, the deviations increase to a maximum magnitude of 283% from the program heating rate at char sample masses of 8mg and decreases down to a maximum deviation of 33% for a char sample of 1.5mg mass. It is clear from the results displayed that the smaller char sample mass minimises the disturbances in the heating rate during the reaction. However, pine char shows the highest deviation from the set program heating of 33%, compared to coal char (7%) and grass char (8%). It is also noted that the pine char has the least content of ash char when compared to that of grass and coal char; this is discussed further in Section 6.3.This low ash content may be directly related to the large heating rate deviations during the progression of the reaction. The instability of the pine char's heating rates during the combustion implies difficulties in modelling the material.

Another factor that could possibly have an effect on the variation of the actual heating rate is the programmed heating rate itself. Figure 5-4 which describes the actual heating rate profiles at the three different heating rates applied at a constant mass for each char sample.

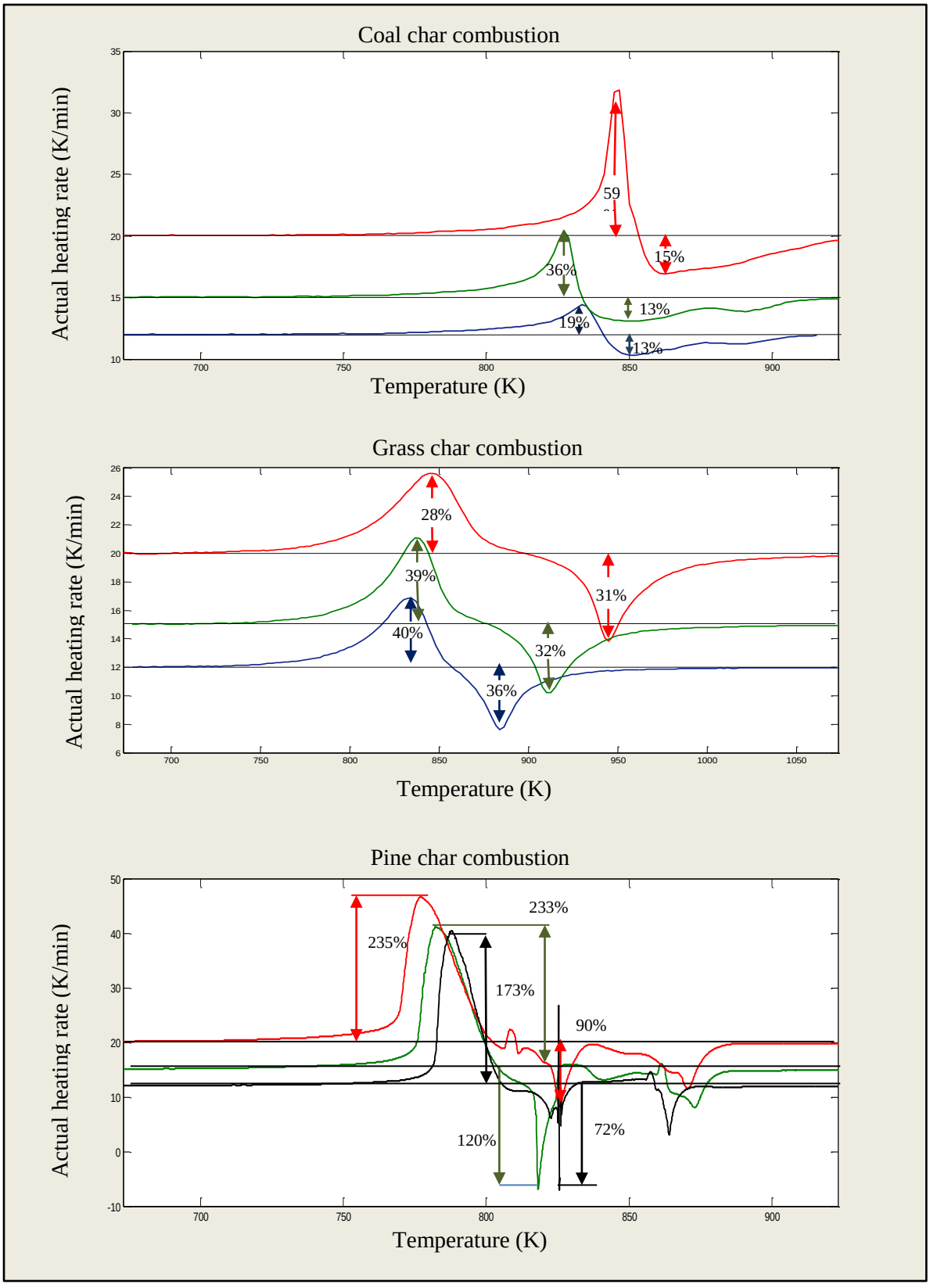

Figure 5-4: Heating rate variations with change in program heating rate

Figure 5-4 shows that for coal char, the magnitude of the heating rate deviations decrease with a decrease in the program heating rate. Grass and pine char on the other hand, displays very small changes in the heating rate deviations with decrease in the programed heating rate.
However, for all the three chars, the temperature range of the heating rate deviations increases as the program heating rate is increased. It can then be concluded that an overall increase in the heating rate disturbances is observed as the program heating rate is increased. From this conclusion, the highest program heating rate (20K/min) was replaced by a lower program heating rate of 8 K/min to reduce the heating rate variations during the reaction. Kastanaki and Vamvuka (2006) confirm such findings as they note that a lower heating rate is more likely to ensure the absence of deviations of sample temperature with respect to the selected temperature value during the conversion.

According to Vyazovkin (1997), the use of inaccurately determined heating rates affects all calculation methods in solid-state kinetic analyses. Vyazovkin (1997) further emphasizes that the actual heating rate of each run, rather than that programmed heating rate, should be used in kinetic analyses. From the results obtained in studying the heating rate variations in the preliminary study, it is clear that completely eliminating the deviations may not be practically feasible during thermo-gravimetric analysis. Therefore, the need to incorporate these variations into the DAE based model is emphasized. This was carried out successfully in this study.

The use of the same particle size, similar mass (±5%), as well as the control of the purge gas flow rates is essential for the replication of the experiments (Vyazovkin, 1997). Since this study is comparative, the particle size (-53μm), mass (±1.5mg) and gas flow rates were kept constant throughout all the analysis (Khalil et al., 2009). The work carried out by Vyazovkin (1997) demonstrated that a two-fold difference in heating rates applied resulted in a more consistent value of E, hence the use of the set of heating rates, 8, 12,15K/min.

5.5. Model Application

Notable observations were made on applying the DAE based model to data obtained prior to the preliminary analysis and the data obtained afterwards. It will also be noted that prior to the preliminary analysis, an average heating rate value was used for kinetics determination in the

DAE based model. The DAE based model could not be successfully applied to the conversions of any of the three materials studied at the initial conditions. The DAE based model was then adapted to the use of instantaneous heating rates measured during the conversion for kinetics determination. Overall, a marked improvement in the DAE model applicability was observed upon the application of the findings observed during the preliminary analysis. Hence, the minimisation of the heating rate fluctuations and the use of instantaneous heating rates in the DAE based model drastically improved the model applicability. Table 5-1 displays the statistical parameters obtained during coal char combustion.

Table 5-1: Model Application

Statistical Parameter	**Prior to Preliminary analysis**	**After Preliminary analysis**
R^2	0.94118	0.9998
RMS error value	0.1029	0.0059

5.6. Conclusion

The reduction of sample and particle size to an average mass of about 1.5mg of char at -53µm allows the combustion reaction to dominantly take place in the chemical reaction controlled regime. The Arrhenius plot method is suitable for the purpose of observing any deviations from one reaction regime to another. The same method was therefore applied to gasification thermo-analytical data to ensure the conversion is chemical reaction controlled.

It was also observed that heating rate fluctuations tend to increase in magnitude as the sample mass is increased. Hence, the reduction in sample size not only confines the reaction to the chemical reaction controlled regime, but also reduces the magnitude of the heating rate deviations from the set point during the reaction progression.

The program heating rate also appears to have an effect on the overall heating rate disturbances during the reaction progression. At higher program heating rates, it is noted that the disturbances take place over a wider temperature/time duration than they do at lower program heating rates. From these findings, the most suitable heating rates identified for the thermo-gravimetric analysis were 8, 12 and 15 K/min. It was noted, however, that the complete elimination of heating rate deviations from the set point is impossible during non-isothermal analysis. This lead to a development to the DAE based model to allow the use of instantaneous heating rates

measured at instantaneous points during the conversion to be used for kinetics evaluation. Therefore, for the execution of the thermo-gravimetric analysis, sample sizes of 1.5mg (±5%), and particle sizes of -53 µm were used.

6. CHARACTERISATION ANALYSIS

This section reports the results of all the characterisation experimental work carried out as described in Section 4.

6.1. Size distribution analysis

The samples were pulverised to -53μm minimum width. The particle size distribution analysis results are presented in Table 6.1.

Table 6-1: Size distribution

Sample	**Coal**	**Grass**	**Pine**
d(0.1)μm	2.497	3.021	5.080
d(0.5)μm	14.701	15.072	26.632
d(0.9)μm	43.003	57.441	69.112

6.2. Calorific value determination

The gross calorific values obtained with the use of the Drycal Bomb Calorimeter are displayed in Table 6-2.

Table 6-2: Gross calorific values

Sample	**Coal**	**Grass**	**Pine**
Gross calorific value(kJ/kg)	28.22	17.05	18.12
	28.07	17.14	18.64
	28.08	17.17	18.82
Average Gross calorific value (kJ/kg)	28.12	17.12	18.52

Three samples were tested to obtain the average gross calorific values as shown in Table 6.2. The results show that the vitrinite-rich coal has the highest calorific value, followed by the pine and grass biomass samples respectively.

6.3. Proximate analysis

Proximate analyses was carried out on the pure samples and the coal-biomass blend samples using the Perkin Elmer TGA.

Table 6-3: Proximate analysis results

Sample	**Coal**	**Grass**	**Pine**	**Coal-Grass 90:10 blend**	**Coal-Pine 90:10 blend**
Moisture (%)	2.95	5.67	7.45	3.67	3.62
Ash (%)	12.18	7.03	0.21	11.06	10.36
Fixed carbon (%)	49.18	14.29	14.06	44.11	45.21
Volatile matter (%)	35.7	73.01	78.29	41.16	40.81

The coal sample under study is a low ash, high volatile coal. The grass and pine samples have extremely high volatile contents in the order of about 75%, with very low fixed carbon content. The pine biomass has the lowest ash content of about 0.2%, whereas the grass char consists of an ash content of about 7%.

6.4. Ultimate analysis

Ultimate analysis was carried out for the determination of the chemical elemental components of the three fuels and their blends. The results are presented in Table 6-4.

Table 6-4: Ultimate analysis results (dry ash free basis)

Sample	**Coal**	**Grass**	**Pine**	**90:10 Coal/Grass blend**	**90:10 Coal/pine blend**
wt.% C	79.53	50.06	51.44	75.99	75.10
wt.% H	5.61	6.53	6.52	5.77	5.74
wt.% N	1.61	0.56	0.13	1.55	1.50
wt.% S	0.87	0.14	0.11	0.74	0.73
wt.% O (by difference)	12.30	42.87	41.84	15.93	16.94

It can be noted that the pine sample contains the lowest proportions of S and N. The coal sample contains the highest amount of C, N and S and the lowest H content. The grass sample on the other hand, contains intermediate values of each.

6.5. Mineralogical Assay

As detailed in Section 3, it is believed that some mineral components are capable of catalytic behavior during gasification of the fuels. On the other hand, the same mineral matter and others are also capable of fouling and scaling combustion units. There is therefore a need to identify the mineral component and their distribution in the fuels in order to identify any catalytic correlations during conversion. XRD analysis and ICP-OES analysis were carried out on the samples.

6.5.1.1. XRD analysis

Quantification of the groups identified was not feasible with this analysis due to the high amount of organic carbon contained in the samples. Figures 6-1 to 6-3 display the results obtained from the analysis.

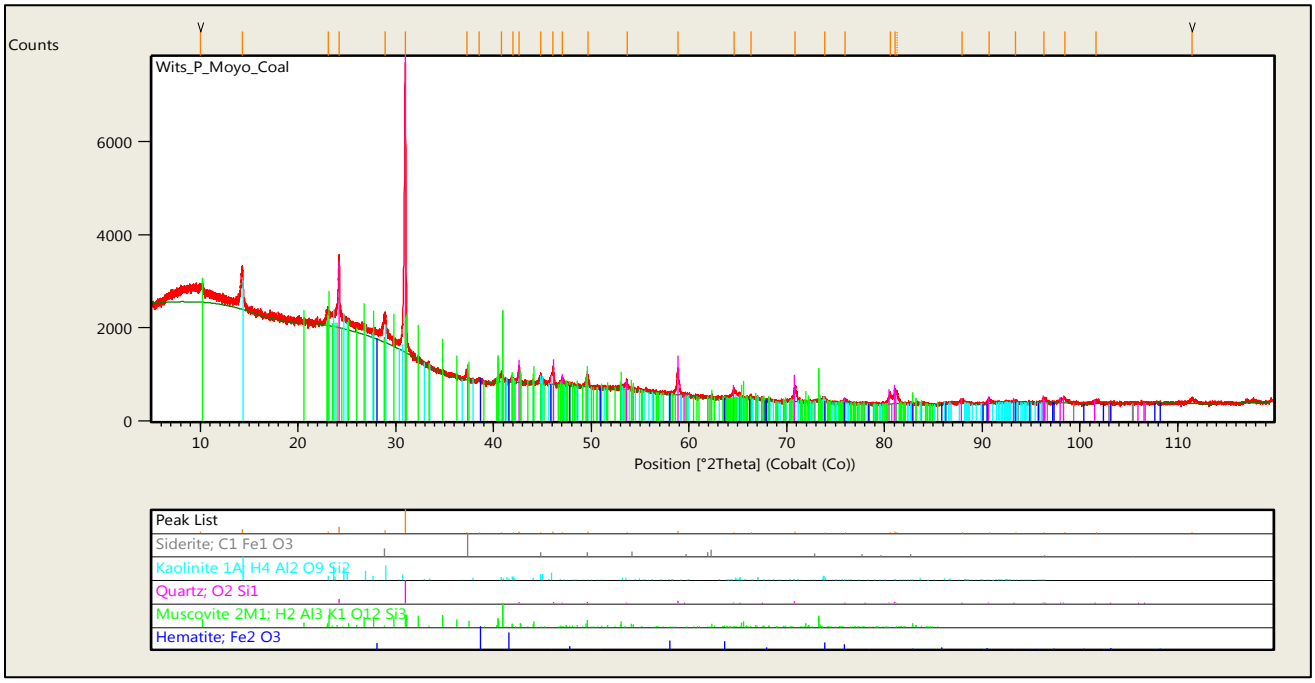

Figure 6-1: XRD coal results

For the coal sample, siderite, kaolinite, quartz, muscovite and hematite mineral groups were identified in the sample.

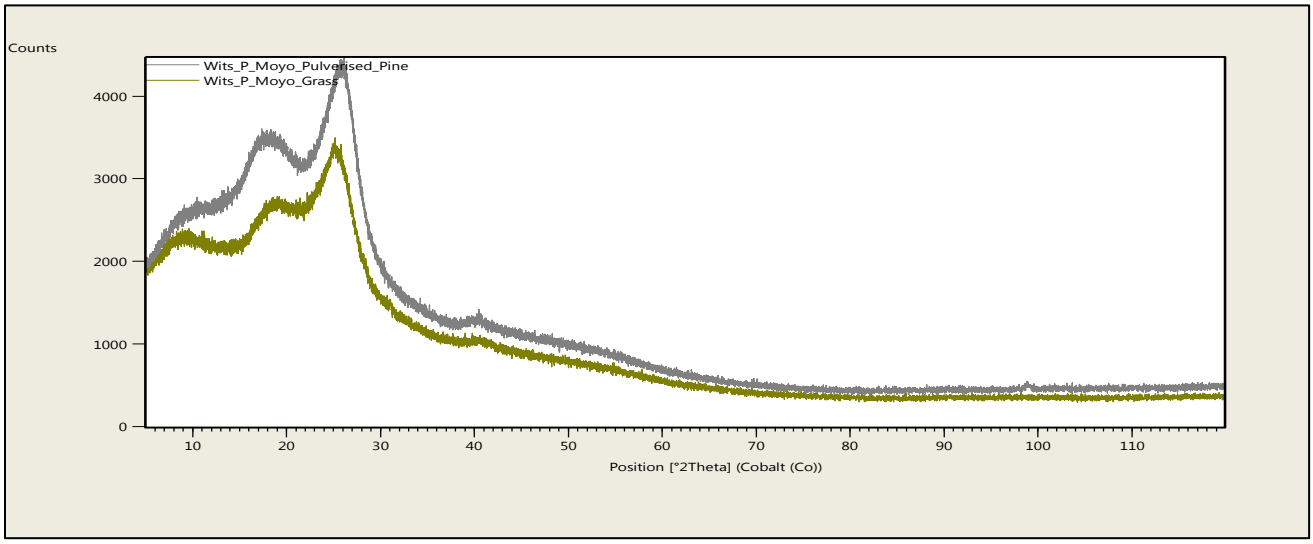

Figure 6-2 : XRD biomass results

As presented by Figure 6-2, no mineral groups were identified for both biomass samples.

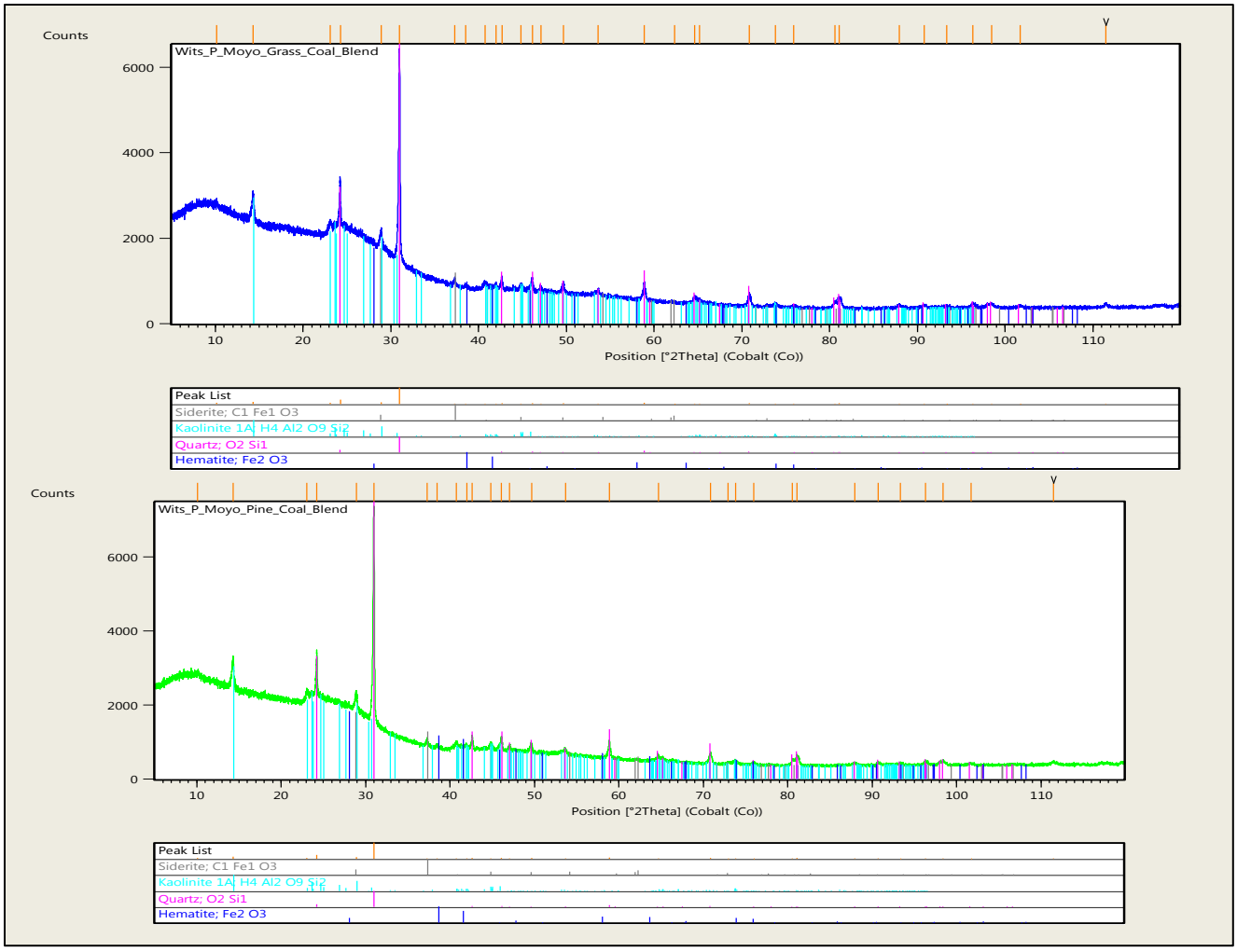

Figure 6-3: XRD 90:10 coal-biomass blends results

Figure 6-3 shows that for both coal- biomass blends, only siderite, kaolinite , quartz and hematite mineral groups were identified. The muscovite mineral group which is observed in the coal is not seen in the two blends. Hence, with this procedure, only the mineral groups could be identified instead of the elemental components of the ash. Combining this fact with the impossibility of quantification leads to the conclusion that the analysis is not suitable for the mineralogical assay of the samples under study.

6.5.1.2. ICP-OES analysis

The results for this analysis are summarized in Table 6-5.

Table 6-5: Mineralogical Assay of raw material ash

CHEMICAL ASH COMPOSITION ANALYSIS											
Compound	**wt.% Content**										
	SiO_2	**Al_2O_3**	**Fe(tot)**	**Fe_2O_3**	**TiO_2**	**CaO**	**MgO**	**K_2O**	**MnO**	**P_2O_5**	**SO_3**
Coal	68,00	20,00	2,47	3,53	2,28	1,69	0,56	1,28	0,05	0,73	0,62
Grass	73,80	0,75	0,60	0,86	0,04	5,95	2,67	9,06	0,10	3,02	2,94
Pine	8,36	2,97	5,75	8,22	0,14	40,10	15,10	3,39	4,65	1,79	8,36
Coal/Grass 90:10 blend	68,70	18,30	2,29	3,27	2,08	2,00	0,77	1,95	0,06	0,93	0,85
Coal/Pine 90:10 blend	68,10	20,00	2,48	3,55	2,28	1,68	0,60	1,20	0,06	0,71	0,69

From the results shown in Table 6-5, the coal and grass samples appear to contain relatively high amounts of SiO_2 as compared to pine. The pine ash on the other hand consists of the highest % content of the alkali CaO and MgO groups. According to Capucine Dupont et al. (2011), Zhang et al. (2008), and Zhu et al. (2008), the alkaline (Na, K) and the earth (Ca, Mg) metallic species are recognized to have catalytic effects. The Fe, Ni, and Zn contents in most coal ash have also been identified as catalytic species (Hernández et al., 2010). As noted in Section 2.9, Dupont et al. (2011) identified that the gasification reaction rate for woody biomasses correlates with the ratio of K/Si, confirming the catalytic effect of the K and reflecting an inhibiting effect of Si. The total catalytic species for each material was quantified; a ratio of the K_2O to SiO_2 was also evaluated for each material. This is presented in Table 6-6.

Table 6-6: Mineralogical assay summary

Material	Total catalytic species (Fe_2O_3,K_2O,MgO,CaO) %	Total inhibiting species(SiO_2) %	Total K_2O %	Ratio K_2O/ SiO_2
Coal	7.06	68,00	1,28	0.02
Grass	18.58	73,80	9,06	0.123
Pine	66.81	8,36	3,39	0.41
Coal-Grass 90:10 blend	7.99	68,70	1,95	0.03
Coal-Pine 90:10 blend	7.03	68,10	1,20	0.02

From the table above, it can be seen that the pine ash contains the highest content of the total catalytic species and the corresponding highest ratio of the K_2O to SiO_2. The grass sample contains the second highest total catalytic species, followed by the coal/grass blend and the coal and coal/pine blend. The K_2O/ SiO_2 ratio implies a probable reactivity order of pine, grass, coal/grass 90:10 blend, coal pine and coal respectively from the most reactive material to the least. This order was compared to the order in which the kinetics obtained present themselves.

6.6. Coal Petrography and Rank

As mentioned in Section 1, the distinguishing property of the coal used in this study is its high vitrinite maceral content. The main reason behind the selection of this coal is the high reactivity of the vitrinite maceral. This translates to relatively shorter reaction times, hence shorter high temperature exposure of the thermo-gravimetric equipment used. The coal sample was obtained from three different float fractions of the South African coal, all extracted as floats at a relative density of 1.5. The maceral content of the three float fractions and their mass contribution is presented on Table 6-7.

Table 6-7: Petrographic and rank analysis

Sample	**1**	**2**	**3**
Mass (g)	255	189	144
Vitrinite %	80.5	81.1	71.4
Liptinite %	4.8	7.5	9.7
Inertinite %	7.8	8.6	14.7
Total Mineral matter %	7.0	3	4.3
Rank	Medium Rank C		

From Table 6-7, it can be concluded that the coal sample used in this study, is a high vitrinite coal of medium rank C. The coal rank implies that the coal is a high volatile bituminous coal.

6.7. Conclusion

The coal sample under study is a low ash, high volatile and vitrinite-rich coal of medium rank C. The grass and pine samples have extremely high volatile contents in the order of about 75%, with very low fixed carbon content. The pine biomass has the lowest ash content of about 0.2%, whereas the grass char consists of an ash content of about 7%. From the ultimate analysis, it was observed that the pine sample contains the lowest proportions of S and N. As expected, the coal sample contains the highest amount of C, N and S and the lowest H content.

Using the XRD procedure for mineralogical assay did not yield successful results with the samples studied. Only the mineral groups could be identified instead of the elemental components of the ash. Quantification of the identified mineral groups was also not possible due to the large content of organic matter in the samples. The mineralogical assay obtained from the ICP-OES procedure lead to the conclusion that the pine sample is potentially the most reactive material from the three samples studied. It is anticipated that the order of reactivity from the most reactive to the least is given as: pine, grass, coal/grass 90:10 blend, coal pine and coal respectively. This order was then compared with the actual kinetic analysis carried out in the following chapter.

7. THEMO-GRAVIMETRIC ANALYSIS

Also noted by Khalil et al. (2009), the TGA furnace was purged with N_2 gas for a minimum of 20 minutes before the heating program is engaged. The repeatability of the experiments was checked by repeating one of each of the three tests required per sample per conversion. The relative difference between the conversion curves produced averaged an RMS error of 0.0016. The thermo-gravimetric curves presented in this study have been normalized according to the Equation [7-1].

$$X = \frac{x_0 - x}{x_0 - x_{ash}} \qquad [7\text{-}1]$$

Here, the conversion, X, will be used in the analysis as defined on Equation [7-1]. x_0 is the initial char mass fraction, x is the mas fraction of the char at a given time during the conversion and x_{ash} is the mass fraction of the ash contained in the char.

7.1. Combustion

The samples were spread in uniform layer in the crucibles (Kastanaki and Vamvuka, 2006), and heated at the three heating rates, (8, 12, 15K/min) from ambient temperature to 750°C. It is highlighted that the actual conversion reactions were completed at a maximum temperature of 640°C, for coal char combustion. A constant air flow rate of 70ml/min was maintained throughout the analysis. For all the analysis carried out, Arrhenius plots were analysed in order to ensure that there is no shift in the data, specifically from a high E at lower temperature to a lower E at a higher temperature. This would correspond to the shift from the chemical reaction controlled regime to the pore diffusion controlled regime.

7.1.1. Coal char

The results from the combustion of coal char are observed in Figures 7-1 to 7-3. The Arrhenius plots for the coal char combustion analysis is displayed in Figure 7-1.

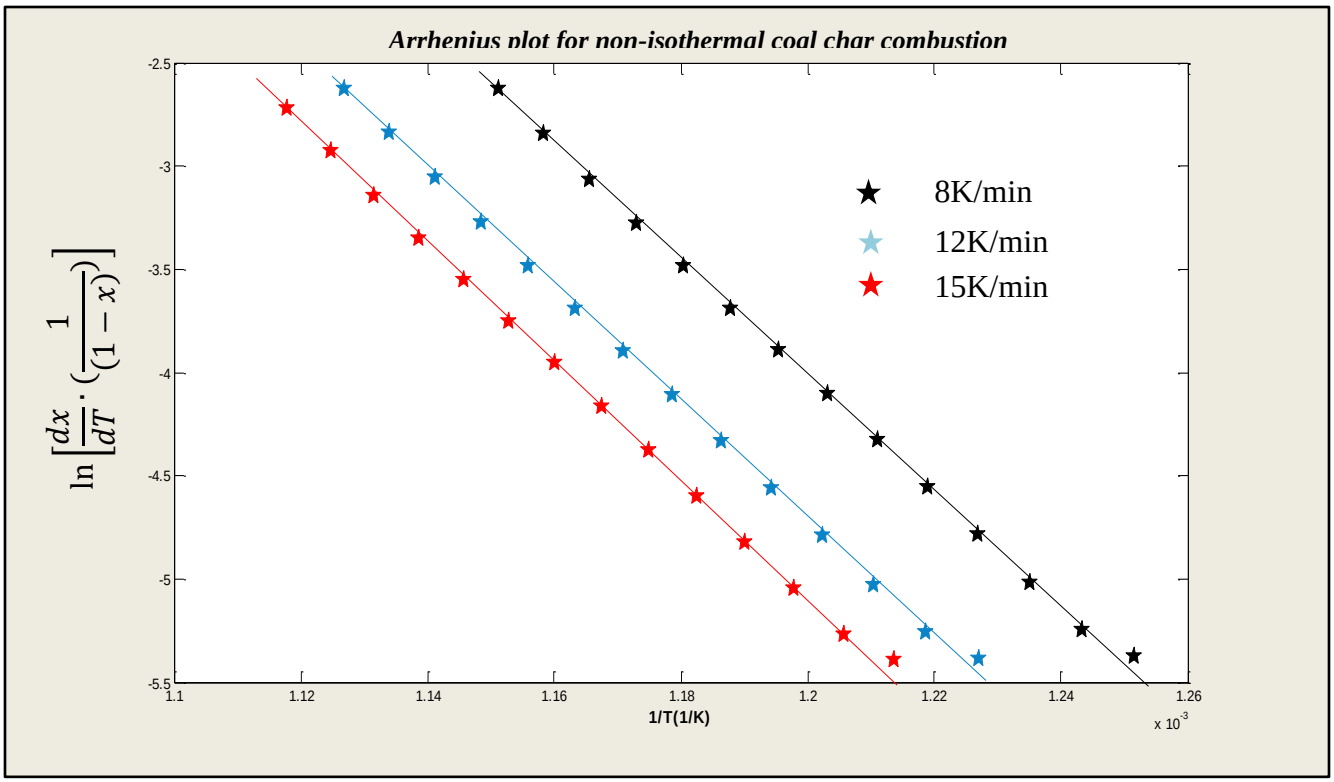

Figure 7-1: Arrhenius plot for non-isothermal coal char combustion

Clearly, no shift in the data is observed and the reaction is then considered to be within the chemical reaction controlled regime. The obtained conversion vs. temperature profiles were then applied to the DAE based model under four different conditions. The DAE model is adapted to two reaction models, the first order and the RPM. These adaptations were further developed to handle instantaneous heating rates calculated at each point along the conversion, and use this range of values for kinetics evaluation instead of just the single programmed heating rate. The single heating rate and the instantaneous heating rate DAE based model versions for each reaction model were applied on the data. Model accuracy was then evaluated to obtain the most suitable model. Table 7-1 displays results obtained.

Table 7-1: Evaluation of model accuracy

Plot	Heating rate used (K/min)			First Order		RPM	
	E calculation	A calculation	φ calculation	Program /Const β R^2 and RMS error	Actual Inst β R^2 and RMS error	Program /Const β R^2 and RMS error	Actual Inst β R^2 and RMS error
i	8 & 12	8	12	0.9824 0.0560	0.9847 0.0510	0.9986 0.0160	0.9991 0.0128
ii	8 & 15	8	15	0.9834 0.0545	0.9864 0.0491	0.9990 0.0130	0.9994 0.0105
iii	12 & 15	12	15	0.9850 0.0518	0.9889 0.0458	0.9998 0.0057	0.9998 0.0061
iv	12 & 8	12	8	0.9824 0.0560	0.9846 0.0511	0.9985 0.0161	0.9990 0.0132
v	15 & 8	15	8	0.9833 0.0545	0.9864 0.0492	0.9991 0.0130	0.9994 0.0101
vi	15 & 12	15	12	0.9850 0.0518	0.9890 0.0457	0.9998 0.0053	0.9998 0.0059
Average model accuracy				**0.9836 0.0541**	**0.9867 0.0487**	**0.9988 0.0115**	**0.9994 0.0098**

As shown in Table 7-1, the accuracy of the model is overall improved by the use of the actual instantaneous heating rates measured throughout the reaction progression which is in agreement with Vyazovkin (1997). The most suitable model for the combustion of the coal char is the RPM adapted DAE based model. This model proved to be the most suitable model for the combustion and gasification of all the chars studied in this work. The plots obtained with the application of this model are presented on Figure 7-2.

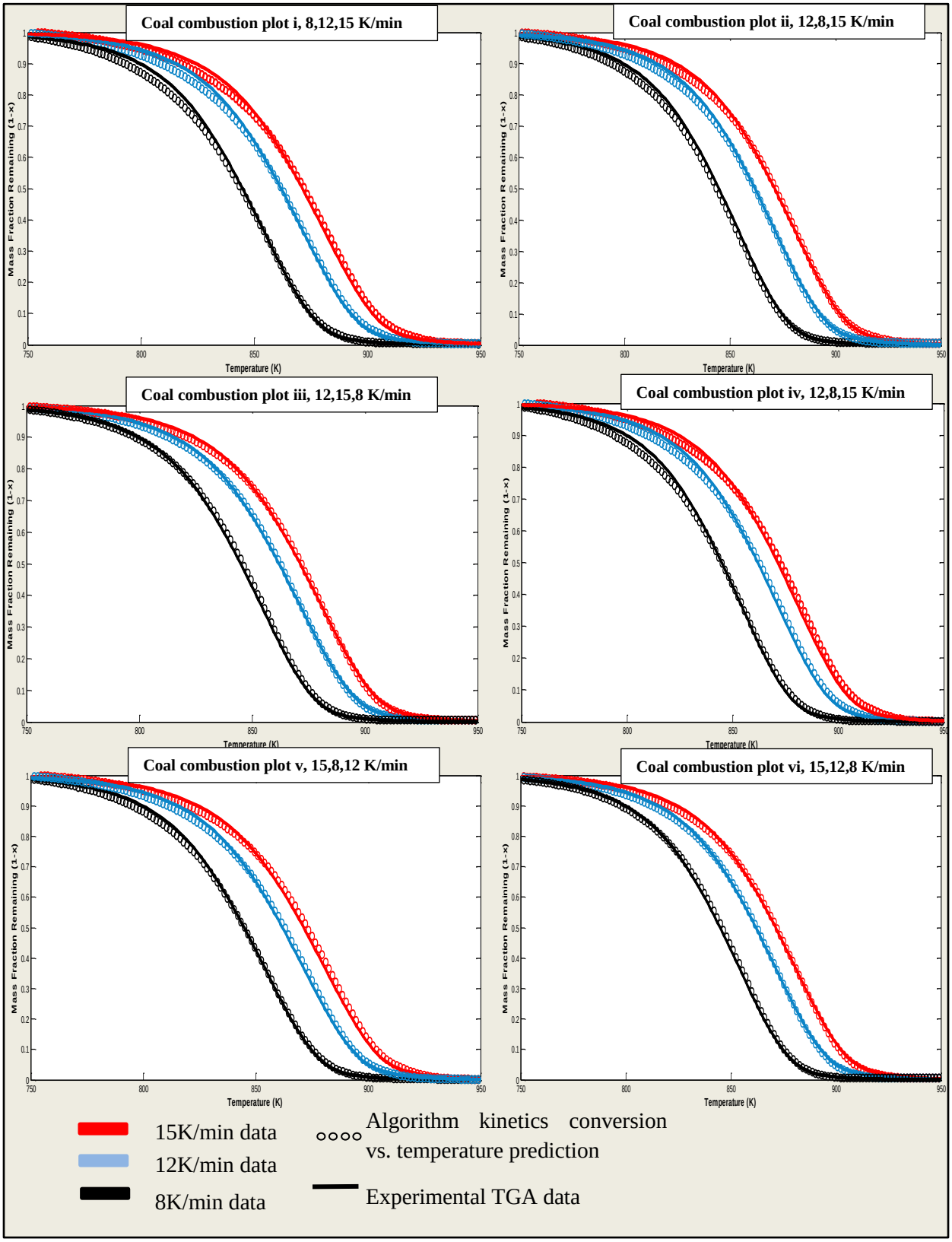
Coal combustion plot i, 8,12,15 K/min
Coal combustion plot ii, 12,8,15 K/min
Coal combustion plot iii, 12,15,8 K/min
Coal combustion plot iv, 12,8,15 K/min
Coal combustion plot v, 15,8,12 K/min
Coal combustion plot vi, 15,12,8 K/min
Mass Fraction Remaining (1-x)
Temperature (K)
15K/min data
12K/min data
8K/min data
Algorithm kinetics conversion vs. temperature prediction
Experimental TGA data

Figure 7-2: Application of the instantaneous heating rate and RPM adapted DAE based model. The figure presents plots of conversion (1-X) vs. temperature.

It is clear that visual inspection would definitely not be adequate for the identification of the most suitable plot. Using the statistical parameters described in Section 4.2 and presented on Table 7-1, the most suitable plot is plot vi. The plot is obtained from the use of data obtained at heating rates 15 and 12 K/min to determine the reaction kinetics. The obtained kinetics provide the most accurate fit for all three data sets. The raw kinetics obtained from the DAE based model for each plot are also presented in Table 7-2.

Table 7-2: DAE based model kinetics

Plot	**Heating rate used(K/min)**			**Kinetics**				**Error evaluation**	
	E calculation	**A calculation**	**φ calculation**	**E (Kj/mol)**	**A ($s^{-1}m^{-1}$)**	**f_o**	**φ**	**R^2**	**RMS**
i	8 ,12	8	12	123.99 404.88	50966 5.5E+19	1.013 0.005	12.04	0.9991	0.0128
ii	8,15	8	15	124.25 800	46350 2.7E+41	1.007 0.007	18.03	0.9994	0.0105
iii	12,15	12	15	305.57 135.81 136.92 137.39	1E-7 4.2E+5 2.7E+5 2.8E+5	0.006 0.034 0.111 0.856	18.53	0.9998	0.0061
iv	12,8	12	8	123.99 305.57	50966 1 E+14	1.017 0.003	11.51	0.9996	0.0132
v	15,8	15	8	124.25 305.57	46350 2.9E+14	1.010 0.006	16.58	0.9994	0.0101
vi	15,12	15	12	305.57 135.81 136.92 137.39	1 E-7 4.2E+5 2.7E+5 2.8 E+5	0.006 0.028 0.122 0.851	18.53	0.9998	0.0059

Figure 7-3 shows the best conversion vs. temperature fit for the modeling of coal char combustion. The derivative temperature plot is also presented on the same figure. This figure is the ultimate result that is demonstrated for all the other analysis. The rest of the results are presented in Appendix C.

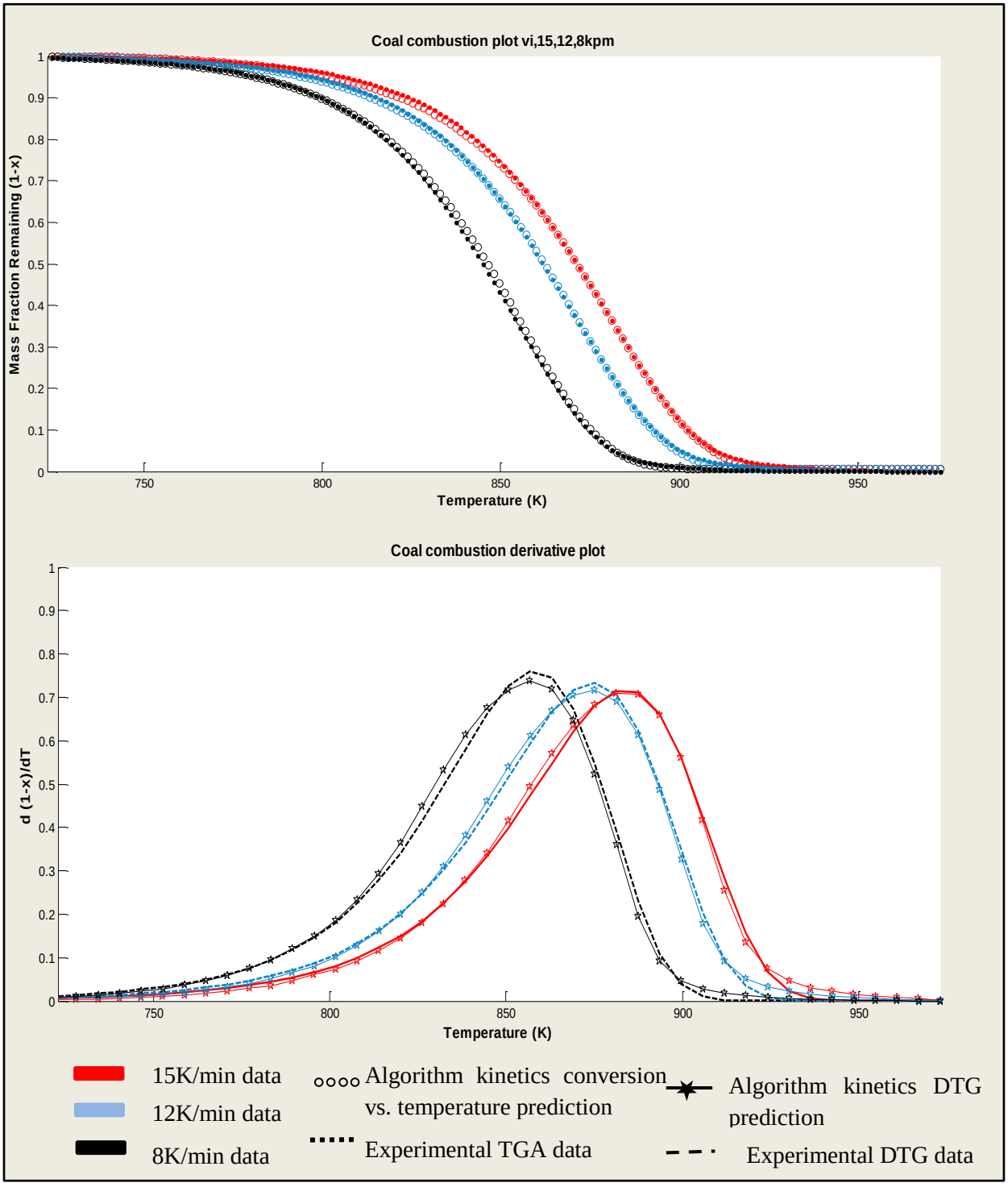

Figure 7-3: Modelling of coal char combustion with the most suitable set of heating rates.

The reaction kinetics obtained from the model are also presented in Table 7-3.

Table 7-3: The actual algorithm determined kinetics

Reaction	**Kinetics**			
	E (Kj/mol)	**A ($s^{-1}m^{-1}$)**	f_o	φ
1	305.57	1e-007	0.006	18.53
2	135.81	4.1982e+005	0.028	
3	136.92	2.6813e+005	0.122	
4	137.39	2.8202e+005	0.851	

The f_0 value denotes the mass fraction of the total reactive mass dissociating according to the particular reaction (1, 4). The higher the f_o value, the greater the reactive mass fraction dissociating according to the particular reaction. The reaction representing majority of the reactive mass (reaction 4); will then be referred to as the major reaction taking place during the conversion. The smaller the f_o value, the smaller the reactive mass fraction dissociating according to the particular reaction. For very small reactive mass fractions, the higher the probability of the reaction being spurious. This is because the DAE based model allocates f_0 values of zero to spurious reactions.

As observed in Table 7-3, reaction 1 does not correspond with any of the reactions observed during the conversion. It also has a negligible mass fraction component of the reactive mass, it will therefore not be considered for kinetic analysis. Reaction 2 represents a very small fraction of the reacting mass as well and will also not be considered for kinetic analysis. As noted by Vittee (2012), even though the reactions may be considered for the simulation of the conversion, they will not be discussed in length when analyzing the kinetic values. The parameters of the remaining two reactions presented are very close to one another and are most likely representing a single reaction. These were therefore lumped together and considered as a single reaction for kinetic analysis as presented on Table 7-4. This analysis will be carried out for all the experimental work presented on this chapter and only the grouped/lumped kinetics will be presented. The actual algorithm determined kinetics are presented in Appendix C.

Table 7-4: The grouped kinetics for coal char combustion

Reaction	Kinetics				Error evaluation	
	E (Kj/mol)	A ($s^{-1}m^{-1}$)	f_o	φ	R^2	RMS
1	137.39	2.82E+05	1.00	18.5	0.9998	0.0059

The heating rate variations occurring during the reaction progression are presented in Appendix C.

7.1.2. Grass char

The combustion of grass char was successfully modeled to R^2 value of 0.99989 and a corresponding RMS error value of 0.0045. The conversion vs. temperature as well as the time derivative of the mass fraction (DTG) curves are presented on Figure 7-4.

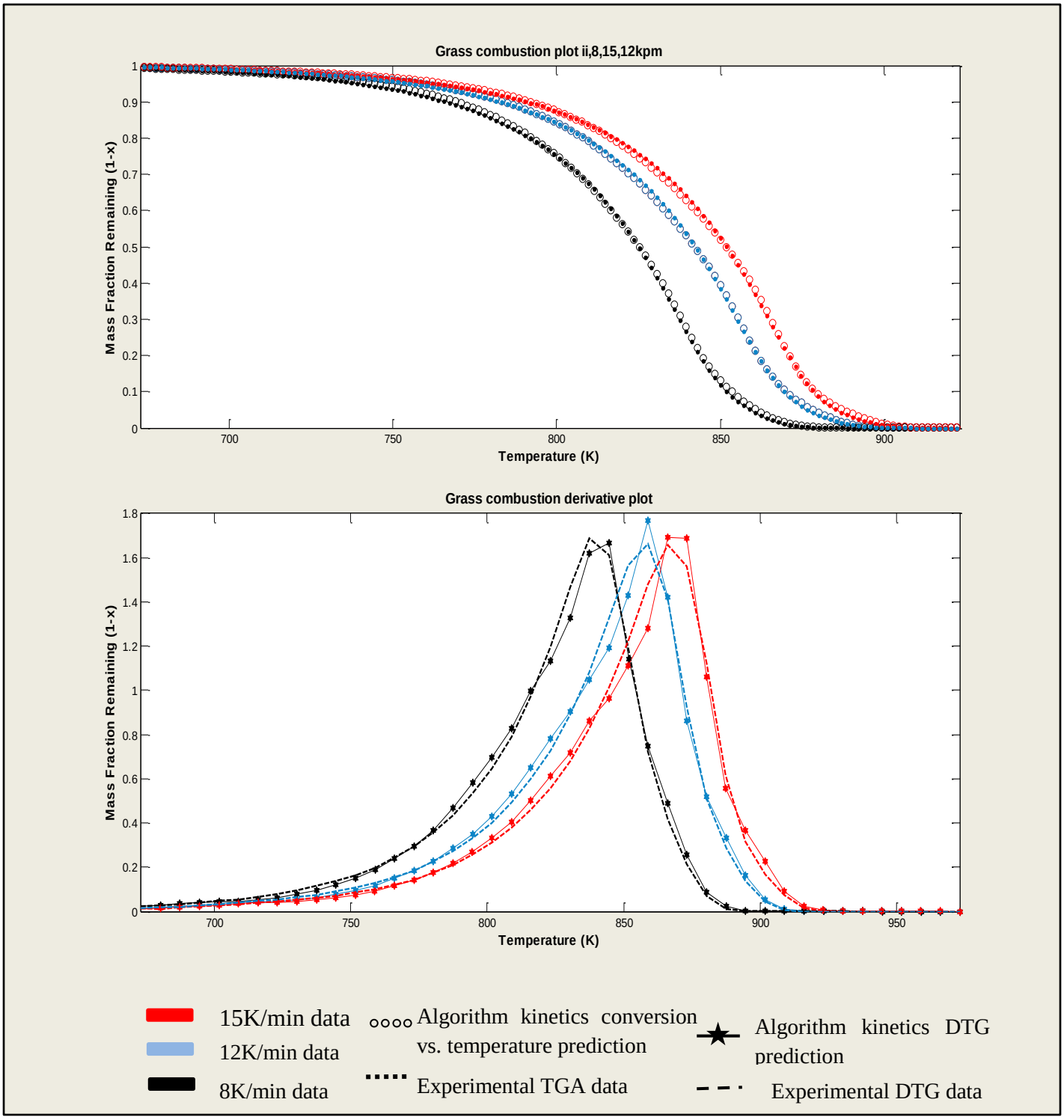

Figure 7-4: Modelling of grass char combustion.

Except for minor over prediction of the reaction rate at its maximum point, the DAE based model excellently simulates the reaction progression. The intrinsic kinetics obtained are displayed in Table 7-5.

Table 7-5: Grass char combustion reaction kinetics

Reaction	Kinetics				Error evaluation	
	E (Kj/mol)	A ($s^{-1}m^{-1}$)	f_o	φ	R^2	RMS
1	127.8	1.60 E+5	0.19	10.5	0.9999	0.0045
2	130.5	2.17 E+5	0.80			

The structural parameter identified for the grass char combustion is 10.5. As implied by the Arrhenius plot, two reactions are required for the modeling of the conversion. According to Wornat et al. (1996), variations in composition, particularly of the catalytic inorganic elements, tend to lead to particle to particle variations in intrinsic reactivities in biomass chars. This may be attributed to the two different sets of reaction kinetics describing the combustion behavior of the grass char.

7.1.3. Pine char

The most accurate model fit for pine char combustion present an R^2 value of 0.9997 with a corresponding RMS error value of 0.0068. The fits are presented in Figure 7-5.

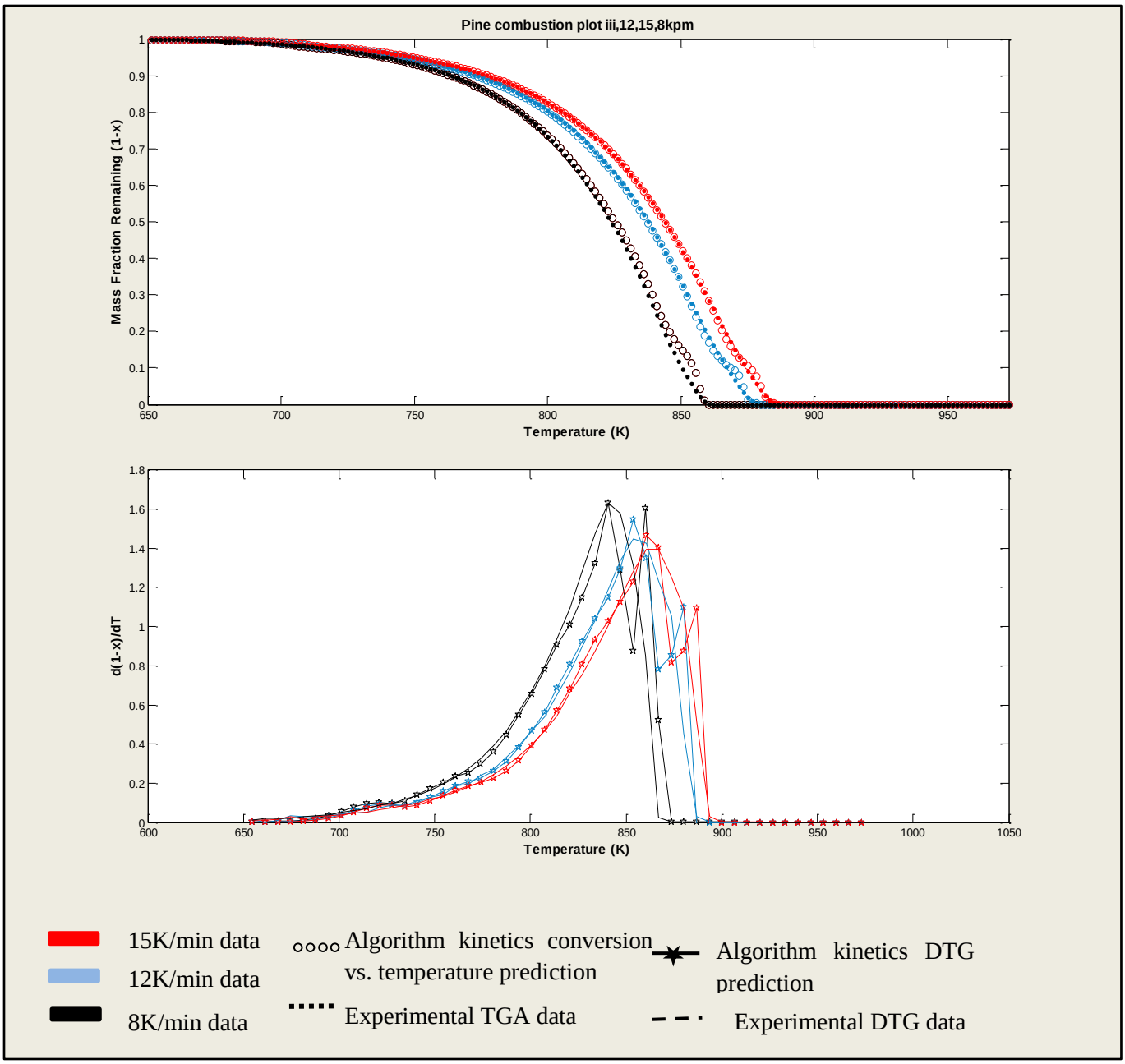

Figure 7-5: Modelling of pine char combustion

The instability in the pine char combustion reaction in terms of heating rate is demonstrated in Figure 7-5. Even though the use of instantaneous heating rates still provides a better fit, the decrease and increase in the heating rates within the last 20% of the reacting mass provides a significant deviation of the algorithm plot from the experimental TGA plots. The more sensitive DTG curves show more significant disturbances on the algorithm plots during this period. A number of sharp peaks denoting the effect of sudden drops and increases of the heating rate on

the model evaluated reaction rate. Table 7-6 displays the reaction kinetics obtained for pine char combustion.

Table 7-6: Pine char reaction kinetics

Reaction	Kinetics				Error evaluation	
	E (Kj/mol)	A ($s^{-1}m^{-1}$)	f_o	φ	R^2	RMS
1	255.48	2.80E+15	0.05	8.29	0.9997	0.0068
2	222.28	2.23E+12	0.04			
3	193.68	7.88E+09	0.16			
4	183.30	5.34E+08	0.73			

A total of 4 reactions are identified for pine char combustion. Even though the multiple reactions may be explained by the composition of biomass chars, it may also be attributed to the relatively large heating rate variations occurring during the reaction.

7.1.4. Coal-Grass 90:10 char blend

The coal and grass samples were blended according to the energy input ratio of 90:10 for the coal and biomass respectively. The samples were charred and the resultant char combusted to yield the following results demonstrated by Figure 7-6 upon model application.

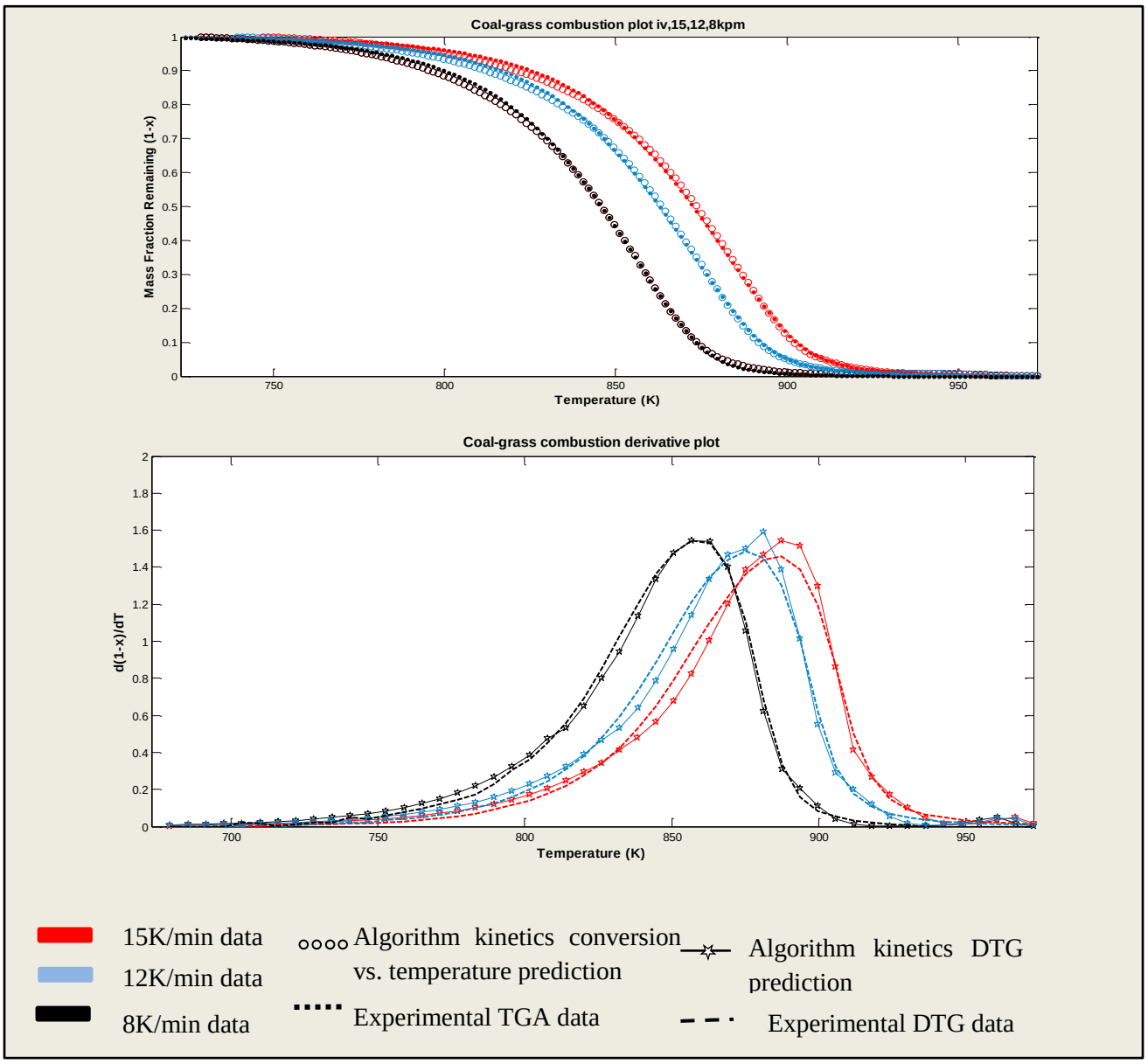

Figure 7-6: Modelling of coal-grass 90:10 char combustion

The conversion vs. temperature fits are almost perfect with only a very slight over prediction of the reaction rate within the 90% to 70% conversion interval. An over prediction of the maximum reaction rate is observed for the 12 K/min and 15 K/min run on the DTG curves. However, this does not disqualify the prediction as a RMS value of 0.0079 with a corresponding R^2 value of 0.9997 confirms the fits to be of high accuracy.

Table 7-7: Coal-grass 90:10 char combustion reaction kinetics

Reaction	Kinetics				Error evaluation	
	E (kJ/mol)	A ($s^{-1}m^{-1}$)	f_o	φ	R^2	RMS
1	125.68	5.38E+4	1.00	18.98	0.9997	0.0079

Despite the presence of two different chars reacting according to different reaction kinetics, only one dominant reaction is identified for the combustion of the blend. This may be considered to imply synergetic behavior between the two material chars during combustion. The structural parameter observed (18,98), is almost identical to that observed during coal char combustion (18,5). It must also be noted that due to the high volatile content of the grass sample, its actual mass contribution to the char blend is further reduced to 6% as presented in Table 7-8.

Table 7-8: Mass contribution of biomass in the blended chars

Biomass	%Biomass by energy input	Coal char fraction by mass	Biomass char fraction by mass
Grass	10%	0.94	0.06
Pine	10%	0.96	0.04
Grass	50%	0.65	0.35
Pine	50%	0.74	0.26

The char mass fractions in the blends were evaluated using the average char yield values obtained during the char formation stage of the experimentation. These are reported on Table 7-9.

Table 7-9: Average char yield during char formation.

Material	Ave char yield %
Coal	63.46
Grass	20.84
Pine	14.53

The char fraction by mass is then evaluated using the following Equation [7-2].

$$\frac{Coal\ char\ fraction\ by\ mass}{Biomass\ char\ fraction\ by\ mass} = \frac{Ave\ coal\ char\ yield\ \%}{Ave\ biomass\ char\ yield\%} * \frac{z * CV_{biomass}}{(1-z) * CV_{coal}} \quad [7\text{-}2]$$

Where z is the coal energy input fraction in the blend, $CV_{biomass}$ is the calorific value of the biomass and CV_{coal} is the calorific value of the coal.

7.1.5. Coal-Grass 50-50 char blend

A blend of 50% biomass and 50% coal by energy input was also used for the combustion conversion. This was mainly to observe the effect of blending the coal with biomass. With the initial char blend containing only 6% biomass, there is a possibility that there will not be any significant change in the kinetics. The 50:50 blend was modeled to a high accuracy of 0.0024 RMS error value and a corresponding R^2 value of 0.99996. Figure 7-7 displays the experimental graphs and corresponding algorithm plots.

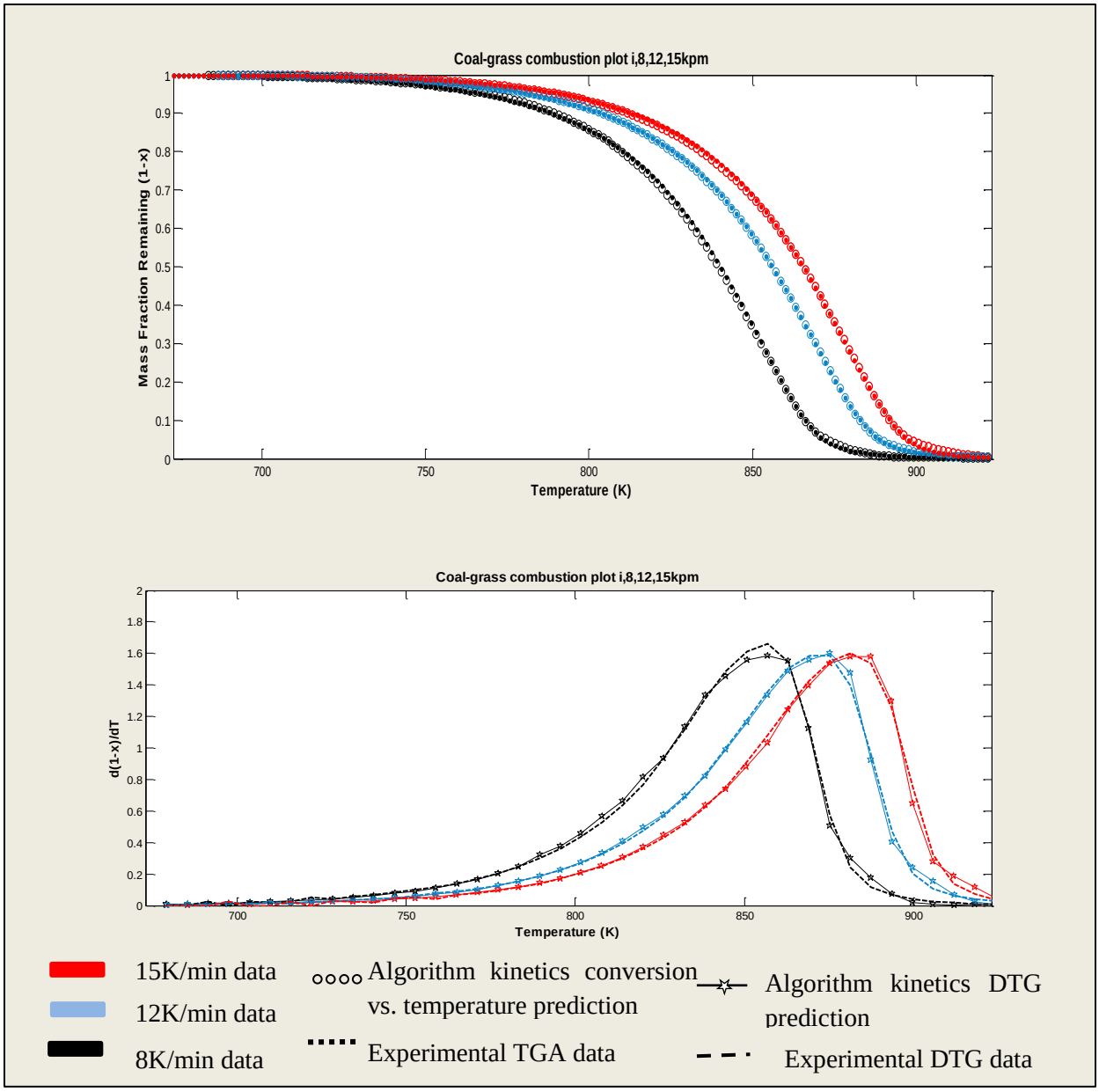

Figure 7-7: Modelling of Coal grass 50:50 char blend combustion

As observed in Figure 7-7, the algorithm conversion vs. temperature plots sit directly on top of the experimental conversion vs. temperature curves. An excellent prediction is also observed on the DTG experimental curves by the DAE based model. Table 7-10 displays the kinetics obtained during the reaction. A single reaction is also sufficient for the modeling of the blend. The structural parameter calculated (15.94) lies in between that of the grass (10.5) and the coal (18.5) chars. This may imply structural changes in the char blend.

Table 7-10: Reaction kinetics for coal-grass 50-50 char blend combustion

Reaction	Kinetics				Error evaluation	
	E (Kj/mol)	A ($s^{-1}m^{-1}$)	f_o	φ	R^2	RMS
1	135.94	3.09E+05	1.00	15.94	0.99996	0.0024

7.1.6. Coal-Pine 90:10 blend

The coal and pine 90:10 blend modeled to an accuracy of 0.0081 RMS error, and a corresponding R^2 value of 0.9996. Figure 7-8 displays the graphical results obtained.

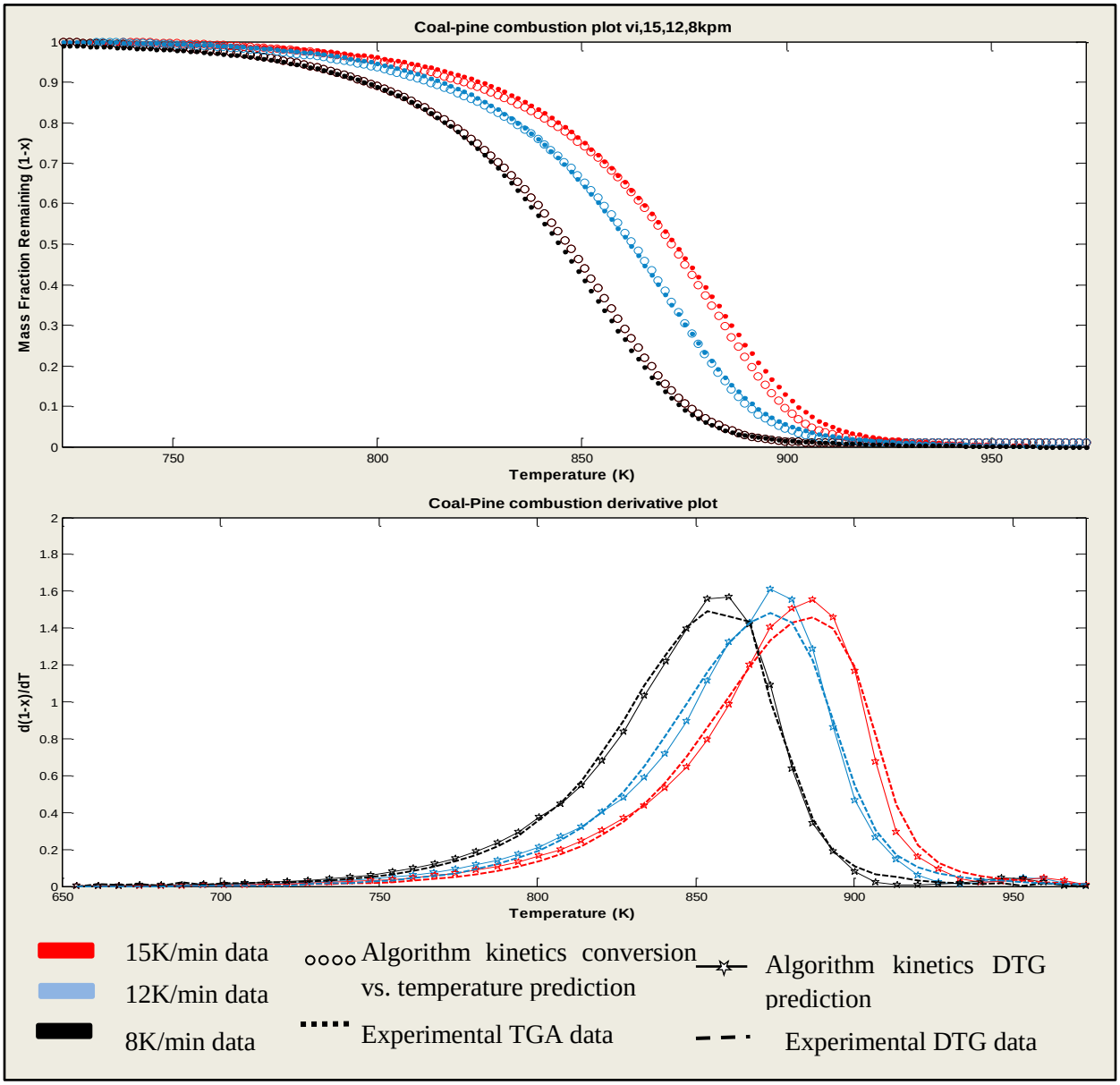

Figure 7-8: Modelling of coal-pine 90:10 char blend combustion

An almost perfect fit is observed for the 12 K/min run, a slight under prediction of the reaction rate is observed throughout most of the reaction at the 8K/min and 15K/min program heating rates. The maximum reaction rates are however over predicted by the DAE model.

Two reactions were identified at a structural parameter of 18.98, which is quite comparable to that of the pure coal char (18.53). Table 7-11 outlines the kinetics determined.

Table 7-11: Coal-pine 90:10 char blend reaction kinetics

Reaction	Kinetics				Error evaluation	
	E (Kj/mol)	A ($s^{-1}m^{-1}$)	f_o	φ	R^2	RMS
1	125.58	6.2e+4	0.42	18.98	0.9996	0.0081
2	135.04	1.93e+5	0.57			

7.1.7. Coal-Pine 50-50 char blend

For the 50:50 pine and coal blend, the graphical results obtained are displayed on Figure 7-9.

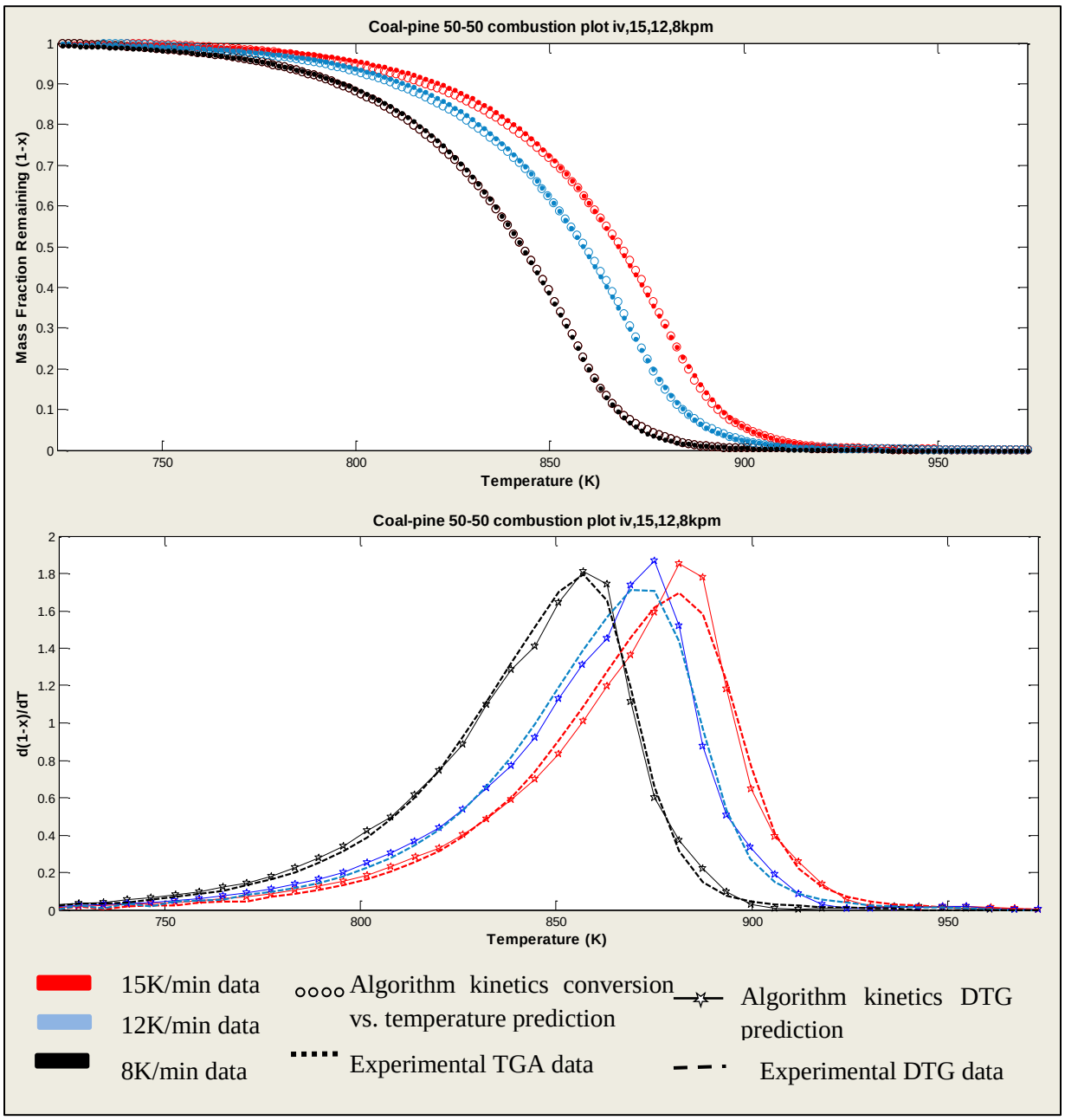

Figure 7-9: Modelling of Coal-pine 50:50 char blend combustion

The fits displayed above present only slight over projections in the maximum reaction rates for heating rates 12 and 15 K/min. For the same heating rates, a slight under prediction of the reaction rate is observed within the 90% to 70% conversion range. The conversion was modeled to an average accuracy of 0.0056. One reaction was identified for the conversion; again implying

the possibility of synergetic effects between the coal char and biomass chars; the structural parameter obtained was 17.88. Table 7-12 outlines the reaction kinetics obtained. Only one reaction was suitable for the modeling of the combustion of the blend despite the multiple reactions obtained during pine char combustion. It is also noted that the blend under discussion consists of approximately 25% by mass of pine char.

Table 7-12: Coal-pine 50:50 char blend reaction kinetics

Reaction	**Kinetics**				**Error evaluation**	
	E (Kj/mol)	**A ($s^{-1}m^{-1}$)**	f_o	φ	**R^2**	**RMS**
1	138.33	3.94e+005	1.00	17.88	0.9998	0.0056

7.2. Gasification

The gasification thermo-gravimetric analysis was carried out at the same heating rates of 8, 12 and 15K/min. The samples were heated from ambient temperature to 1200°C. The actual conversion however, was completed at a maximum temperature of 1125°C, for coal char gasification. Arrhenius plots were carried out for each char blend, from which no continuous deviations in the gradient were observed. These plots are located in the Appendix C. Similar to the combustion thermo-gravimetric analysis, sample masses of 1.5mg were uniformly distributed to cover the base of the crucible. A constant CO_2 flow rate of 65ml/min was used in conjunction with a simultaneous N_2 flow rate of 5ml/min. All the blends were successfully modelled by the RPM adapted DAE based model. The structural parameter range for each material were confined to within a ±5% range from those determined during the combustion experimental analysis. This is because the char was prepared in the same way as for the combustion tests, its structural parameters are therefore expected to be the same.

7.2.1. Coal char

The gasification of coal char was modeled to an accuracy of 0.0040 RMS value with a corresponding R^2 value of 0.9999. The experimental and model predicted plots are presented by Figure 7-10.

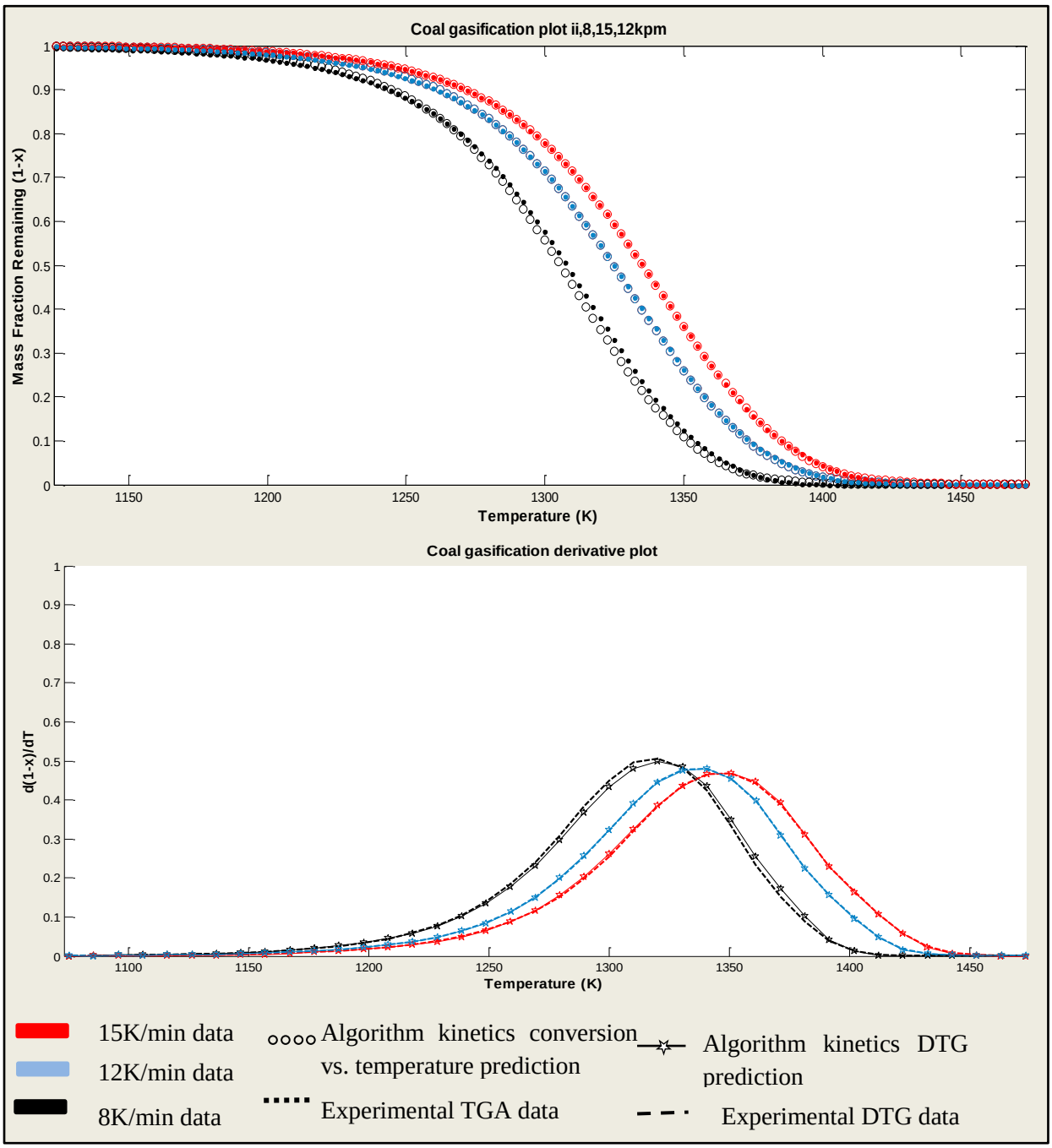

Figure 7-10: Modelling of coal char gasification.

Figure 7-10 demonstrates an almost perfect prediction of the experimental curves by the DAE based model kinetics. Three reactions were identified during this conversion and these are presented in Table 7-13. The same structural parameter as that identified during char combustion was suitable for the description of the conversion.

Table 7-13: Coal char gasification reaction kinetics

Reaction	Kinetics				Error evaluation	
	E (Kj/mol)	A ($s^{-1}m^{-1}$)	f_o	φ	R^2	RMS
1	304.3	1.82e+9	0.28	18.5	0.99985	0.0040
2	300.61	1.14e+9	0.15			
3	272.91	5.05e+7	0.56			

7.2.2. Grass char

Grass char gasification was modeled to excellent accuracy of an RMS of 0.0032 and a corresponding R^2 value of 0.9999. The conversion vs. temperature and DTG plots are presented in Figure 7-11.

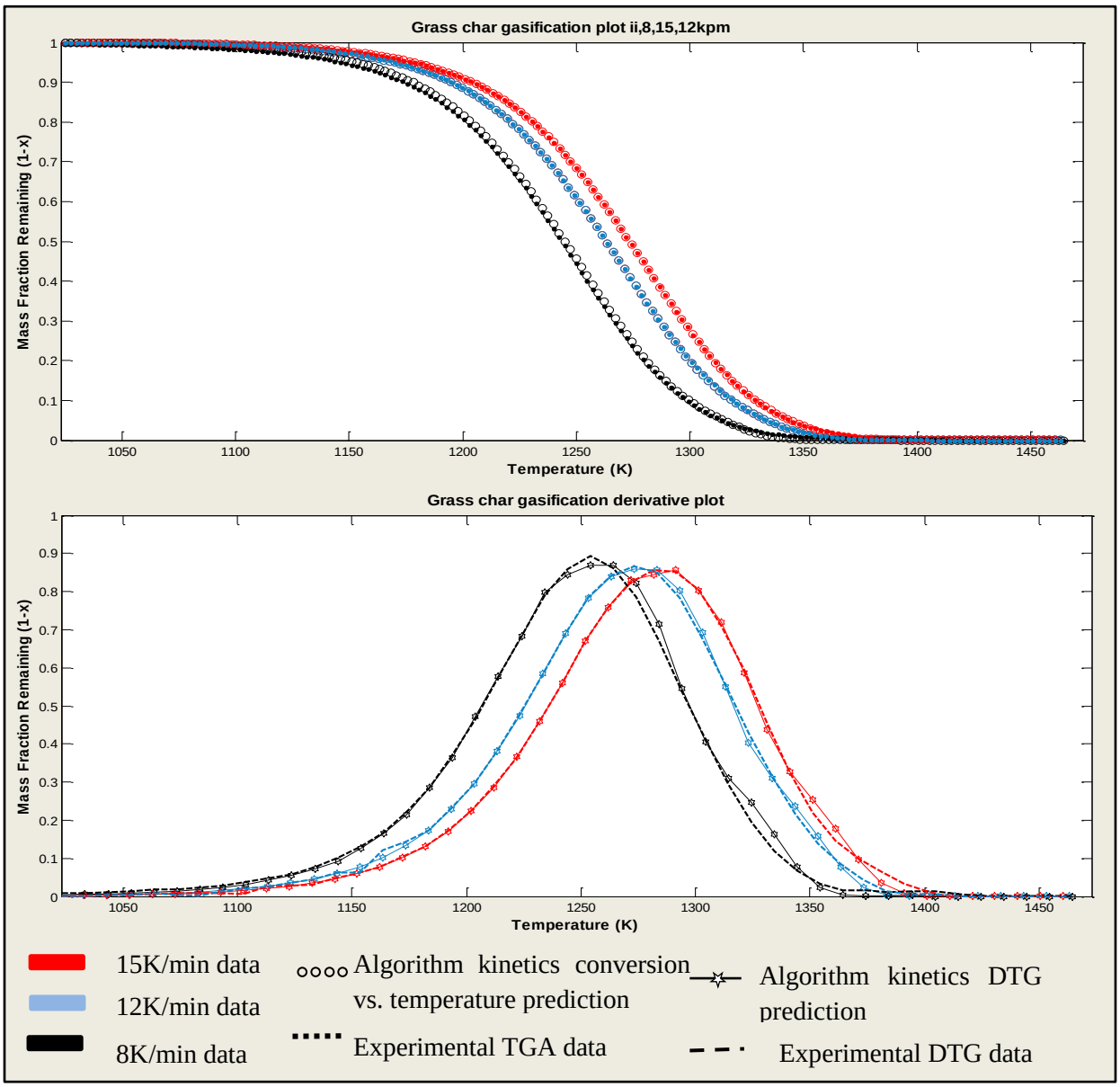

Figure 7-11: Modelling of grass char gasification.

The Figure above presents excellent fits demonstrated by the DAE based model. Four reactions were identified for the modeling of the conversion and are presented in Table 7-14. The structural parameter identified was 10.03 which compares very well with that obtained during combustion (10.5).

Table 7-14: Grass char gasification kinetics.

Reaction	Kinetics				Error evaluation	
	E (Kj/mol)	A ($s^{-1}m^{-1}$)	f_o	φ	R^2	RMS
1	260.19	1.90e+8	0.23	10.03	0.9999	0.0032
2	272.38	2.89e+8	0.27			
3	275.83	3.73e+8	0.27			
4	300.03	1.49e+9	0.22			

7.2.3. Pine char

Pine char was modeled to an accuracy of 0.0030 RMS value and a corresponding R^2 value of 0.9999.

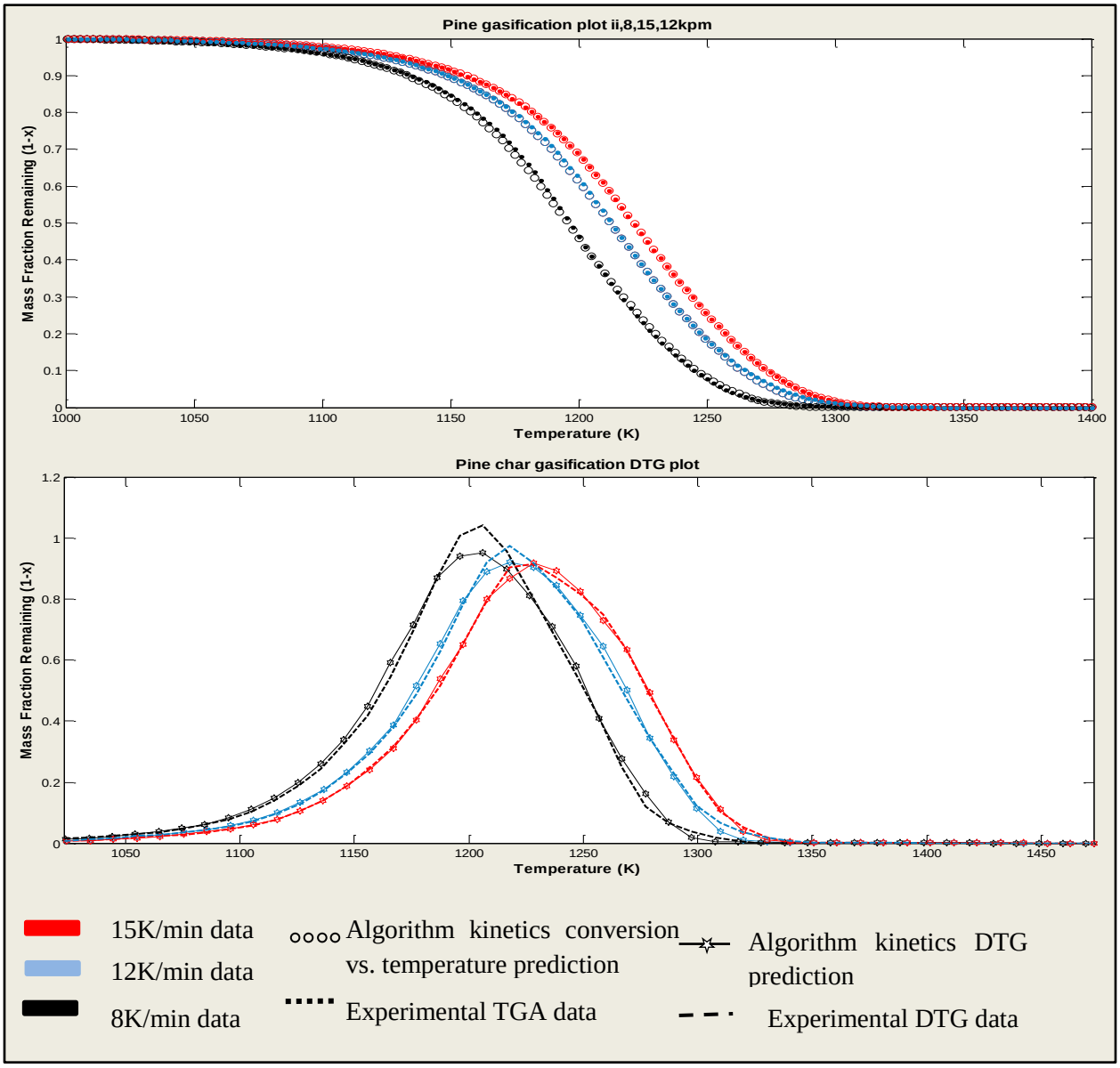

Figure 7-12: Modelling of pine char gasification.

Figure 7-12 above demonstrates the conversion vs. temperature and DTG plots for the three heating rates predicted. A slight under prediction of the reaction rate is observed around the maximum point for the 8K/min test. The same structural parameter determined during pine char combustion was found suitable for the modeling of the gasification of the material. Four reactions were identified for the modeling of the pine char as presented in Table 7-15.

Table 7-15: Pine char gasification reaction kinetics.

Reaction	Kinetics				Error evaluation	
	E (Kj/mol)	A ($s^{-1}m^{-1}$)	f_o	φ	R^2	RMS
1	280.04	3.96e+9	0.35	8.29	0.9999	0.0030
2	272.96	8.97e+8	0.22			
3	274.81	9.97e+8	0.20			
4	293.45	3.21e+9	0.22			

7.2.4. Coal-Grass 90:10 char blend

For the 10% grass by heat input blend, the model accuracy was evaluated at 0.0081 and 0.9996, RMS error value and R^2 statistic respectively.

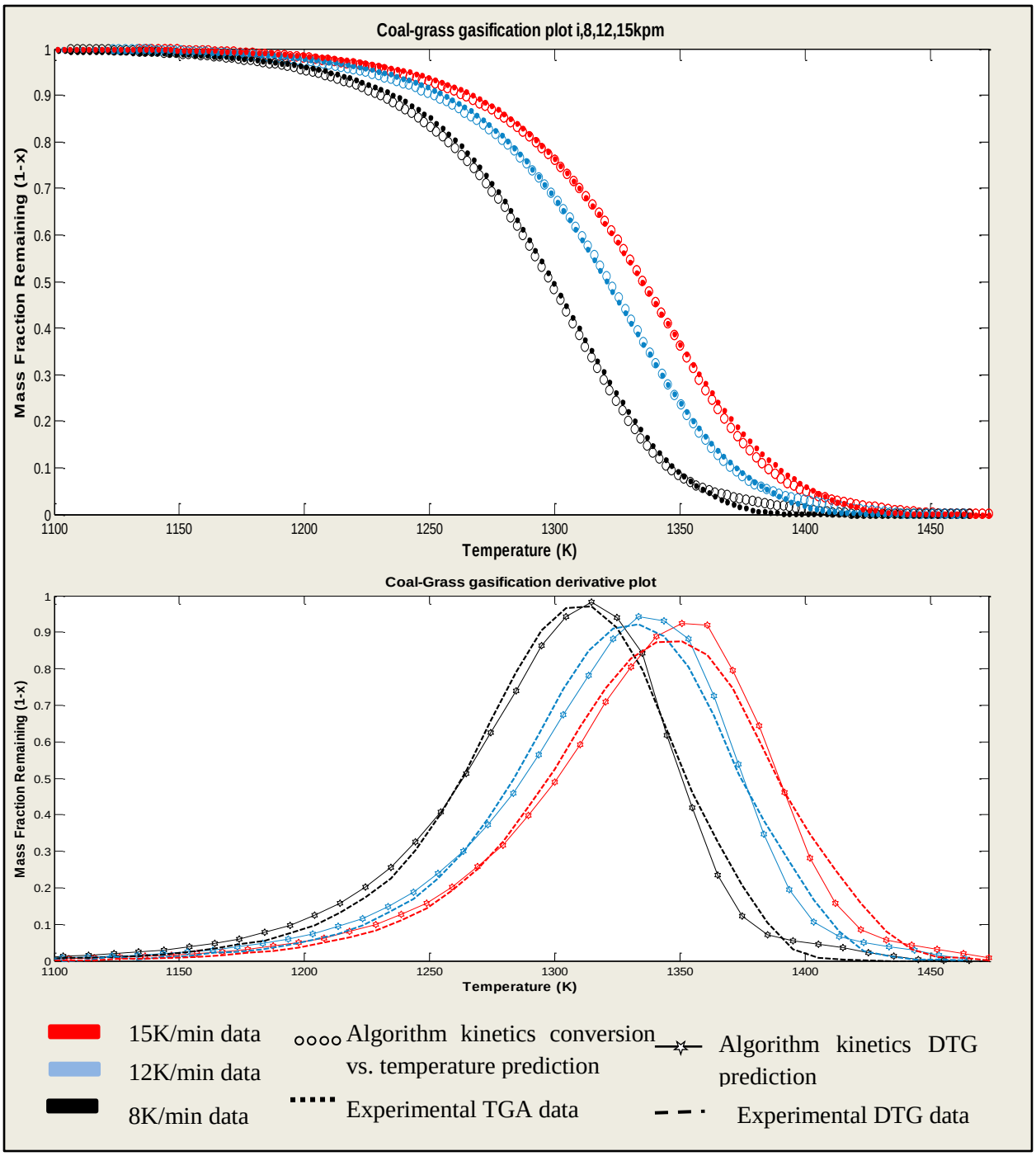

Figure 7-13: Modelling of coal-grass 90:10 char blend gasification

As observed in Figure 7-13, the DAE based model fairly accurately describes the reaction progression of the blend during gasification. A slight under prediction of the reaction rate is observed towards the completion of the reaction during all the tests. The same structural parameter as determined during combustion was also found suitable for the modeling of the

blend during gasification. Two reactions were determined for the modeling of the blend as presented by Table 7-16.

Table 7-16: Coal-grass 90:10 char blend gasification kinetics.

Reaction	**Kinetics**				**Error evaluation**	
	E (Kj/mol)	**A ($s^{-1}m^{-1}$)**	f_o	φ	**R^2**	**RMS**
1	230.36	1.43e+6	0.60	18.99	0.9996	0.0081
2	222.30	5.36e+5	0.41			

7.2.5. Coal-Pine 90:10 char blend

The coal- pine 90:10 blend was modeled to an accuracy of 0.0077 RMS error value and 0.9996 R^2 statistic. The conversion vs. temperature and DTG plots are outlined in Figure 7-14.

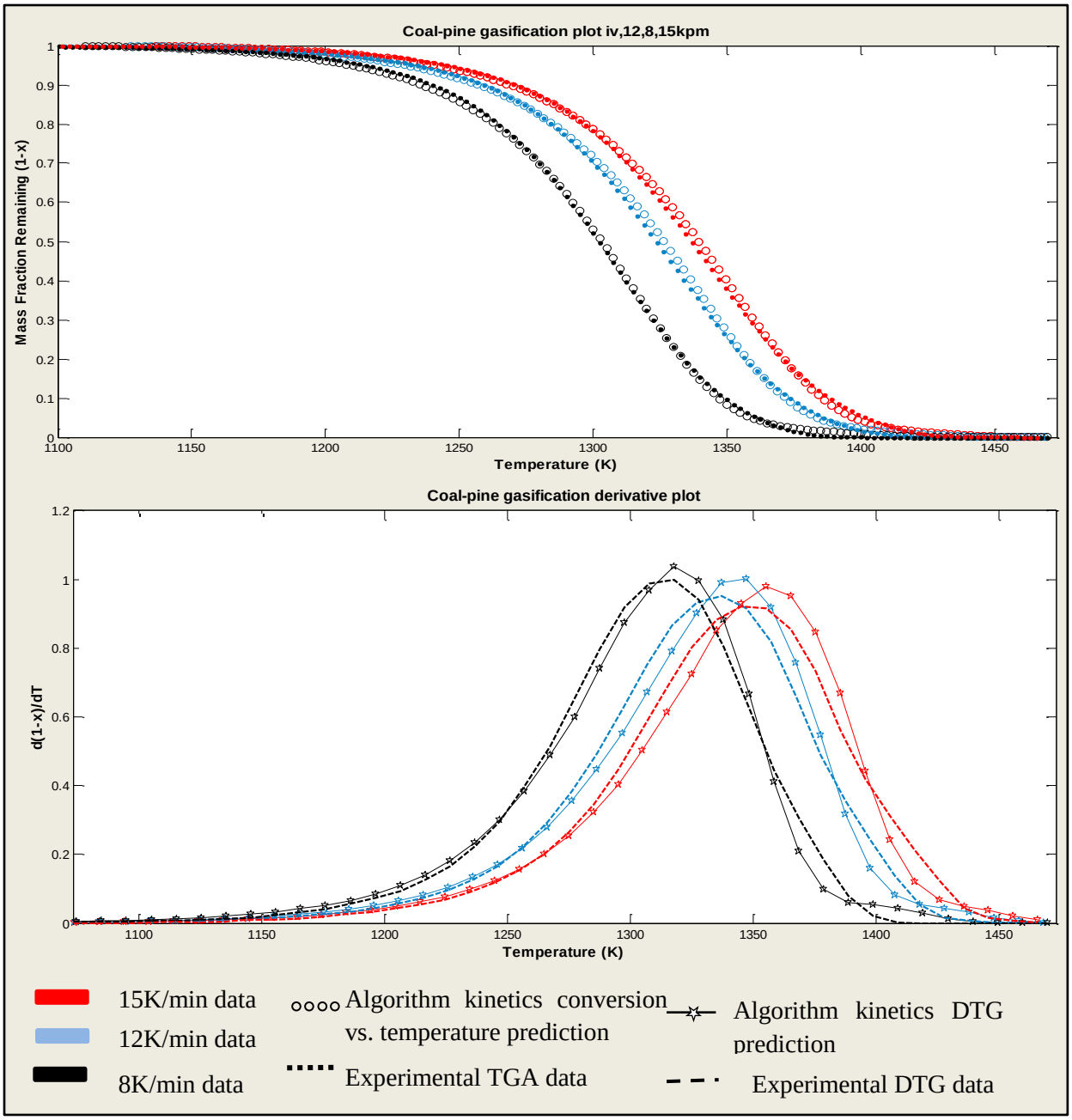

Figure 7-14: Modelling of coal-pine 90:10 gasification.

Throughout the three tests carried out, it can be observed that the DAE based model slightly over predicts the reaction rate towards the maximum point and under predicts it as it completes. This does not, however, denounce the fact that overall, the DAE based model adequately predicts the reaction progression. The same structural parameter of 18.99 as determined during the

combustion of the blend was found suitable for the modeling of the gasification process. Table 7-17 displays the kinetics observed during the conversion.

Table 7-17: Coal-pine 90:10 gasification kinetics

Reaction	Kinetics				Error evaluation	
	E (Kj/mol)	A ($s^{-1}m^{-1}$)	f_o	φ	R^2	RMS
1	239.01	3.40e+6	0.28	18.99	0.9996	0.0077
2	231.34	1.21e+6	0.71			

7.2.6. Isothermal gasification of coal char

Coal char was then gasified isothermally at temperatures, 1268K, 1298K, and 1318K. The experimental data was analyzed using the RPM adapted DAE based model which successfully modeled the non-isothermal coal char gasification conversion. The DAE based model modeled the conversion to a reasonable accuracy of 0.0051 RMS error and a corresponding R^2 value of 0.9991. Figure 7-15 displays the obtained experimental and model predictions.

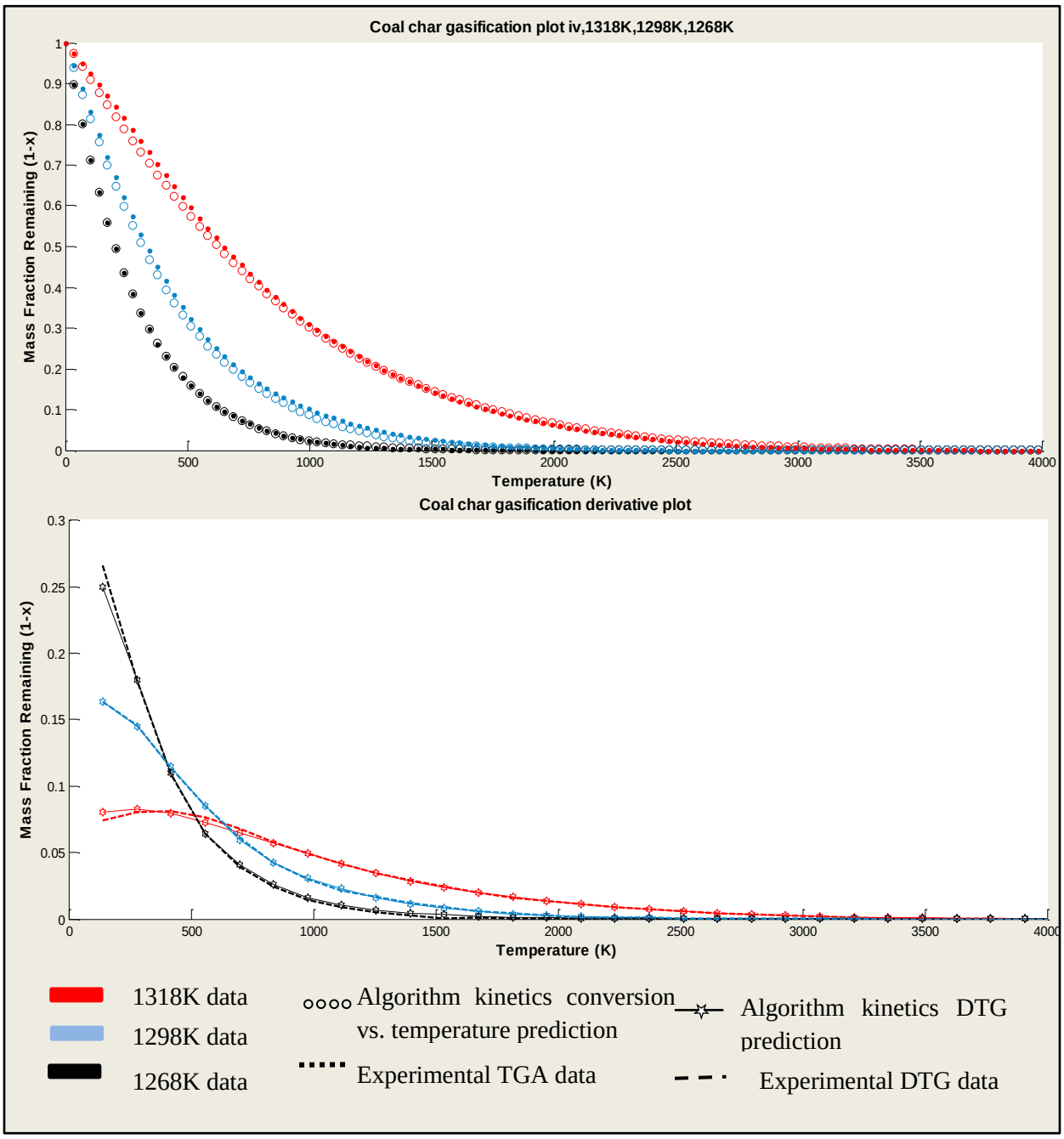

Figure 7-15: Modelling of isothermal coal char gasification

Minor deviations are observed at the beginning of the reaction for temperatures 1318K and 1298K. As the reaction proceeds, a slight over prediction of the reaction is observed between 500 and 1000s duration of the conversion for the 1318K conversion. The DAE based model

prediction then accurately predicts the rest of the conversion for the three different temperatures. The kinetics obtained are presented in Table 7-18.

Table 7-18: Isothermal Coal char gasification kinetics

Reaction	**Kinetics**				**Error evaluation**	
	E (Kj/mol)	**A ($s^{-1}m^{-1}$)**	f_o	φ	**R^2**	**RMS**
1	359.22	9.00E+11	0.10	17.0	0.99912	0.0051
2	322.34	1.18E+10	0.37			
3	298.41	5.91E+08	0.44			
4	166.24	1.80E+03	0.07			

As observed in Table 7-18, a different set of kinetics is obtained upon the modeling of isothermal gasification of coal char as compared to the non-isothermal kinetics. A 11% reduction in the structural parameter is observed from 18.99 to 17.0. This isothermally determined set of kinetics was then used for non-isothermal modeling of the conversion. Figure 7-16 reports the results obtained when using isothermally determined kinetics to predict non-isothermal reaction progression.

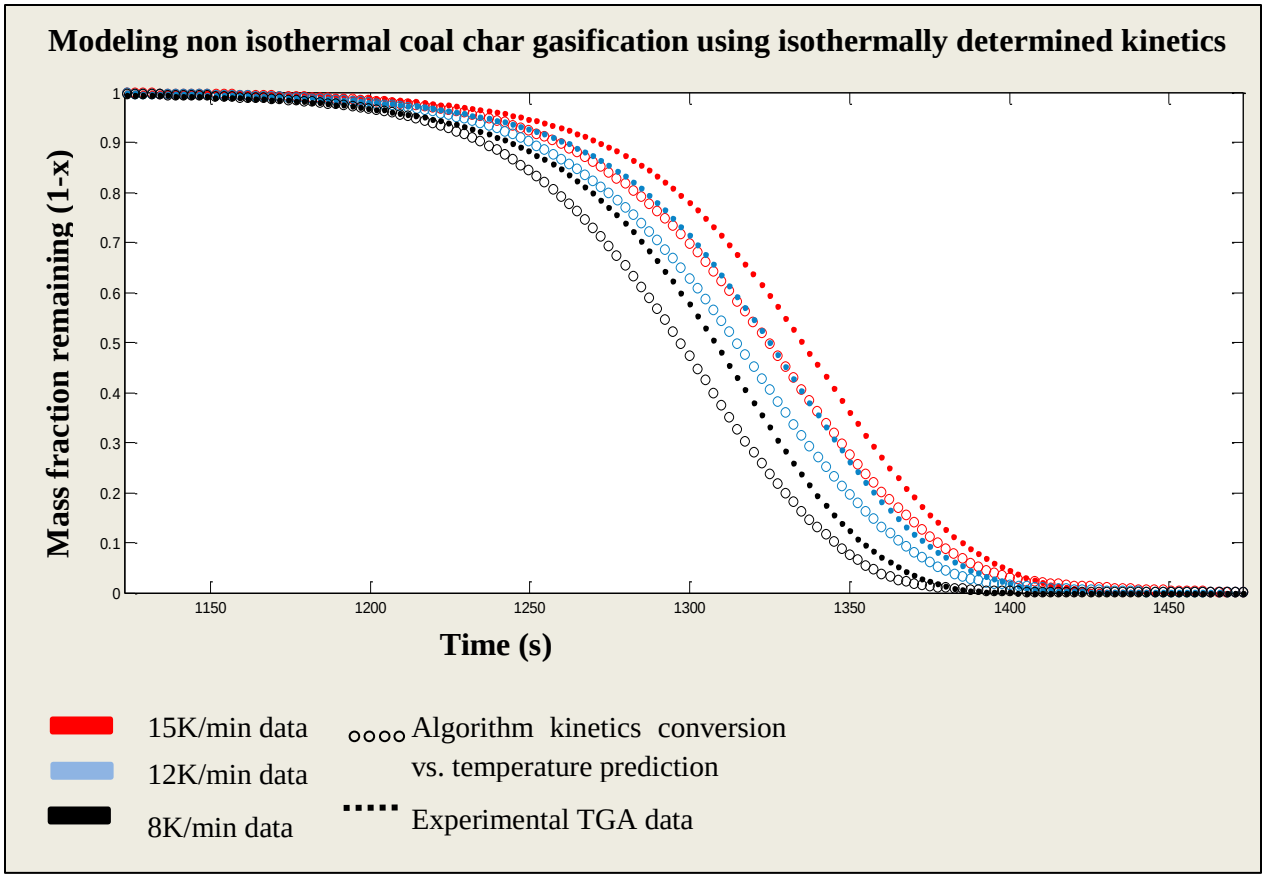

Figure 7-16: Modelling of non-isothermal coal char gasification using isothermally determined kinetics.

From visual observation, it is clear that the isothermally determined kinetics are not suitable for the modeling of non-isothermal behavior of the coal char. Non-isothermally determined kinetics were in turn used to predict isothermal reaction progression. The results obtained are demonstrated by Figure 7-17.

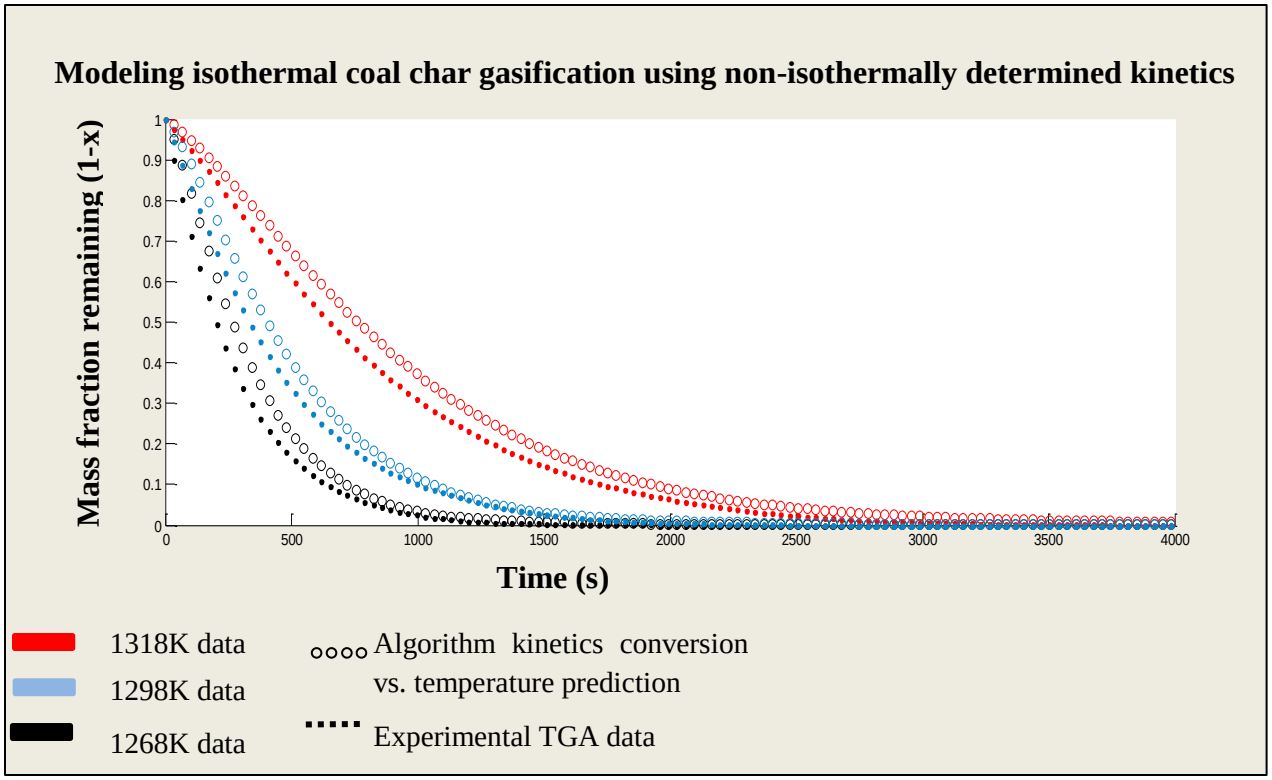

Figure 7-17: Modelling of isothermal coal char gasification using non-isothermally determined kinetics

As displayed in Figure 7-17, it is observed that the non-isothermally determined kinetics are also not suitable for the modeling of the material's non-isothermal behavior during the conversion.

A method proposed by Njapha (2003) normalizes the isothermal conversion data for various reaction models with respect to time. Njapha (2003) presents the isothermal char conversion as a function of normalized time, $t/t_{0.9}$. $t_{0.9}$ is the time at which the conversion reaches 90%. Njapha normalized the SCM reaction equations at the three regimes as described on Table 7-19.

Table 7-19: Normalized time SCM equations

Regime	Model Equation	Normalized Time Model Equation
Chemical reaction controlled	$t = \tau_{chemical\ reaction}[1-(1-X)]^{\frac{1}{3}} \ldots [7-3]$	$\frac{t}{t_{0.9}} = \frac{1-(1-X)^{1/3}}{0.54} \ldots [7-4]$
Ash diffusion controlled	$t = \tau_{ash\ diffusion}[1-3\left(1-X\right)^{\frac{2}{3}}+2(1-X)\right] \ldots$[7-5]	$\frac{t}{t_{0.9}} = \frac{1-3(1-X)^{\frac{2}{3}}+2(1-X)}{0.55} \ldots [7-6]$
External mass transfer controlled	$t = \tau_{mass\ transfer}X \ldots [7-7]$	$\frac{t}{t_{0.9}} = \frac{X}{0.9} \ldots [7-8]$

The parameter τ as shown in the equations above is dependent on the regime in which the reaction is taking place. The parameter is a function of the reacting gas and particle properties at the different regimes. It is eliminated by the normalization of the reaction model equation as presented on Table 7-19. A plot of normalised time against the massfraction remaining $(1-X)$, can then be produced for a particular reaction model at a given regime. These plots are then compaired to those of the actual char conversion experiments to identify the most suitable model describing the char conversion. The RPM is also normalized according to the equations outlined on Table 7-20.

Table 7-20:Normalized time RPM equation

	Model Equation	Normalized Time Model Equation
RPM	$t = \tau_{RPM}\left(\sqrt{1-\Psi\ln(1-X)}-1\right) \ldots$[7-9]	$\frac{t}{t_{90}} = \frac{\sqrt{1-\Psi\ln(1-X)}-1}{\sqrt{1-\Psi\ln(1-0.9)}-1} \ldots [7-10]$ (Kaitano, 2007)

The outlined method can then be applied in this study to ensure that the isothermal coal char conversion can be defined as occuring in the chemically controlled regime according to the RPM at the DAE based model determined structural parameter Ψ. The results obtained upon plotting the mass farction remaining against the normalised time are shown on Figure 7-18.

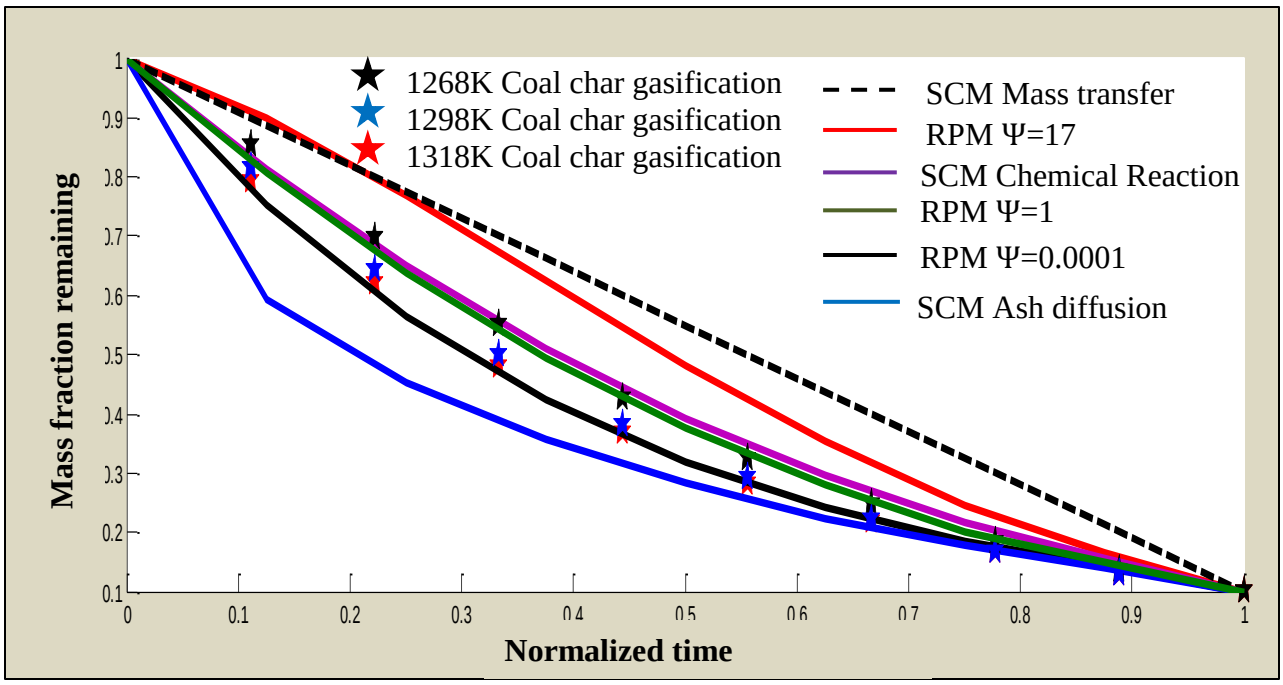

Figure 7-18: Conversion vs. normalized time plots.

According to this method, it can be seen that the most suitable reaction model describing the isothermal coal char gasification is the RPM at a structural parameter in the range between 1 and 0. However, the DAE based model identified a structural parameter of 17. Clearly, more than one structural parameter would be best used to describe the conversion of the coal during gasification at the different isothermal temperatures. To ensure the method is applicable to multiple reactions occuring at a given structural parameter, a RPM multiple reaction conversion is simulated according to the kinetics specified on the Table 7-21. A single reaction at the same structural parameter will also be simulated as detailed on Table 7-21.

Table 7-21: Specified reaction kinetics

Reaction	Kinetics			
	E (Kj/mol)	A ($s^{-1}m^{-1}$)	f_o	φ
1	350	10E+ 11	0.4	17.0
2	300	10E+ 9	0.4	
3	250	10E+ 7	0.1	
4	400	10E+ 14	0.05	
5	360	10E+ 12	0.05	
1	300	10E + 9	1.0	17.0

The simulated conversion is then plotted as a function of the conversion against the normalized time. The results are displayed on Figure 7-19.

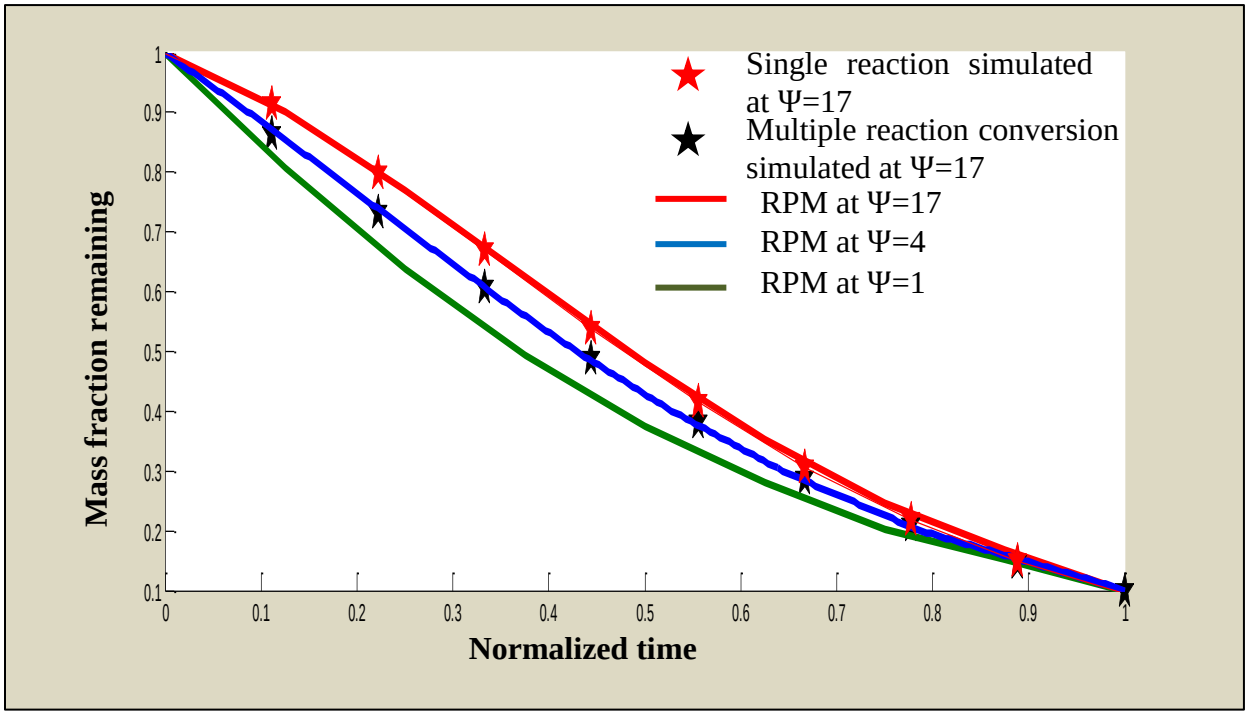

Figure 7-19: Conversion vs. normalized time plots: Simulated RPM reactions.

Clearly, the normalisation method identifies a different structural parameter than that specified during the simulation. Even though the method adequately describes the conversion of a

simulated single reaction, it does not correctly described the progression of a multiple reaction conversion.

7.3. Discussion of Results

There is need to further analyse and compare the kinetics obtained during the conversions of the materials studied in this research. Clearly the determined kinetics are able to predict the progression of the conversions with high accuracy. The kinetics of the different materials has been compared to one another, and also, to literature values obtained during other studies in this section.

7.3.1. The compensation effect

Vyazovkin (2008) notes that there is a fundamental flaw in the use of single heating rate methods for kinetics determination. The methods tend to produce differing sets of the kinetic triplets, most of which provide a satisfactory description of the same dataset. This is observed in Table 7-23; the various plots using different heating rate conversion data for the determination of kinetics produce different sets of the kinetic triplet. This occurs due to the mutually compensating correlation of E and A, and is known as the compensation effect (Vyazovkin, 2008). Vyazovkin (2008) describes the correlation by Equation [7-11].

$$\log A_i = aE_i - b \qquad [7\text{-}11]$$

Where a and b are constants and E and A are the activation energy and grouped pre-exponential factor associated with the reaction i. Vyazovkin (2008) goes on to demonstrate that for the same reaction, an increase in E would normally be associated with a corresponding increase in the logarithm of A. This is explained by an increase in A defining an increase in the reaction rate, whilst an increase in E relates to a decrease in the reaction rate. Hence, the same reaction profile may be maintained by simultaneously increasing or decreasing the two parameters (Vyazovkin, 2008). This effect is very useful in the identification of the correct Arrhenius parameters. Given the two constants are known, iso-conversional methods can adopt this effect to model independently calculate A. In this study, this compensation effect is used for the comparison of the Arrhenius parameters obtained during the conversion of the different chars.

Table 7-22: Combustion kinetics

Char Sample	E (Kj/mol)	A ($s^{-1}m^{-1}$)	f_o	φ
Coal	137.39	2.82E+5	1.00	18.5
Pine	255.48	2.80E+15	0.049	8.29
	222.28	2.23E+12	0.038	
	193.68	7.88E+9	0.164	
	183.30	5.34E+8	0.735	
Grass	127.8	1.60 E+5	0.19	10.5
	130.5	2.17 E+5	0.80	
Coal-Grass 90:10	125.68	5.38E+4	1.00	18.98
Coal-Pine 90:10	125.58	6.2e+4	0.42	18.98
	135.04	1.93e+5	0.57	
Coal-Grass 50:50	135.94	3.09E+5	1.00	15.94
Coal-Pine 50:50	138.33	3.94e+5	1.00	17.88

Considering Table 7-22, it must be noted that the comparison of the obtained kinetics is impossible without the elimination of the compensation effect. A simultaneous increase or decrease in E and A is observed with each material. For example, when comparing the coal-grass 90:10 char blend with the coal char during combustion, one can conclude that a decrease of 11.38 Kj/mol in the E is observed. This conclusion would, however, be completely ignoring the 2.30E+05 $s^{-1}m^{-1}$ drop in the corresponding value of A. The compensation effect will therefore be used for the calculation of E upon eliminating the effect of the change in A. The calculated E value (E_c) will be considered as the corrected E, this is the value; of E upon the elimination of the compensation effect on the Arrhenius parameters determined. This value will be evaluated by the application of Equation [7-11], by substituting A in order to determine E_c . E_c will then be compared to the actual E.

Clearly a baseline reaction must be established for comparison. This reaction was determined from the coal char combustion kinetics in Table 7-23. This reaction must be suitably described by two different sets of kinetics using the different heating rate sets. The two most accurate reactions identified by the DAE based model represent the exact same reaction. However, the third most accurate reaction presents a different set of kinetics.

Table 7-23: Coal char combustion kinetics

Plot	Heating rate used(K/min)			Kinetics				Error evaluation	
	E calculation	A calculation	φ calculation	E (Kj/mol)	A ($s^{-1}m^{-1}$)	f_o	φ	R^2	RMS
i	8 ,12	8	12	123.99	5.10E+04	1.0	12.04	0.9991	0.0128
ii	8,15	8	15	124.25	4.64E+04	1.0	18.03	0.9994	0.0105
iii	12,15	12	15	137.39	2.82E+05	1.0	18.53	0.9998	0.0061
iv	12,8	12	8	123.99	5.10E+04	1.0	11.51	0.9990	0.0132
v	15,8	15	8	124.25	4.64E+04	1.0	16.58	0.9994	0.0101
vi	15,12	15	12	137.39	2.82E+05	1.0	18.53	0.9998	0.0059

The kinetics from combinations vi and v were used to evaluate the constants a and b from Equation [7-11]. This coal char combustion reaction was then used as the basis of comparison for all the reactions occurring in the other materials under study. The E_c value may therefore be referred to as the coal char equivalent E. Since the constants a and b have been evaluated based on coal char combustion, the E_c becomes the corresponding E for coal char combustion given the A used in the equation. The equation defining coal char combustion may therefore be described by the Equation [7-12];

$$\log A_i = 0.06E_i - 2.75 \qquad [7\text{-}12]$$

All the reactions taking place in the combustion of the biomass and the biomass-coal char blends were then analyzed in comparison to the reaction taking place during the coal char combustion. The difference between the E of a particular char and the E_c was evaluated in terms of percentages. A weighted sum of the percentage differences is presented as the overall percentage difference between E_c and E. As shown on Table 7-24, if a char has an E that is lower than the corresponding E_c, (coal equivalent activation energy), it is then more reactive than the coal char during combustion. For such a char, the magnitude difference is shown by a negative percentage value. If a char is less reactive than the coal char, its E will be higher than the calculated E_c, and hence a positive percentage difference. Note that since the different chars use their own A's to

evaluate the E_c (coal equivalent activation energy),both parameters, the A and the E, are then considered and compared with the coal char combustion kinetics.

Table 7-24: Kinetic analysis on combustion kinetics

Char Sample	E (Kj/mol)	A ($s^{-1}m^{-1}$)	f_o	φ	E_C	Total weighted % difference
Coal	137.39	2.82E+5	1.00	18.5	137.39	0%
Pine	255.48	2.80E+15	0.049	8.29	299.67	-6.0%
	222.28	2.23E+12	0.038		249.25	
	193.68	7.88E+9	0.164		209.36	
	183.30	5.34E+8	0.735		190.34	
Grass	127.8	1.60E+5	0.19	10.5	133.26	-4.0%
	130.5	2.17E+5	0.80		135.48	
Coal-Grass 90:10	125.68	5.38E+4	1.00	18.98	125.31	0.3%
Coal-Pine 90:10	125.58	6.2E+4	0.42	18.98	126.37	-0.1%
	135.04	1.93E+5	0.57		134.63	
Coal-Grass 50:50	135.94	3.09E+5	1.00	15.94	138.05	-2.0%
Coal Pine 50:50	138.33	3.94E+5	1.00	17.88	139.82	-1.1%

This is how the table was created: For Pine, if A=2.80E+15$m^{-1}s^{-1}$, the corresponding E_c, evaluated by Equation [7-12] (which represents how coal would behave), is 299.67. The actual E for that particular reaction (255.48kj/mol) is lower than the E_c, implying that the reaction is more reactive than that of coal char combustion. Using the reactive mass contribution, the differences in the E's and E_c's are summed into a weighted average percentage.

From Table 7-24, it is observed that pine char and grass char are definitely more reactive than the coal char, with the two biomass E's proving 6.0% and 4.0% lower than that of coal char. As compared to coal char, pine char appears to be the most reactive material, followed by the grass char. When the coal and biomass char blends are compared to the coal char reactivity, no significant differences in the kinetics are observed for the 90:10 biomass blends. For the 90:10 coal and grass blend, the E obtained proves to be 0.3% higher than that of coal char. The 90:10 coal and pine char blend appears to react with an E 0.1 % lower than that of coal char.

Considering the magnitude of the differences observed, it is concluded that the 10% biomass by energy input of the biomass component has no significant effect on the reactivity of the coal char during combustion. As the percentage is increased up to 50% biomass by energy input, it must be noted that the difference in E's increases to 2% (grass-coal char blend) and 1.1% (pine-coal char blend) lower than that of the coal char. It may then be concluded that the biomass component tends to increase the reactivity of the coal char at a 50% blend. It is also highlighted at this stage that the biomass and coal char blends were created using an energy input ratio of the raw samples before char formation. Due to the high volatile content of the biomass materials, the biomass component is further reduced after char formation. Table 7-25 below summarises the biomass contribution in the blends used.

Table 7-25: Biomass contribution by mass during blending

Biomass	**%Biomass by energy input**	**Coal char fraction by mass**	**Biomass char fraction by mass**
Grass	10%	0.94	0.06
Pine	10%	0.96	0.04
Grass	50%	0.65	0.35
Pine	50%	0.74	0.26

The same approach was used on the evaluation of gasification kinetics, yielding the results presented in Table 7-26. However, two distinct reactions were identified during the gasification conversion. The major reaction was identified and used as the baseline reaction. The secondary reaction was then evaluated as based on the major reaction; this lead to a total weighted percentage difference on the coal char gasification. This value was then eliminated from the results obtained on the other materials, resulting in an overall % difference in the E's based on the coal char gasification. The equation defining the coal char gasification is presented by Equation [7-13];

$$\log A_i = 0.04E_i - 2.80 \qquad [7\text{-}13]$$

Table 7-26: Kinetic analysis of gasification kinetics.

Char Sample	E (Kj/mol)	A ($s^{-1}m^{-1}$)	f_o	φ	E_c	Total weighted % difference	Overall % difference
Coal	304.3	1.82E+9	0.28	18.53	313.36	-1.0%	0%
	300.61	1.14E+9	0.15		308.08		
	272.91	5.05E+7	0.56		272.91		
Pine	280.04	3.96E+9	0.35	8.29	322.12	-12.0%	-11%
	272.96	8.97E+8	0.22		305.37		
	274.81	9.97E+8	0.20		306.57		
	293.45	3.21E+9	0.22		319.76		
Grass	260.19	1.90E+8	0.23	10.03	287.86	-7.0%	-6.0%
	272.38	2.89E+8	0.27		292.59		
	275.83	3.73E+8	0.27		295.47		
	300.03	1.49E+9	0.22		311.10		
Coal-Grass 90:10	230.36	1.43E+6	0.60	18.99	232.69	-0.5%	0.5%
	222.30	5.36E+5	0.41		221.62		
Coal-Pine 90:10	233.49	1.83E+6	1.00	18.99	235.47	-1.0%	0.0%

Table 7-26 reports an E decrease of 11% for pine char and 6% for grass char as compared to the coal char gasification kinetics. The pine char proves more reactive than grass char during gasification and combustion. Similar results are observed for the 10% biomass blends, where very minor changes in E are observed. The coal–grass blend reports a 0.5% increase in E, whilst the coal-pine blend reports no difference in activation energies when compared to the coal char. Clearly, due to the low biomass char contribution by mass, the 90:10 blends also present minimal changes in E during gasification.

7.3.2. Comparison of the determined kinetics with literature values

The E's obtained in the current study are therefore compared to some literature values on Table 7-27.

Table 7-27: Comparison of E's obtained with literature values

Combustion		
Author	**Sample**	**Activation Energy (Kj/mol)**
This study	Vitrinite-rich South African coal char	137
This study	Pine dust char	183-255.
This study	Grass char	133-135
Sahu et al. (2010)	Coal char	133
Sahu et al.(2010)	Saw dust char	74-117
Filho and Milioli (2008)	Brazillian bituminous coal	104
Muthuraman et al.(2010)	Indonesian Coal	151
CO_2 Gasification		
This study	Vitrinite-rich South African coal char	272-305
This study	Pine dust char	251-280
This study	Grass char	270-300
Zhu et al. (2008)	Wheat straw char	145
Zhu et al.(2008)	Coal char	197
Seo et al.(2010)	Pinus densiflora	172
Senneca (2007)	Pinus radiata	259
Senneca (2007)	Pine seed shell	201
Liu et al. (2000)	Coal char	170-250
Vittee (2012)	Coal char	228-262

From Table 7-27, the E's obtained during the combustion of the coal and grass chars in this study are comparable to those reported in literature. The pine char combustion however, was found to have an E range higher than those obtained in literature. The E's observed during gasification of all the material chars proved to be somewhat higher than those reported in

literature. It is however noted, that as observed in Section 7.3.1, it is not advisable to compare the E of one material without considering it's A. The higher E's obtained, especially during gasification, may be attributed to the corresponding A's. However, in this study, a grouped pre-exponential factor is determined as shown by Equation [2-11].

$$A = \frac{A_o S_0}{1 - \epsilon_o} \qquad [2\text{-}11]$$

To evaluate the actual pre-exponential factor, there is need for the measurement of the initial area per unit volume and the initial porosity of the chars which is not within the scope of this study.

According to Liu and Niksa (2004), Zolin (2001) reported structural values in the range of 2.2 to 19 for nine coal chars of different rank. Charpenay et al. (1992) used structural parameter values up to 50, for the modeling of the combustion of a Pittsburg coal. Sadhukhan et al. (2010) identified structural parameters in the range of 5.2-8.0. Ahmed and Gupta (2011) used two different structural parameters, 9.0 and 2.1 for woodchips char gasification in steam and CO_2 respectively.

7.3.3. Evaluation of interactions between the components of the char blends.

The approach carried out by Gil et al. (2010(a)), Sadhukhan et al. (2008), Vuthaluru (2004) and Moghtaderi et al. (2004) was adopted in this study to identify if any interactions between the components of the blends occurred during gasification or combustion. Gil et al. (2010(a)) studied the co-combustion of coal and sawdust, whereas the other authors studied pyrolysis of coal with wood waste and sawdust. The method adopted was carried out by calculating the theoretical derivative temperature curves of the blends as the weighted sum total of the conversion curves of each individual component Gil et al. (2010(a)). This method will be referred to as the additive method.

$$\frac{dm}{dt} = x_{coal}\left(\frac{dm}{dt}\right)_{coal} + x_{biomass}\left(\frac{dm}{dt}\right)_{biomass} \qquad [7\text{-}14]$$

Here $(dm/dt)_{coal}$ and $(dm/dt)_{biomass}$ represent the rates of mass loss of the individual fuels of proportions x_{coal} and$x_{biomass}$. The results obtained upon the application of this method to the blends used in this study are detailed in the sections below.

7.3.3.1. Coal-Grass blends

The two curves obtained for each conversion (the calculated curve and the actual experimental curve) were compared with the use of the RMS error value and the R^2 value as explained in Section 4.2. Figure 7-20 displays the results obtained during the combustion and gasification of the coal-grass blends.

Table 7-28: Evaluation of interactions between the components of the coal-grass char blends using the additive method.

Coal/Grass 90/10		
Conversion	**R^2**	**RMS**
Combustion	0.9997	0.0076
Gasification	0.9994	0.0094
Coal/Grass 50/50		
Combustion	0.9991	0.0129

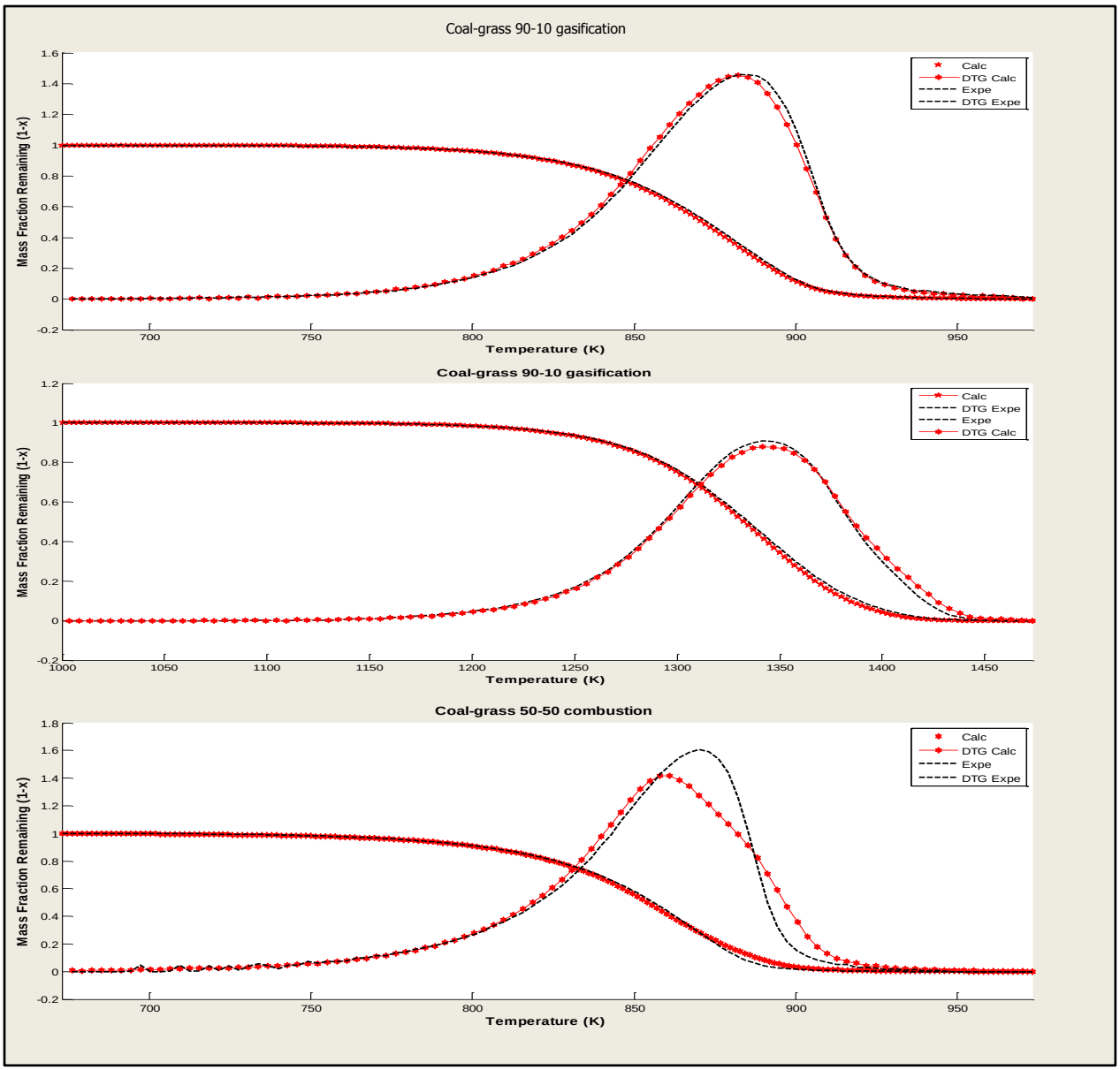

Figure 7-20: Evaluation of interactions between the components of the coal-grass char blends using the additive method.

The statistical evaluation parameters are displayed in Table 7-28. For the 90:10 blend of grass and coal, the RMS error values are 0.0076 and 0.0094 for combustion and gasification respectively. As the biomass component in the blend is increased to 50% by energy input, the RMS error value increases to 0.0129. Sadhukhan et al. (2008) carried out the same analysis of the pyrolysis of coal and biomass blends (wood waste), and obtained RMS error values of 0.0023 and 0.014. According to Sadhukhan et al. (2008), these values demonstrated the absence of synergetic effects during the conversion. Sadhukhan et al. (2008) however also visually

compared the experimental curve obtained with the virgin samples used in the conversion and used this as an additive measure for the identification of the synergetic effects.

Figure 7-21 gives a closer look at the differences between the coal-grass 50-50 blend DTG experimental curve during combustion and the calculated DTG curve.

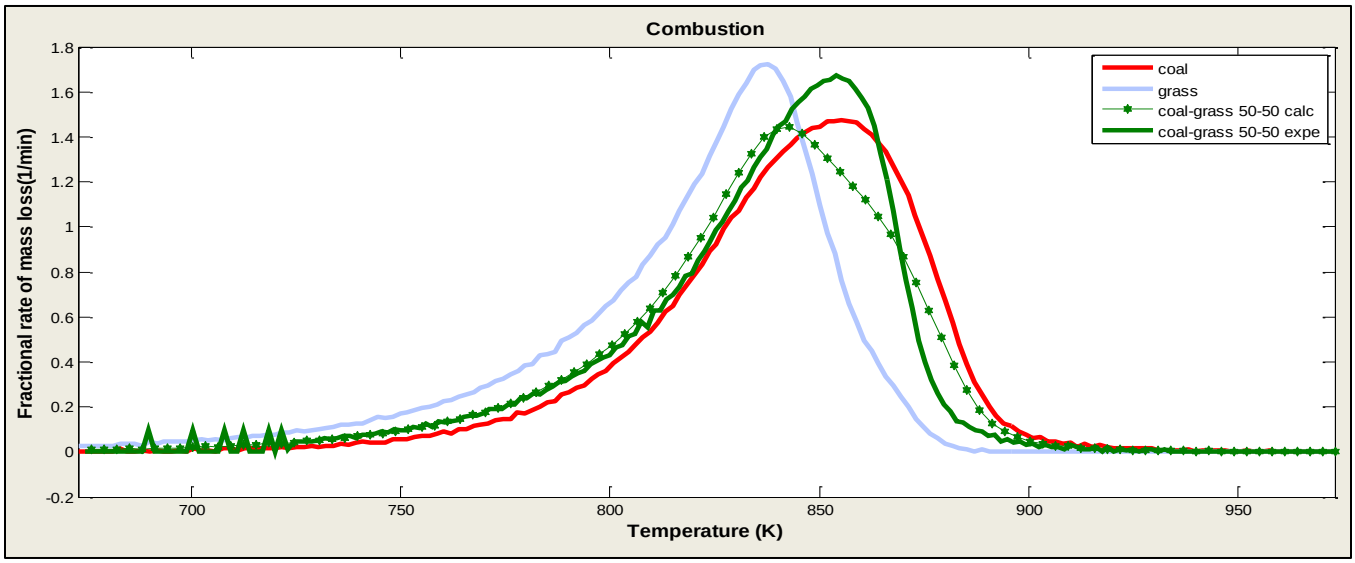

Figure 7-21: Qualitative analysis of coal and grass char combustion (DTG curves).

Figure 7-21 shows that grass char degradation commenced at the low temperature of 680K, compared to that of coal char which commenced at about 730K. During grass char combustion, the reaction rate increased continuously to a sharp maximum reaction rate at 840K. This was then followed by a progressive decrease in the reaction rate to completion at a temperature of 890K. The coal char reaction rate increased from zero to a maximum point at 855K. A steady decrease was then observed thereafter to a final temperature of 915K.The predicted DTG curve for the 50:50 blend appears to have two maximum points at temperatures of about 845K and 880K. The smaller peak at about 880K is distinguished by the change in the slope of reaction rate decrease. The two peaks can be explained as due to the two different components reacting simultaneously in the blend. The actual 50:50 blend DTG curve, presents a smooth increase in the reaction rate, commencing at the same temperature of 730K as the coal char combustion. The reaction rate increases to a single sharp maximum point at about 855K. It is noted that during this period, until about 840K, the predicted curve and the actual experimental curve a relatively agreeable. This, however, changes beyond 840K, where the actual experimental curve presents a further increase in the reaction rate to a single pronounced maximum point at about 855K. A

15% increase in the maximum reaction rate was observed on the experimental 50:50 blend DTG curve. A continuous decrease in the reaction rate was then experienced up to about 905K. It is again noted that the decrease in reaction rate at this point occured at temperatures lower than that of the coal char and yet higher than that of grass char degradation.

7.3.3.2. Coal Pine blend

The coal-pine blend results are displayed on Figure 7-22 and Table 7-29.

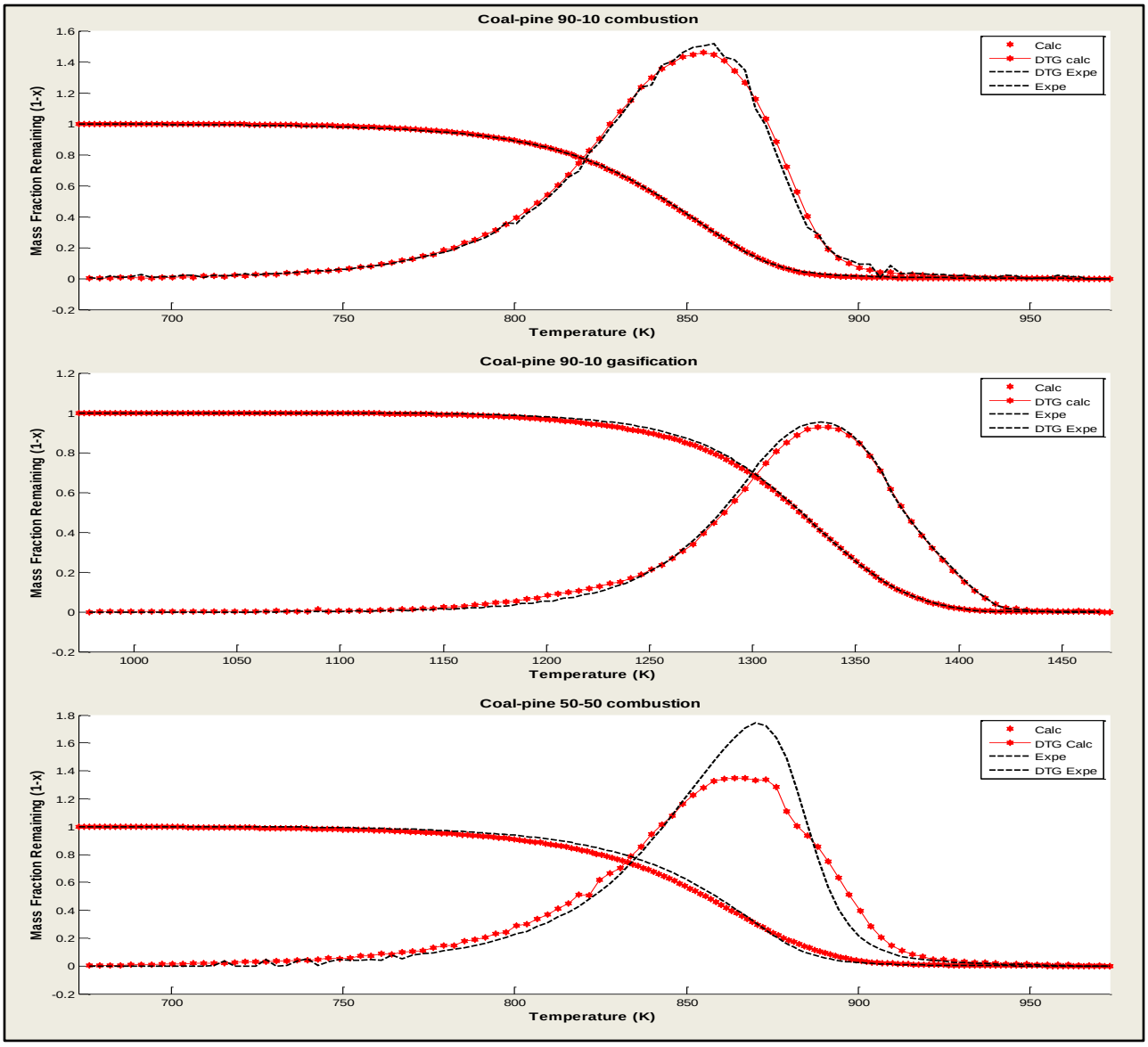

Figure 7-22: Evaluation of interactions between the components of the coal-pine char blends using the additive method.

Table 7-29 outlines the statistical parameters observed.

Table 7-29: Evaluation of interactions between the components of the coal-grass char blends using the additive method.

Coal-Pine 90:10		
Conversion	**R^2**	**RMS**
Combustion	0.9999	0.0040
Gasification	0.9993	0.0107
Coal-Pine 50:50		
Combustion	0.9968	0.0239

A similar observation was noted with the pine and coal blend. A very low RMS value of 0.0040 is obtained when comparing the two conversion curves during combustion. During gasification, an RMS value of 0.0107 was obtained. For the 50:50 blend, the RMS value for combustion increases to 0.0239. Figure 7-23 allows qualitative analysis of the DTG curves for the 50:50 blend during combustion.

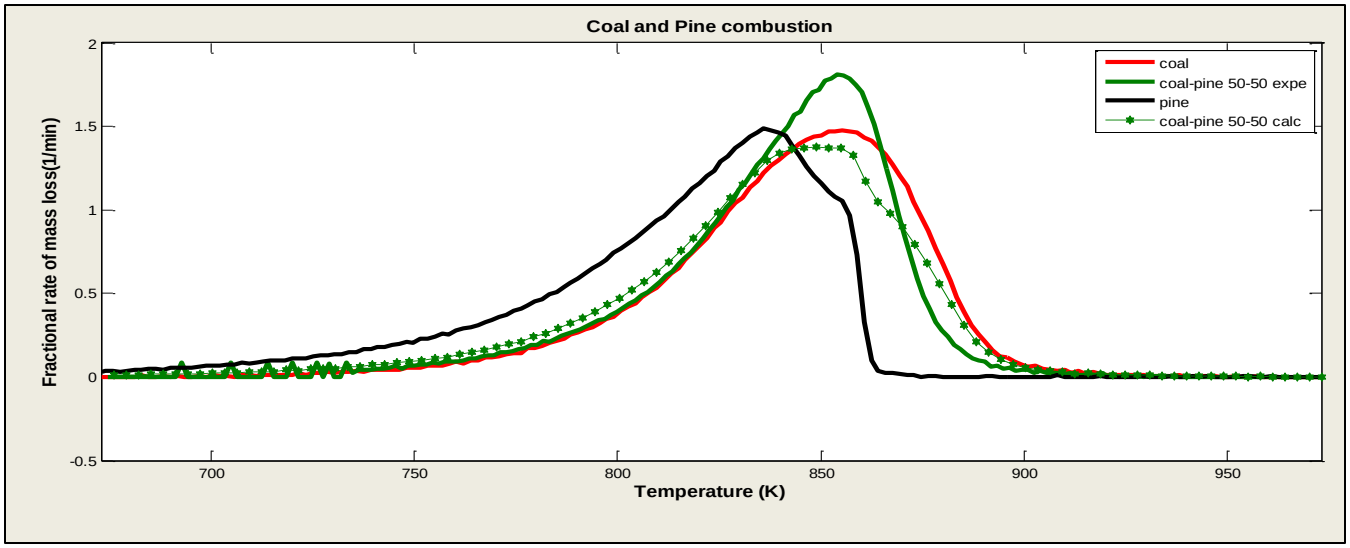

Figure 7-23: Qualitative analysis of coal and pine char combustion.

From Figure 7-23 clearly the pine char conversion commences at a lower temperature of approximately 673K as compared to the grass char and coal char. The shape of the pine char DTG curve shows the existence of more than one reaction taking place during the conversion. The reaction rate constantly increases from about 673K to a maximum at about 835K. The rate then slowly drops to the second peak observed at about 855K. A sharp decrease in the rate then

follows until the reaction terminates at about 865K. The coal char presents a progressive increase in the reaction rate from 730K to a maximum at 855K. A continuous decrease in the reaction rate is observed until approximately 815K. Clearly, the predicted DTG curve for the 50:50 blend can be defined to have two peaks at temperatures of 850K and 875K. This may be attributed to the degradation of the two char components respectively. The actual 50:50 blend DTG curve presents a smooth increase in the reaction rate, commencing at the same temperature as the coal char degradation (730K). The reaction rate increases to a single sharp maximum point at about 855K. At this point, it is observed that a 40% increase in the maximum point of the reaction was observed when compared to the calculated curve. This was followed by a continuous decrease in the reaction rate. It must be noted, however, that the decrease in the reaction rate is at a rate faster than that of the coal char, and yet slower than that of the pine char. At this point, it is clear that the curve prediction differs from the experimental curve. It can therefore be concluded that synergetic effects were present during the combustion of the blends.

7.4. Conclusions

It is clear from the presented results that the DAE based model is capable of efficiently modeling the combustion and gasification of the coal and biomass chars and their blends. It can therefore be concluded that the model is a robust and accurate method for kinetics determination. Multiple reactions were identified during the conversion of some of the chars in this study. This may be explained by the heterogeneous nature of the both the coal and biomass chars. As highlighted by Vittee (2012), the model identifies a single structural parameter for the multiple reactions identified. All the materials were successfully modeled by the RPM to accuracies in the range of RMS values of 0.0024 to 0.0081, and corresponding R^2 values of 0.9996 to 0.99996. The first order reaction model yielded results in the order of RMS values 0.0154 to 0.0507 and corresponding R^2 values of 0.9987 to 0.9866 respectively.

The successful application of the RPM for the modeling of the combustion and gasification of all the chars and char-blends studied serves to confirm the findings obtained by Bhatia and Vartak (1996) as highlighted in Section 2.4.2. Whilst Rafsanjani and Jamshidi (2008) state that the RPM is the most widely used in the modeling of char gasification, Bhatia and Vartak (1996) further state that the RPM found extensive application in the interpretation of gas-solid reaction rate data. It is found that the RPM is suitable for the modeling of both the gasification and combustion of coal and biomass chars.

As observed by Vittee (2012), the use of isothermal kinetics for non-isothermal conditions or vice versa, does not yield accurate results. For coal char gasification, the kinetics obtained at a particular temperature program may not be suitable for application in another. The plots of conversion against normalized time as described by Kaitano (2007) and Njapha (2003) were applied in this study. The normalized method was not able to correctly evaluate the structural parameters when multiple reactions are taking place during the conversion. There is therefore need to further study isothermal conversion and possibly adapt the normalization to multiple reaction behavior.

The 90:10 coal and biomass blends by heat input, corresponding to 6 and 4% biomass char input by mass for grass and pine char respectively, show no or little synergetic effects during both combustion and gasification. The RMS values of the relative errors are smaller for combustion of this blend than for gasification. This is expected since the biomass component in the char is so small. However, as the composition is increased to 50:50 coal and biomass blends by heat input, the char mass contribution in the blends increases to 35 and 26% for grass and pine char respectively. This is demonstrated by Table 7-8 in Section 7.1.4. The different DTG curves and increase in the RMS values imply the possibility of synergetic effects are observed with RMS error values of 0.0129 and 0.0239 for the grass and pine blend respectively. For both blends, an increase in the maximum reaction rate was observed in magnitudes of 15% and 40% from the calculated curves for coal-grass and coal-pine 50:50 blends respectively. These findings are similar to those observed by Duong et al. (2010). Duong et al. (2010) blended biomass (woody biomass and switch grass) and bituminous coal during combustion and gasification. Duong et al. (2010) states that the blending of the biomass with the coal for the most part increased the reactivity of the blends beyond that predicted by the additive method applied on Section 7.3.2.

The compensation effect has been applied to the observed grouped kinetics with the assumption that the structural parameter has negligible effect on E. The results obtained show considerable consistency of the theory with minimal deviations in E observed for the 90:10 coal and biomass blends. A decrease in the E during the combustion of the 50:50 coal-biomass blends is observed in the magnitudes of 2% and 1.1% for grass char and pine char blends respectively. It may then be concluded that the addition of biomass to the coal char during combustion leads to a reduction in E. The theory also shows that grass char and pine char have significantly lower E's during

both the combustion and gasification processes as compared to coal char. From Section 6.5 the high catalytic alkali oxide content in the ash contained in the pine char as compared to that in the pine would imply that the pine char is typically the most reactive component. The results obtained confirm this presumption and show that pine char is more reactive than grass char during both combustion and gasification. The pine char presents an E 6% lower than that of coal char whilst the grass char presents an E 4% lower than that of coal during combustion. During gasification, the pine char appears to be reacting with an E 11% lower than that of coal char and grass char with an E 6% lower. It is therefore concluded that the compensation effect is a suitable method of kinetics analysis. The high vitrinite coal char is also less reactive than the two biomasses studied. Pine char is the most reactive material followed by grass char and finally the coal char, during both combustion and gasification, in terms of activation energy.

The structural parameters identified were in the range of 8.3 to 18.9 and were found in line with those observed in literature. Similar structural parameters were also identified for a single material in the two different gas atmospheres.

8. CONCLUSIONS AND RECOMMENDATIONS

This research study was aimed at the determination of the intrinsic reaction kinetics of gasification and combustion of biomass and coal chars under non-isothermal and isothermal conditions. This was carried out to fulfill the following objectives:

- To validate the modified DAE based model by application on combustion and gasification thermo-analytical data.
- To identify the suitable reaction models for biomass and biomass-coal char blends in gasification and combustion.
- To investigate the effect of the presence of biomass on coal char combustion and gasification using the DAE based model.
- To analyze the reaction kinetics of non-isothermal gasification.

These objectives were successfully addressed in the study and the outcomes are presented in this chapter.

8.1. Summary

A woody and herbaceous biomass, pine chips and highveld grass, were selected for blending with a vitrinite-rich coal during gasification and combustion using thermo-gravimetry. The blends under the named conversion processes were utilised for an intrinsic kinetic study by the application of an iso-conversional DAE based model. The RPM and first order reaction models were used in conjunction with the DAE based model. Efforts were applied to ensure that the experimental conditions describe the chemical reaction controlled regime. Upon application, the model determines the activation energy, (E), the grouped pre-exponential factor, (A), and the mass fraction of the material reacted, (f_o). The DAE based model applied strikes a balance between modelistic and model free methods. E is evaluated model independently whilst A is evaluated model dependently. The approach used by the model has been recommended for the evaluation of solid state kinetics in literature (Khawam and Flanagan, 2005) and has in turn shown successful results in this study.

8.2. Conclusions

8.2.1. Preliminary analysis and Characterisation

Upon the completion of the preliminary analysis, it was concluded that the reduction of sample and particle size to an average mass of about 1.5mg of char at -53µm allows the combustion reaction to dominantly take place in the chemical reaction controlled regime. The same conditions were applied during the gasification tests. The Arrhenius plot method was found suitable for the purpose of observing any deviations from one reaction regime to another and was applied to all the thermo-analytical data obtained to ensure kinetic regime dominance. The heating rate fluctuations tended to increase in magnitude as the sample mass is increased. Hence, the reduction in sample size not only confines the reaction to the chemical reaction controlled regime, but also reduces the magnitude of the heating rate deviations from the set point during the reaction progression. At higher program heating rates, it was noted that the disturbances take place over a wider temperature/time duration than they do at lower program heating rates. From these findings, the most suitable heating rates identified for the thermo-gravimetric analysis were 8, 12 and 15 K/min. It was noted, however, that the complete elimination of heating rate deviations from the set-point is impossible during non-isothermal analysis. This lead to a development to the DAE based model to allow the use of instantaneous heating rates measured at instantaneous points during the conversion to be used for kinetics evaluation.

From the characterization experimental analysis, it was observed that the coal sample under study is a low ash, high volatile and high vitrinite coal of medium rank C. The grass and pine samples have extremely high volatile contents in the order of about 75%, with very low fixed carbon content. The pine biomass has the lowest ash content of about 0.2%, whereas the grass char consists of an ash content of about 7%. From the ultimate analysis, it has been observed that the pine sample contains the lowest proportions of S and N. As expected, the coal sample contained the highest amount of C, N and S, and the lowest H content of the 3 materials analysed.

The use of XRD analysis for mineralogical assay of the materials was found unsuitable during this study. The mineralogical assay obtained from the ICP-OES procedure lead to the conclusion that the pine sample is potentially the most reactive material from the three samples studied. The

alkali oxide content implied that the order of reactivity from the most reactive to the least is given as: pine, grass and coal respectively. This result was confirmed by the kinetic analysis.

8.2.2. Model application

From the kinetic analysis carried out in this study, it can be concluded that the DAE based model has been successfully validated on application to combustion and gasification thermo-analytical data of the coal, biomass, and their blends. The DAE based model was capable of efficiently modeling the combustion and gasification of the coal and biomass chars and their blends. The use of instantaneous heating rates measured as the reaction progressed showed an improvement in the model accuracy during kinetics determination. All the materials and blends were successfully modelled using the RPM. The observed accuracies were in the range of 0.0021-0.0081 RMS error values, and 0.99996 and 0.9996 R^2 values. It is therefore concluded that the model is a robust and accurate method for kinetics determination.

It is highlighted that multiple reactions were identified during the conversions of most of the chars under study. This may be explained by the heterogeneous nature of the both the coal and biomass chars. As noted by Vittee (2012), the model identifies a single structural parameter for the multiple reactions identified. The structural parameters identified were in the range of 8.3 to 18.9, and can be concluded to be in line with those observed in literature. It is therefore concluded that, in this study, the RPM has proven to be a very reliable reaction model for the description of coal and biomass char combustion and gasification.

8.2.3. Kinetic analysis

The compensation effect was successfully applied to the observed grouped kinetics. The results obtained show considerable consistency of the theory with minimal deviations in E observed for the 90:10 coal and biomass char blends. It was then concluded that negligible effects were observed on the reaction kinetics of both combustion and gasification of coal upon the addition of 10% biomass (highveld grass/pine) by heat input. A decrease in E during the combustion of the 50:50 coal-biomass blends was observed in the magnitudes of 2% and 1%, for grass char and pine char blends respectively. From this observation it was concluded that the addition of

biomass at a ratio of 50% by heat input to the coal char during combustion lead to a reduction in E and hence, an increase in the reactivity of the material.

The results also show that grass char and pine char have significantly lower E's during both the combustion and gasification processes compared to coal char. This is in line with the prediction obtained from the mineralogical assay results. The pine char presents an E 6% lower than that of coal char, whilst the grass char presents an E 4% lower than that of coal char during combustion. During gasification, the pine char appears to be reacting with an E 11% lower than that of coal char and grass char with an E 6% lower. It is therefore concluded that the compensation effect is a suitable method of kinetics analysis. The high vitrinite coal char is therefore less reactive than the two biomasses studied. Pine char is the most reactive material followed by grass char and, finally the coal char. The reactivity trends of these materials can therefore be attributed to their alkali metal content. However, it cannot be determined in this study whether or not the alkali salts contained in the biomass are the only source of catalytic behaviour during the conversions.
It was observed in this study that the use of isothermal kinetics for non-isothermal conditions or vise-versa does not yield accurate results. For coal char gasification, the kinetics obtained at one temperature program may not be suitable for application in another temperature program of different nature. The plots of conversion against normalized time as described by Kaitano (2007) and Njapha (2003) were applied on the coal char isothermal gasification conversion data for further analysis. The results obtained upon the application of the normalized time method proved the method unsuitable for application on multiple reaction conversions during the current study.

8.2.4. Evaluation of interactions between the components of the char blends.

Upon the evaluation of interactions between the components of the char blends, no synergetic effects were identified during the combustion and gasification of the 90:10 coal and biomass char blends. This was expected since the biomass component in the char was very small (6 and 4% by mass for the grass and pine blend respectively). However, as the biomass proportions were increased to 50% by heat input during combustion, synergetic effects between the blend components were observed. An increase in the maximum reaction rate was observed in magnitudes of 15% and 40% from the calculated curves for coal-grass and coal-pine 50:50 blends respectively.

8.3. Recommendations

The recommendations for future studies in this research area identified during the conduction of this research are presented in this section. The research study is of great benefit in addressing the need for an understanding of the reaction kinetics and thermal properties involved in the conversion processes (Kastanaki and Vamvuka, 2006; Senneca, 2007). In order to modify, design, and develop efficient and economically competitive conversion processes at industrial scale, an understanding of the intrinsic kinetic characteristics of the fuels during the conversion processes is essential. (Mani et al., 2011; Vamvuka et al., 2011; Fermoso et al., 2010; Huang et al., 2010; Gil et al., 2010(a); Kuo-Chao et al., 2009; Fermoso et al., 2008; Roberts and Harris, 2007; Ochoa et al., 2001; Dutta and Wen, 1977).

1. The DAE based model has been applied only to thermo-gravimetric studies, and proven successful. It is therefore recommended that the algorithm be applied to bench scale and pilot scale analysis studies, such as the drop tube furnace.
2. It was observed in the current study that the kinetics obtained during a conversion carried out at a particular temperature program may not be suitable for application in the modeling of a different temperature programmed conversion. It is therefore recommended that kinetic studies for the use in a particular temperature environment be carried out in the temperature program similar to that of the industrial process under study. Further investigations on the applicability of non-isothermal kinetics to isothermal behavior, and vice-versa, should be undertaken on other processes such as combustion and pyrolysis.
3. The mineralogical assay determined during the characterization stage of the study was able to accurately predict the order of reactivity of the materials studied. However, to adequately attribute the reactivities of the substances to their alkali content, there is a need to evaluate the reactivities of the materials by removing the alkali metals from the raw materials. The DAE based model can then be used to evaluate the reactivities to observe the effect of the alkali metals during the processes.
4. In the current study, only two blends were used for the analysis; it is recommended that a more detailed analysis be carried out on a wide set of blends to observe the effect of increasing the biomass content on the blend reactivity.
5. The normalized time method suggested by Njapha (2003) and Kaitano (2007) was found unsuitable for application on multiple reaction conversion during isothermal coal char

gasification analysis. It is therefore recommended that isothermal behaviour be further studied to possibly adapt the method to multiple reaction conversion behaviour.

9. REFERENCES

Abanades, J. C., Alonso, M., 2009. Application of the Random Pore Model to the Carbonation Cyclic Reaction. *American Institute of Chemial Engineers Journal*, 55(5),pp.1246-1255.

Ahmed, I. I., Gupta, A. K., 2011. Kinetics of woodchips char gasification with steam and carbon dioxide. *Applied Energy*, 88(5), pp.1613–1619.

Ahn, D. H., Gibbs, B. M., Ko, K. H., Kim, J. J., 2001. Gasification kinetics of an Indonesian sub-bituminous coal-char with CO_2 at elevated pressure. *Fuel*, 80(11), pp.1651-1658.

Arenillas, A., Rubiera, F., Arias, B., Pis, J. J., Faúndez, J. M., Gordon, A. L., García, X. A., 2004. A TG / DTA study on the effect of coal blending on ignition behaviour. *Journal of Thermal Analysis and Calorimetry*, 76, pp.603–614.

Arenillas, A., Rubiera, F., Pis, J. J., Jones, J. M., Williams, A., 1999. The effect of the textural properties of bituminous coal chars on NO emissions. *Fuel*, 78(14), pp.1779-1785.

Baxter, L., Koppejan, J., 2004. Biomass-coal Co-combustion : Opportunity for Affordable Renewable Energy Primary motivations for co-firing. *Fuel*, 84(10), pp. 1295-1302.

Bhat, A., Ram Bheemarasetti, J. V., Rajeswara Rao, T., 2001. Kinetics of rice husk char gasification. *Energy Conversion and Management*, 42(18), pp.2061–2069.

Bhatia, S. K. Vartak, B. J., 1996. Reaction of microporous solids: The discrete random pore model. *Carbon*, 34(11), pp.1383–1391.

Biagini, E., Lippi, F., Petarca, L., Tognotti, L., 2002. Devolatilization rate of biomasses and coal ± biomass blends : an experimental investigation. *Fuel*, 81(8), pp.1041-1050.

Bockelie, M., Davis, K., Fry, A., Sarofim, A., No date. Enhanced methane production by co-gasification of potassium-rich biomass and coal. *Reaction Engineering International*, Utah, pp.1-20.

Bos, A. N. R., Lefferts, L., Marin, G. B., Steijns, M. H. G. M., 1997. Kinetic research on heterogeneously catalysed processes: A questionnaire on the state-of-the-art in industry. *Applied Catalysis A:General*, 160, pp.185–190.

Braun, R. L., Burnham, A. K., 1987. Analysis of Chemical Reaction Kinetics Using a Distribution of Activation Energies and Simpler Models. Energy and Fuels, 1(2), pp.153-161.

Brown, M. E., Gallagher, P. K., 2008. Handbook of Thermal analysis and Calorimetry. Introduction to recent advances, techniques and applications of thermal analysis and calorimetry. Chapter 1. Vol. 5. Elsevier B.V., pp. 1-12.

Charpenay, S., Serio, M. A., Solomon, P.R., 1992. The prediction of coal char reactivity under combustion conditions. *Twenty-Fourth Symposium (International) on Combustion/ The Combustion Institute*, pp.1189–1197.

Chimica, I. & Federico, N., No date. Combustion and gasification rates of lignocellulosic chars. ThermalNet. Intelligent Energy Europe , pp.1-53.

Dash, S., Murthy, P, N., Nath, L., Chowdhury, P., 2010. Kinetic modeling on drug release from controlled drug delivery systems. *Acta Poloniae Pharmaceutica - Drug Research*, 67(3), pp. 217-223.

Davidson, R. M., Doig, A., Ekmann, J. M., Fernando, R., Harding, N. S., Moreea-Taha, R., Morrison, G. F., Ramezan, M., Rousaki, K., Smith, I. M., Smouse, S. M., Winslow, J. C., 2007. Cofiring biomass with other fuels. Coal online, available at http://www.coalonline.org/site/coalonline/content/home as assessed on 12/05/2012.

Department of Energy and Minerals., 2004. Capacity Building in Energy Efficiency and Renewable Energy: Economic and Financial Calculations and Modeling for the Renewable Energy Strategy Formulation. Report No. 2.3.4-19. February.pp.58-68.

De Micco, G., Nasjleti, A., Bohe, A. E., 2012. Kinetics of the gasification of a Rio Turbio coal under different pyrolysis temperatures. *Fuel*, 95, pp. 537-543.

Duong, D., Lantos, G., Tillman, D.,Kawecki, D., Coleman, A., 2010.Biomass Cofiring and Its Effect on the Combustion Process. *The 35th International Technical Conference on Clean Coal & Fuel Systems,* Clearwater, FL, USA. June 6-10.

Draper, N. R. W., Smith, H., 1981. Applied Regression Analysis, 2nd ed. John Wiley & Sons Inc., New York, USA.

Dupont, C., Nocquet, T., Da Costa Jr, A. J., Verne-Tournon, C., 2011. Kinetic modelling of steam gasification of various woody biomass chars: Influence of inorganic elements. *Bioresource technology*, 102, pp.9743–8.

Dutta, S., Wen, C. Y., Belt, R. J., 1977. Reactivity of Coal and Char. 1. In Carbon Dioxide Atmosphere. *Industrial and Engineering Chemistry Process Design and Development*, 16(1), pp.20-30.

Duz, M. Z., Tonbul, Y., Baysal, A., Akba, O., Saydut, A., Hamamci, C., 2005. Pyrolysis kinetics and chemical composition of Hazro coal according to the particle size. *Journal of Thermal Analysis and Calorimetry*, 81, pp.395–398.

European Commission., 2009. DIRECTIVE 2009/28/EC of the European Parliament and of the Council of 23 April 2009 on the promotion of the use of energy from renewable sources and amending and subsequently repealing Directives 2001/77/EC and 2003/30/EC, pp.16-62.

Everson, R. C., Neomagus, H. W. J. P., Kasaini, H., Njapha, D., 2006. Reaction kinetics of pulverized coal-chars derived from inertinite-rich coal discards: Gasification with carbon dioxide and steam. *Fuel*, 85(7-8), pp.1076–1082.

Fakir, Q., 2011. Kinetics of pyrolysis and combustion of a South African coal using the distributed. MSc Dissertation. University of Witwatersrand. Johannesburg, South Africa.

Feng, B., Bhatia, S. K., 2002. On the validity of thermogravimetric determination of carbon gasification kinetics. *Chemical Engineering Science*, 57(15), pp.2907-2920

Fermoso, J., Arias, B., Pevida, C., Plaza, M. G., Rubiera, F., Pis, J. J., 2008. Kinetic models comparison for steam gasification of different nature fuel chars. *Journal of Thermal Analysis and Calorimetry*, 91, pp.779-786.

Fermoso, J., Gil, M. V., Pevida, C., Pis, J. J., Rubiera, F., 2010. Kinetic models comparison for non-isothermal steam gasification of coal–biomass blend chars. *Chemical Engineering Journal*, 161(1-2), pp.276-284.

Fermoso, J., Stevanov, C., Moghtaderi, B., Arias, B., Pevida, C., Plaza, M.G., Rubiera, F., Pis , J. J., 2009. High-pressure gasification reactivity of biomass chars produced at different temperatures. *Journal of Analytical and Applied Pyrolysis*, 85(1-2), pp.287-293.

Fernando, R., 2005. Fuels for biomass co-firing.(October).IEA Clean Coal Centre available at http://www.iea-coal.org.uk as assessed on 27/07/2012.

Filho, C. G. D. S., Milioli, F. E., 2008. A thermogravimetric analysis of the combustion of a Brazilian mineral coal, Quim. Nova, 31(1), p. 98-103

Fisher, E. M., Dupont, C., Darvell, L. I., Commandré, Saddawi, A., Jones, J.M., Grateau, M., Nocquet, T., Salvador, S., 2012. Combustion and gasification characteristics of chars from raw and torrefied biomass. *Bioresource technology*, 119, pp.157–65.

Gil, M. V., Casal, D.,Pevida, C., Pis, J. J., Rubiera, F., 2010(a). Thermal behaviour and kinetics of coal/biomass blends during co-combustion. *Bioresource technology*, 101, pp.5601–8.

Gil, M. V., Fermoso, J., Pevida, C., Pis, J.J., Rubiera, F., 2010(b). Intrinsic char reactivity of plastic waste (PET) during CO_2 gasification. *Fuel Processing Technology*, 91(11), pp.1776-1781.

Henrich, E., Burkle, S., Meza-Renken, Z. I., Rumpel, S., 1999. Combustion and gasification kinetics of pyrolysis chars from waste and biomass. *Journal of Analytical and Applied Pyrolysis* , 49, pp.221–241.

Hernandez, J. J., Aranda-Almansa, G., Serrano, C., 2010. Co-Gasification of Biomass Wastes and Coal−Coke Blends in an Entrained Flow Gasifier: An Experimental Study. *Energy & Fuels*, 24(4), pp.2479-2488.

Higman, C., van der Burgt, M., 2008. Gasification, second edition., Elsevier Inc., Burlington, USA, pp.1-456.

Huang, Z., Zhang, J., Zhao, Y., Zhang, H., Yue, G., Suda, T., Narukawa, M., 2010. Kinetic studies of char gasification by steam and CO_2 in the presence of H_2 and CO. *Fuel Processing Technology*, 91(8), pp.843-847.

Hurt, R. H., Calo, J. M., 2001. Semi-Global Intrinsic Kinetics for Char Combustion Modeling. *Combustion and Flame*, 125(3), pp.1138-1149.

Ioannou, Z., Zoumpoulakis, L., Halikia, I., Teloniati, T., 2009. Overall kinetic study of non-isothermal decomposition of calcium carbonate. *Mineral Processing and Extractive Metallurgy*, 118(2), pp.98-104.

Irfan, M. F., Usman, M, R., Kusakabe, K., 2011. Coal gasification in CO_2 atmosphere and its kinetics since 1948: A brief review. *Energy*, 36(1), pp.12-40.

Ishida, M., Wen, C. Y., 1971.Comparison of zone-reaction model and unreacted-core shrinking model in solid-gas reactions- Isothermal analysis. *Chemical Engineering Science*, 26, pp.1031–1041.

Kaitano, R., 2007. Characterisation and reaction kinetics of high ash chars derived from inertinite-rich coal discards. *PhD Dissertation*. North-West University. Potchefstroom, South Africa.

Kastanaki, E., Vamvuka, D., 2006. A comparative reactivity and kinetic study on the combustion of coal–biomass char blends. *Fuel*, 85, pp.1186–1193.

Khalil, R., Varhegyi, G., Jaschke, S., GrØnli, G. M., Hustad, J., 2009. CO_2 Gasification of Biomass Chars : A Kinetic Study. *Energy and Fuels*, 23(1), pp.94–100.

Khawam, A. & Flanagan, D. R., 2005. Role of isoconversional methods in varying activation energies of solid-state kinetics. *Thermochimica Acta*, 436(1-2), pp.101–112.

Kim, Y. T., Seo, D. K., Hwang, J., 2011. Study of the Effect of Coal Type and Particle Size on Char-CO_2 Gasification via Gas Analysis. *Energy and Fuels*, 25(11), pp.5044–5054.

Klose, W., Wolki, M., 2005. On the intrinsic reaction rate of biomass char gasification with carbon dioxide and steam. *Fuel*, 84(7-8), pp.885–892.

Koko, M., 2012. A 1-D Simulation Tool for Biomass Co-Firing Development and Application, Co-firing Biomass with coal. Copenhagen. March 27-28.pp.1-29.

Kuo-Chao, L., Keng-Tung, W., Chien-Song, C., Wei-The1, T., 2009. A New Study on Combustion Behavior of Pine Sawdust Characterized by the Weibull Distribution. *Chinese Journal of Chemical Engineering*, 17(5), pp.860-868.

Lahijani, P., Zainal, Z. A., Mohamed, A. R., 2012. Catalytic effect of iron species on CO_2 gasification reactivity of oil palm shell char. *Thermochimica Acta*, (546), pp.24–31.

Le Manquais, K., Snape, C., McRobbie, I., Barker, J., Pellegrini, V., 2009. Comparison of the Combustion Reactivity of TGA and Drop Tube Furnace Chars from a Bituminous Coal. *Energy and Fuels*, 23, pp.4269–4277.

Liu, G., Tate, A. G., Bryant, G. W., Wall, T. F., 2000. Mathematical modeling of coal char reactivity with CO 2 at high pressures and temperatures. *Fuel*, (79), pp.1145–1154.

Liu, G., Niksa, S., 2004. Coal conversion submodels for design applications at elevated pressures. Part II. Char gasification. *Progress in Energy and Combustion Science*, 30(6), pp.679-717.

Liu, H., Kaneko, M., Luo, C., Kato, S., Kojima, T., 2004. Effect of pyrolysis time on the gasification reactivity of char with CO_2 at elevated temperatures. *Fuel*, 83(7-8), pp.1055-1061.

Livingston, W. R., 2012. Recent developments in biomass co-firing in large coal-fired utility. Copenhagen. March, Babcock Energy.

Lu, G. Q., Do, D. D., 1994. Comparison of structural models for high-ash char gasification. *Carbon* , 32(2), pp.247–263.

Maciejewska, A.,Veringa, H., Sander, J., Peteves, S. D., 2006. Of biomass pre-treatment, Institute for Energy European Commission. Institute for Energy, Petten (Netherlands).

Mani, T., Mahinpey, N., Murugan, P., 2011. Reaction kinetics and mass transfer studies of biomass char gasification with CO_2. *Chemical Engineering Science*, 66(1), pp.36-41.

Marbek Resource Consultants Ltd., 2007. A catalogue of renewable energy sources, Durban.

Miles, T. R., Miles Jr, T. R., Baxter, L. L., Jenkins, B. M., Oden, L. L., 1993. Alkali Slagging Problems with Biomass Fuels. *First Biomass Conference of the Americas: Energy, Environment, Agriculture, and Industry*,(1).

Mitsuoka, K., Hayashi, S., Amano, H., Kayahara, K., Sasaoka, E., Uddin, M. A., 2011. Gasification of woody biomass char with CO_2: The catalytic effects of K and Ca species on char gasification reactivity. *Fuel Processing Technology*, 92(1), pp.26-31.

Miura, K., Hashimoto, K., Silveston, P. L., 1989. Factors affecting the reactivity of coal chars during gasification , and indices representing reactivity. *Fuel* , 68, pp.1461-1475.

Moghtaderi, B., Meesri, C. & Wall, T. F., 2004. Pyrolytic characteristics of blended coal and woody biomass. *Fuel*, 83(6), pp.745–750.

Muthuraman, M., Namioka, T. Yoshikawa., K., 2010. A comparative study on co-combustion performance of municipal solid waste and Indonesian coal with high ash Indian coal: A thermogravimetric analysis, *Fuel Processing Technology*.91(5),pp. 550-558.

Njapha, D., 2003. Determination of the kinetic models and associated parameters for the low temperature combustion and gasification of high ash coal chars. *PhD Thesis*. North-West University Potchefstroom, South Africa.

Ochoa, J., Cassanello, M. C., Bonelli, P, R., Cukierman, A. L., 2001. CO_2 gasification of Argentinean coal chars: a kinetic characterization. *Fuel Processing Technology*, 74(3), pp.161-176.

Otero, M., Calvo, L. F., Gil, M. V., Garcia, A. I., Moran, A., et al., 2008. Co-combustion of different sewage sludge and coal: a non-isothermal thermogravimetric kinetic analysis. *Bioresource technology*, 99, pp.6311–9.

Ozawa, T., 1992. Estimation of activation energy by isoconversion methods.*Thermochimica Acta*, 203, pp.159–165.

Please, C. P., McGuinness, M. J., McElwain, D. L. S., 2003. Approximations to the Distributed Activation Energy Model for the Pyrolysis of Various Coals. *Combustion and Flame*, 133, pp.107-117.

Pitt, G. J., 1962. The Kinetics of the Evolution of Volatile Products from Coal. *Fuel*, 41, pp.264-274.

Qi, C., Zhang, J., Lin, X., Liu, Q., Wang, X., 2011. Investigation on Pulverized Coal Combustion Behavior by Non-Isothermic Integral Thermogravimetry Method. *Journal of Iron and Steel Research, International*, 18(8), pp.1–8.

Rafsanjani, H. H., Jamshidi, E., 2008. Kinetic study and mathematical modeling of coal char activation. *Chemical Engineering Journal*, 140(1-3), pp.1–5.

Roberts, D. G., Harris, D. J., 2007. Char gasification in mixtures of CO_2 and H_2O: Competition and inhibition. *Fuel*, 86(17-18), pp.2672-2678.

Roberts, D. G., Hodge, E. M., Harris, D. J., Stubington, J. F., 2010. Kinetics of Char Gasification with CO_2 under Regime II Conditions: Effects of Temperature, Reactant, and Total Pressure. *Energy & Fuels*, 24(10), pp.5300–5308.

Rostami, A. A., Hajalgol, M. R., Wrenn, S. E., 2004. A Biomass Pyrolysis Sub-model for CFD Applications. *Fuel*, 83, pp.1519-1525.

Rotaru, A., Goêa, M., 2009. Computational thermal and kinetic analysis: Complete standard procedure to evaluate the kinetic triplet form non-isothermal data. *Journal of Thermal Analysis and Calorimetry*, 97(2), pp.421-426.

Rotliwala, Y. C., Parikh, P. A., 2011. Thermal degradation of rice-bran with high density polyethylene: A kinetic study. *Korean Journal of Chemical Engineering*, 28(3), pp.788–792.

Sadhukhan, A. K., Gupta, P., Goyal, T., Saha, R. K., 2008. Modelling of pyrolysis of coal-biomass blends using thermogravimetric analysis. *Bioresource technology*, 99(17), pp.8022–6.

Sadhukhan, A. K., Gupta, P., Saha, R. K., 2010. Modelling of combustion characteristics of high ash coal char particles at high pressure: Shrinking reactive core model. *Fuel*, 89(1), pp.162-169.

Sahu, S. G., Sarkar, P., Chakraborty, N., & Adak, a. K. (2010). Thermogravimetric assessment of combustion characteristics of blends of a coal with different biomass chars. *Fuel Processing Technology*, 91(3), 369–378.

Saloojee, F., 2011. Kinetics of pyrolysis and combustion of a South African coal using the distributed. *MSc Dissertation*. University of Witwatersrand. Johannesburg, South Africa.

Scott, S. A., Dennis, J. S., Davidson, J. F., Hayhurst, A. N., 2006(a). An algorithm for determining the kinetics of devolatilisation of complex solid fuels from thermo-gravimetric experiments. *Chemical Engineering Science*, 61(8), pp.2339-2348.

Scott, S. A., Dennis, J. S., Davidson, J. F., Hayhurst, A. N., 2006(b). Thermogravimetric measurements of the kinetics of pyrolysis of dried sewage sludge. *Fuel*, 85(9), pp.1248-1253.

Senneca, O., 2007. Kinetics of pyrolysis, combustion and gasification of three biomass fuels. *Fuel Processing Technology*, 88(1), pp.87-97.

Seo, D. K., Lee, S. K., Kang, W. M., Hwang, J., Yu, T., 2010. Gasification reactivity of biomass chars with CO_2. *Biomass and Bioenergy*, 34(12), pp.1946-1953.

Sima-Ella, E., Yuan, G., Mays, T., 2005. A simple kinetic analysis to determine the intrinsic reactivity of coal chars. *Fuel*, 84(14-15), pp.1920-1925.

Sis, H., 2009. Application of Model-free Methods for Analysis of Combustion Kinetics of Coals with Different Ranks. *Energy Sources, Part A: Recovery, Utilization, and Environmental Effects*, 31(12), pp.1016-1027.

Smith, I. W., Tyler, R. J., 1972. Internal burning of pulverized semi-anthracite: the relation between particle structure and reactivity. *Fuel*, 51(4), pp.312-321.

Spiro, C. L., McKee, D. W., Kosky, P. G., Lamby, E. J., Maylotte, D. H., 1983. Significant parameters in the catalysed CO_2 gasification of coal chars. *Fuel*, 62(3), pp.323-330.

Srivastava, S., Zulfequar, M., Kumar, A., 2010. Study of crystallization kinetics in glassy Se_{100-x} Bi_x using iso-conversional methods. *Journal of Non Oxide Glasses*, 2(2), pp.97-106.

Starink, M. J., 2003. The determination of activation energy from linear heating rate experiments : a comparison of the accuracy of isoconversion methods. *Thermochimica Acta*, 404 (1-2), pp.163-176.

Szekely, J., Evans, J. W., 1970. A structural model for gas-solid reactions with a moving boundary. *Chemical Engineering Science*, 25(6), pp.1091-1107.

The Biomass Corporation., 2008. Why Biomass. Available at *www.biomasscorp.com*, As assessed on 20/06/2012.

Thybaut, J. W., Marin, G. B., o date. Catalysis,Testing of catalytic processes. *Encyclopedia of life support systems*.

Tiwari, P., Deo, M., 2012. Detailed Kinetic Analysis of Oil Shale Pyrolysis TGA Data. *AIChE Journal*, 58(2), pp.505-515.

Turkdogan, E. T., Koump V., Vinters J. V., Perzak T. F.,1968. Rate of oxidation of graphite in carborn dioxide. *Carbon*,6, pp.101-107.

Umeki, K., Roh, S., Min, T., Namioka, T., Yoshikawa, K., 2010. A simple expression for the apparent reaction rate of large wood char gasification with steam. *Bioresource Technology*,101(11), pp.4187-4192.

Vamvuka, D., Karouki, E., Sfakiotakis, S., 2011. Gasification of waste biomass chars by carbon dioxide via thermo-gravimetry. Part I: Effect of mineral matter. *Fuel*, 90(3), pp.1120-1127.

Vittee, T., 2012. Determination of Kinetics of Char Reactivity with Carbon Dioxide Using Thermogravimetry and the Distributed Activation Energy Model. MSc Dissertation. University of Witwatersrand. Johannesburg, South Africa.

Vuthaluru, H., 2004. Thermal behaviour of coal/biomass blends during co-pyrolysis. *Fuel Processing Technology*, 85(2-3), pp.141–155.

Vyazovkin, S., 1997. ADVANCED ISOCONVERSIONAL METHOD Non-linear iso-conversional method. *Journal of Thermal Analysis*, 49, pp.1493-1499.

Vyazovkin, S., 2008. Handbook of Thermal Analysis and Calorimetry, Isoconversional kinetics. Chapter 13, pp. 503-537.

Wagner, N. J., Coertzen, M., Matjie, R. H., van Dyk, J. C., 2008. Coal Gasification, Applied coal petrography: The role of petrograhy in coal utilization . Chapter 5.pp.119-144.

Walker, P. L., Vastola, F. J., Hart, P. J., 1967. Tracer studies on carbon-oxygen reaction. *Fundamentals of gas-surface interactions*, 18,pp. 307-315

Williams, A., Pourkashanian, M., Jones, J. M., 2001. Combustion of pulverised coal and biomass. *Progress in Energy and Combustion Science*, 27(6), pp.587–610.

Wornat, M. J., Hurt, R. H., Davis, K. A., Yang, N. Y. C., 1996. Single-particle combustion of two biomass chars. *Twenty-Sixth Symposium (International) on Combustion/ The Combustion Institute*, pp.3075–3083.

Yuan, S., Chen, X., Li, J., Wang, F., 2011. CO_2 Gasification Kinetics of Biomass Char Derived from High-Temperature Rapid Pyrolysis. *Energy and fuels*, pp.2314-2321.

Zhang, Y., Ashizawa, M., Kajitani, A. S., Miura, A. K., 2008. Proposal of a semi-empirical kinetic model to reconcile with gasification reactivity profiles of biomass chars. *Fuel*, 87(4-5), pp.475–481.

Zhu, W., Song, W., Lin, W., 2008. Catalytic gasification of char from co-pyrolysis of coal and biomass. *Fuel Processing Technology*, 89(9), pp.890-896.

Zolin, A., 2001. Reactivity of solid fuels. *PhD Dissertation*, Department of Chemical Engineering, Technical University of Denmark, Denmark.

Zou, J. H., Zhou, Z. J., Wang, F. C., Zhang, W., Dai, Z. H., Liu, H. F., Yu, Z. H., 2007. Modeling reaction kinetics of petroleum coke gasification with CO_2. *Chemical Engineering and Processing: Process Intensification*, 46(7), pp.630-636.

10.APPENDICES

10.1. APPENDIX A: THE MAT LAB CODE

The Mat lab code used in this study is outlined in this appendix. The first order reaction model code is outlined first, followed by the RPM code at constant heating rates. The major changes applied to the model to allow the simulation and use of instantaneous heating rates is explained last.

The first order reaction model constant heating rate code.

The first order reaction model DAE based algorithm code is made up of a set of 9 scripts of code. The first four scripts are basic scripts that were used together with the RPM code as well. These are namely, the 'AEerror2','chi', 'term' and 'rsquared' scripts. The scripts of code are displayed on below.

The AEerror2 code serves to evaluate Equation [2-27] outlined in Section 2.5. Using this code the activation energy is evaluated by minimizing the differences between the right and left hand side of the equation. The code evaluates the difference between the equation sides and reports it as an error value which was in turn minimized by the FMINBND function for the evaluation of the activation energy at varying points along the conversion.

```
function error = AEerror2(E,T1,T2,T0,B1,B2)
%This uses the EXPINT function to find the integral from X to inf of Exp(-
t)/t dt

T1;
T2;
T0=T0;
E;
R=8.314;

first=T0*exp(-E*1000/(R*T0));
aa=E*1000/(R*T0);bb=exp(-aa)/aa;
second=(E*1000/R)*EXPINT(aa);
third=T1*exp(-E*1000/(R*T1));
cc=E*1000/(R*T1);dd=exp(-cc)/cc;
fourth=(E*1000/R)*EXPINT(cc);

fifth=first;
```

```
sixth=second;

seventh=T2*exp(-E*1000/(R*T2));
ee=E*1000/(R*T2);ff=exp(-ee)/ee;
eighth=(E*1000/R)*EXPINT(ee);

%LHS of EQ 2-23
ls=(1/B1)*(first-second-third+fourth);

%RHS of EQ 2-23
rs=(1/B2)*(fifth-sixth-seventh+eighth);
error = sqrt((1-rs/ls)^2);
```

The chi script calculates the Ψ_i values by evaluating the exponential of Equation [2-27].

```
function error = chi(E,PE,T1,T0,B1,B2);
%This uses the approximation for integral from X to inf of exp(-t)/t dt
T1;
T0=T0;
E;%;
A=PE;
R=8.314;

%% Temperature Integral
%terms in Equation 2-27

first=T0*exp(-E*1000/(R*T0));
aa=E*1000/(R*T0);bb=exp(-aa)/aa;
second=(E*1000/R)*EXPINT(aa);
third=T1*exp(-E*1000/(R*T1));
cc=E*1000/(R*T1);dd=exp(-cc)/cc;
fourth=(E*1000/R)*EXPINT(cc);

%% Original Ln(Chi) Expression
%RHS of EQ 2-22
rhs=(A/B1)*(first-second-third+fourth);
error = exp(rhs);
```

The 'term' script of code is a simple function of the exponential term $(\frac{-E}{RT})$.

```
function y=term(T,E)

y=exp(-E*1000./(8.314*T));
```

The 'rsquared' code is used for the evaluation of the statistical parameters that measure the quality of fit (R^2 and RMS error values).

```
function c=rsquared(fit, expe)
global act_pred
expdash(1:length(expe),:)=mean(fit);

act_pred=sum((expe-fit).^2);
act_mean=sum((expe-expdash).^2);
rsqrd=1-(act_pred/act_mean);
difference= ((expe-fit).^2);
rms=sqrt(sum(difference)/length(difference));
error=rms;

c=[rsqrd error];
```

The rest of the code discussed in this section is used only with the first order constant/programmed heating rate algorithm. This code contains the scripts, 'findfirst', 'funcfirst', 'firstmodel', 'Aifirst' and 'fiterror'.

The ‘Aifirst’ script evaluates the pre-exponential factor according to Equation [2-27].

```
function y = Aifirst(E,T1,T2,T0,B1,B2, x)


%% terms in Equation 2-27

first=T0*exp(-E*1000/(R*T0));
aa=E*1000/(R*T0);
bb=exp(-aa)/aa;
second=(E*1000/R)*expint(aa);
third=T1*exp(-E*1000/(R*T1));
cc=E*1000/(R*T1);
dd=exp(-cc)/cc;
fourth=(E*1000/R)*expint(cc);

Ai=-B1/(first-second-third+fourth);

y=Ai;
```

The ‘firstmodel’ script allows the simulation of the first order reaction model conversion vs. Temperature data for a given set of kinetics.

```
function c=firstmodel(f0,E,PE,b,T0,Tup,m)

B=b/60;%K/sec

s=size(E');
nn=s(:,1);
T=linspace(T0,Tup,m);
```

```
for i=1:m
    for j=1:nn
        term1(j)=quad(@term,T0,T(i),[],[],E(j));
        chi2(i,j)=chi(E(j),PE(j),T(i),T0,B,B);
        chi2(i,nn+1)=1;
    end
end
size(chi2)
fi=chi2*f0;
hold on

%% Plots
plot(T', fi,'ro');
%First Derivative Plot
hold on
x=T';y=100.*fi;
deriv=-diff(y)./diff(x);
x=x(2:length(x));
plot(x,deriv,'k.')
c=[T' fi];
```

The ‘funcfirst’ function evaluates the actual kinetics by application of the algorithm. The code uses the conversion vs. Temperature data, as well as the program heating rates and the ‘AEerro2’ and ‘Aifirst’ scripts of code to evaluate the set of kinetics for the candidate reactions taking place during the conversion. In the ‘funcfirst’ code then calculates the Ψ matrix using the ‘chi’ script. Using the lsqnonneg function, the matrix is inverted and the f_0 column evaluated. The non-zero values in the f_0 column then correspond to the actual conversion kinetics of the non-spurious reactions identified.

```
function c = funcfirst(T1,T2,B,Tr,xx,B1,B2,T0);

%% Constant Known terms and Settings
%global phi

warning off
options2=optimset('TolX',1e-6,'LevenbergMarquardt','off');
n=length(T1);

%% Chi Check

for i=1:n
    E(i)=FMINBND('AEerror2',0,800,options2,T1(i),T2(i),T0,B1,B2);
    PE(i)=Aifirst(E(i),T1(i),T2(i),T0,B1,B2); %added x into input for Ai2.m
    PE(1)=0.0000001;
    chi_check20(i)=chi(E(i),PE(i),T1(i),T0,B1,B2);
    chi_check100(i)=chi(E(i),PE(i),T2(i),T0,B1,B2);
end
check=[chi_check20' chi_check100'];
a=isfinite(PE');
PE=PE(a);
E=E(a);
```

```
q=length(Tr);

%% reduces no of data points in TGA set
npoints=q;
nn=length(E);
Tr1i=Tr;

%% Calculation of F0 - Scott eq. 9
for i=1:npoints
    for j=1:nn
        term1(j)=quad(@term,T0,Tr1i(i),[],[],E(j));
         chi2(i,j)=chi(E(j),PE(j),Tr(i),T0,B,B);
        chi2(i,nn+1)=1;
    end
end

%%
options3=optimset('TolX',10);
f0=lsqnonneg(chi2,xx);
[length(f0) length(E') length(PE')];
E(n+1)=0;PE(n+1)=0;
E';

c=[f0 E' PE'];
```

The ‘fiterror’ code serves to prepare the experimental data into suitable columns of temperature and conversion for application in the ‘funcfirst’ code. The ‘fiterror’ code also analyses the kinetic triplet output from the ‘funcfirst’ code and provides a well formatted kinetic triplet result.

```
function error = fiterror(data1,data2,nrxns,rnTGA,nTGA,b1,b2,nexp)
global kinetics triplet fitdata1
format SHORT G %Best number display format for viewing answers
B1=b1./60;%1st heating rate K/sec
B2=b2./60;%2nd heating rate K/sec
R=8.314; %j/molK

%% Generating TGA points
TT1=data1(:,1);
x1=data1(:,2);

TT2=data2(:,1);
x2=data2(:,2);

%% reducing TGA points
Tr1=linspace(TT1(1),TT1(length(TT1)),nTGA)';
Tr2=linspace(TT2(1),TT2(length(TT2)),nTGA)';

Xr1=interp1q(TT1,x1,Tr1);
Xr2=interp1q(TT2,x2,Tr2);
TT1=Tr1;
TT2=Tr2;
```

```
x1=Xr1;
x2=Xr2;

x1(length(x1))=x1(length(x1)-1);
X=linspace(x1(1),x1(end),nrxns)';

T1=interp1q(flipud(x1),flipud(TT1),X);
T2=interp1q(flipud(x2),flipud(TT2),X);

%% Generating TGA points with reduced number of points

Xtga=x2;
Tr1=TT2;
b2=B2;
T0=Tr1(1);
%% Using Simulated Data to Calculate Triplet
data3=funcfirst(T1,T2,b2,Tr1,Xtga,B1,B2,T0);

f0p=data3(:,1);Ep=data3(:,2);PEp=data3(:,3);
I=find(f0p>=(0.00));
k=find(f0p>=(0.05));
l=length(f0p)-1;

f0p=f0p(I);
Epp=Ep(I)';
PEpp=PEp(I)';
Epp(k)';
PEpp(k)';
Ep=Epp(1:(end-1));
PEp=PEpp(1:(end-1));
m=nexp;

ff=f0p(1:nrxns);
kinetics=[ff Ep' PEp' [1:1:nrxns]'];
nonsp= find(kinetics(:,1)>0.001);
E_found=[kinetics(nonsp,1) kinetics(nonsp,2)];
A_found=[kinetics(nonsp,1) kinetics(nonsp,3)];
triplet=[ E_found A_found(:,2) kinetics(nonsp,4)];

error=triplet
```

The ‘findfirst’ code runs the whole algorithm, by commanding the ‘fiterror’ function. The code then simulates conversions at the three heating rates using the algorithm kinetics and compares these to the experimental data using the ‘rsquared’ coded function. The ’findfirst’ code gives an output of the kinetic triplet determined, the R^2 and RMS error values, as well as the DTG and conversion vs. Temperature algorithm plots and experimental curves.

```
function c=findfirst(data1, data2, data3,b1,b2,b3,nrxns,m,ntga,rntga)

format short g
global triplet fit error
```

```
error=fiterror(data1,data2,nrxns,rntga,ntga,b1,b2,m);
expe=data3;

fit=firstmodel([(triplet(:,1))' 0]', triplet(:,2)', triplet(:,3)', b3,
expe(1,1), expe(200,1), m);
Arate=firstmodel([(triplet(:,1))' 0]', triplet(:,2)', triplet(:,3)', b2,
expe(1,1), expe(200,1), m);
fit1=firstmodel([(triplet(:,1))' 0]', triplet(:,2)', triplet(:,3)', b1,
data1(1,1), data1(200,1), m);
fit2=firstmodel([(triplet(:,1))' 0]', triplet(:,2)', triplet(:,3)', b2,
data2(1,1), data2(200,1), m);
close all
hold off
plot(Arate(:,1), Arate(:,2), 'ro');

xlim([973 1423]);
ylim([0 1])

% Create xlabel
xlabel('Temperature (K)','FontWeight','demi','FontSize',12);

% Create ylabel
ylabel('Mass Fraction Remaining (1-x)','FontWeight','demi','FontSize',12);
 hold on

plot(fit(:,1),fit(:,2),'ko','LineWidth',1.0,'MarkerSize',6.0,
'MarkerEdgeColor',[0 0 0]);
plot(fit1(:,1),fit1(:,2),'co','LineWidth',1.0,'MarkerSize',6.0,
'MarkerEdgeColor',[0 0 0]);
plot(fit2(:,1),fit2(:,2),'bo','LineWidth',1.0,'MarkerSize',6.0,
'MarkerEdgeColor',[0 0 0]);
plot(data1(:,1), data1(:,2), 'g.')
x=data1(:,1);y=100.*data1(:,2);
xr=linspace(x(1),x(end),50);
yr=spline(x,y,xr);
deriv=-diff(yr)./diff(xr);
xr=xr(2:length(xr));
plot(xr,deriv,'g')

plot(data2(:,1), data2(:,2), 'c.')
x=data2(:,1);y=100.*data2(:,2);
xr=linspace(x(1),x(end),50);
yr=spline(x,y,xr);
 deriv=-diff(yr)./diff(xr);
 xr=xr(2:length(xr));
 plot(xr,deriv,'c')

plot(data3(:,1), data3(:,2), 'b.')
x=data3(:,1);y=100.*data3(:,2);
xr=linspace(x(1),x(end),50);
yr=spline(x,y,xr);
deriv=-diff(yr)./diff(xr);
xr=xr(2:length(xr));
plot(xr,deriv,'b')
```

```
rsqrd=rsquared(fit(:,2), expe(:,2));
rsqrd1=rsquared(fit1(:,2), data1(:,2));
rsqrd2=rsquared(fit2(:,2), data2(:,2));

error=((rsqrd+rsqrd1+rsqrd2)./3);

triplet
c=error;
```

The RPM constant heating rate code

The RPM constant heating rate code is presented below. The code consists of nine scripted functions. The first three are used in the first order code and have since been presented. The last six are namely, 'Ai3', 'rpmodel', 'findphi', 'phicalc2', 'phierror21' and 'funcrpm'.

The Ai3 code evaluates the pre-exponential factors of the candidate reactions according to the RPM function.

```
function y = Ai3(E,T1,T0,B1)
%NOTE: B1 must be input in K/sec when using it as a stand-alone


%% Constant Known terms
T0=T0;
R=8.314; %j/molK
first=T0*exp(-E*1000/(R*T0));

aa=E*1000/(R*T0);
bb=exp(-aa)/aa;

second=(E*1000/R)*expint(aa);
third=T1*exp(-E*1000/(R*T1));

cc=E*1000/(R*T1);
dd=exp(-cc)/cc;

fourth=(E*1000/R)*expint(cc);

Ai= -0.8797*B1/(first-second-third+fourth);

y=Ai;
```

The ‘rpmodel’ code simulates the reaction progression using a set of specified kinetics according to the RPM.

```
c=rpmodel(f0,E,PE,b,T0,Tup,m,phi)

B=b/60;%K/sec
s=size(E');
nn=s(:,1);

 T=linspace(T0,Tup,m);
for i=1:m
    for j=1:nn
        term1(j)=quad(@term,T0,T(i),[],[],E(j));
        chi2(i,j)=exp((PE(j)/B)*(term1(j)));
        chi2(i,nn+1)=1;
        chinew(i,j)=exp((1-(phi/2*(log(chi2(i,j))+2/phi))^2)/phi);
        chinew(i,nn+1)=1;
    end
end
size(chinew)
fi=chinew*f0;

I=find(fi<=(f0(end)));
c=[T' fi];

hold on

%% Plots
plot(c(:,1), c(:,2),'ro')
%First Derivative Plot

x=c(:,1);y=100.*c(:,2);
deriv=-diff(y)./diff(x);
x=x(2:length(x));
 plot(x,deriv,':')
```

Similar to the funcfirst code, the funcrpm code evaluates the actual kinetics by application of the RPM adapted algorithm. The code uses the conversion vs. Temperature data, as well as the program heating rates and the 'AEerro2' and 'Ai3' scripts of code to evaluate the set of kinetics for the candidate reactions taking place during the conversion. In the 'funcrpm' code calculates the Ψ matrix. Using the lsqnonneg function, the matrix is inverted and the f_0 column evaluated. The non-zero values in the f_0 column then correspond to the actual conversion kinetics of the non-spurious reactions identified.

```
function c = funcrpm(T1,T2,B,Tr,xx,B1,B2,T0,phi);

%% Constant Known terms and Settings
warning off
options2=optimset('TolX',1e-6,'LevenbergMarquardt','off');
n=length(T1);
```

```
%% Chi Check

for i=1:n
    E(i)=FMINBND('AEerror2',0,800,options2,T1(i),T2(i),T0,B1,B2);
    PE(i)=Ai3(E(i),T1(i),T2(i),T0,B1,B2); %added x into input for Ai2.m
    PE(1)=0.0000001;
    chi_check20(i)=chi(E(i),PE(i),T1(i),T0,B,B2);
    chi_check100(i)=chi(E(i),PE(i),T2(i),T0,B,B2);
end
check=[chi_check20' chi_check100'];

a=isfinite(PE');
PE=PE(a);
E=E(a);

q=length(Tr);

%% reduces no of data points in TGA set
npoints=q;
nn=length(E);

Tr1i=Tr;

%% Calculation of F0
for i=1:npoints
    for j=1:nn
        term1(j)=quad(@term,T0,Tr1i(i),[],[],E(j));
        chi2(i,j)=exp((PE(j)/B)*(term1(j)));
%Lines from rpmodel.m
        chi2(i,nn+1)=1;
%Lines from rpmodel.m
        chirpm(i,j)=exp((1-(phi/2*(log(chi2(i,j))+2/phi))^2)/phi); % this is
the analogous expression of 1-x... chi??   %Lines from rpmodel.m
        chirpm(i,nn+1)=1;
    end
end

options3=optimset('TolX',10);


f0=lsqnonneg(chirpm,xx);

[length(f0) length(E') length(PE')];

E(n+1)=0;PE(n+1)=0;
E';

c=[f0 E' PE'];
```

The ‘phierror 21’ code is very similar to the ‘fiterror’ code discussed for the first order reaction model. The code prepares the experimental data for algorithm application and calls upon the funcrpm code for kinetics determination, (i.e. E, A, and f_0). The ‘phierror21’ code then evaluates the error values between the simulated algorithm plots and the experimental data curves. The ‘phierror21’ code therefore gives an output of this error value which is in turn minimized by the ‘phicalc’ function for the determination of the structural parameter.

```
function error = phierror21(phi,data1,data2,nrxns,rnTGA,nTGA,b1,b2,nexp)
global kinetics triplet fitdata1

format SHORT G %Best number display format for viewing answers

B1=b1/60;%1st heating rate K/sec
B2=b2/60;%2nd heating rate K/sec
R=8.314; %j/molK

%% Generating TGA points
TT1=data1(:,1);
x1=data1(:,2);

TT2=data2(:,1);
x2=data2(:,2);

%% reducing TGA points
Tr1=linspace(TT1(1),TT1(length(TT1)),nTGA)';
Tr2=linspace(TT2(1),TT2(length(TT2)),nTGA)';

Xr1=interp1q(TT1,x1,Tr1);
Xr2=interp1q(TT2,x2,Tr2);

TT1=Tr1;
TT2=Tr2;
x1=Xr1;
x2=Xr2;
x1(length(x1))=x1(length(x1)-1);

X=linspace(x1(1),x1(end),nrxns)';
% X=linspace(0.99999999,x1(end),nrxns)'; ***Original working line***

T1=interp1q(flipud(x1),flipud(TT1),X);
T2=interp1q(flipud(x2),flipud(TT2),X);

%% Generating TGA points with reduced number of points
Xtga=x2;
Tr1=TT2;

T0=Tr1(1);
%% Using Simulated Data to Calculate Triplet
```

```
data3=funcrpm(T1,T2,B2,Tr1,Xtga,B1,B2,T0,phi);


f0p=data3(:,1);Ep=data3(:,2);PEp=data3(:,3);

I=find(f0p>=(0.00));
k=find(f0p>=(0.05));

l=length(f0p)-1;

f0p=f0p(I);
Epp=Ep(I)';
PEpp=PEp(I)';
Epp(k)';
PEpp(k)';
Ep=Epp(1:(end-1));
PEp=PEpp(1:(end-1));
m=nexp;

ff=f0p(1:nrxns);
kinetics=[ff Ep' PEp' [1:1:nrxns]'];
nonsp= find(kinetics(:,1)>0.001);
E_found=[kinetics(nonsp,1) kinetics(nonsp,2)];
A_found=[kinetics(nonsp,1) kinetics(nonsp,3)];
triplet=[ E_found A_found(:,2) kinetics(nonsp,4)];

%% Sangtong-Ngam Method Sigma Curve Fit by Least Squares
Tup=Tr1(end);
fitdata1=rpmodel(f0p,Ep,PEp,b2,T0,Tup,m,phi);

TT1p=fitdata1(:,1);
x1p=fitdata1(:,2);
xexp=x2;
length(xexp);
length(x1p);
hold on

difference= (x1p-xexp).^2;
square=sqrt(difference/length(difference));

error=sum(square)
```

The ‘phicalc2’ code is unique to the RPM adapted algorithm and is used for the evaluation of the structural parameter. A possible range of values is specified for the structural parameter. The code uses the range to identify a suitable value by reducing the error in the differences between the simulated algorithm determined kinetics plots and the experimental data at a given heating rate. This is carried out by minimizing the ‘phierror2’ function within the specified boundaries.

```
function d = phicalc2(data1, data2, nrxns,rnTGA,nTGA,b1,b2,nexp)

options2=optimset('TolX',1e-5,'LevenbergMarquardt','off');

phi=fminbnd('phierror2',1,30,options2,data1,data2,nrxns,rnTGA,nTGA,b1,b2,nexp
);


d=phi;
```

The ‘findphi’ code runs the whole RPM adapted algorithm, by calling upon the ‘phicalc2’ function. The code then simulates conversions at the three heating rates using the algorithm kinetics and compares these to the experimental data using the ‘rsquared’ coded function. The ’findfirst’ code gives an output of the RPM kinetics determined, the R^2 and RMS error values, as well as the DTG and conversion vs. temperature algorithm plots and experimental curves.

The instantaneous heating rate codes:

The major developments on the DAE based model codes was on the simulation codes ‘rpmodel’ and ‘firstmodel’. The models were edited to accept data consisting of three columns, conversion, temperature and heating rate. The rest of the code was then corrected to make use of a set of values of the heating rate during kinetics evaluation, instead of a single value.

The ‘rpmodel1’ was used for data simulation at a specified set of kinetics and instantaneous heating rates.

```
function c=rpmodel1(f0,E,PE,m,data)

T=data(:,1)
B=data(:,3)./60
s=size(E');
nn=s(:,1);
T0=T(1)



for i=1:m
    for j=1:nn
        term1(j)=quad(@term,T0,T(i),[],[],E(j));
        chi2(i,j)=exp((PE(j)/B(i))*(term1(j)));%note: it is NOT -A/B*I(T),
but +A/B*I(T) ****WINNER***
        chi2(i,nn+1)=1;
        chi2(i,j)=chi(E(j),PE(j),T(i),T0,B(i),B);
        chi2(i,nn+1)=1;
    end

I=find(fi<=(f0(end)));


c=[T fi];

hold on

%% Plots
plot(c(:,1), c(:,2),'ro')
%First Derivative Plot
x=c(:,1);y=100.*c(:,2);
deriv=-diff(y)./diff(x);
x=x(2:length(x));
 plot(x,deriv,':')
```

The ‘firstmodel1’ code was in turn used for the simulation of conversion data at a given set of the kinetic triplet and a corresponding set of instantaneous heating rates.

```
function c=rpmodel1(f0,E,PE,m,data)

T=data(:,1)
B=data(:,3)./60
s=size(E');
nn=s(:,1);
T0=T(1)

for i=1:m
    for j=1:nn
        term1(j)=quad(@term,T0,T(i),[],[],E(j));
        chi2(i,j)=exp((PE(j)/B(i))*(term1(j)));
        chi2(i,nn+1)=1;
        chi2(i,j)=chi(E(j),PE(j),T(i),T0,B(i),B);
        chi2(i,nn+1)=1;
    end
end

size(chi2);
fi=chi2*f0;
for i=1:(length(fi)-1)
    if fi(i+1)> fi(i)
         fi(i+1)=0;

    else
        fi(i+1)=fi(i+1);
    if fi(i+1)<=0
         fi(i+1)=0;

          if fi(i+1)== NaN
         fi(i+1)=0;

    else
        fi(i+1)=fi(i+1);
          end
    end

    end
end

I=find(fi<=(f0(end)));

c=[T fi];

hold on

%% Plots
plot(c(:,1), c(:,2),'ro')
%First Derivative Plot

x=c(:,1);y=100.*c(:,2);
```

```
deriv=-diff(y)./diff(x);
x=x(2:length(x));
 plot(x,deriv,':')
```

10.2. APPENDIX B: TGA SEQUENCES

This appendix outlines the sequences used to conduct the thermo-gravimetric analysis on the TA instruments TGA. The char production sequence is detailed first, followed by the combustion and gasification sequences.

Char Production

TA Instruments Thermal Analysis -- DSC-TGA Standard

Method Log:

i. Select Gas: 1
ii. Flow rate 70.0 ml/min
iii. Ramp 20.00°C/min to 1250.00°C
iv. Select Gas: 1
v. Flow rate 40.0 ml/min
vi. Air cool: On
vii. Equilibrate at 700.00°C
viii. Air cool: Off
ix. Isothermal for 15.00 min
x. Equilibrate at 30^0C

The method log outlined provides the sequential steps undergone by the TGA during the char formation stage. It is noted that the gases 1 and 2 represent N_2 and air respectively. After the chars were prepared, the char samples were reweighed and distributed to cover the base of the crucibles in preparation for the gasification and combustion experiments. These sequences are outlined as follows:

Non-Isothermal Combustion

TA Instruments Thermal Analysis -- DSC-TGA Standard

Method Log:

i. Select Gas: 1
ii. Flow rate 70ml/min
iii. Equilibrate at 30^0C
iv. Select Gas: 2
v. Flow rate 70ml/min
vi. Isothermal for 1.00 min
vii. Data storage: On
viii. Ramp 8.00°C/min to 750.00°C
ix. Isothermal for 1.00 min
x. Data storage: Off
xi. Select Gas: 1
xii. Flow rate 70.0 mL/min
xiii. Equilibrate at 30^0C

Non-Isothermal gasification

TA Instruments Thermal Analysis -- DSC-TGA Standard

Method Log:

i. Select Gas: 1
ii. Flow rate 70ml/min
iii. Equilibrate at 30^0C
iv. Select Gas: 1
v. Flow rate 5ml/min
vi. External event : On
vii. Isothermal for 1.00 min
viii. Data storage: On
ix. Ramp 8.00°C/min to 750.00°C
x. Isothermal for 1.00 min
xi. Data storage: Off
xii. External event: Off
xiii. Select Gas: 1

xiv. Flow rate 70.0 mL/min

xv. Equilibrate at 30^0C

For the gasification tests, CO_2 was used. The CO_2 was accessed into the reaction chamber from an external flow meter which was permanently set at a volumetric flow rate of 65ml/min. The external event step opens up the valve that allows the reactive gas to flow into the TGA furnace. The isothermal gasification sequence is outlined below:

Isothermal gasification

TA Instruments Thermal Analysis -- DSC-TGA Standard
Method Log

i. Select Gas: 1

ii. Flow rate 70ml/min

iii. Equilibrate at 995^0C

iv. Select Gas: 1

v. Flow rate 5ml/min

vi. External event : On

vii. Data storage: On

viii. Isothermal for 100.00 min

ix. Data storage: Off

x. External event: Off

xi. Select Gas: 1

xii. Flow rate 70.0 mL/min

xiii. Equilibrate at 30^0C

For the isothermal analysis, the sample was equilibrated at the reaction temperature whilst in inert atmosphere to avoid the reaction commencing at lower temperatures. When the reaction temperature was reached, the reactive gas was switched on and the reaction commences. At the end of each test, the TGA was purged with N_2 gas flow whilst the equipment cools down to room temperature.

10.3. APPENDIX C: THERMO-GRAVIMETRIC ANALYSIS RESULTS

10.3.1. Combustion Analysis

Below are the detailed thermo-gravimetric analysis results obtained during the combustion tests.

Coal Char Combustion

The coal char combustion analysis results are already outlined in Chapter 7. The variation in heating rate during the combustion reaction is displayed on Figure 10-1.

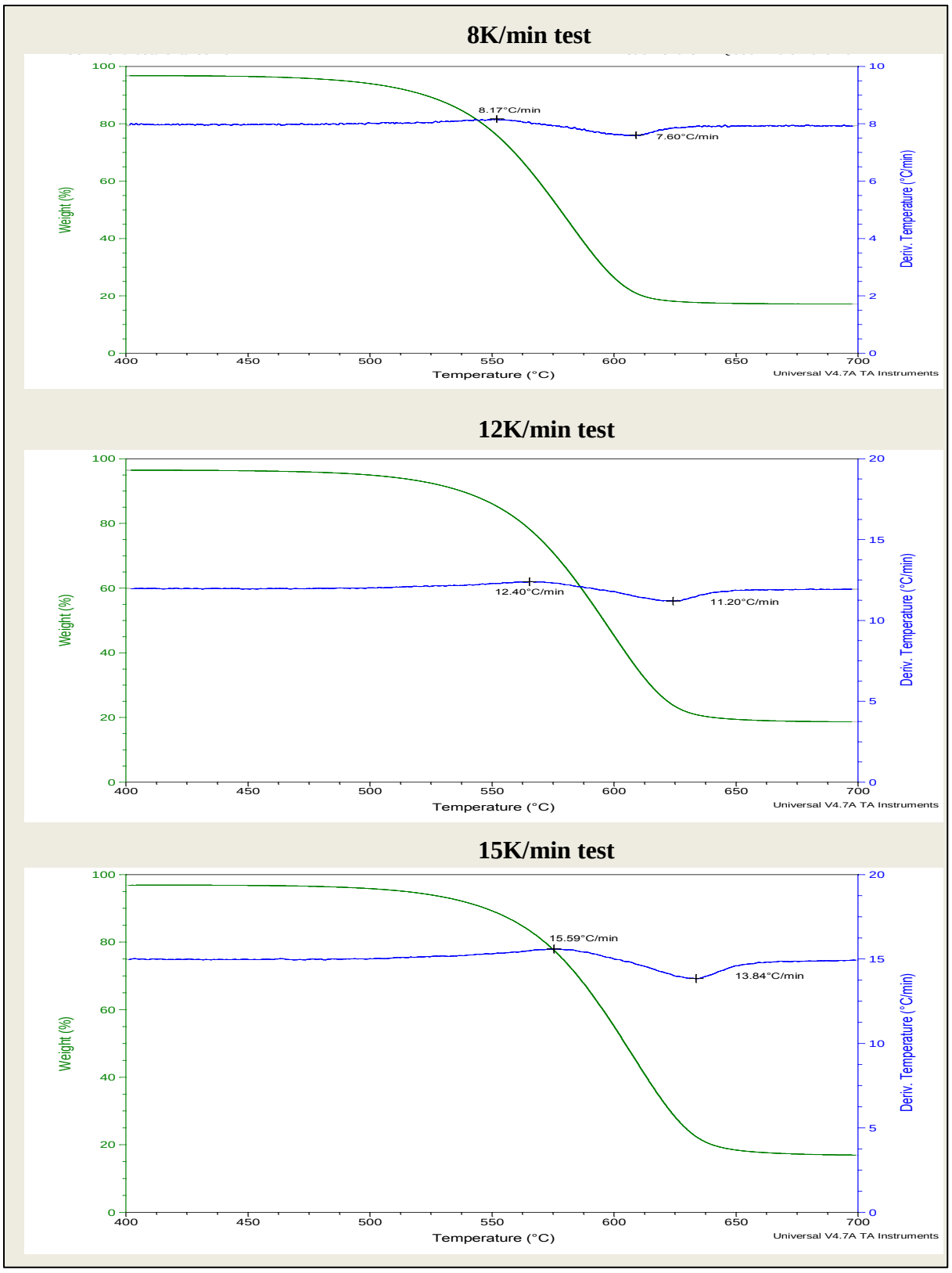

Figure A10-1: Heating rate variations during coal char combustion

Grass Char Combustion

The grass char combustion results are displayed in Figures 10-2 to 10-4. The Arrhenius plot is displayed on Figure 10-2. Even though a change in slope is observed, the change in gradient denotes an increase in E at higher temperatures as observed in Section 5. It was therefore concluded that the reaction is taking place within the kinetic regime. However, instead of two reactions being identified during pine char combustion as indicated by the Arrhenius plot, only one reaction was obtained using the DAE based model and averaging out the kinetics.

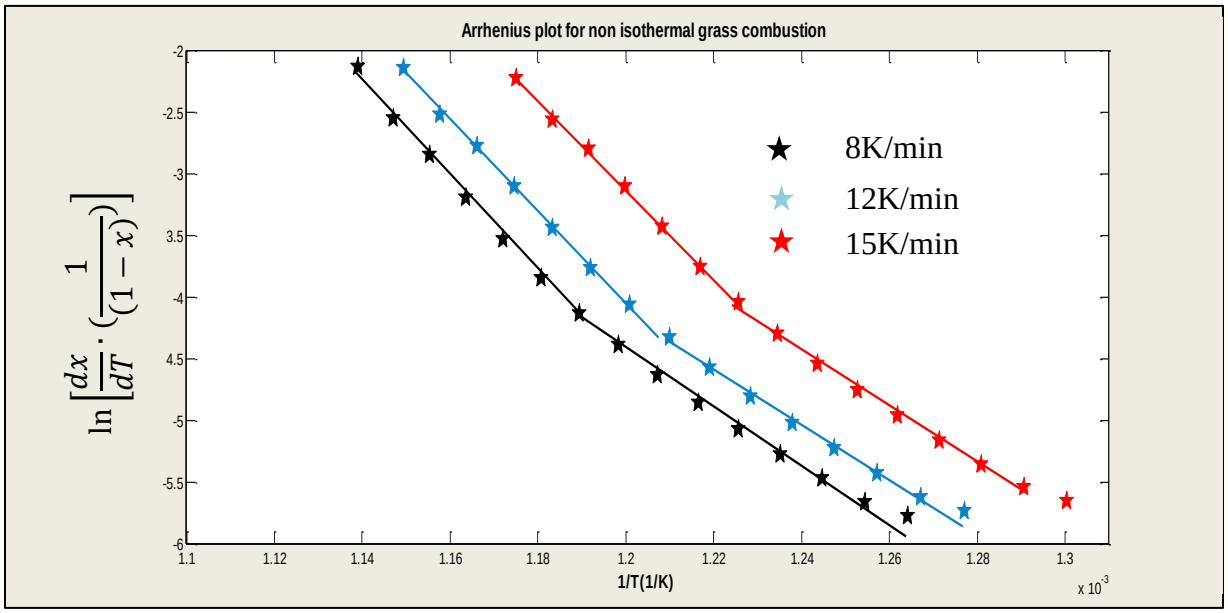

Figure A10-2: Grass char combustion Arrhenius plot

Table A10-1: Grass char combustion model evaluation.

Plot	Heating rate used (K/min)			First order		RPM	
	E calculation	**A calculation**	***φ* Calculation**	**Const B R^2 and RMS**	**Var B R^2 and RMS**	**Const B R^2 and RMS**	**Var B R^2 and RMS**
i	8 ,12	8	12	0.98557 0.0514	0.98845 0.0453	0.99952 0.0094	0.99984 0.0054
ii	8,15	8	15	0.98631 0.0501	0.99039 0.0420	0.99959 0.0086	0.99989 0.0045
iii	12,15	12	8	0.98759 0.0477	0.99245 0.0381	0.99912 0.0110	0.99976 0.0055
iv	12,8	12	15	0.98557 0.0514	0.98843 0.0453	0.9995 0.0094	0.99981 0.0038
v	15,8	15	12	0.98631 0.0501	0.99032 0.0422	0.99936 0.0102	0.99986 0.0059
vi	15,12	15	8	0.98758 0.0477	0.99258 0.0378	0.99948 0.0088	0.99984 0.0054
Average model accuracy				0.98649 0.0497	0.99044 0.0418	0.99943 0.0096	0.99983 0.0051

From the model evaluation above, the RPM adapted DAE based instantaneous model was evaluated as the most accurate model grass char combustion modelling. This model was then applied onto the experimental data and the graphical results and kinetics are displayed on Figure 10-3 and Table 10-2.

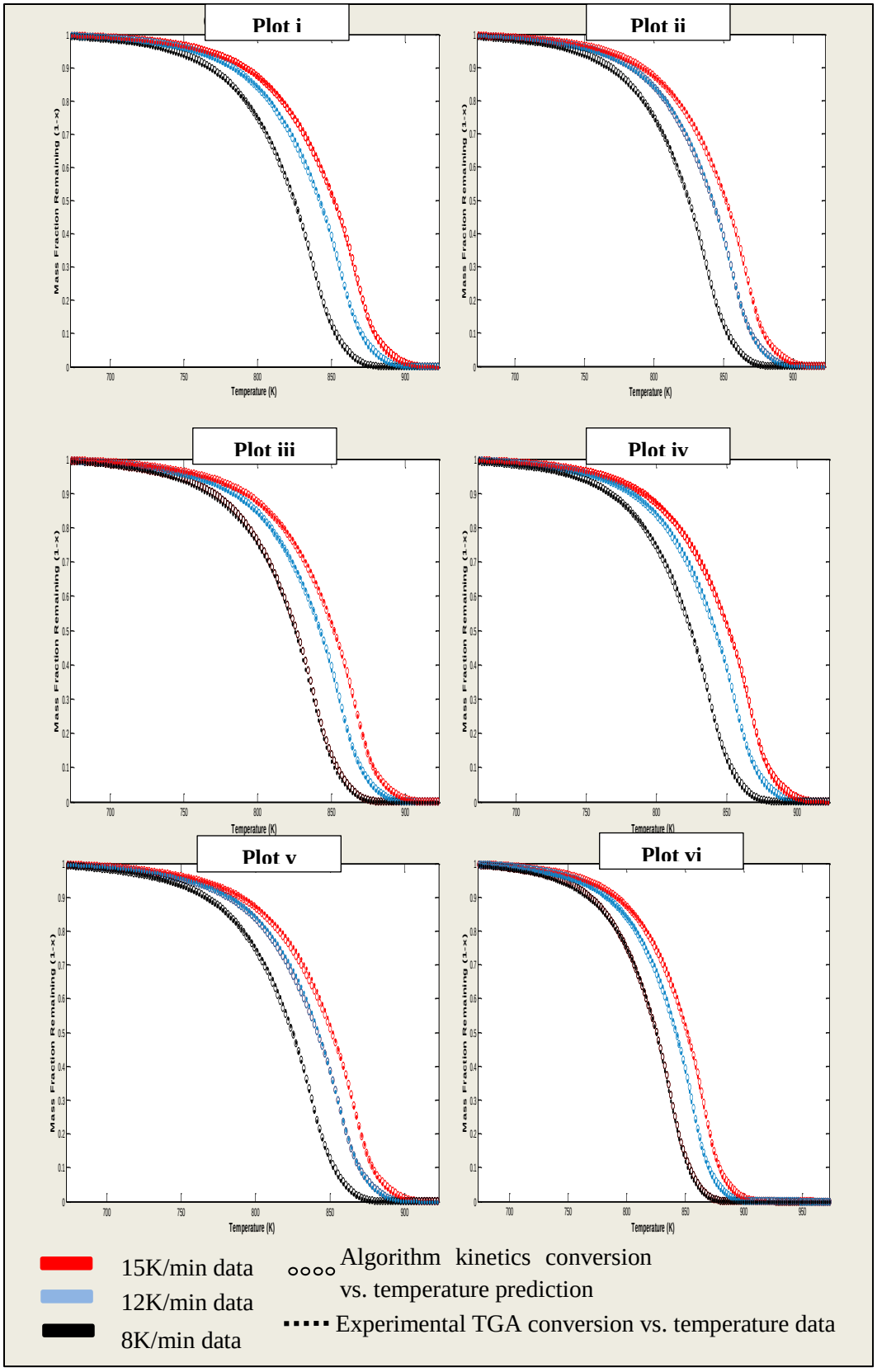

Figure A10-3: Grass char combustion modelling.

Table A10-2: Grass char combustion kinetics.

Plot	Heating rate used(K/min)			Kinetics				Error evaluation	
	E calculation	A calculation	φ calculation	E	A	f_o	φ	R^2	RMS
i	8 ,12	8	12	92.7 125.9 127.1	22806 1.21e+5 1.33e+5	0.01 0.12 0.87	10.5	0.9998	0.0054
ii	8,15	8	15	118.1 127.8 130.5	2.03e+6 1.60e+5 2.17e+5	0.01 0.19 0.80	10.5	0.9999	0.0045
iii	12,15	12	15	196.5 126.3 130.7 137.3 141.4	1.4e+12 1.28e+6 2.78e+5 5.73e+5 9.09e+5	0.01 0.02 0.14 0.06 0.77	14.5	0.9998	0.0055
iv	12,8	12	8	92.7 125.9 127.1	22833 1.21e+5 1.33e+5	0.01 0.38 0.61	10.0	0.9998	0.0059
v	15,8	15	8	112.4 127.8 130.5	3.47e+5 1.60e+5 2.18e+5	0.01 0.28 0.71	10.5	0.9999	0.0049
vi	15,12	15	12	196.5 130.2 131.7	1.4e+12 2.35e+5 2.77e+5	0.01 0.34 0.66	8.61	0.9998	0.0054

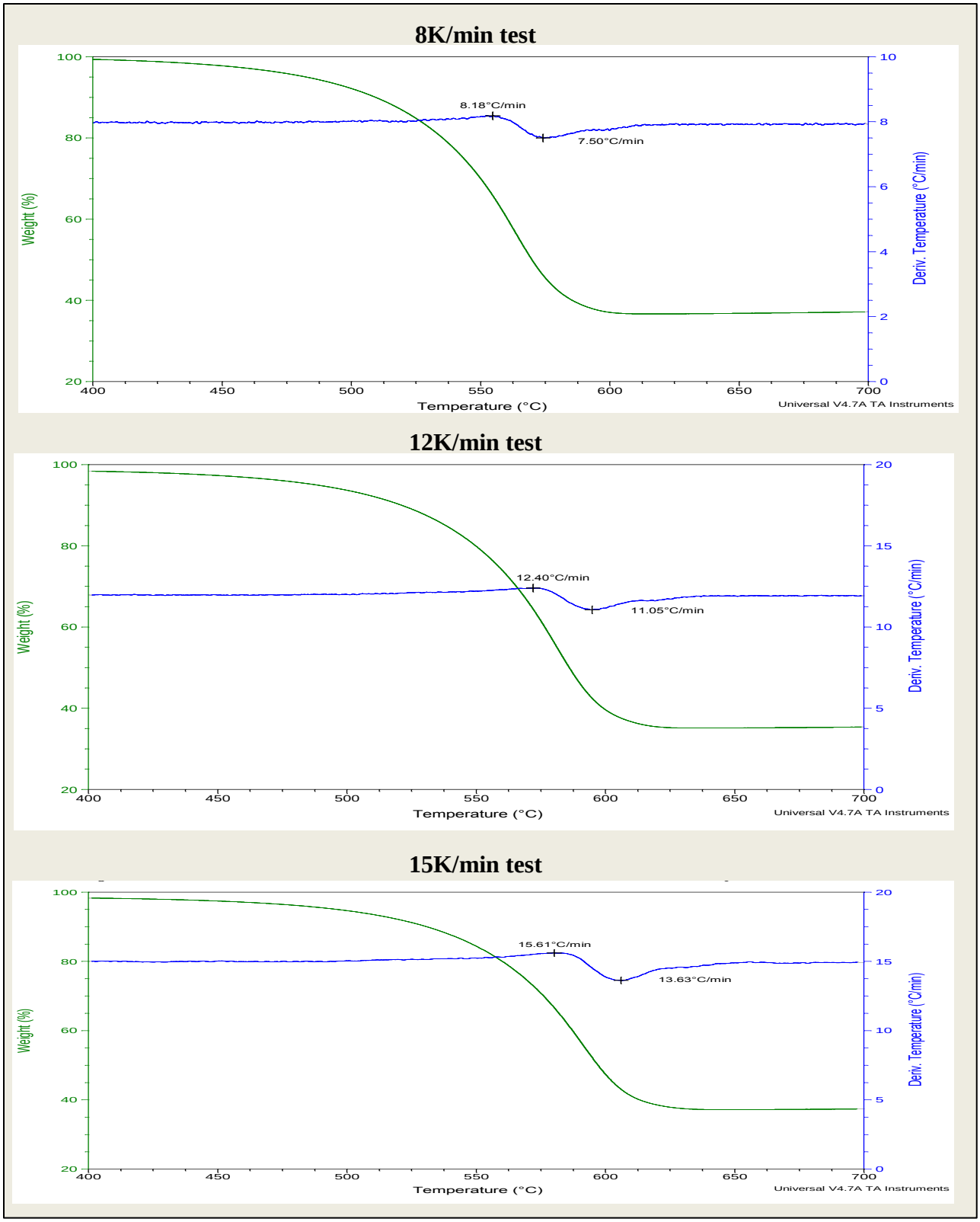

Figure A10-4: Heating rate variations during grass char combustion.

Pine char combustion

The thermo-gravimetric analysis results for pine char combustion are displayed in an order similar to that of grass char combustion.

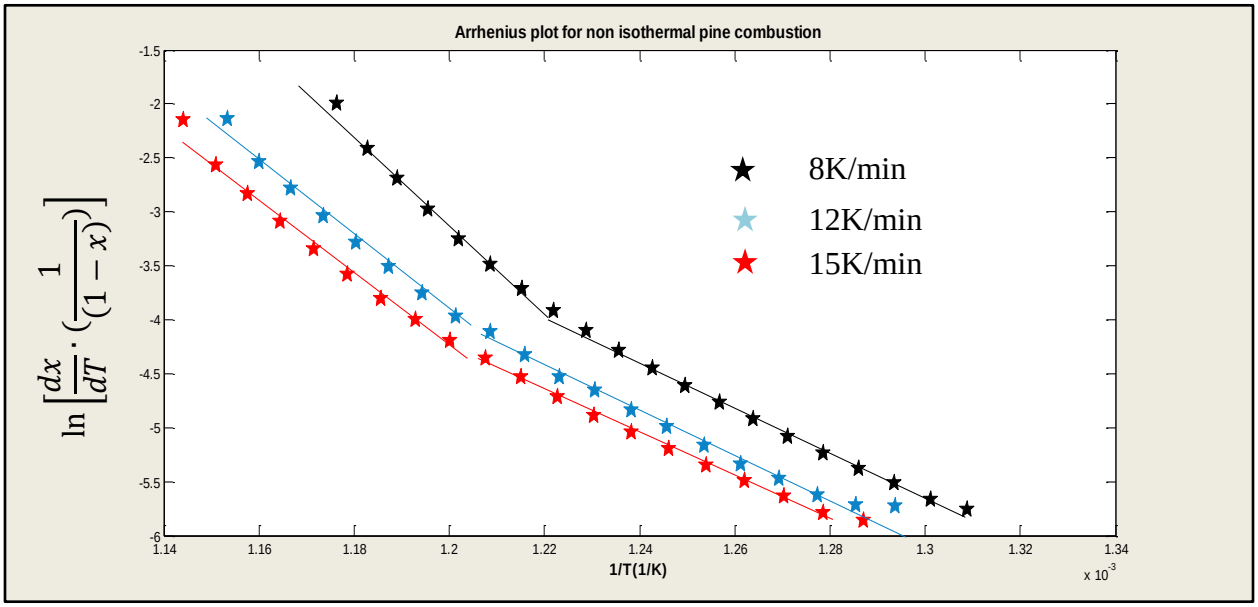

Figure A10-5: Arrhenius plot for pine char combustion

Table A10-3: Pine char combustion model evaluation

Plot	Heating rate used (K/min)			First Order		RPM	
	E calculation	A calculation	φ calculation	Const B R^2 and RMS	Var B R^2 and RMS	Const B R^2 and RMS	Var B R^2 and RMS
i	8 ,12	8	12	0.99515 0.0299	0.99828 0.0176	0.99886 0.0140	0.99968 0.0077
ii	8,15	8	15	0.99649 0.0254	0.99872 0.0154	0.99935 0.0103	0.99964 0.0078
iii	12,15	12	15	0.99814 0.0184	0.99855 0.0167	0.9995 0.0073	0.99971 0.0068
iv	12,8	12	15	0.99514 0.0300	0.99811 0.0184	0.99786 0.0184	0.99952 0.0089
v	15,8	15	12	0.99646 0.0256	0.99868 0.0156	0.9994 0.0099	0.99964 0.0076
vi	15,12	15	8	0.99814 0.0184	0.99864 0.0161	0.99953 0.0071	0.99966 0.0071
Average model accuracy				0.99659 0.0246	0.99850 0.0166	0.99908 0.0111	0.99964 0.0077

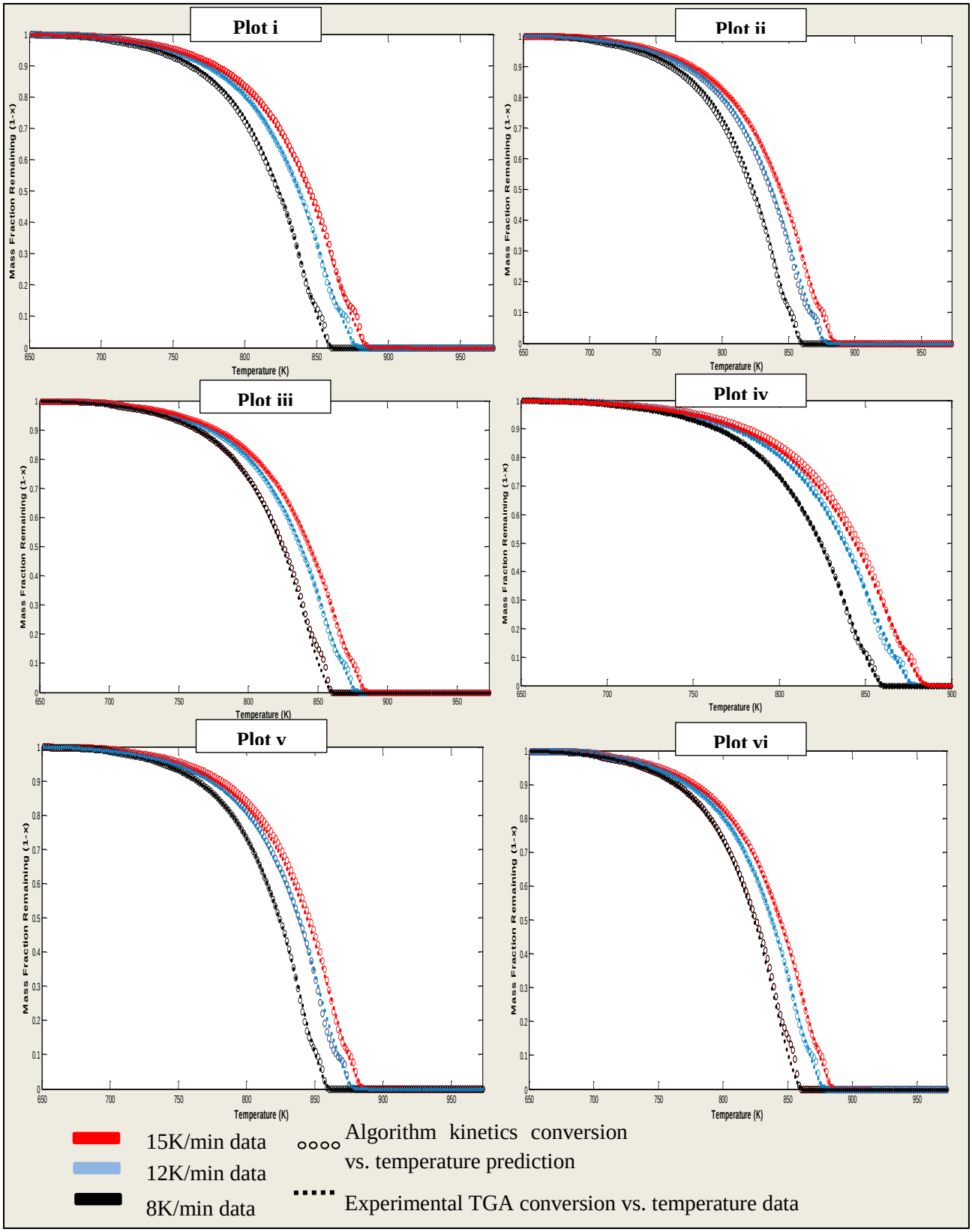

Figure A10-6: Pine char combustion modeling.

Table A10-4: Pine char combustion kinetics.

Plot	Heating rate used(K/min)			Kinetics determined				Error	
	E calculation	A calculation	φ calculation	E	A	f_o	φ	R^2	RMS
i	8 ,12	8	12	284.24	6.94e+18	0.01	8.02	0.9997	0.0077
				217.16	9.40e+12	0.01			
				189.62	3.36e+10	0.01			
				163.02	9.47e+7	0.09			
				149.76	4.46e+6	0.23			
				144.69	2.00e+6	0.63			
ii	8,15	8	15	314.86	1.37e+21	0.01	6.89	0.9996	0.0078
				240.4	4.38e+14	0.01			
				217.68	4.16e+12	0.01			
				198.38	8.86e+10	0.02			
				172.81	4.2e+8	0.04			
				171.17	3.10e+8	0.08			
				154.05	8.76e+6	0.83			
iii	12,15	12	8	387.82	3.40e+26	0.01	8.286	0.9997	0.0068
				277.86	5.01e+17	0.01			
				297.57	4.69e+18	0.01			
				260.63	6.17e+15	0.01			
				253.77	1.27e+15	0.01			
				260.32	2.41e+15	0.01			
				242.4	1.06e+14	0.01			
				219.43	1.58e+12	0.01			
				223.6	2.53e+12	0.03			
				193.02	7.39e+9	0.07			
				194.121	8.19e+9	0.09			
				83.8818	6.20e+8	0.53			
				1.76	3.09e+8	0.20			
iv	12,8	12	15	284.24	6.9e+18	0.01	8.29	0.9995	0.0089
				217.16	9.40e+12	0.01			
				189.62	3.36e+10	0.01			
				188.34	2.18e+10	0.01			
				168.0	2.58e+8	0.02			
				166.5	1.92e+8	0.02			
				149.76	4.46e+6	0.67			
				144.69	1.97e+6	0.24			
v	15,8	15	12	314.87	1.37e+21	0.01	7.43	0.9995	0.0076
				258.66	4.38e+14	0.01			
				229.05	2.94e+11	0.01			
				204.66	8.86e+10	0.01			
				198.38	7.55e+8	0.06			
				175.87	7.63e+6	0.90			
vi	15,12	15	8	387.83	3.40e+26	0.01	8.29	0.9997	0.0071
				277.87	5.01e+17	0.01			
				297.57	4.69e+18	0.01			
				253.77	1.27e+15	0.01			
				242.4	1.06e+14	0.01			
				234.98	2.07e+13	0.01			
				219.43	1.58e+12	0.02			
				193.42	8.37e+9	0.05			
				193.02	7.40e+9	0.11			
				183.88	6.20e+8	0.55			
				181.76	3.09e+8	0.20			

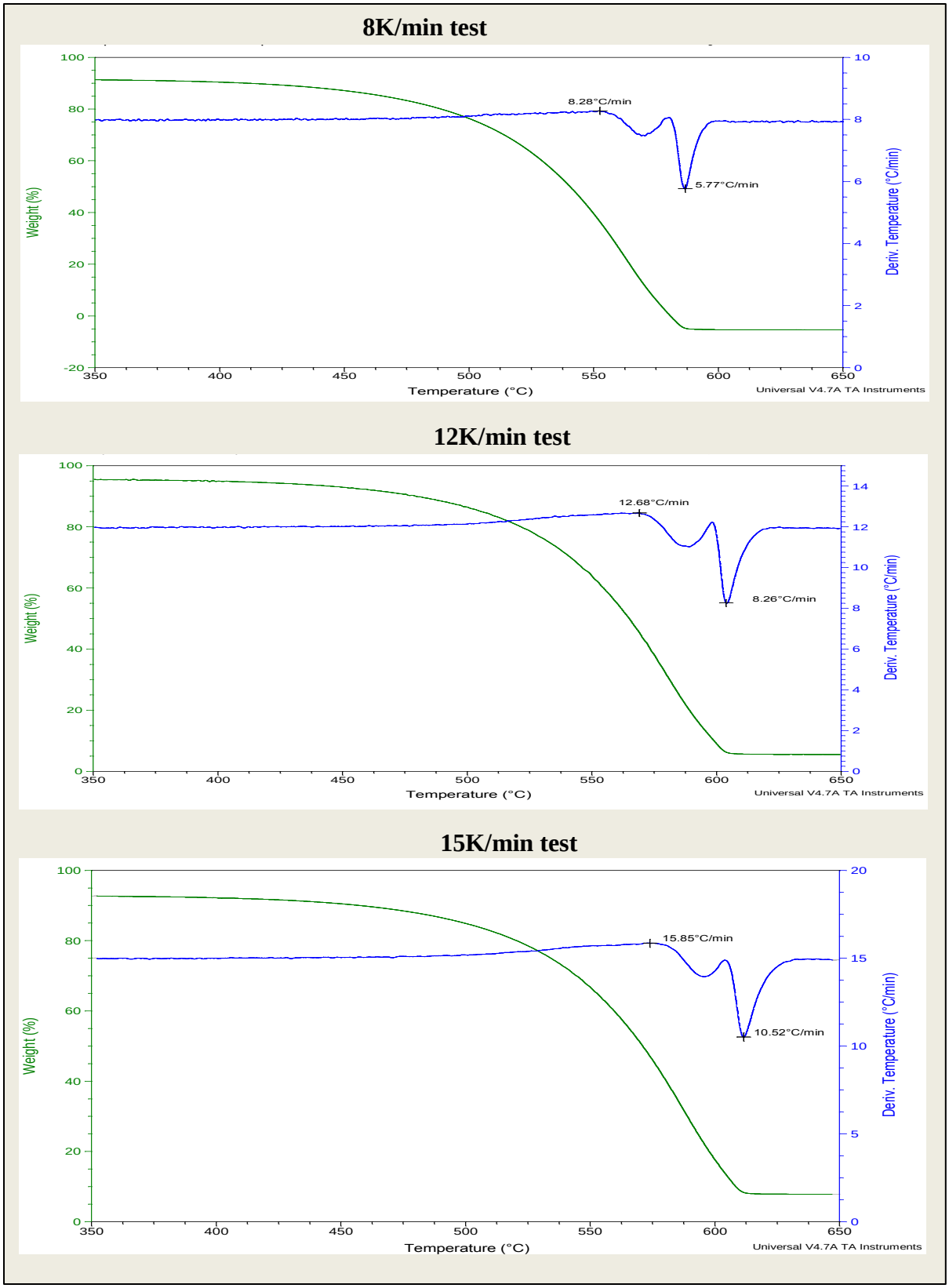

Figure A10-7: Heating rate deviations during pine char combustion.

Coal-grass char blends combustion

Coal-grass 90:10 char blend combustion

The results obtained during the combustion of the coal-grass 90:10 blend are displayed in the following figures and tables.

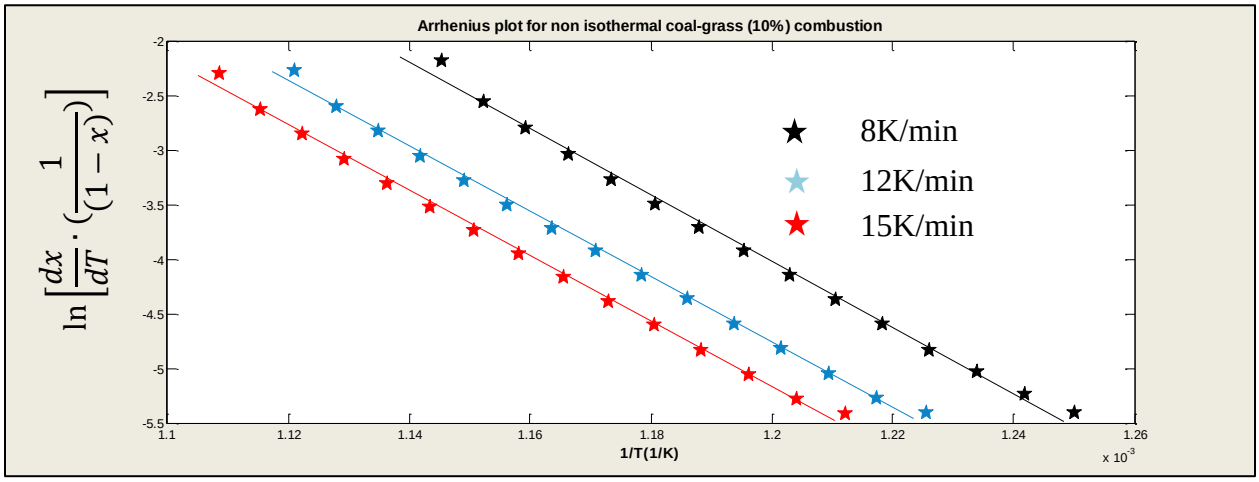

Figure A10-8: Arrhenius plot for coal-grass 90:10 cha blend combustion.

Table A10-5: Coal-grass 90:10 cha blend combustion model evaluation.

Plot	Heating rate used (K/min)			First Order		RPM	
	E calculation	A calculation	φ calculation	Const B R^2 and RMS	Var B R^2 and RMS	Const B R^2 and RMS	Var B R^2 and RMS
i	8 ,12	8	12	0.98047 0.0591	0.98468 0.0509	0.98466 0.0111	0.99778 0.0199
ii	8,15	8	15	0.98047 0.0591	0.98572 0.0505	0.99665 0.0245	0.9982 0.0179
iii	12,15	12	8	0.98051 0.0590	0.98655 0.0507	0.99931 0.0111	0.99963 0.0082
iv	12,8	12	15	0.98046 0.0591	0.98455 0.0511	0.99616 0.0261	0.99762 0.0206
v	15,8	15	12	0.98047 0.0590	0.98565 0.0506	0.9967 0.0243	0.99829 0.0175
vi	15,12	15	8	0.98052 0.0590	0.98661 0.0506	0.99931 0.0111	0.99965 0.0079
Average model accuracy				0.98048 0.0591	0.98563 0.0507	0.99547 0.0180	0.99853 0.0153

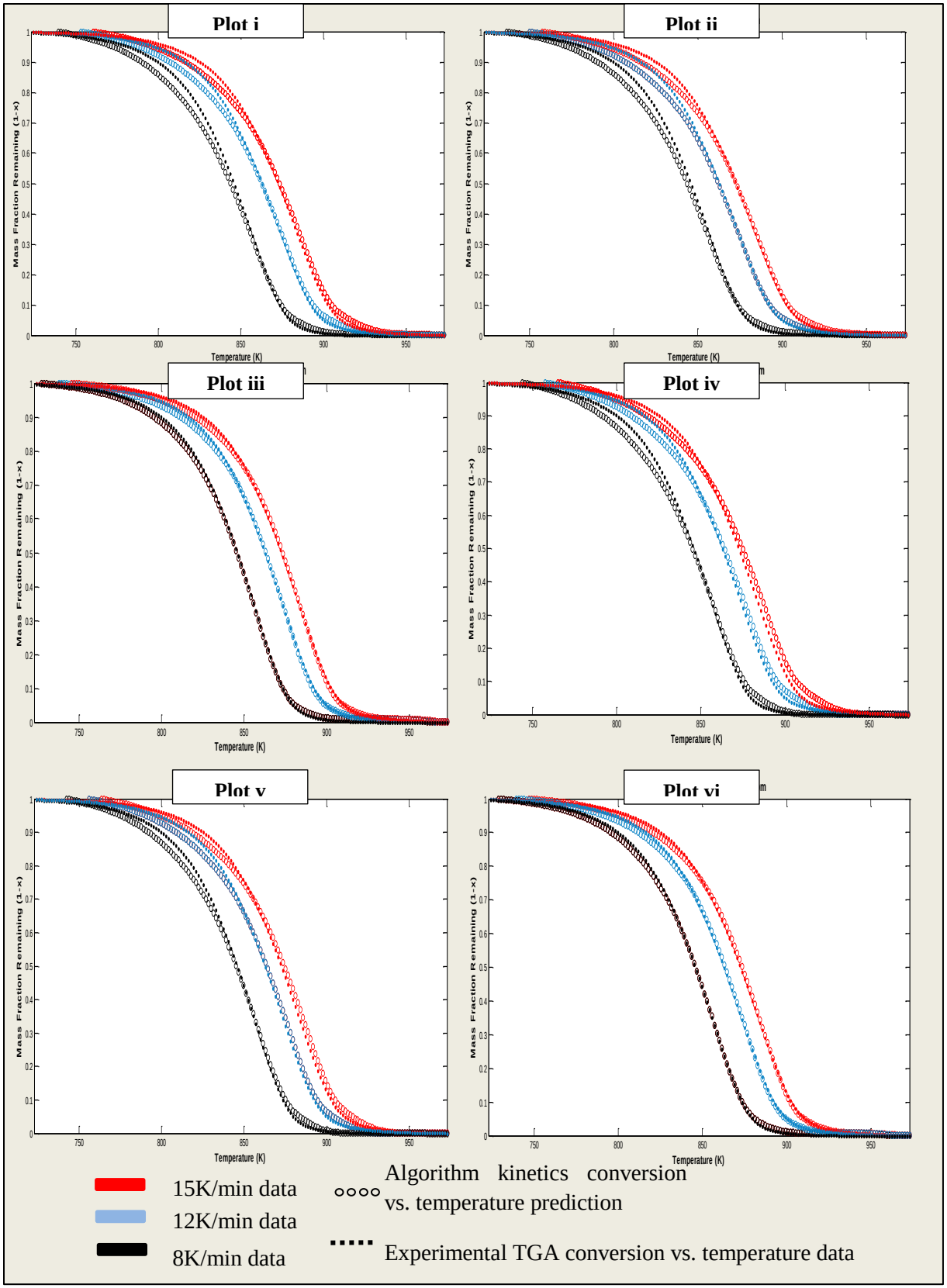

Figure A10-9: Modelling of coal-grass 90:10 cha blend combustion.

Table A10-6: Coal-grass 90:10 cha blend combustion kinetics.

Plot	Heating rate used(K/min)			Rpm kinetics					
	E calculation	A calculation	φ calculation	E	A	f_o	φ	R^2	RMS
i	8 ,12	8	12	114.22 115.05	1.3e+4 4.3e+3	1.00 0.01	11.2	0.9978	0.0199
ii	8,15	8	15	117.75 185.77	2.1e+4 5.24e+7	1.00 0.01	11.9	0.9982	0.0179
iii	12,15	12	8	125.68	5.4e+4	1.00	19.4	0.9996	0.082
iv	12,8	12	15	114.29	1.3e+4	1.03	9.9	0.9976	0.206
v	15,8	15	12	117.79	2.1e+4	1.02	10.2	0.9983	0.175
vi	15,12	15	8	125.68	5.4e+4	1.00	18.9	0.9997	0.0079

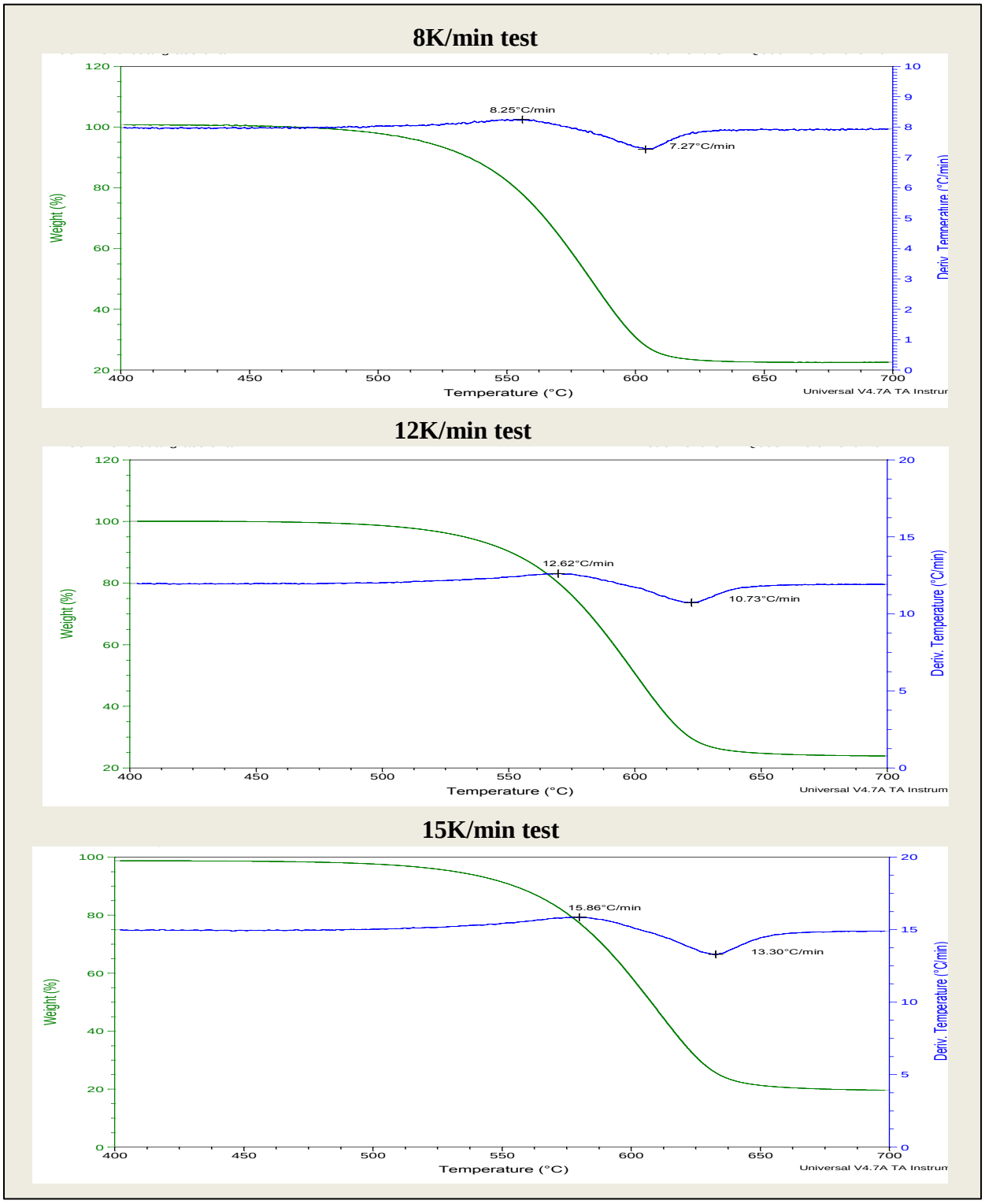

Figure A10-10: Heating rate deviations during coal-grass 90:10 cha blend combustion.

Coal-grass 50:50 char blend combustion

The figures and tables below display the results analysis obtained during the combustion of the coal-grass 50:50 char blend.

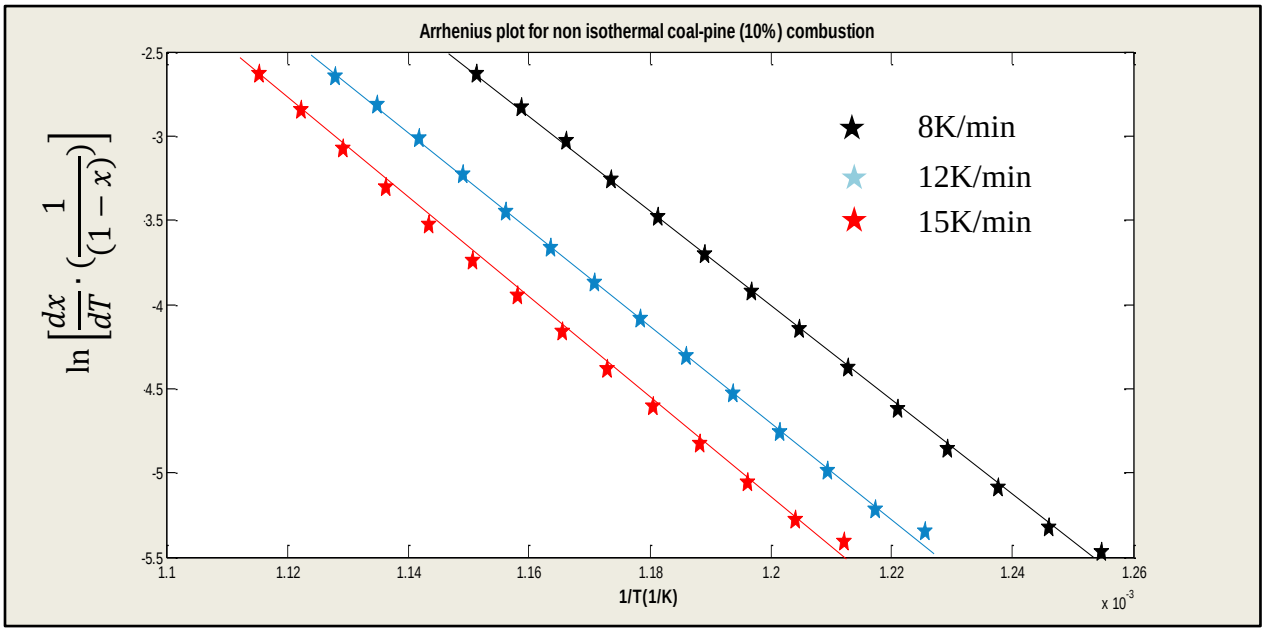

Figure A10-11: Arrhenius plot for coal-grass 50:50 char blend combustion.

Table A10-7: Cal-grass 50:50 char blend model evaluation.

Plot	Heating rate used (K/min)			First order		RPM	
	E calculation	A calculation	φ calculation	Const B R^2 and RMS	Var B R^2 and RMS	Const B R^2 and RMS	Var B R^2 and RMS
i	8 ,12	8	12	0.98574 0.0510	0.98836 0.0454	0.99968 0.0076	0.99996 0.0024
ii	8,15	8	15	0.98516 0.0521	0.98924 0.0444	0.99925 0.0100	0.99988 0.0041
iii	12,15	12	8	0.98418 0.0538	0.98917 0.0455	0.99688 0.0186	0.99926 0.0092
iv	12,8	12	15	0.98573 0.0511	0.98837 0.0454	0.99966 0.0078	0.99994 0.0031
v	15,8	15	12	0.98516 0.0521	0.98924 0.0444	0.9991 0.0107	0.99983 0.0046
vi	15,12	15	8	0.98418 0.0538	0.98917 0.0455	0.99893 0.0119	0.99975 0.0058
Average model accuracy				0.985025 0.0523	0.988925 0.0451	0.998917 0.0111	0.99977 0.0049

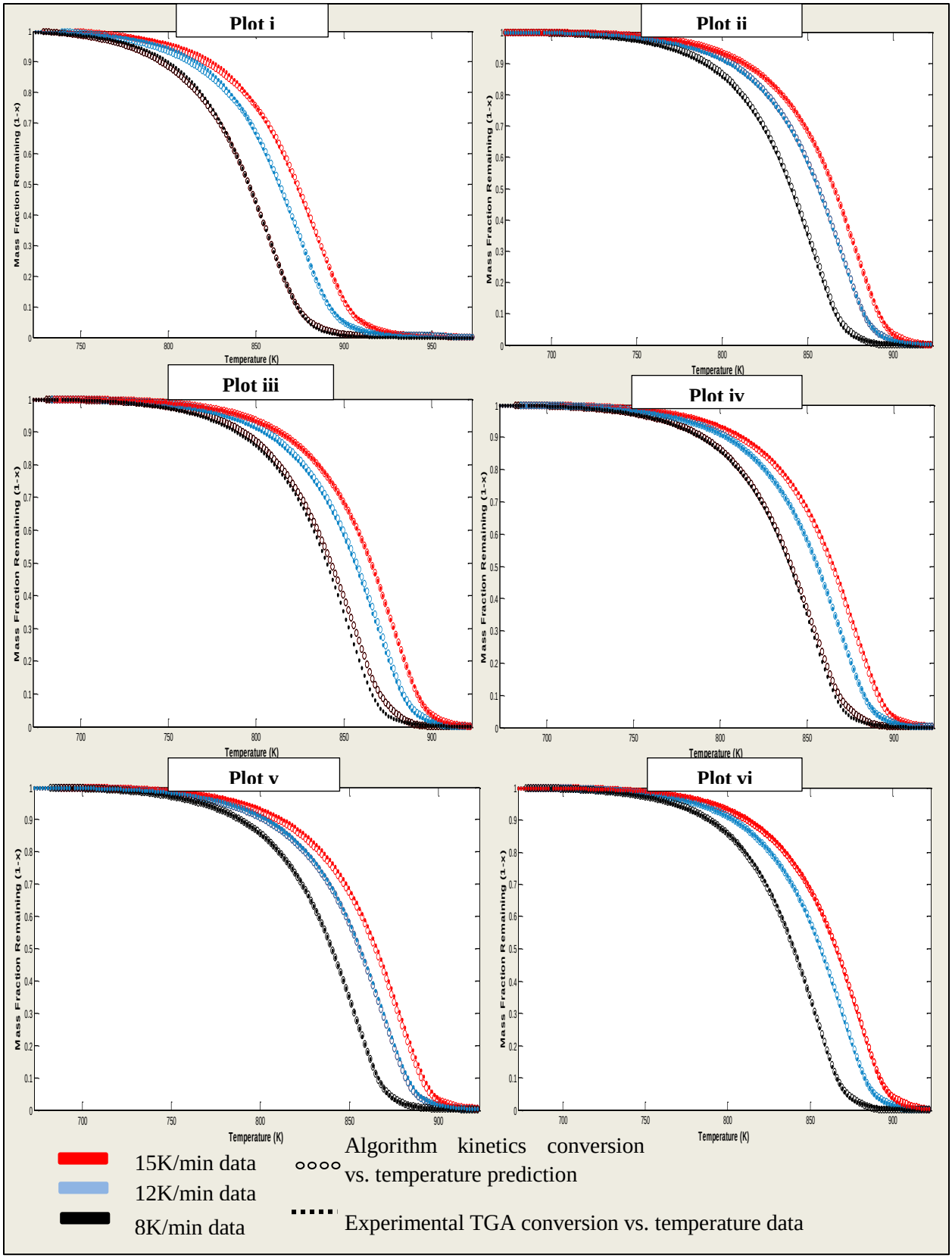

Figure A10-12: Modelling of coal-grass 50:50 char blend combustion

Table A10-8: Coal-grass 50:50 char blend combustion kinetics.

Plot	Heating rate used(K/min)			Rpm kinetics					
	E calculation	A calculation	φ calculation	E	A	f_o	φ	R^2	RMS
i	8 ,12	8	12	135.94	3.09e+5	1.00	15.9	0.99996	0.0024
ii	8,15	8	15	136.8 146.96	5.71e+5 1.49e+6	0.11 0.89	14.2	0.99988	0.0041
iii	12,15	12	8	114.97 138.08 175.45	1.27e+5 6.53e+5 7.75e+7	0.01 0.36 0.63	13.0	0.99926	0.0092
iv	12,8	12	15	135.96	3.09e+5	1.0	15.3	0.99994	0.0031
v	15,8	15	12	132.53 140.64 137.83 136.84 146.96 194.7	1.19e+6 1.83e+6 7.38e+5 5.94e+5 1.49e+6 2.29e+8	0.01 0.01 0.01 0.01 0.94 0.01	17.0	0.99983	0.0046
vi	15,12	15	8	114.97 137.48 141.33 175.45	1.27e+5 5.45e+5 8.45e+5 7.75e+7	0.01 0.35 0.13 0.50	13.6	0.99975	0.0058

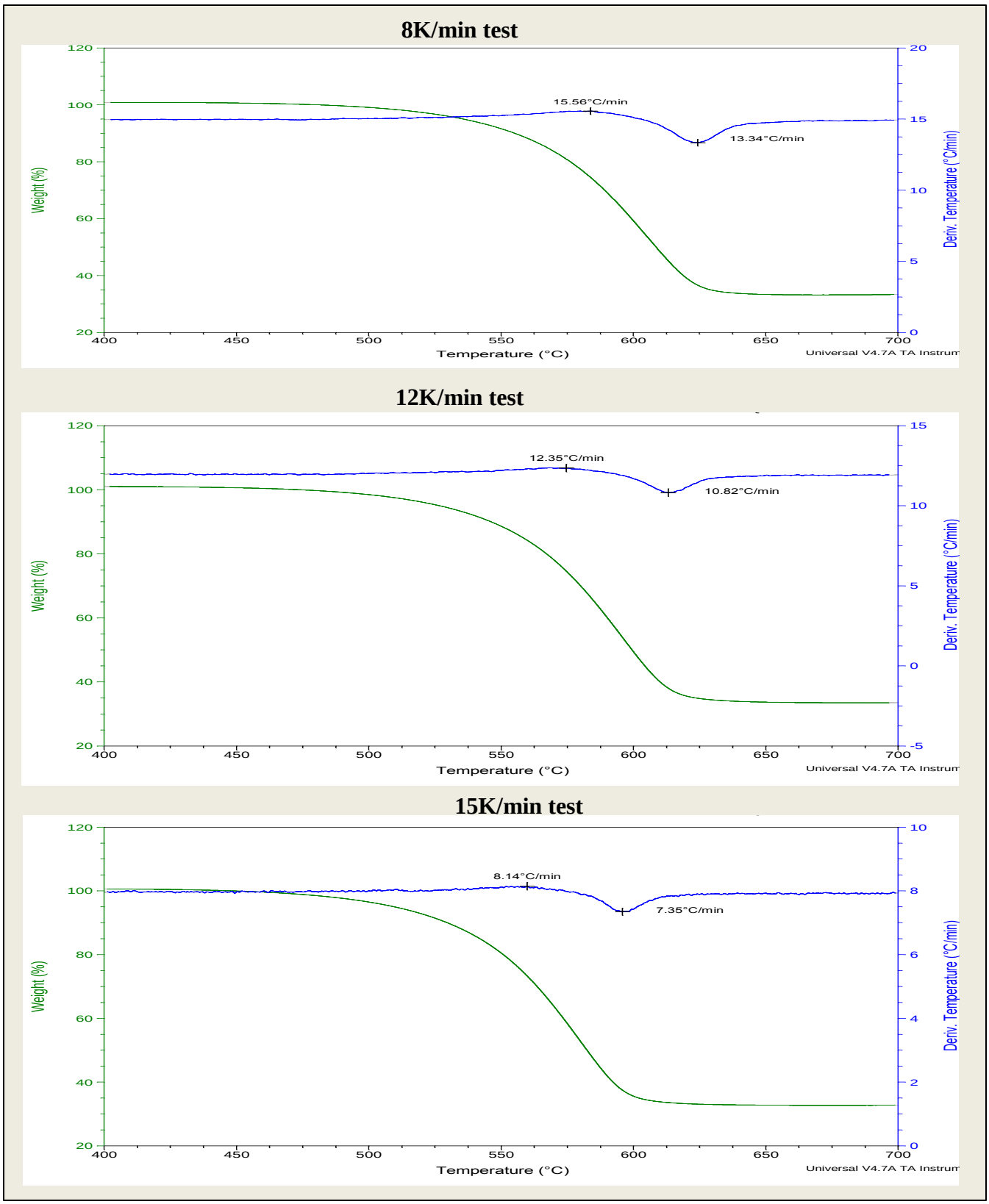

Figure A10-13: Heating rate deviations during coal-grass 50:50 char blend combustion

Coal-pine char blends combustion

Coal-pine 90:10 char blend combustion

The results obtained during the analysis of the coal-pine 90:10 char blend combustion are detailed as follows:

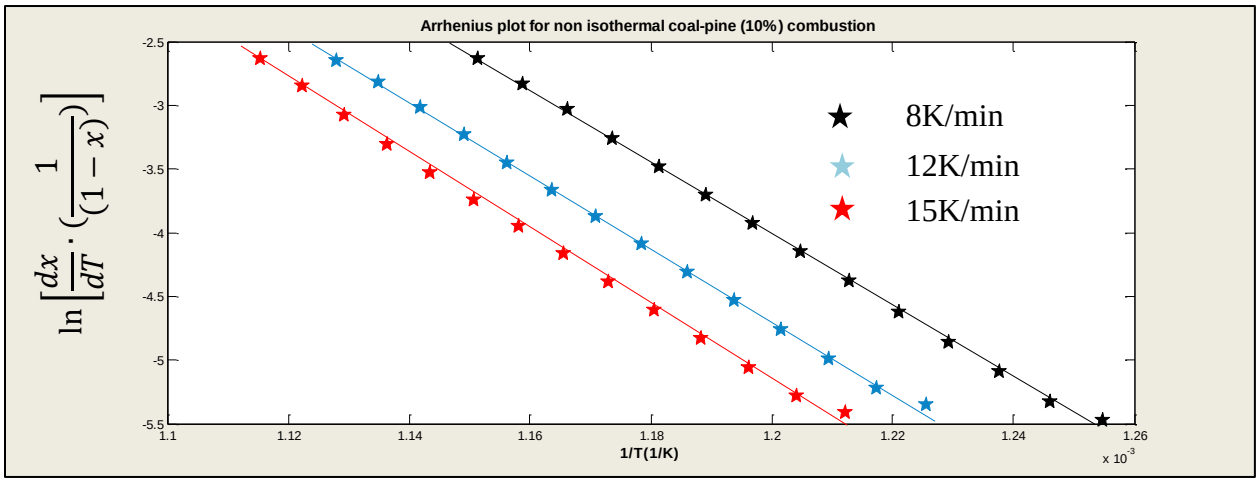

Figure A10-14: Arrhenius plot for coal-pine 90:10 char blend combustion.

Table A10-9: Coal-pine 90:10 char blend combustion model evaluation.

Plot	Heating rate used (K/min)			First Order		RPM	
	E calculation	A calculation	φ calculation	Const B R^2 and RMS	Var B R^2 and RMS	Const B R^2 and RMS	Var B R^2 and RMS
i	8 ,12	8	12	0.98241 0.0553	0.98484 0.0500	0.99892 0.0136	0.99958 0.0086
ii	8,15	8	15	0.97894 0.0605	0.98375 0.0534	0.99935 0.0100	0.99952 0.0092
iii	12,15	12	8	0.9723 0.0695	0.98216 0.0577	0.99761 0.0171	0.99873 0.0125
iv	12,8	12	15	0.9823 0.0554	0.9846 0.0503	0.9989 0.0136	0.99954 0.0093
v	15,8	15	12	0.97893 0.0605	0.98375 0.0534	0.99925 0.0097	0.9995 0.0081
vi	15,12	15	8	0.97237 0.0694	0.98213 0.0578	0.9989 0.0125	0.99937 0.0090
Average model accuracy				0.97697 0.0631	0.98328 0.0545	0.99880 0.0126	0.99933 0.0096

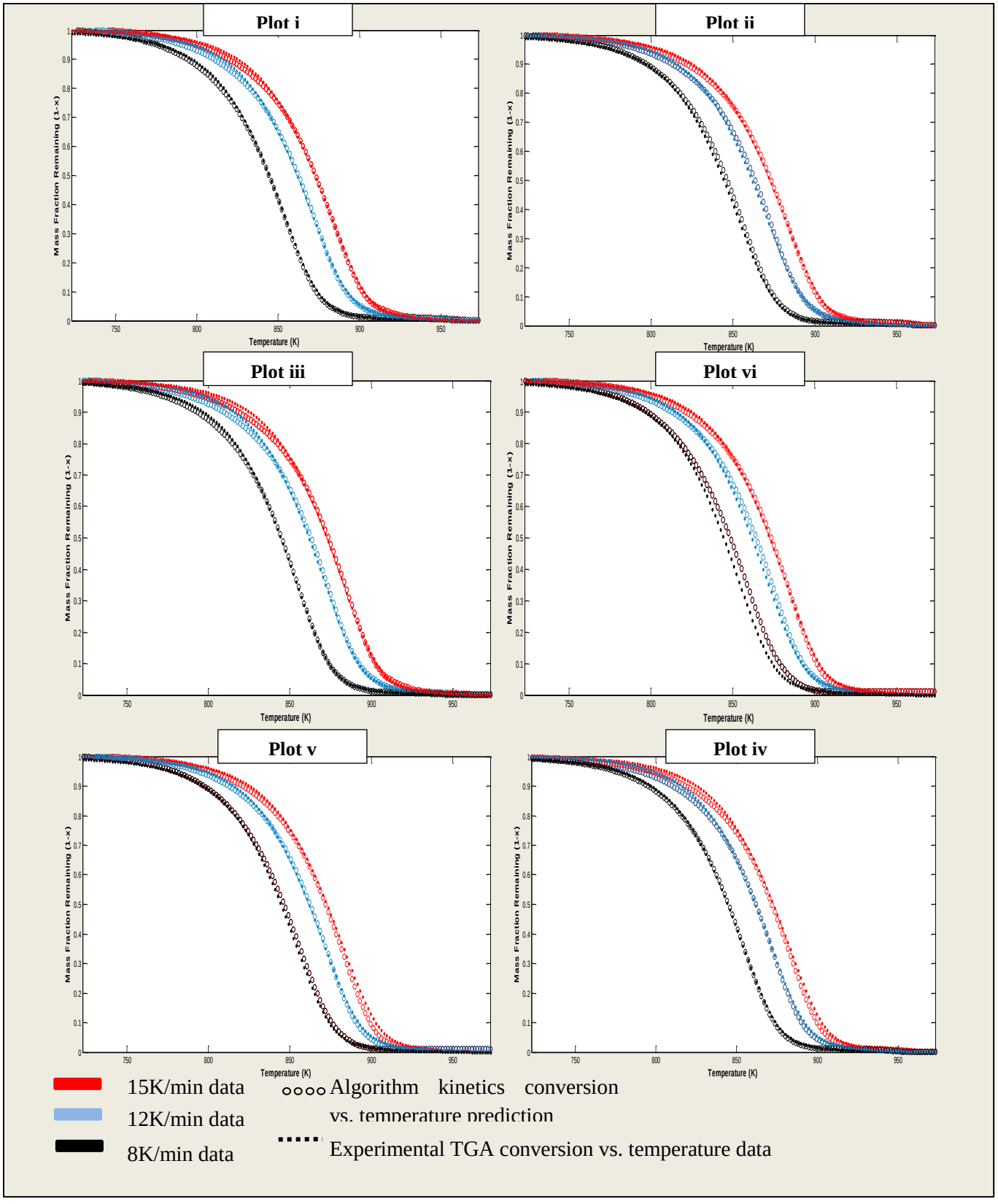

Figure A10-15: Modelling of coal-pine 90:10 char blend combustion.

Table A10-10: Coal-pine 90:10 char blend combustion kinetics.

Plot	Heating rate used(K/min)			Kinetics determined					
	E calculation	A calculation	φ calculation	E	A	f_o	φ	R^2	RMS
i	8 ,12	8	12	122.91	3.49e+4	1.00	21.8	0.9996	0.0086
ii	8,15	8	15	123.35 125.56 135.19 742.31	6.1e+4 6.1e+4 1.97e+005 1.48e+038	0.12 0.03 0.84 0.01	19.0	0.9995	0.0092
iii	12,15	12	8	305.57 118 130.67 165.38	1e-007 3.0e+4 1.26e+5 1.21e+7	0.01 0.11 0.44 0.44	19.0	0.999	0.0125
iv	12,8	12	15	125.65 122.8 294.7	6.8e+4 3.4e+4 4.87e+13	0.09 0.91 0.00 1	19.1	0.9995	0.0093
v	15,8	15	12	125.58 135.04 461.82	6.2e+4 1.93e+5 9.1e+022	0.42 0.57 0.01	19.0	0.9996	0.0081
vi	15,12	15	8	305.57 118 130.67 165.38	1e-7 3.0e+4 1.26e+5 1.21e+7	0.01 0.05 0.66 0.29	19.0	0.9995	0.0090

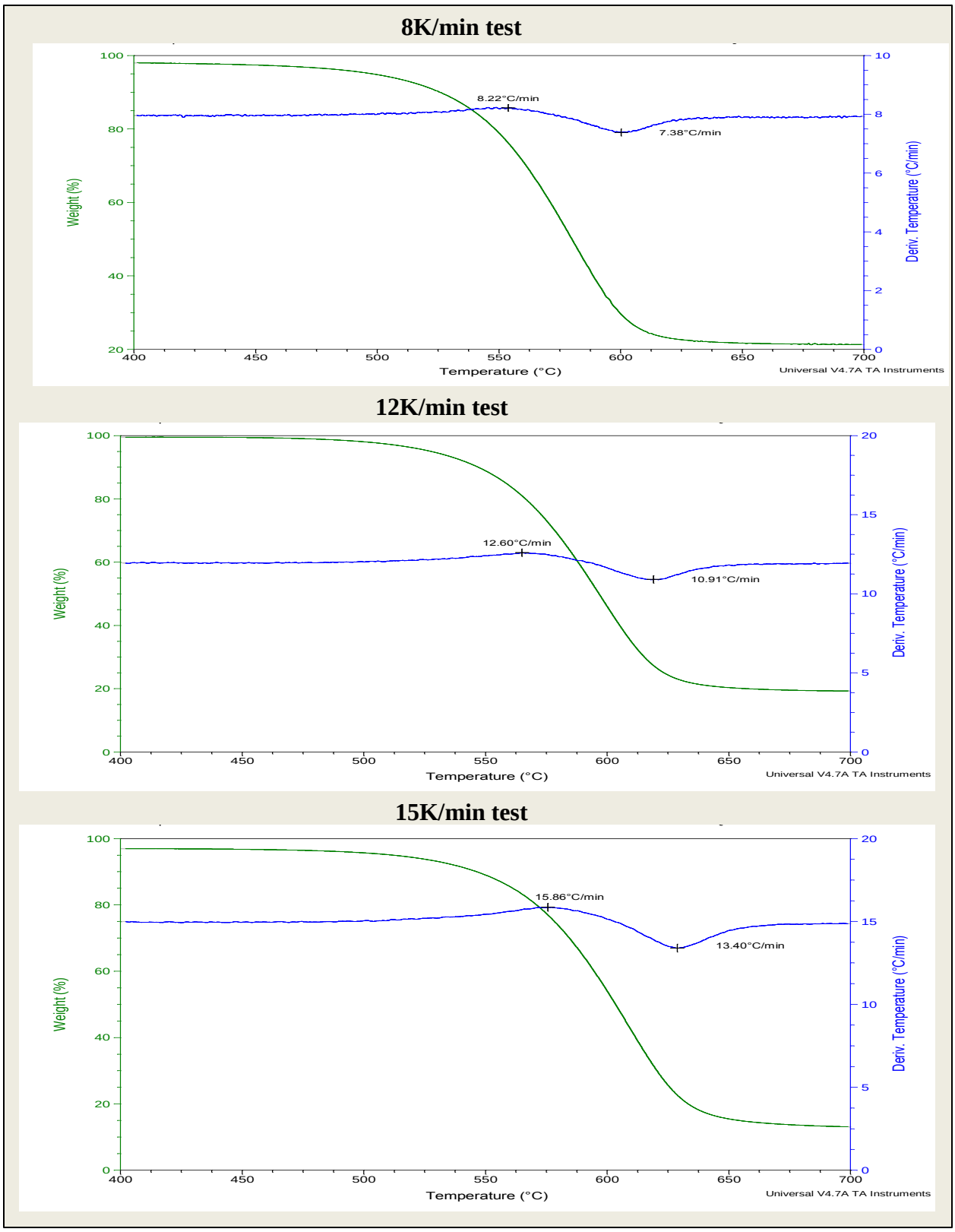

Figure A10-16: Heating rate deviations during coal-pine 90:10 char blend combustion.

Coal-Pine 50:50 char combustion

The figures and tables below outline the results obtained during coal-pine 50:50 char blend combustion.

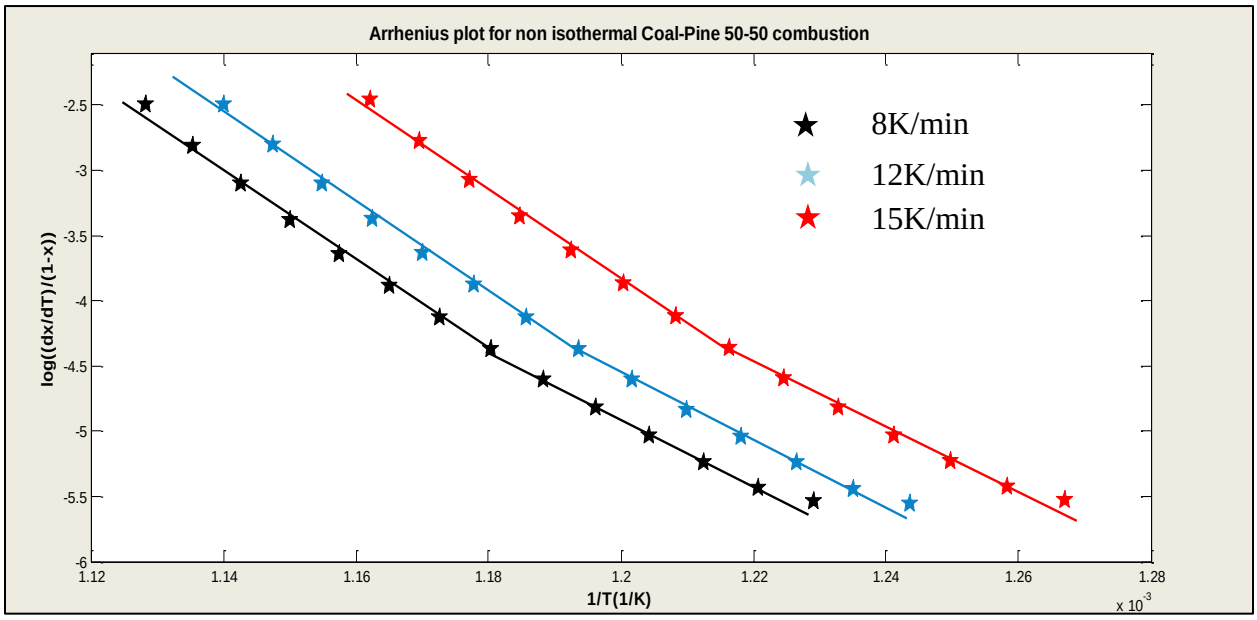

Figure A10-17: Arrhenius plots for coal-pine 50:50 char blend combustion.

Table A10-11: Coal-pine 50:50 char blend combustion model evaluation.

Plot	Heating rate used (K/min)			First order		RPM	
	E calculation	A calculation	φ calculation	Const B R^2 and RMS	Var B R^2 and RMS	Const B R^2 and RMS	Var B R^2 and RMS
i	8 ,12	8	12	0.98281 0.0564	0.98621 0.0496	0.99682 0.0243	0.99879 0.0150
ii	8,15	8	15	0.98215 0.0575	0.98622 0.0506	0.99775 0.0204	0.99898 0.0137
iii	12,15	12	8	0.98097 0.0593	0.98573 0.0527	0.99956 0.0090	0.99982 0.0058
iv	12,8	12	15	0.9828 0.0565	0.98613 0.0497	0.99675 0.0245	0.9988 0.0149
v	15,8	15	12	0.98216 0.0575	0.98623 0.0505	0.99746 0.0216	0.99899 0.0137
vi	15,12	15	8	0.98098 0.0594	0.98574 0.0526	0.99962 0.0084	0.99983 0.0056
Average model accuracy				0.98198 0.0578	0.98604 0.0510	0.99799 0.0180	0.99920 0.0115

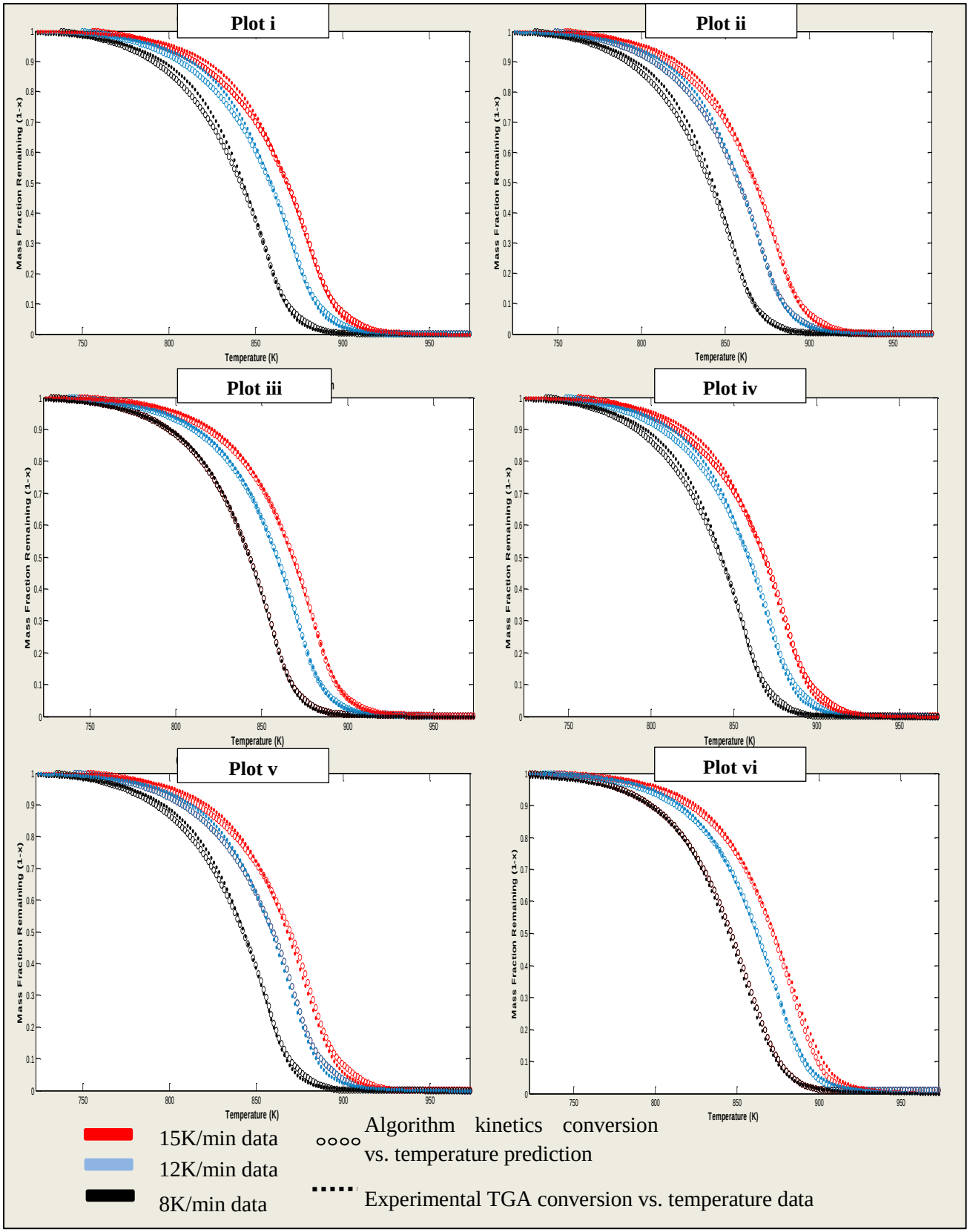

Figure A10-18: Modeling of coal-pine 50:50 char blend combustion.

Table A10-12: Coal-pine 50:50 char blend combustion kinetics.

Plot	Heating rate used(K/min)			Rpm kinetics					
	E calculation	**A calculation**	***φ* calculation**	**E**	**A**	**F0**	***φ***	**R^2**	**RMS**
i	8 ,12	8	12	129.86	1.40e+5	1.02	10.7	0.9988	0.0150
ii	8,15	8	15	127.73	9.1e+4	1.01	15.4	0.9989	0.0137
iii	12,15	12	8	138.33	3.94e+5	1.00	17.7	0.9998	0.0058
iv	12,8	12	15	129.86	1.40e+5	1.02	10.0	0.9988	0.0149
v	15,8	15	12	127.73	9.1e+4	1.01	13.6	0.9989	0.0137
vi	15,12	15	8	138.33	3.94e+5	1.00	17.9	0.9998	0.0056

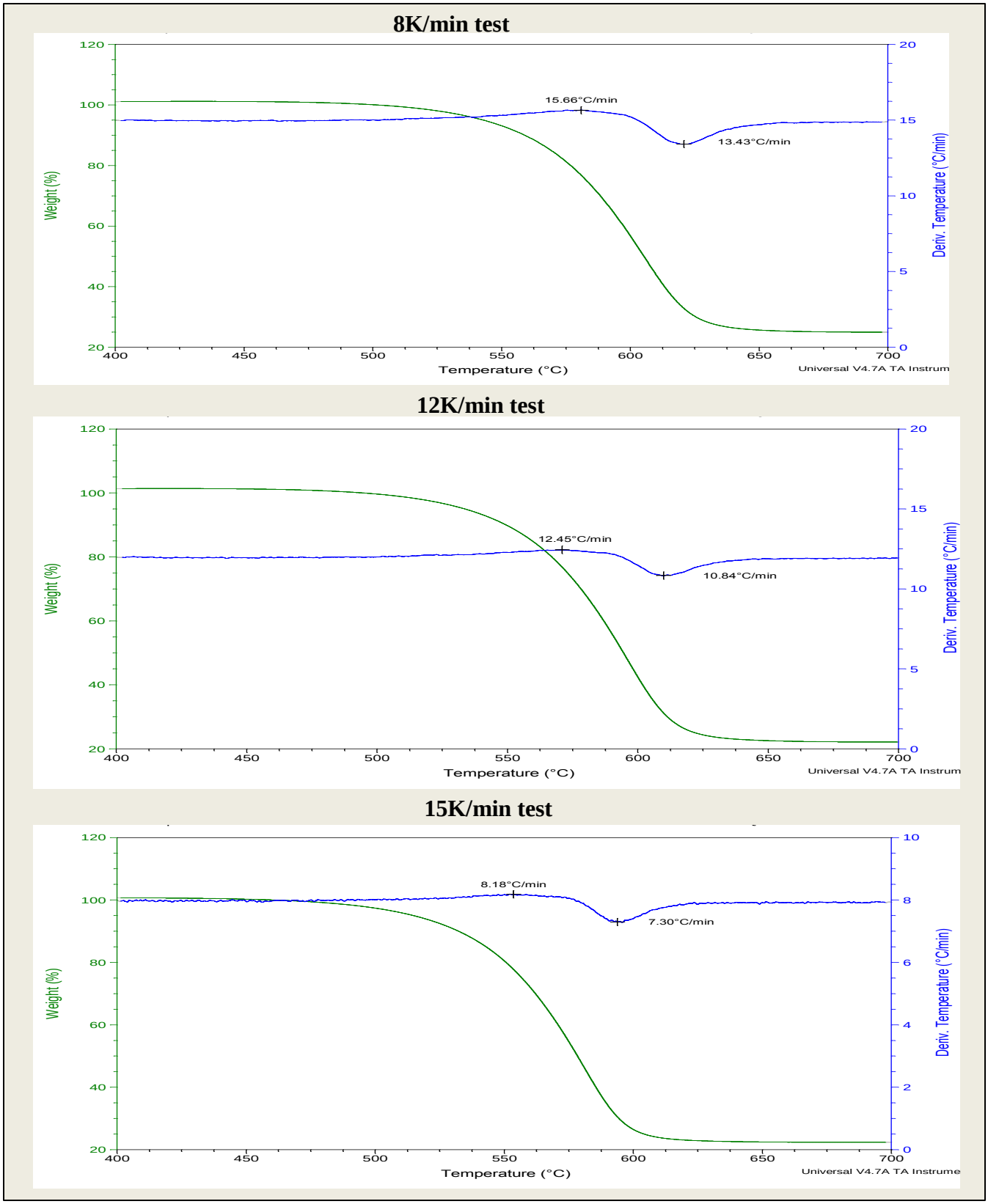

Figure A10-19: Heating rate deviations during coal-pine 50:50 char blend combustion.

10.3.2. Gasification Analysis

Coal char gasification

The coal char gasification analysis is outlined in the following tables and figures.

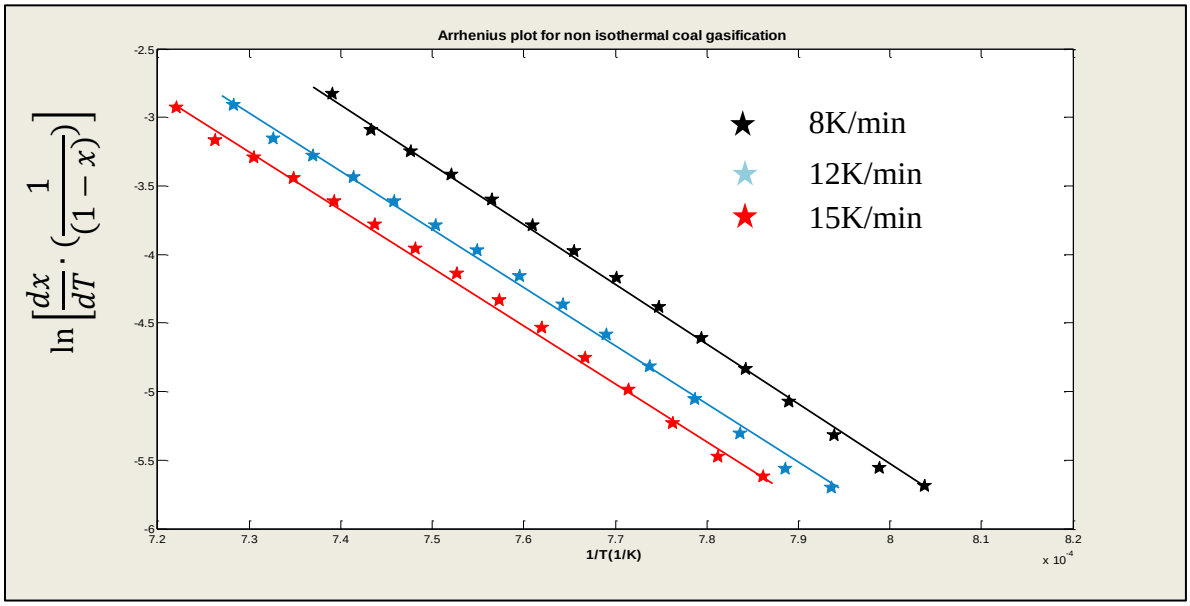

Figure A10-20: Arrhenius plot for coal char gasification

Table A10-13: Coal char gasification model evaluation.

Plot	Heating rate used (K/min)			First order		RPM	
	E calculation	A calculation	φ calculation	Const B R^2 and RMS	Var B R^2 and RMS	Const B R^2 and RMS	Var B R^2 and RMS
i	8 ,12	8	12	0.99859 0.0151	0.99843 0.0155	0.9999 0.0048	0.99993 0.0056
ii	8,15	8	15	0.99797 0.0182	0.99797 0.0181	0.9999 0.0043	0.99963 0.0040
iii	12,15	12	8	0.99652 0.0238	0.99655 0.0246	0.9999 0.0043	0.99985 0.0047
iv	12,8	12	15	0.99856 0.0153	0.99832 0.0161	0.99975 0.0083	0.99988 0.0053
v	15,8	15	12	0.99798 0.0182	0.99801 0.0181	0.9976 0.0115	0.99758 0.0068
vi	15,12	15	8	0.99652 0.0238	0.99654 0.0246	0.9999 0.0041	0.99985 0.0046
Average Model Accuracy				0.99769 0.0191	0.99764 0.0195	0.99949 0.0062	0.99945 0.0052

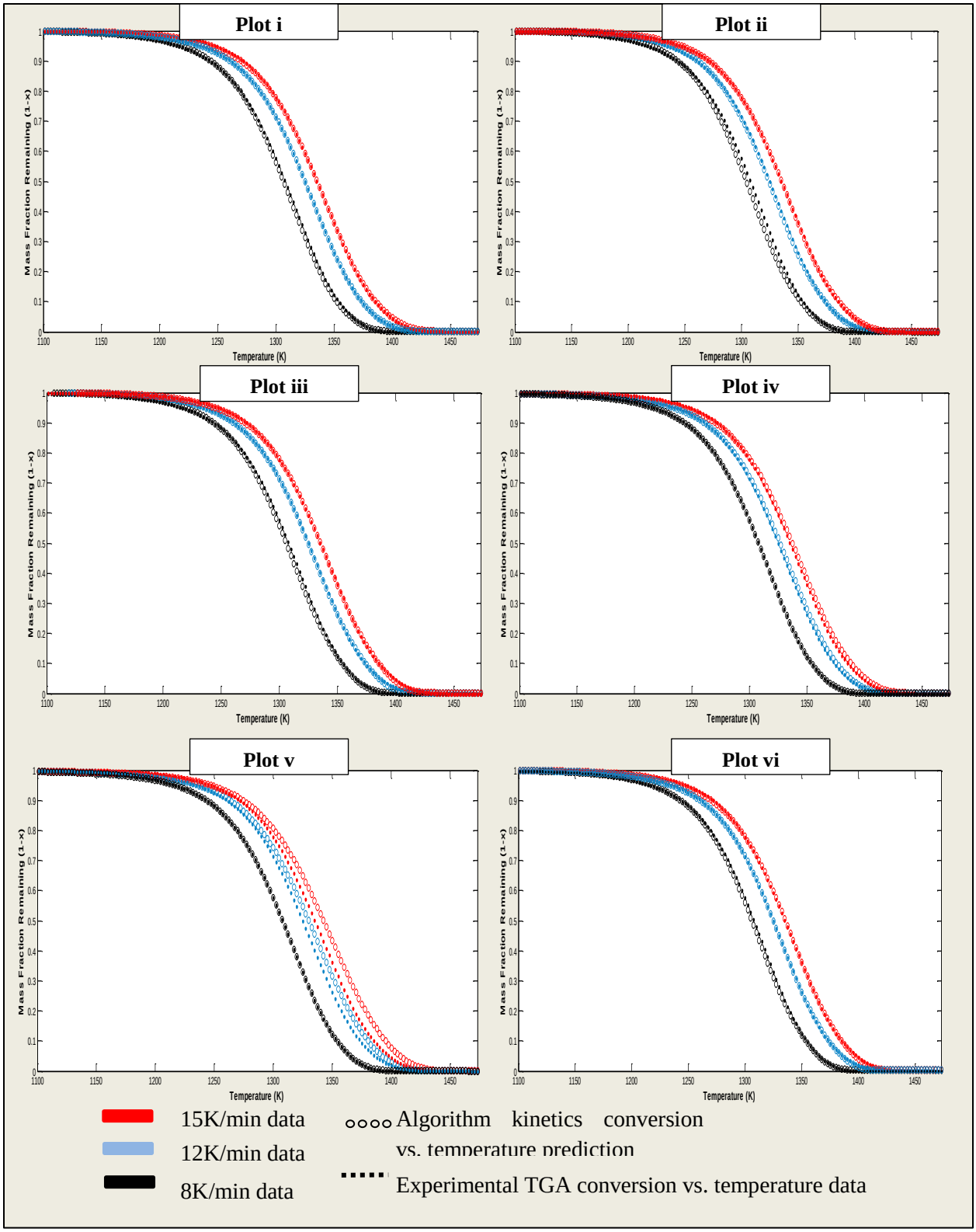

Figure A10-21: Modelling of coal char gasification.

Table A10-14: Coal char gasification kinetics.

Plot	Heating rate used(K/min)			Kinetics determined					
	E calculation	A calculation	φ calculation	E	A	F0	φ	R^2	RMS
i	8 ,12	8	12	324.61 316.13 313.22 265.59 118.47	2.20e+10 5.766e+9 4.16e+9 2.60e+7 22.43	0.05 0.06 0.24 0.59 0.06	18.5	0.9997	0.0056
ii	8,15	8	15	313.06 304.3 300.61 272.91 265.56	7.41e+9 1.82e+9 1.14e+9 5.05e+7 1.186e+7	0.08 0.20 0.15 0.52 0.04	18.5	0.9999	0.0040
iii	12,15	12	8	305.57 288.21 289.35 287.25	1e-7 4.68e+8 4.67e+8 1.80e+8	0.01 0.37 0.05 0.58	18.0	0.9998	0.0047
iv	12,8	12	15	323.72 324.44 313.22 311.23 265.59	2.24e+10 2.28e+10 4.16e+9 3.26e+9 2.60e+7	0.01 0.09 0.01 0.39 0.48	12.0	0.9997	0.0053
v	15,8	15	12	305.57 288.21 286.82 287.25	1e-7 4.68e+8 3.92e+8 1.80e+8	0.01 0.11 0.30 0.58	18.0	0.9996	0.0068
vi	15,12	15	8	305.57 288.21 286.82 287.25	1e-7 4.68e+8 3.91e+8 1.80e+8	0.01 0.18 0.22 0.59	18.5 31	0.9999	0.0046

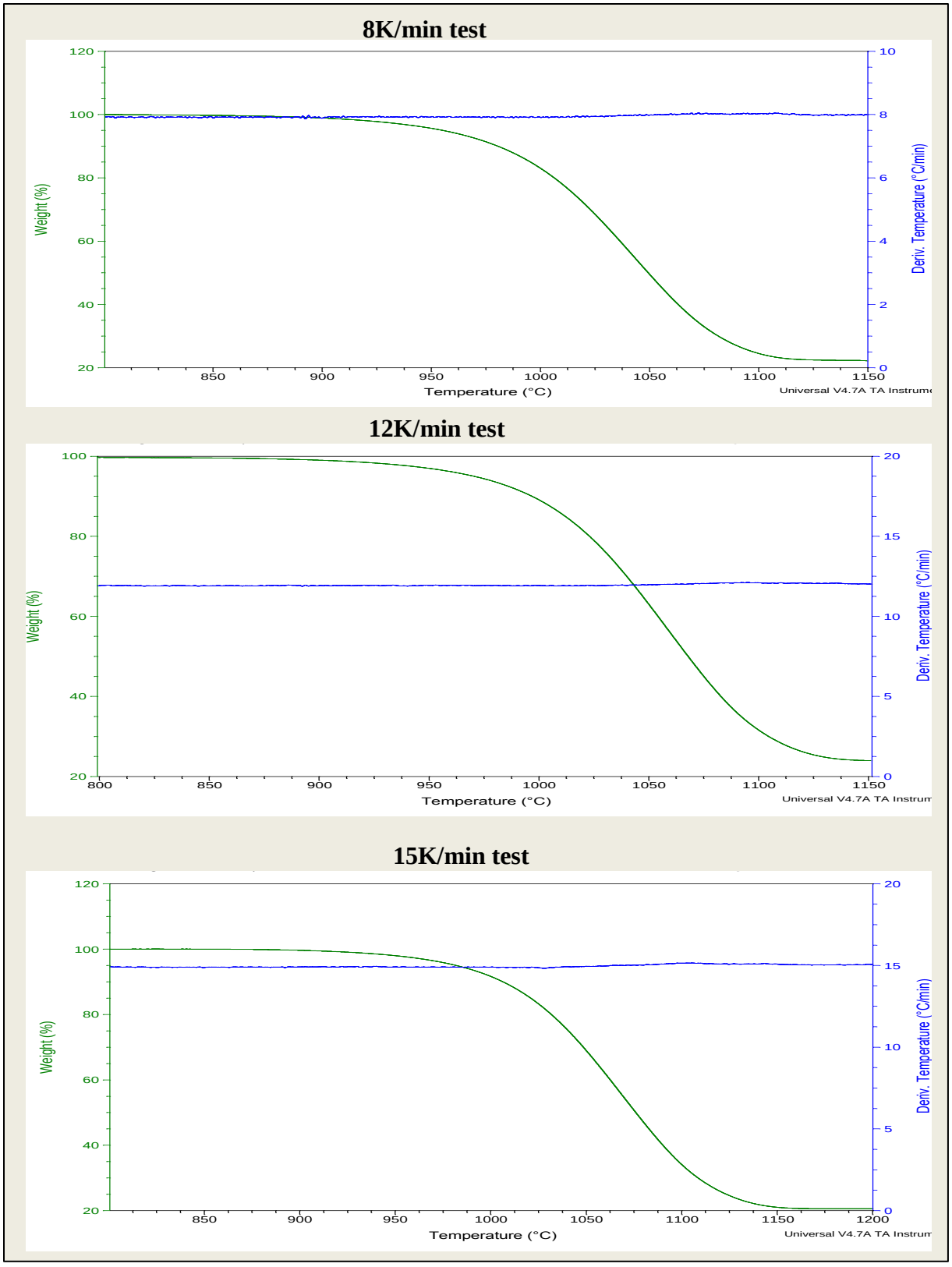

Figure A10-22: Heating rate deviations during coal char gasification.

Grass char gasification

The results obtained during coal char gasification analysis are detailed below.

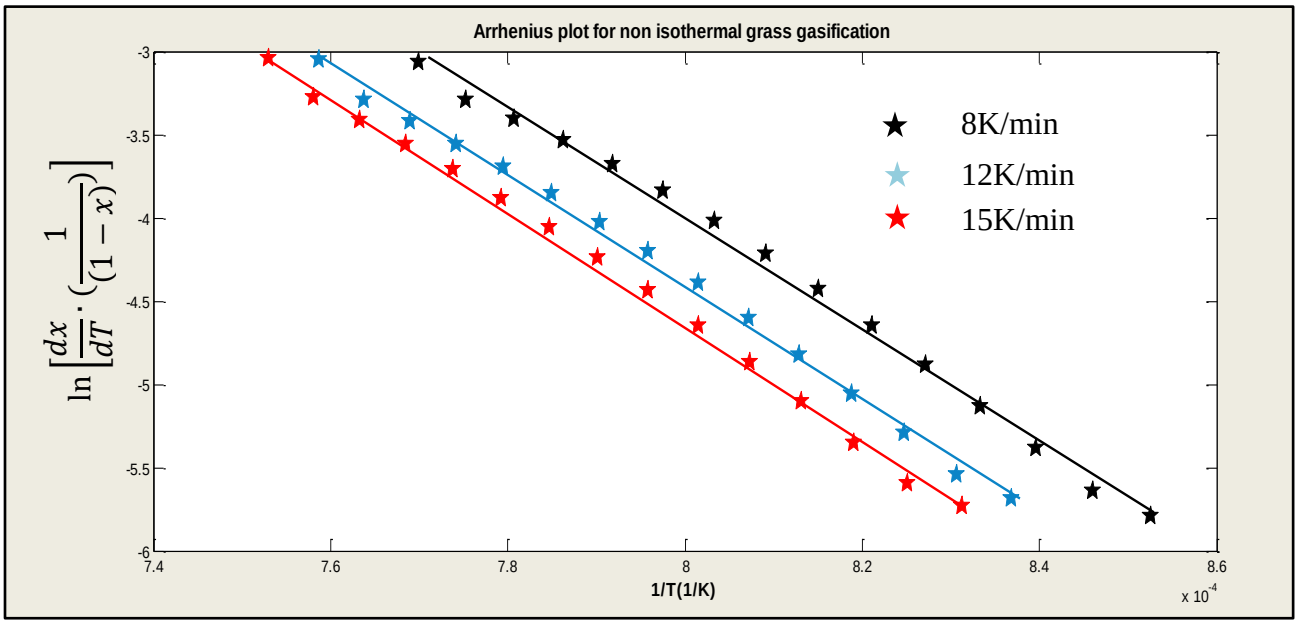

Figure A10-23: Arrhenius plot for grass char gasification.

Table A10-15: Grass char gasification model evaluation.

Plot	Heating rate used (K/min)			First order		RPM	
	E calculation	A calculation	φ calculation	Const B R^2 and RMS	Var B R^2 and RMS	Const B R^2 and RMS	Var B R^2 and RMS
i	8 ,12	8	12	0.9984 0.0173	0.9961 0.0184	0.9999 0.0035	0.9999 0.0033
ii	8,15	8	15	0.9988 0.149	0.9980 0.0153	0.9999 0.0031	0.9999 0.0032
iii	12,15	12	8	0.9993 0.0113	0.9983 0.0117	0.9998 0.0042	0.9998 0.0041
iv	12,8	12	15	0.9984 0.0174	0.9963 0.0187	0.9999 0.0044	0.9999 0.0044
v	15,8	15	12	0.9988 0.0151	0.9981 0.0159	0.9998 0.0052	0.9998 0.0048
vi	15,12	15	8	0.9993 0.0113	0.9986 0.0118	0.9999 0.0036	0.9999 0.0033
Average Model Accuracy				0.99883 0.0369	0.99757 0.0153	0.999867 0.0040	0.99987 0.0039

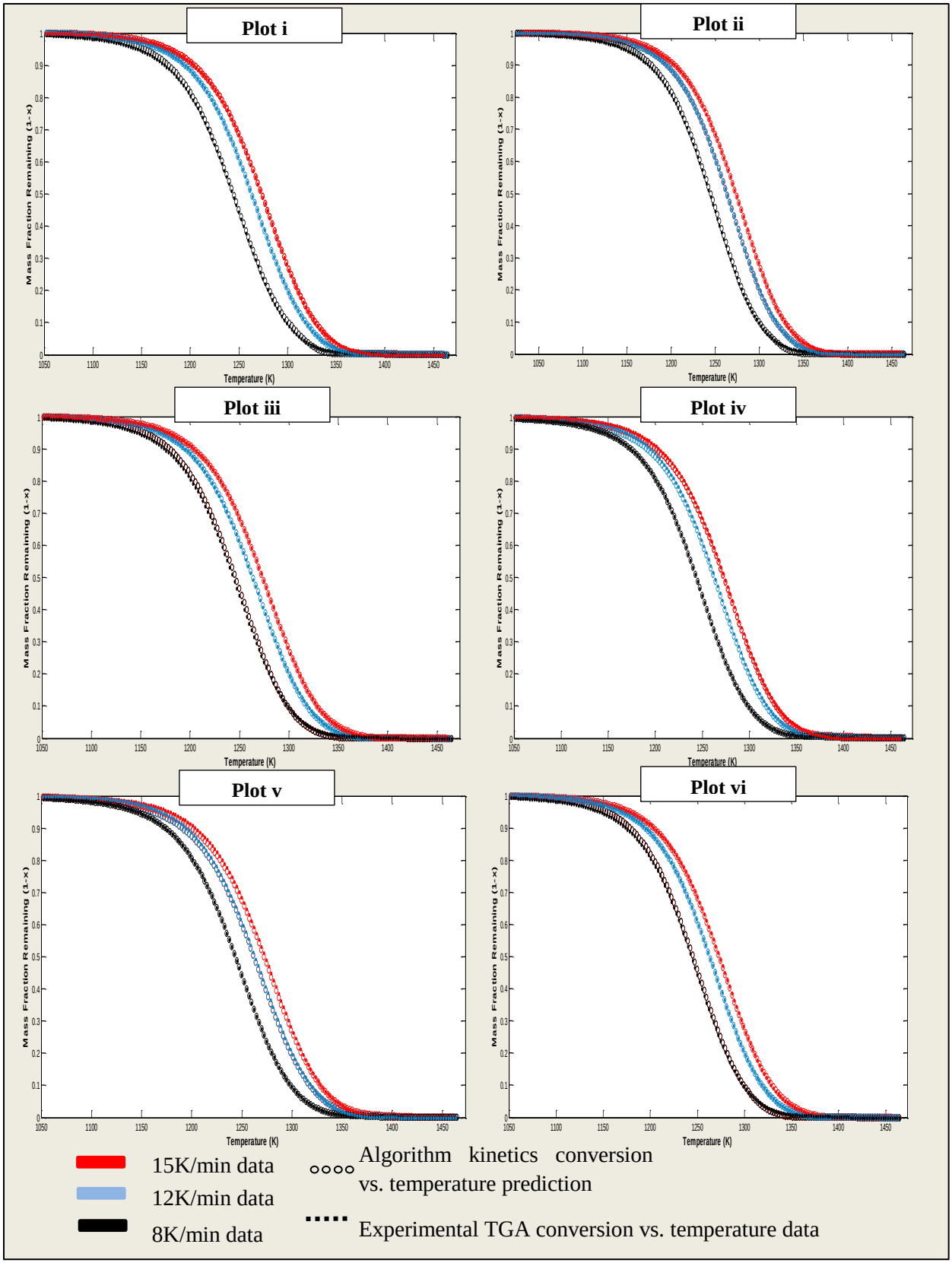

Figure A10-24: Modelling of grass char gasification.

Table A10-16: Grass char gasification kinetics.

Plot	Heating rate used(K/min)			Rpm kinetics					
	E calculation	A calculation	φ calculation	E	A	F0	φ	R^2	RMS
i	8 ,12	8	12	255.08 255.05 261.54 263.07 332.89	1.14e+8 9.87e+7 1.08e+8 1.08e+8 3.19e+10	0.20 0.01 0.28 0.29 0.21	10.0	0.9999	0.0033
ii	8,15	8	15	254.78 260.19 260.5 272.38 275.83 300.03	1.98e+8 1.90e+8 1.87e+8 2.89e+8 3.73e+8 1.49e+9	0.01 0.20 0.02 0.27 0.27 0.22	10.0	0.9999	0.0032
iii	12,15	12	8	270.04 272.48 270.88 275.79 302.34 305.06 252.69	9.07e+8 9.65e+8 4.88e+8 6.40e+8 4.56e+9 5.39e+9 1.94e+7	0.01 0.03 0.23 0.05 0.38 0.03 0.26	10.0	0.9999	0.0041
iv	12,8	12	15	254.74 255.47 256.4 265.64 270.42 332.89 305.57	1.49e+8 8.89e+7 9.25e+7 1.28e+8 1.85e+8 3.19e+10 4.60e+8	0.05 0.05 0.28 0.27 0.17 0.15 0.01	10.0	0.9999	0.0044
v	15,8	15	12	134.3 254.78 259.16 260.05 264.78 271.52 275.83 282.04 287.66 300.03 305.57	4.2e+3 1.98e+8 2.32e+8 2.07e+8 2.00e+8 2.86e+8 3.74e+8 5.64e+8 6.28e+8 1.49e+9 6.33e+8	0.01 0.01 0.03 0.09 0.37 0.03 0.05 0.24 0.08 0.09 0.01	7.7	0.9999	0.0048
vi	15,12	15	8	272.48 271.87 284.13 306.04 306.74 252.69	9.65e+8 6.58e+8 1.21e+9 5.35e+9 5.08e+9 1.93e+7	0.05 0.16 0.38 0.17 0.07 0.17	6.5	0.9999	0.0037

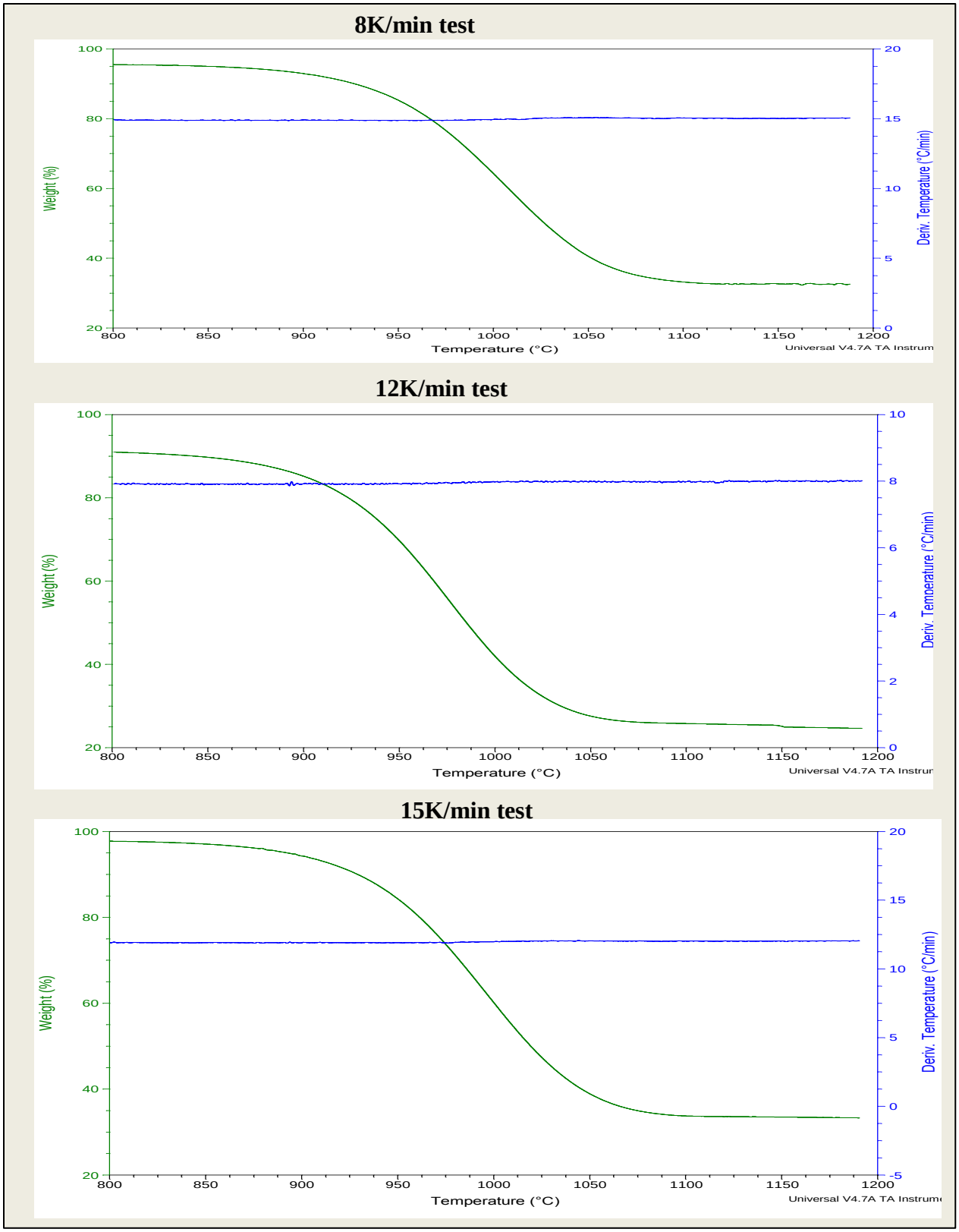

Figure A10-25: Heating rate deviations during grass char gasification

Pine char gasification

The pine char gasification analysis results are outlined in the following figures and tables.

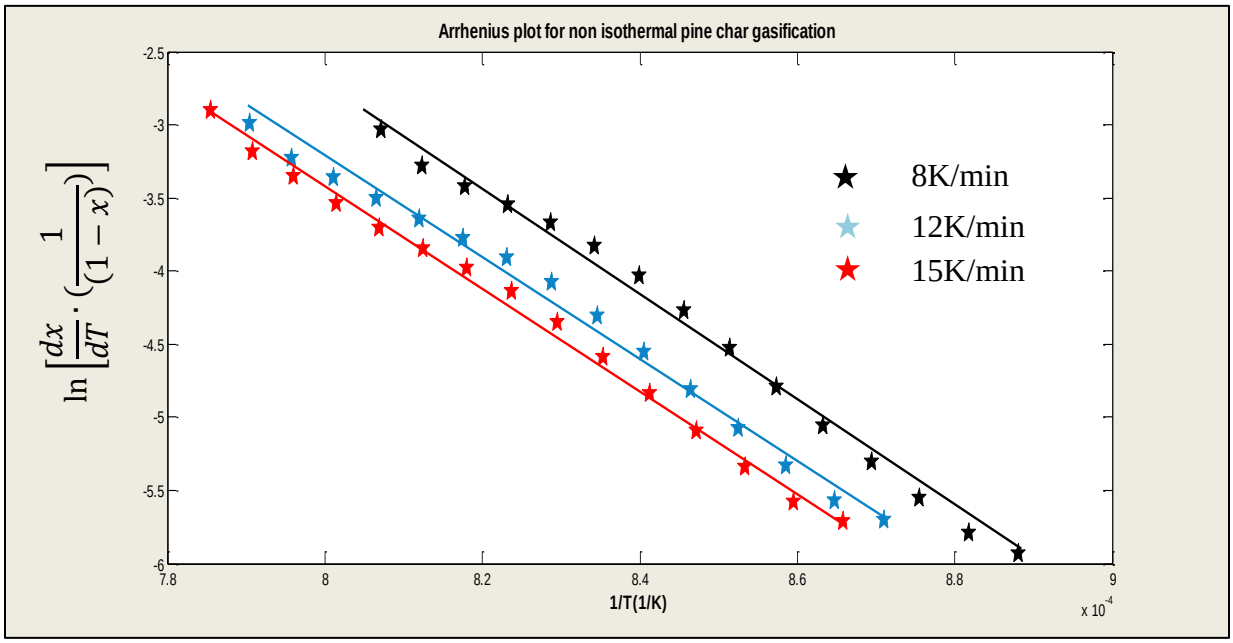

Figure A10-26: Arrhenius plots for pine char gasification.

Table A10-17: Pine char gasification model evaluation.

Plot	Heating rate used (K/min)			First Order		RPM	
	E calculation	A calculation	φ calculation	Const B R^2 and RMS	Var B R^2 and RMS	Const B R^2 and RMS	Var B R^2 and RMS
i	8 ,12	8	12	0.99914 0.0130	0.99936 0.0113	0.9999 0.0047	0.9999 0.0043
ii	8,15	8	15	0.99929 0.0118	0.9993 0.0118	0.9999 0.0030	0.9999 0.0030
iii	12,15	12	8	0.99958 0.0090	0.99932 0.0116	0.9997 0.0058	0.9997 0.0058
iv	12,8	12	15	0.99913 0.0131	0.99936 0.0112	0.9995 0.0082	0.9997 0.0067
v	15,8	15	12	0.9993 0.0117	0.99934 0.0114	0.9999 0.0039	0.9999 0.0038
vi	15,12	15	8	0.99955 0.0092	0.99928 0.0120	0.9998 0.0050	0.9999 0.0037
Average Model Accuracy				0.99933 0.0113	0.99932 0.0116	0.99979 0.0051	0.99983 0.0046

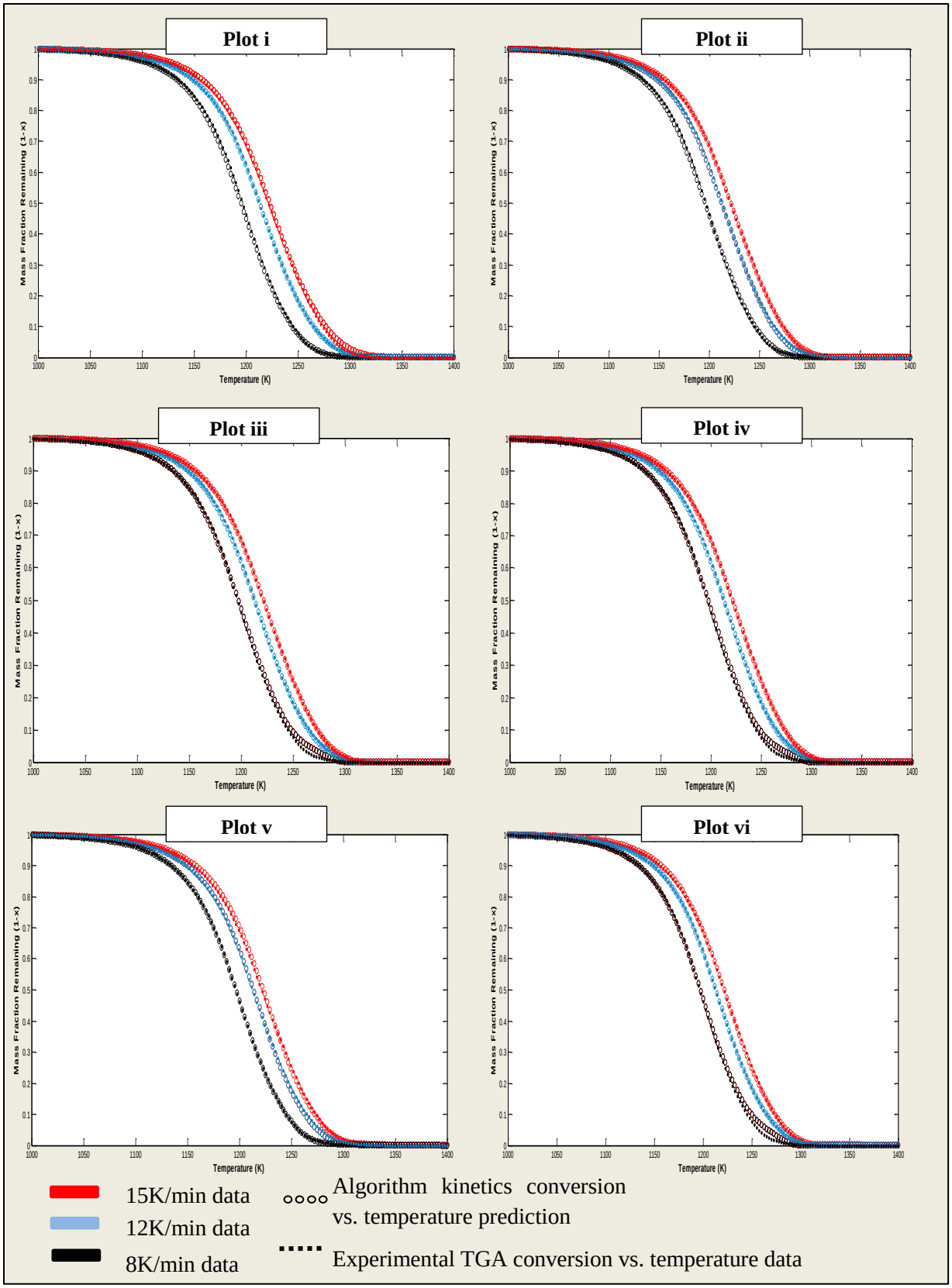

Figure A10-27: Modelling of pine char gasification.

Table A10-18: Pine char gasification kinetics.

Plot	Heating rate used(K/min)			Kinetics determined					
	E calculation	A calculation	φ calculation	E	A	F0	φ	R^2	RMS
i	8 ,12	8	12	269.92 267.26 252.79 249.18 228.63	1.20e+9 8.71e+8 1.091e+8 7.03e+7 5.50e+6	0.35 0.05 0.16 0.22 0.22	8.2	0.9999	0.0043
ii	8,15	8	15	303.77 280.04 272.96 274.81 293.45	2.73e+11 3.96e+9 8.97e+8 9.97e+8 3.21e+9	0.01 0.34 0.22 0.20 0.22	8.3	0.9999	0.0030
iii	12,15	12	8	335.96 288.1 310.52 325.83 574.81	8.37e+12 9.44e+9 3.59e+10 1.47e+11 1.28e+21	0.02 0.35 0.47 0.02 0.13	8.0	0.9997	0.0058
iv	12,8	12	15	267.26 262.71 249.18 242.47 228.63	8.70e+8 4.92e+8 7.00e+7 3.28e+7 5.50e+6	0.04 0.43 0.02 0.31 0.19	8.3	0.9997	0.0067
v	15,8	15	12	242.04 268.84 276.22 276.07 293.45 323.57	1.90e+9 9.72e+8 1.05e+9 9.41e+8 3.21e+9 1.25e+10	0.01 0.51 0.08 0.23 0.16 0.01	8.3	0.9999	0.0038
vi	15,12	15	8	324.28 335.96 285.6 278.07 310.52 325.83	8.37e+12 6.94e+9 2.75e+9 3.59e+10 1.47e+11 1.28e+21	0.01 0.24 0.18 0.23 0.20 0.12	8.0	0.9999	0.0037

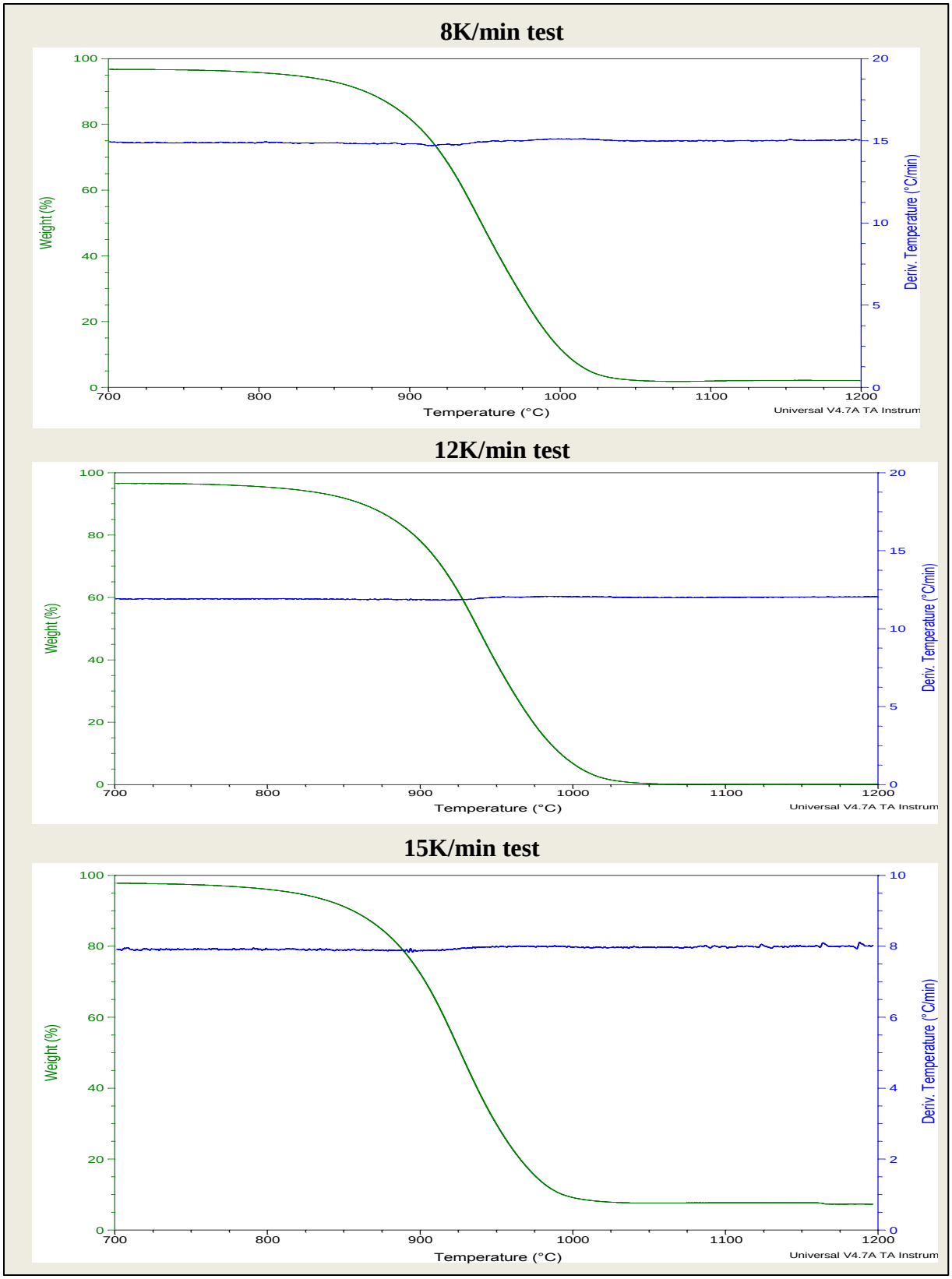

Figure A10-28: Pine char gasification kinetics.

Coal-grass 90:10 char blend gasification

The coal-grass 90:10 char blend gasification analysis results are presented below.

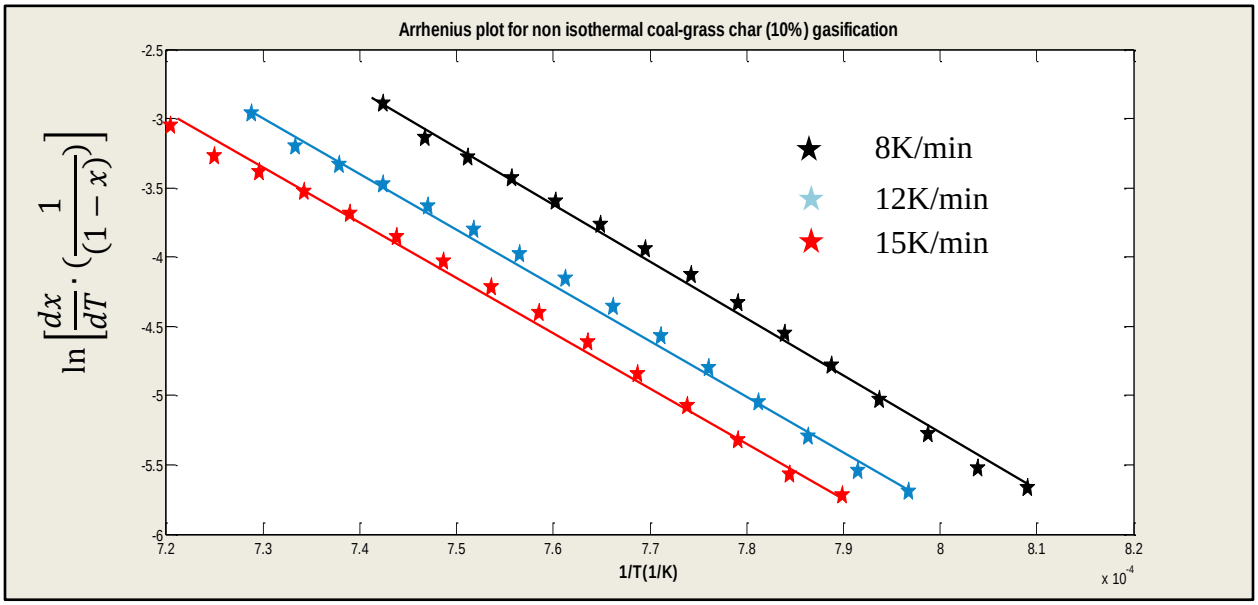

Figure A10-29: Arrhenius plots for coal-grass 90:10 char blend gasification.

Table A10-19: Coal-grass 90:10 char blend gasification model evaluation.

Plot	Heating rate used (K/min)			First order		RPM	
	E calculation	A calculation	φ calculation	Const B R^2 and RMS	Var B R^2 and RMS	Const B R^2 and RMS	Var B R^2 and RMS
i	8 ,12	8	12	0.99107 0.0379	0.99123 0.0363	0.99959 0.0080	0.99959 0.0081
ii	8,15	8	15	0.98789 0.0441	0.98732 0.0445	0.99864 0.0143	0.99875 0.0140
iii	12,15	12	8	0.98052 0.0560	0.98119 0.0575	0.99361 0.0313	0.99399 0.0307
iv	12,8	12	15	0.99107 0.0379	0.99118 0.0364	0.99932 0.0101	0.99949 0.0089
v	15,8	15	12	0.98788 0.0441	0.98731 0.0447	0.99813 0.0166	0.99815 0.0168
vi	15,12	15	8	0.9806 0.0559	0.98127 0.0537	0.99442 0.0296	0.99445 0.0297
Average Model Accuracy				0.98651 0.0460	0.98658 0.0455	0.99728 0.0183	0.99740 0.0180

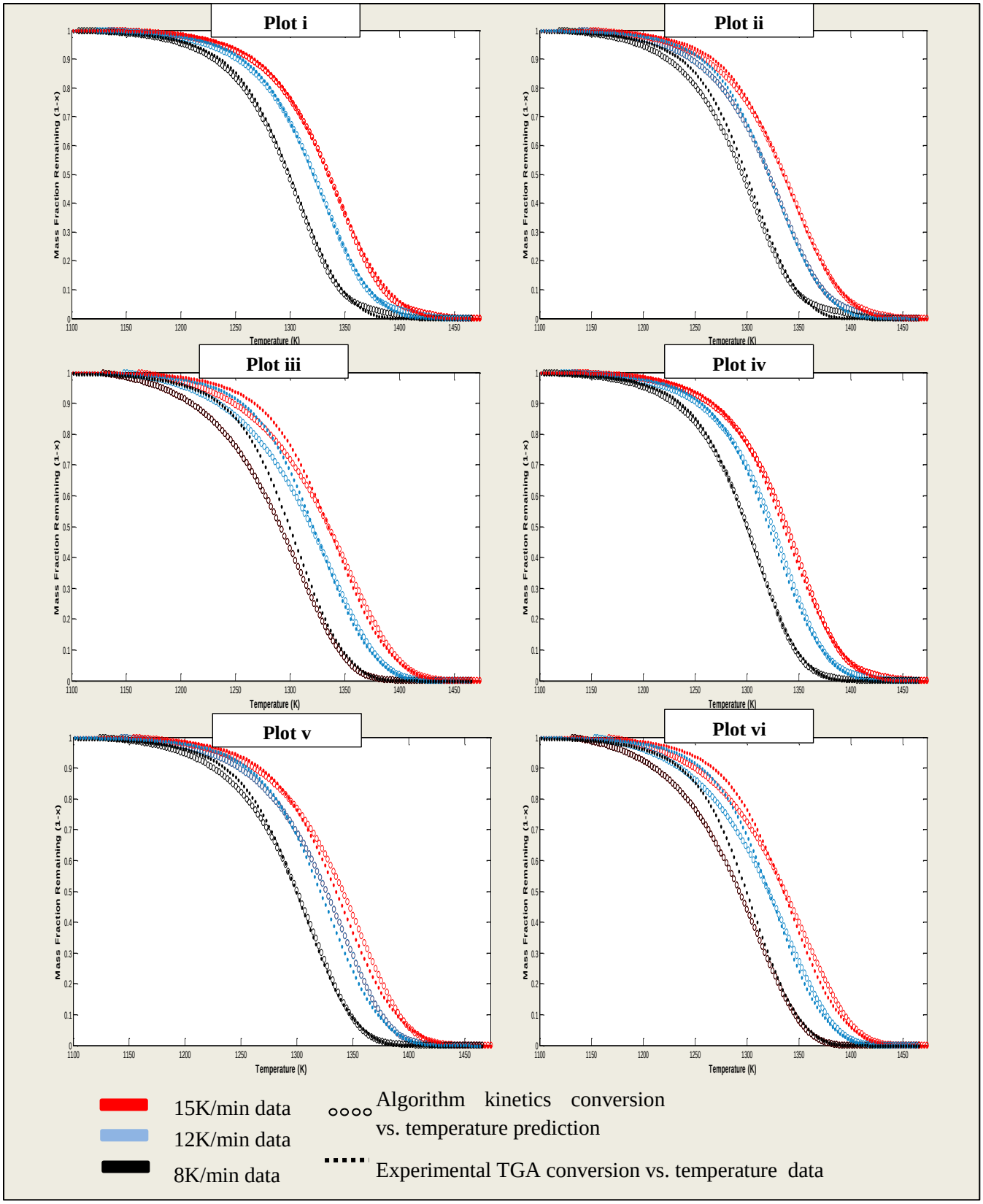

Figure A10-30: Modelling of coal-grass 90:10 char blend gasification.

Table A10-20: Coal-grass 90:10 char blend gasification kinetics.

Plot	Heating rate used(K/min)			Kinetics determined					
	E calculation	A calculation	φ calculation	E	A	F0	φ	R^2	RMS
i	8 ,12	8	12	236.78 230.36 222.3 287.63	3.46e+6 1.43e+6 5.36e+5 6.20e+7	0.03 0.52 0.41 0.04	18.9	0.9996	0.0081
ii	8,15	8	15	207.97 203.19 345.53	1.63e+5 9.20e+5 9.44e+9	0.75 0.22 0.04	18.9	0.9988	0.0140
iii	12,15	12	8	184.6	2.1e+4	1.02	9.7	0.9940	0.0307
iv	12,8	12	15	230.36 222.3 174.97	1.4313e+6 5.3601e+5 3.7e+3	0.41 0.52 0.07	18.9	0.9995	0.0089
v	15,8	15	12	203.19	9.2e+4	1.00	18.7	0.9982	0.0168
vi	15,12	15	8	184.6	2.2e+3	1.03	9.1	0.9945	0.0297

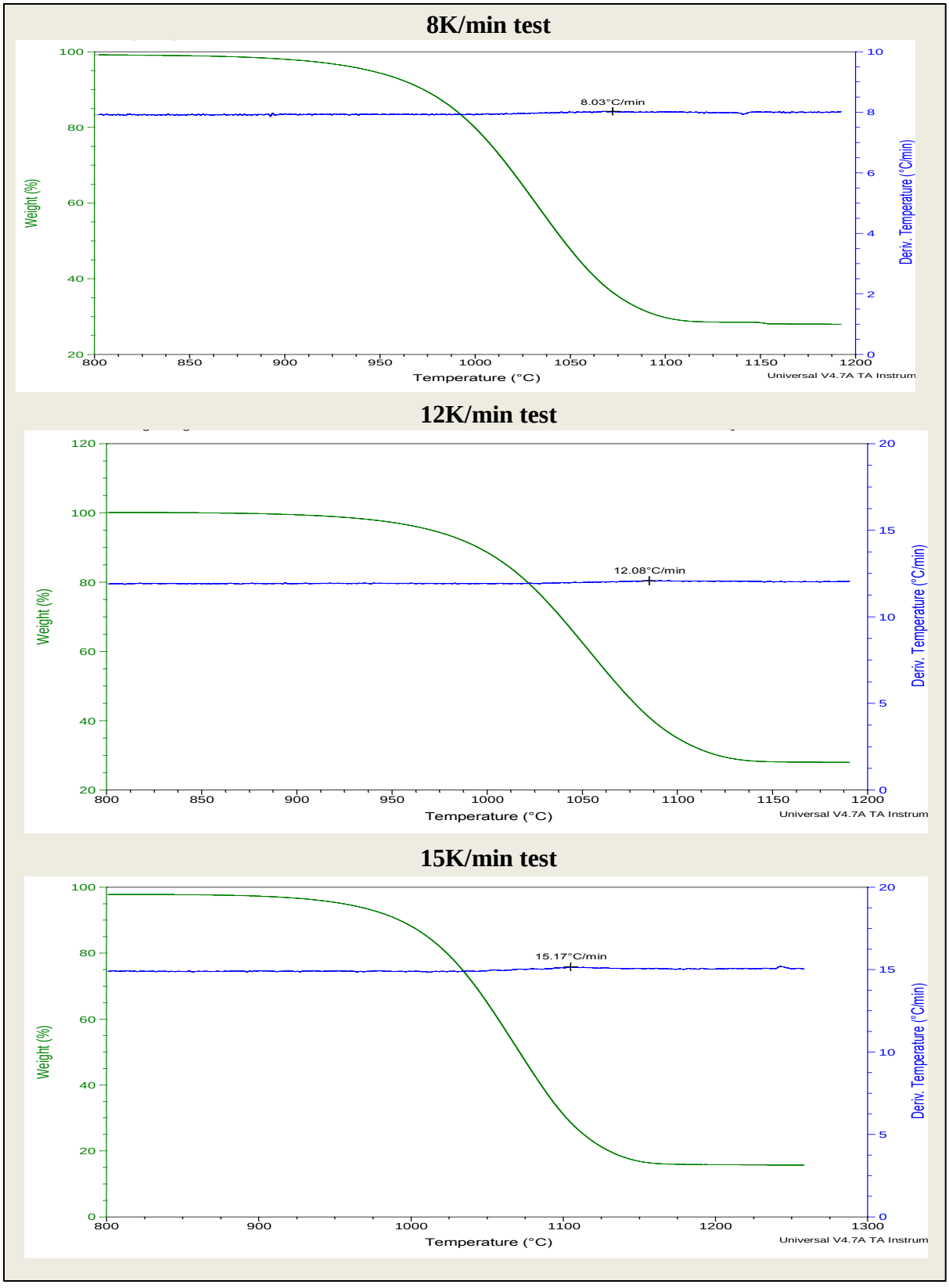

Figure A10-31: Heating rate deviations during coal-grass 90:10 char blend gasification.

Coal-pine 90:10 char blend gasification

The results obtained during coal-pine90:10 char blend gasification are outlined in the tables and figures that follow:

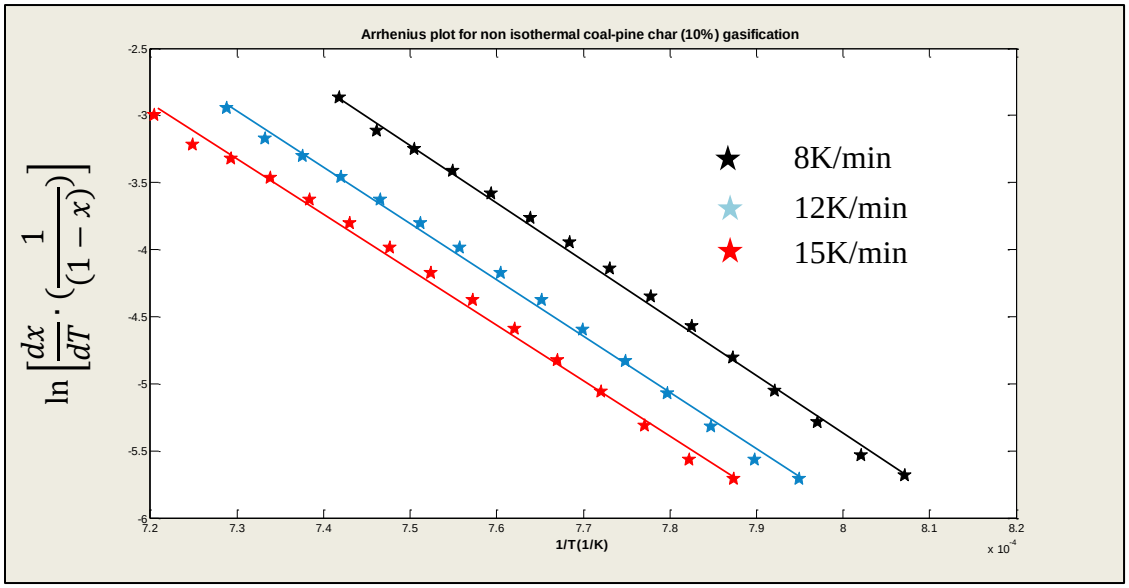

Figure A10-32: Arrhenius plot for coal-pine 90:10 char blend gasification.

Table A10-21: Coal-pine 90:10 char blend gasification model evaluation.

Plot	Heating rate used (K/min)			First order		RPM	
	E calculation	A calculation	φ calculation	Const B R^2 and RMS	Var B R^2 and RMS	Const B R^2 and RMS	Var B R^2 and RMS
i	8 ,12	8	12	0.99048 0.0390	0.98976 0.0386	0.99954 0.0086	0.99961 0.0089
ii	8,15	8	15	0.98897 0.0420	0.98895 0.0420	0.99924 0.0106	0.99927 0.0104
iii	12,15	12	8	0.9858 0.0477	0.98663 0.0487	0.9978 0.0184	0.99738 0.0200
iv	12,8	12	15	0.99048 0.0390	0.98974 0.0386	0.99955 0.0083	0.99962 0.0077
v	15,8	15	12	0.98897 0.0420	0.98896 0.0420	0.99889 0.0129	0.9989 0.0128
vi	15,12	15	8	0.9858 0.0477	0.98662 0.0488	0.99815 0.0171	0.99776 0.0188
Average Model Accuracy				0.98842 0.0429	0.98844 0.0431	0.99886 0.0127	0.99876 0.0131

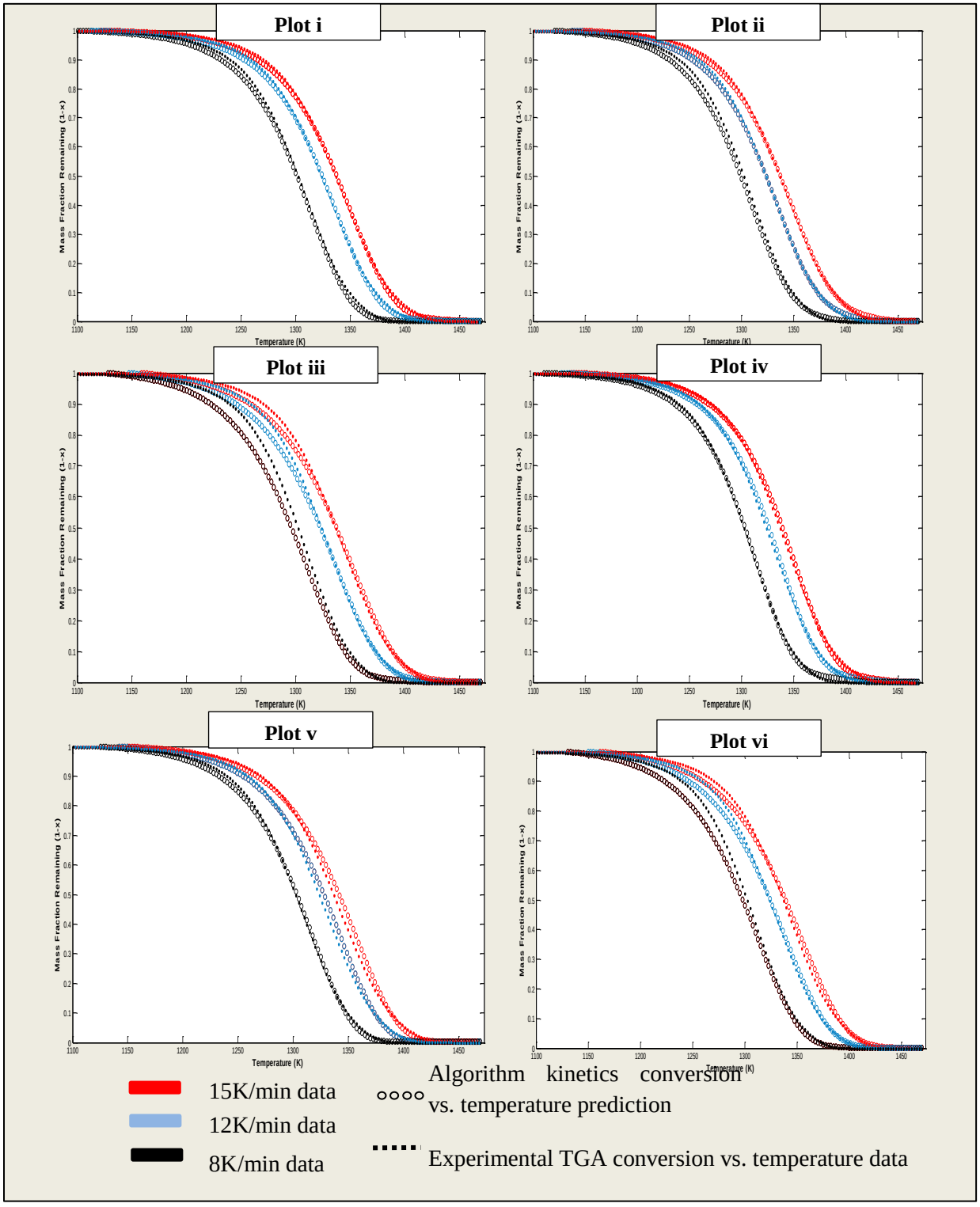

Figure A10-33: Modelling of coal-pine 90:10 char blend gasification

Table A10-22: Coal-pine 90:10 char blend gasification kinetics.

Plot	Heating rate used(K/min)			Kinetics determined					
	E calculation	A calculation	φ calculation	E	A	F0	φ	R^2	RMS
i	8 ,12	8	12	240.93 231.34 149.26	4.38e+6 1.21e+6 3.8e+2	0.27 0.70 0.03	18.9	0.9996	0.0089
ii	8,15	8	15	219.53 203.74	4.11e+5 5.1e+4	0.84 0.17	29.2	0.9993	0.0104
iii	12,15	12	8	200.3 305.57	7.4e+4 2.90e+8	1.00 0.02	18.9	0.9974	0.0200
iv	12,8	12	15	239.01 231.34 305.57	3.40e+6 1.21e+6 2.90e+8	0.28 0.71 0.02	18.9	0.9996	0.0077
v	15,8	15	12	223.05 219.53	6.49e+5 4.12e+5	0.12 0.89	18.9	0.9989	0.0128
vi	15,12	15	8	200.3 240.07	7.3e+4 1.21e+6	0.99 0.02	17.9	0.9978	0.0188

Fi

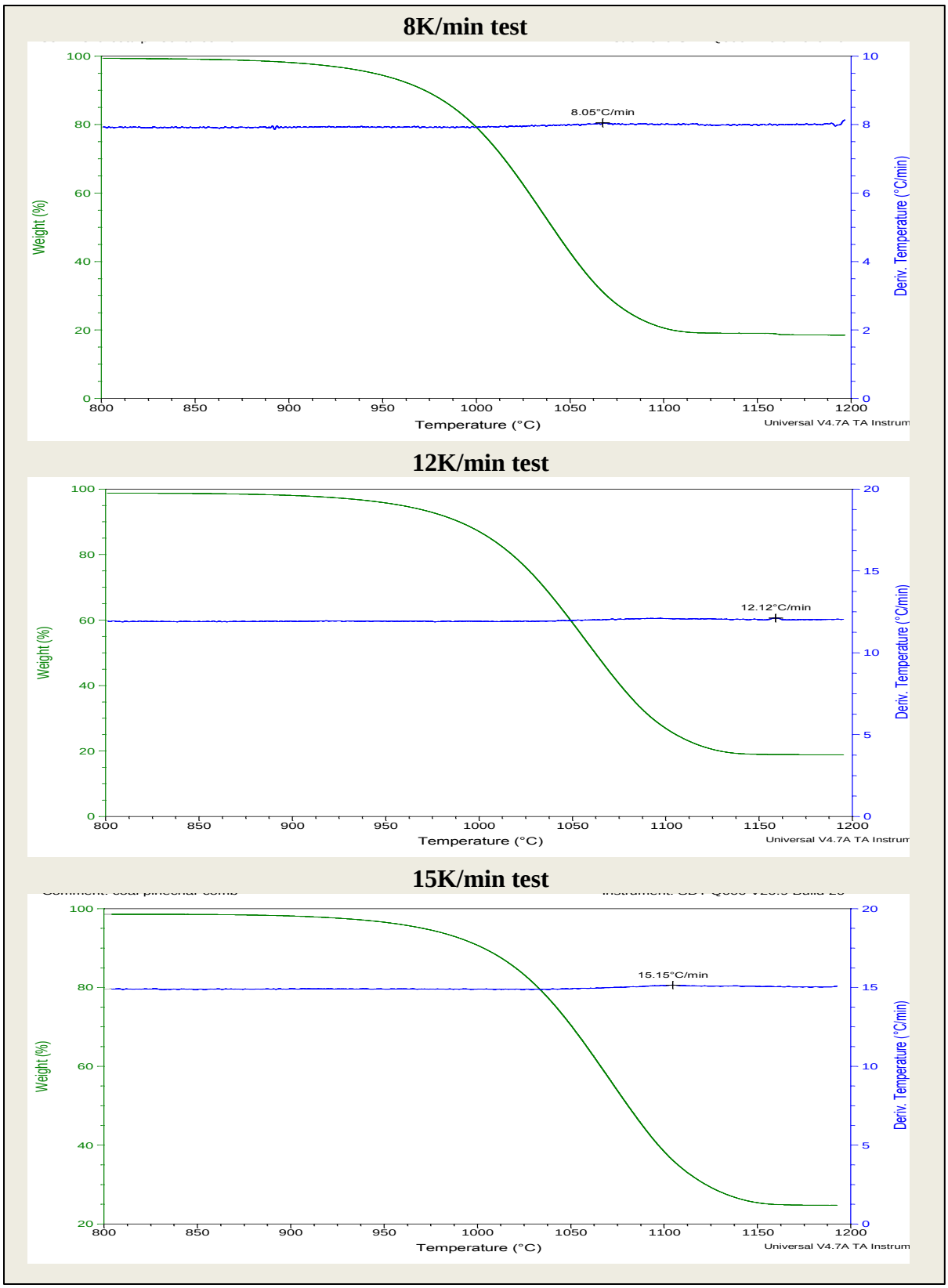

Figure A10-34: Heating rates deviations during coal-pine 90:10 char blend gasification

Isothermal coal char gasification

The results obtained during isothermal coal char gasification are displayed in the following figures and tables:

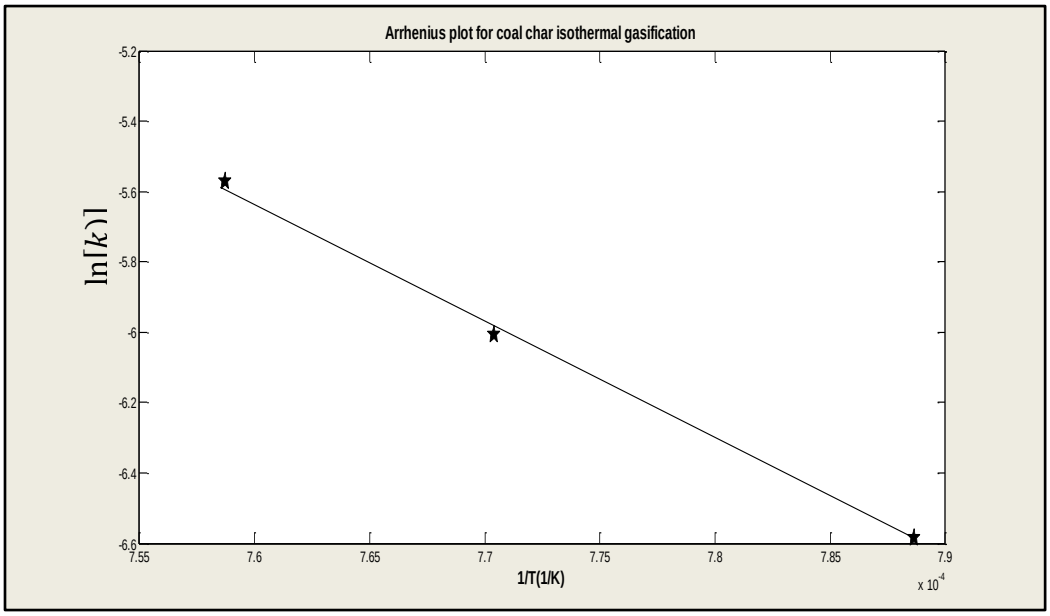

Figure A10-35: Arrhenius plot for isothermal coal char gasification.

As observed in all the previous analysis, the instantaneous heating rates RPM adapted DAE based model is most suitable for modeling char gasification. Therefore, isothermal coal char gasification was only modeled by the instantaneous temperature RPM adapted DAE based model.

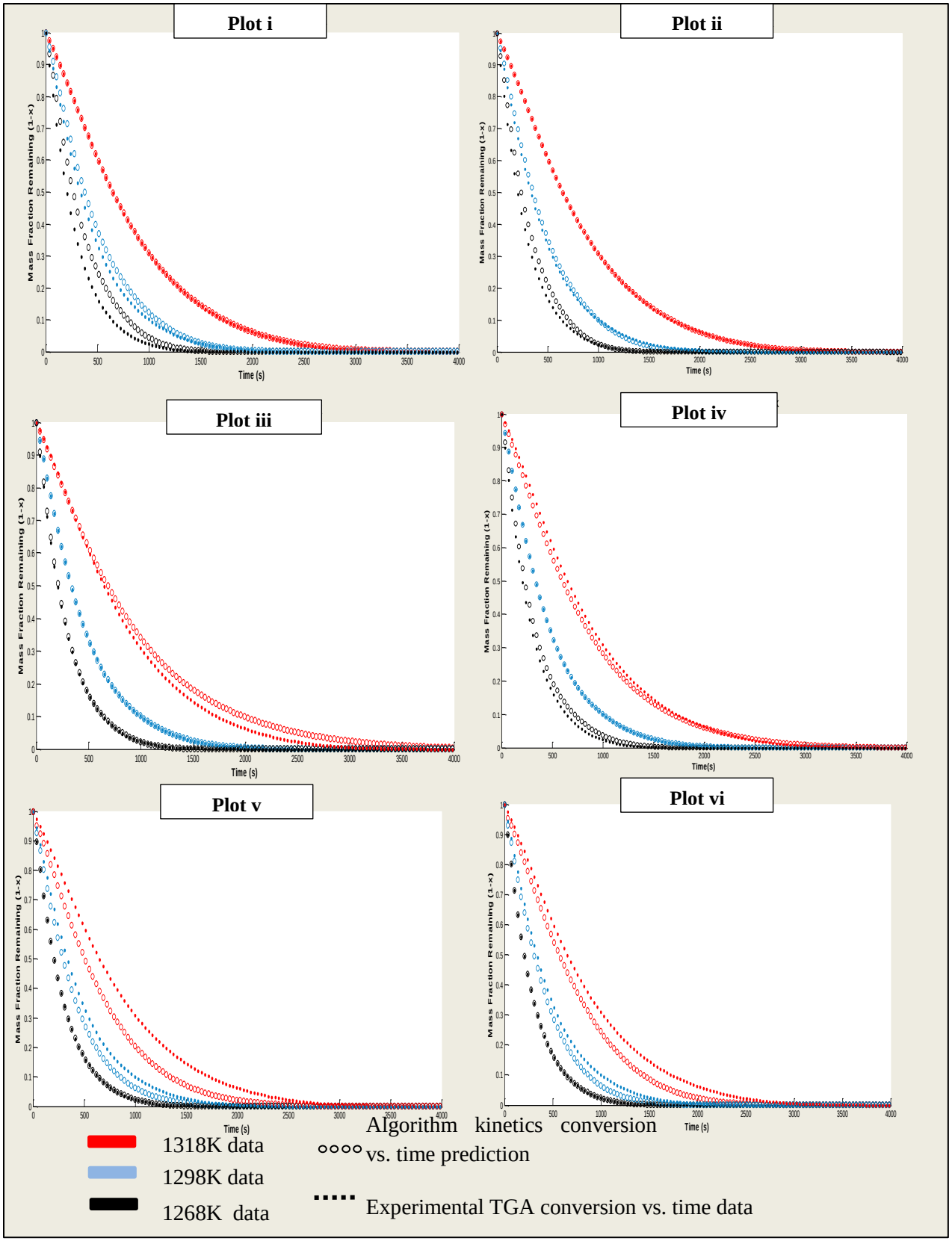

Figure A10-36: Modelling of isothermal coal char gasification.

Table A10-23: Isothermal coal char gasification kinetics.

Plot	Heating rate used(K/min)			Kinetics determined					
	E calculation	A calculation	φ calculation	E	A	F0	φ	R^2	RMS
i	8 ,12	8	12	302.29 300.03 277.27 274.66 215.53	3.90e+9 3.0e+9 1.98e+8 1.47e+8 2.73e+5	0.04 0.02 0.29 0.07 0.57	11.7	0.9854	0.0148
ii	1268,1318	1268	1298	321.98 319.62 296.28 293.81 247.9	2.52e+10 1.92e+10 1.20e+9 9.04e+8 5.88e+6	0.04 0.02 0.29 0.07 0.57	11.7	0.9952	0.0083
iii	1298,1318	1318	1268	363.67 330.61 327.71 310.73	1.51e+12 3.10e+10 2.24e+10 2.18e+9	0.08 0.20 0.28 0.42	18.0	0.9988	0.0040
iv	1298	1268	1318	317.32 314.22 281.66 279.93 229.65	2.18e+10 1.54e+10 3.32e+8 2.68e+8 1.19e+6	0.01 0.07 0.20 0.28 0.42	6.8	0.9967	0.0558
v	1318	1268	1298	395.37 336.26 313.74 312.09 284.03 280.06 247.9 180.19	5.87e+14 1.32e+11 9.60e+9 7.85e+9 3.04e+8 1.96e+8 5.88e+6 6.45e+3	0.03 0.03 0.07 0.01 0.15 0.10 0.35 0.26	17.0	0.9926	0.0150
vi	1318,1298	1298	1268	429.38 365.68 344.01 342.81 318.93 318.39 298.41 166.24	1.30e+16 1.93e+12 1.52e+11 1.30e+11 7.34e+9 6.49e+9 5.91e+8 1.8e+3	0.03 0.03 0.08 0.01 0.15 0.10 0.35 0.26	17.0	0.9991	0.0051

10.4. APPENDIX D: PRESENTATIONS AND FUTURE PUBLICATIONS

The appendix presents a poster presented at the annual Fossil Fuel Foundation 2012 Conference held in Johannesburg.

10.4.1. Fossil Fuel Foundation 2012 Conference Poster presentation

THE APPLICATION OF A DISTRIBUTED ACTIVATION ENERGY BASED MODEL TO THE COMBUSTION OF BIOMASS AND COAL CHAR BLENDS

Patience Moyo , Shezhaad Kauchali ,Nicola Wagner : School of Chemical and Metallurgical Engineering

1. INTRODUCTION

- Combustion is a major process for energy conversion in the globe.
- Co-firing of coal with biomass offers the advantage of a reduction in greenhouse gas emmisions and major pollutants.
- The determination of combustion kinetics of coal and biomass is a crucial area of study for the design and optimization of energy systems.

Pine wood chips (PW) and highveld grass (HG), were selected for blending with a vitrinite-rich coal (VC) during combustion using thermo-gravimetry.

2. STUDY AIM AND OBJECTIVES

AIM: To validate the Distributed Activation Energy based model (DAEBM) by application to thermo-analytical data.

OBJECTIVES:

- To determine and analyze the kinetics of the combustion of coal and biomass char blends under non isothermal conditions.
- To investigate the effect of the presence of biomass on coal combustion.

3. METHODOLOGY

CHARACTERIZATION ANALYSES

- Proximate analysis
- Ultimate analysis
- ICP-OES analysis
- Gross calorific value determination

Figure 1: Thermo-gravimetric Analyser

SAMPLE BLENDING

(90:10 and 50:50 coal-biomass heat input ratios)

THERMO-GRAVIMETRIC ANALYSIS (TGA)

- Char prep: Samples heated from 25°C to 1250°C in N_2
- Combustion: Chars heated at heating rates of 8K/min, 12K/min and 15K/min from 25°C to 750°C in air.

MODEL APPLICATION AND KINETICS DETERMINATION

4. THE DAEBM

TGA data at two heating rates (β_1, β_2) is discretized by the selection of n values of conversion as candidate parallel reactions. Where:

$$\frac{M(t)}{M_0} = \omega_\infty + \sum_{i=1}^{n} (f_{i,0}) \exp\left[-\frac{A_i}{\beta}\int_{T_0}^{T} \exp(-E_i/RT(t))dT\right] \quad \text{-[1]} \quad \text{(Scott et al. [1])}$$

$M(t)/M_0$: Normalized sample mass; ω_∞: Mass fraction inerts; $f_{i,0}$: The initial mass fraction of M_0 which decomposes with activation energy E_i and pre-exponential factor A_i; $\Psi_i(\beta_i, T_o)$

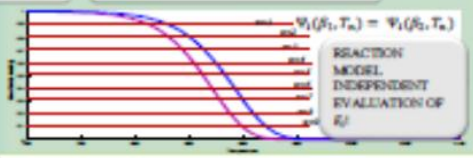

For the known reaction model($f(x)$),a point of maximum reaction rate is analytically evaluated,x_{max}.A_i is calculated by the substitution.....

$$\ln \Psi_i(x_{max}, T_{max}) = \int_0^{x_{max}} \frac{dx}{f(x)} = -\frac{A_i}{\beta}\left[\int_{T_0}^{T} \exp(-E_i/RT(t))dT\right] \quad \text{-[2]}$$

The evaluation and inversion of equation [1] calculates the $f_{i,0}$ values. The DAEBM outputs E_i, A_i and $f_{i,0}$ for the actual reaction/s taking place!!

5. RESULTS AND DISCUSSION

Table 1: Coal and Biomass Characterization

Analysis	Proximate analysis (wt%,dry basis)			CV	ICP-OES(% Content)		Ultimate analysis (wt.%, dry ash free basis)				
Sample	Ash	FC	VM	(kJ/kg)	Total catalytic species (Fe_2O_3,SiO_2,Al_2O_3,CaO) %	Ratio K$_2$O/SiO$_2$	C	H	N	S	O
VC	12.6	58.7	36.8	28.1	7.1	0.02	79.5	5.6	1.7	0.9	12.3
HG	7.5	15.2	77.4	17.1	18.6	0.12	50.1	6.5	0.6	0.1	42.9
PW	0.2	15.2	84.6	18.5	6.8	0.45	51.4	6.5	0.1	0.0	42.0

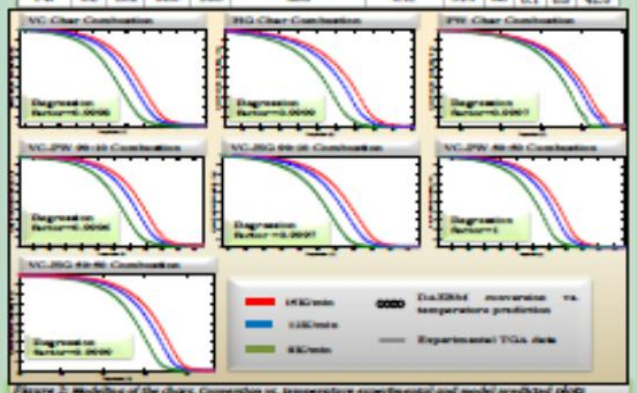

Figure 2: Modelling of the chars. Conversion vs. temperature experimental and model predicted plots

Table 2: Char combustion kinetics

Sample	E$_i$(kJ/mol)	A$_i$(s^{-1})	$f_{i,0}$	ω_∞
VC	127.4	2.82E+5	1.00	16.5
PW	255.5	2.90E+15	0.05	8.3
	193.7	7.88E+9	0.20	
	103.3	5.34E+0	0.74	
HG	127.0	1.60E+5	0.19	10.5
	130.5	2.17E+5	0.80	
VC-HG 90:10	125.7	5.38E+4	1.00	19.0
VC-PW 90:10	125.6	4.2E+4	0.42	19.0
	125.0	1.93E+5	0.57	
VC-HG 50:50	125.9	2.09E+5	1.00	15.9
VC-PW 50:50	128.3	3.94E+5	1.00	17.9

- Kinetic analysis was carried out using the compensation effect:

$$\log A_{i,0} = aE_{a,i} - b \ldots \text{[3]}$$

(Vyazovkin,[2])

- Synergetic behavior was analyzed using the additive method [3]-[4].

6. CONCLUSIONS

- PW char has the least ash, S, and N, and yet the highest catalytic organic matter content. The characterization implies that the PW is the most reactive char.
- The DAEBM successfully modeled all the chars and blends during combustion to high accuracy using the random pore reaction model. The DAEBM is a robust and accurate method of kinetics determination.
- Kinetic analysis considering the E and A values obtained confirms that the PW char is the most reactive material, followed by HG and VC chars respectively.

- Negligible changes were observed in the activation energy for the 90:10 coal-biomass char blends. A decrease in activation energy was observed during the combustion of the 50:50 blends.
- Synergetic behavior between the coal and the biomass was observed for the 50:50 coal-biomass blends.

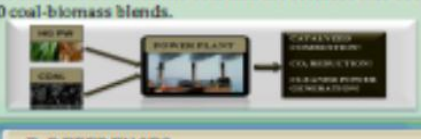

7. REFERENCES

[1] Scott, S. A., Dennis, J. S., Davidson, J. F., Hayhurst, A. N., 2006. An algorithm for determining the kinetics of devolatilization of complex solid fuels from thermogravimetric experiments. Chemical Engineering Science, 61(9), pp.2989-2998.

[2] Vyazovkin, S., 2008. Handbook of Thermal Analysis and Calorimetry , Nonconventional kinetics. Chapter 13, pp. 503-537.

[3] Sadhukhan, A. K., Gupta, P., Goyal, T., Saha, R. K., 2008. Modelling of pyrolysis of coal-biomass blends using thermogravimetric analysis. Bioresource technology, 99(17), pp.8022-6.

[4] Gil, M. V., Casal, D.,Pevida, C., Pis, J. J., Rubiera, F., 2010. Thermal behaviour and kinetics of coal/biomass blends during co-combustion. Bioresource technology, 101, pp.5601-8.

Figure 10-37 Poster presented at the Fossil Fuel Foundation 2013 annual conference

10.4.2. Draft journal article for publication

The Application of a Distributed Activation Energy (DAE) Based Model to the Combustion of Biomass and Coal Chars

P. Moyo[1], S. Kauchali[1], N. Wagner[1]

School of Chemical Engineering, University of Witwatersrand, 1 Jan Smuts avenue, Braamfontein, 2000, Johannesburg, South Africa.
Corresponding author: P. Moyo- patiencem24@gmail.com.

Abstract

A kinetic study on char combustion was conducted using Thermo-gravimetric analysis (TGA) on chars from a high vitrinite coal (VC), highveld grass (HG), and pine wood (PW). The samples were heated from room temperature up to 1023K at heating rates from 8, 12 and 15K/min in air at atmospheric pressure. The chars were modeled by the application of a modified distributed activation energy (DAE) based model. The DAE based model was initially developed by Scott et al. [Scott et al., 2006] for the pyrolysis of complex fuels obeying linear kinetics. The modified DAE model was able to derive the activation energy, E, the grouped pre-exponential factor, A, and the number of reactions occurring in the thermal conversion process. Furthermore, the mass fraction associated with each unique reaction was obtained. The ability to determine multiple reactions distinguishes the DAE based model as a unique and robust method for kinetics determination.

The first order and the random pore reaction models (RPM) were applied to describe the reaction profiles. The combustion of the three chars was successfully modeled using the RPM to high accuracy. The biomass chars were modeled using multiple reactions whereas coal char was modeled with a single reaction. E's and A's in the range of 180-255kJ/mol and 5.34E+8 to 2.80E+15 $s^{-1}m^{-1}$ were determined for the PW char. E's and A's in the range of 127- 138kJ/mol and 1.60E+5 to 2.82E+5 $s^{-1}m^{-1}$ were determined for the rest of the chars and blends during combustion. The structural parameters obtained lie in the range of 8.3 to 18.9. The kinetic analysis shows that PW char is the most reactive char whilst VC char is least reactive.

1. Introduction

Over the years, coal has proven stability in both cost and supply, leading to the fuel gaining renewed interest as an energy source [2]. However, due to coal's high carbon to hydrogen ratio, carbon dioxide control is a major concern for its current and future use. Combustion and gasification are the two main processes used to convert the chemical energy content in coal. Henrich et al. [3] notes that even though char combustion is an old and well known process, the complex heterogeneous reaction mechanisms are not reliably understood. A precise knowledge of the intrinsic kinetic characteristics of the combustion processes is essential for understanding and modeling combustion at industrial scale, so as to develop an efficient and economically competitive clean process [4-13]. The optimization of coal conversion processes not only leads to a significant reduction in carbon dioxide emissions, but an extension of the coal resource lifetimes as well [14].

Coal combustion may be described as a series of sequential events, beginning with drying, followed by devolatilization, homogeneous oxidation of volatile matter and heterogeneous oxidation of solid char, and, finally, the burning out of char [9]. Volatile combustion occurs very fast such that the overall combustion rate is controlled by the relatively slow char combustion process [15,16]. The determination of intrinsic kinetics of combustion of coal and biomass is a crucial area of study for the optimization of energy systems.

The use of coal with carbon dioxide neutral energy sources like biomass, offers the advantage of a reduction in greenhouse gas emissions [17], and is also suggested to have a positive impact on the emission of other pollutants like SO_2 and NO_x [17],[18]. With the endorsements of mandatory targets by the European Council and Kyoto Protocol, for the use of renewable sources and the controlling of CO_2 emissions, the interest in biomass continues to rise [19].

The main purpose of modeling chemical reactions is to obtain the kinetic triplet of the reaction, and use it to reproduce the progression of the reaction under typical industrial operating conditions. The kinetic triplet consists of the reaction model function,$(f(x))$, where x is conversion, the activation energy of the conversion reaction(E), and the pre-exponential factor,(A). An advanced iso-conversion method is applied to thermo-analytical data obtained

from the combustion of coal and biomass chars in this research. The algorithm was intended for the determination of kinetics for a complex fuel dissociating under numerous parallel first order reactions. Saloojee [14] identified that the evaluation of the activation energy using the algorithm is model independent. Vittee [20] extended the use of this algorithm to fuels dissociating according to the random pore reaction model. These adaptations have been suited to both non-isothermal and isothermal conditions, and have proven apparent success in the modeling of coal char combustion and gasification using TGA.

The aim of the current work is to determine the intrinsic reaction kinetics of combustion of biomass and coal chars under non- isothermal conditions. This aim is accomplished by the successful validation of the DAE based model on application to the thermo-analytical data obtained. A kinetic analysis of the behavior of the materials during these processes is presented.

2. Experimental Procedure

A low ash, high volatile, high vitrinite coal (VC) obtained from density fractionation of a South African coal was used in this study. The two types of biomass considered were: highveld grass (HG) and pine wood (PW), obtained from South Africa's Gauteng province. A summary of the characterization analysis of the raw materials is presented on Table 2-1. It is noted that the ash content analysis implies order of reactivity from the most reactive to the least, given as: PW, HG, and VC. This is relative to the catalytic oxides contained in each of the materials [21-24]. Capucine Dupont et al. [21] identified that the reactivity for woody biomass correlates with the ratio of potassium / silica, confirming the catalytic effect of the potassium and reflecting an inhibiting effect of silica. All the samples were milled to a -53μm size.

Table 2-1: *Characterization analysis of the raw samples*

Proximate analysis (wt.%, dry basis)				**Ultimate analysis (wt.%, dry ash free basis)**					**Gross calorific value (MJ/kg)**
	Ash	**FC**	**VM**	**C**	**H**	**N**	**S**	**O**	
VC	12.55	50.67	36.78	79.53	5.61	1.70	0.87	12.30	28.12
HG	7.45	15.15	77.4	50.06	6.53	0.40	0.14	42.87	17.12
PW	0.23	15.19	84.58	51.44	6.52	0.09	0.00	41.95	18.52

Ash content (Oxide wt. %)							
	SiO_2	**Fe_2O_3**	**CaO**	**MgO**	**K_2O**	**Total catalytic species (Fe_2O_3,K_2O,MgO,CaO) %**	**Ratio K_2O/ SiO_2**
VC	68.00	3.53	1.69	0.56	1.28	7.06	0.02
HG	73.80	0.86	5.95	2.67	9.06	18.58	0.12
PW	8.36	8.22	40.10	15.10	3.39	66.81	0.41

3. Char Preparation

All the samples were pyrolysed in an SDT-Q600 thermo-gravimetric analyzer (TGA) in a nitrogen atmosphere. The samples were heated at a constant heating rate of 20K/min up to 1250^0C. When this temperature was reached, the samples were cooled to 700^0C and held at this temperature to ensure the release of all the volatile matter. Even though the results from char production via TGA may not be directly applicable to industrial facilities, char samples are easy to obtain and are very useful for comparison purposes [16].

4. Combustion tests

The conversion tests were carried out using thermo-gravimetric analysis in the SDT-Q600 TGA. The samples were spread in uniform layer in the crucibles, at sample masses of 1.5mg ±5%, and heated at the three heating rates(8,12,15K/min) from ambient temperatures to 750^0C [16]. A constant air flow rate of 70ml/min was maintained throughout the analysis. The conditions specified were selected prior to a preliminary analysis to ensure chemical reaction control during the reactions. For all the analysis carried out, Arrhenius plots were plotted in order to ensure that there is no shift in the data, specifically from a high activation energy at lower temperature to a lower activation energy at a higher temperature. This would correspond to the shift from the chemical reaction controlled regime to the pore diffusion controlled regime. Hence, the

conversion tests were carried out in the chemical reaction controlled regime. The low sample mass and heating rates ensure the minimization of the actual heating rate deviations from the programmed heating rate during the conversions. The tests were repeated to determine the reproducibility, which averaged a RMS error value of 0.0016.

5. Kinetic analysis

The kinetic analysis was carried out with the use of a DAE based model. The DAE based model is an algorithm that was originally designed for the kinetics determination of a material decomposing subject to numerous parallel first order reactions [1]. For such a material:

$$\frac{M(t)}{M_0} = w + \sum_{All\ reactions,i} f_{i,0} exp\left[-A_i \int_0^{\tau} exp(-E_i/RT(t))dt\right] \qquad [3\text{-}1]$$

Where $M(t)$ is the sample mass of initial value M_0 containing a fraction w of inert material. $f_{i,0}$ is the initial mass fraction of M_0 which decomposes with activation energy E_i and pre-exponential factor A_i.

Vittee [20] adapted this algorithm to the dissociation of materials subject to numerous parallel random pore reactions. For this material:

$$\frac{M(t)}{M_0} = w + \sum_{All\ reactions,i} f_{i,0} exp\left[\frac{1 - (\frac{\varphi}{2}\left[-A_i \int_0^{\tau} exp(-E_i/RT(t))dt\right] + \frac{2}{\varphi})^2}{\varphi}\right] \qquad [3\text{-}2]$$

Where φ is the RPM structural parameter. With this algorithm it is possible to find the$f_{i,0}$, A_i and E_i of each reaction using the experimentally measured sample mass. By assuming the range of mass component fractions (f) in the char, the heterogeneity of the reacting compound is catered for [16]. The algorithm is applicable to thermo-gravimetric experiments carried out at two or more different, but constant, heating rates. The Equations [3-1] and [3-2] above become linear matrix problems if the reactions are known, together with each value of E and A. The mass of solid fuel remaining at a time is the sum of the masses of each of the components remaining. The

equations may then be written in a matrix format such that for any set of times $(t_1, t_2, t_3 \ldots.)$ the remaining mass of fuel $M(t)$ is given by equation [3-3].

$$\frac{1}{M_0}\begin{bmatrix} M(t_0) \\ M(t_1) \\ M(t_2) \\ \vdots \\ \vdots \end{bmatrix} = \begin{bmatrix} \Psi_1(t_0) & \Psi_2(t_0) & \ldots & \Psi_n(t_0) & 1 \\ \Psi_1(t_1) & \Psi_2(t_1) & \ldots & \Psi_n(t_1) & 1 \\ \Psi_1(t_2) & \Psi_2(t_2) & \ldots & \Psi_n(t_2) & 1 \\ \vdots & \vdots & \vdots & \vdots & \vdots \\ \vdots & \vdots & \vdots & \vdots & \vdots \end{bmatrix} \times \begin{bmatrix} f_{1,0} \\ f_{2,0} \\ f_{3,0} \\ \vdots \\ w \end{bmatrix} \qquad [3\text{-}3]$$

Such that$M = \Psi f$. Where

$$\Psi_{first\ order} = exp\left[-A_i \int_0^{\tau} exp\left(-\frac{E_i}{RT(t)}\right) dt\right] \qquad [3\text{-}4]$$

And

$$\Psi_{RPM} = \exp\left[\frac{1 - \left(\frac{\varphi}{2}\left[-A_i \int_0^{\tau} exp\left(-\frac{E_i}{RT(t)}\right) dt\right] + \frac{2}{\varphi}\right)^2}{\varphi}\right] \qquad [3\text{-}5]$$

Assuming at a given conversion there is a single reaction dominating, the fraction of initial mass remaining for the *i*th component is given by equation [3-6].

$$f_i(T) = f_{i,0}\, \Psi_i(T) \qquad [3\text{-}6]$$

Where

$$\Psi_i(\beta_1, T_1) = \Psi_i(\beta_2, T_2) \qquad [3\text{-}7](\text{Scott et al. [1]})$$

Taking natural logarithms and substituting the Ψ_i expressions in Equation [3-7], provides nonlinear equations that can be solved for E_i.This gives the exact value of the activation energy given the solid fuel is made up several components when one reaction dominates the overall mass loss at the conversion of interest [1]. It is then assumed that the dominating reaction is at a

conversion corresponding to the maximum rate of decomposition for a single first order reaction when the material is heated at a constant rate. This is at the point when:

$$\frac{d}{dt}\left(\frac{df_i}{dt}\right) = 0 \qquad [3\text{-}8]$$

Solving Equation [3-8] provides the maximum value of Ψ at the maximum rate of decomposition. Taking natural logarithms of Equations [3-4] and [3-5] at this point allows the evaluation of the corresponding pre-exponential factors (A_i). Upon obtaining the set of possible E_i's and A_i's, the matrix Equation [3-3] can then be substituted and inverted to obtain discrete values of E_i and $A_i$of the active reactions, together with the mass fractions of the components ($f_{i,o}$) dissociating according to these reactions. Non zero values of ($f_{i,o}$), are generated by the inversion for all non spurious reactions from the n candidate reactions assumed.

The model accuracy was measured using two methods: the correlation coefficient (i.e. the R^2 statistic), and the root mean square value (RMS) of the differences between the algorithm determined kinetics simulation and the experimental plot. These differences were evaluated for all three heating rate tests and the average values reported.

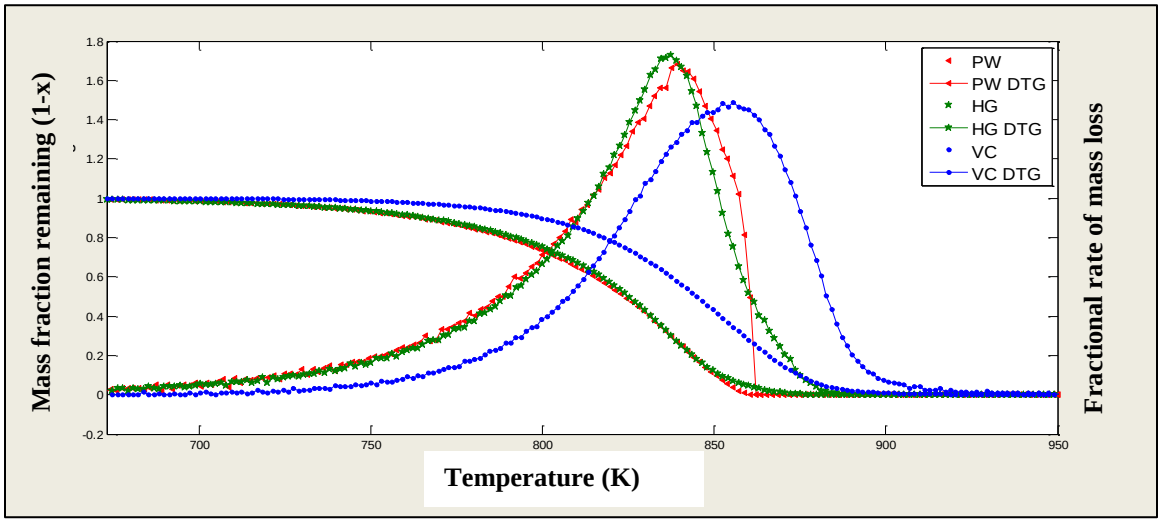

Figure 5-1: *Conversion vs. temperature and DTG curves for the combustion of pure samples.*

6. Results and Discussion

The mass fraction as well as the time derivative of the mass fraction (DTG), as a function of temperature conversion for the pure samples are presented in Figure 4-1. It is observed that the

combustion of biomass samples commences at a lower temperature (710K) than that of coal (760K).The HG and VC char combustion present relatively smooth single peak DTG curves, whereas the PW char DTG curve presents a few deformities on the curve that may be the result of the merging of two or more parallel reactions taking place during the conversion. The maximum reaction rate temperatures are in the order of HG (835K), PW (840K), and VC (855K). According to Kastanaki and Vamvuka [16], there is a possibility of evaluating the reactivity of a substance using its temperature of maximum decomposition (T_{rmax}); the lower the $T_{rmax,}$ the more reactive the substance. According to this theory, the most reactive char would be HG, followed by PW, and the VC being the least reactive.

The char samples were all successfully modelled by the RPM. The first order reaction model proved very unsuitable for the modelling of char combustion. For example, the RPM modelled the conversion to an accuracy of an RMS value of 0.0056, with a corresponding R^2 value of 0.9998. The first order reaction model on the other hand modelled VC char combustion to an accuracy of 0.0457 and 0.989 (RMS error value and R^2 statistic respectively).

The modelling of the three chars is presented in Figure 4-2. The actual kinetics obtained are presented in Table 4-1. As seen on the table, the combustion of PW char is modelled by multiple reactions. Two of the reactions resemble 90% of the reactive matter identified. The remaining five reactions only resemble 10% of the reactive matter, with the last three reactions resembling 1% each. It is also noted that, even though the heating rate variations during the conversion were reduced, they could not be eliminated. Pine char showed the highest heating rate deviations from the set point during the conversion, and particularly towards completion. The trend is observed by the algorithm prediction curves which tend to show a rapid increase in temperature as the reaction approaches completion. This may contribute to the complex kinetics determined during the conversion.Wornat et al. [25] state that variations in composition, particularly of the catalytic inorganic elements, tend to lead to particle to particle variations in intrinsic reactivities in biomass chars. This may be attributed to the multiple different sets of reaction kinetics describing the combustion behavior of the biomass char. The structural parameters identified were in the range of 8.3 to 18.9, and can be concluded to be in line with those observed in literature [26,-29].

Note that due to the differences in the grouped pre-exponential factors obtained, the direct comparison of the Activation energies is not possible. Vyazovkin [30] notes that there is a fundamental flaw in the use of single heating rate methods for kinetics determination. The methods tend to produce differing sets of the kinetic triplets, most of which provide a satisfactory description of the same dataset. This is observed when the algorithm is allowed to use different sets of two heating rates for kinetics determination.

In the present work, various sets of the 3 heating rates were used for kinetics determination, of which the most accurate was selected. The phenomena occurs due to the mutually compensating correlation of E and A, and is known as the compensation effect [30]. The correlation is described by the Equation [4-1].

$$logA_i = aE_i - b \qquad [4\text{-}1]\ [30]$$

Where a and b are constants associated with the reaction i. The different sets of kinetics obtained for the conversion of one material can then be used to determine the two constants, hence defining the compensation correlation for the particular conversion. This compensation correlation was evaluated for coal char combustion and used as a baseline for the comparison of all the kinetics evaluated relative to coal combustion. The equation defining coal char combustion was found to be:

$$\mathrm{l}ogA_i = 0.06E_i - 2.75 \qquad [4\text{-}2]$$

The compensation effect was therefore eliminated on algorithm determined kinetics by substituting the pre-exponential factor and determining the coal char equivalent activation energy using Equation [4-2]. The difference between the coal char equivalent E and the algorithm determined E is evaluated as a percentage. The results obtained show that HG char and PW char have significantly lower activation energies during combustion. The PW char being the most reactive followed by HG, and lastly VC, as suggested by the mineralogical assay.

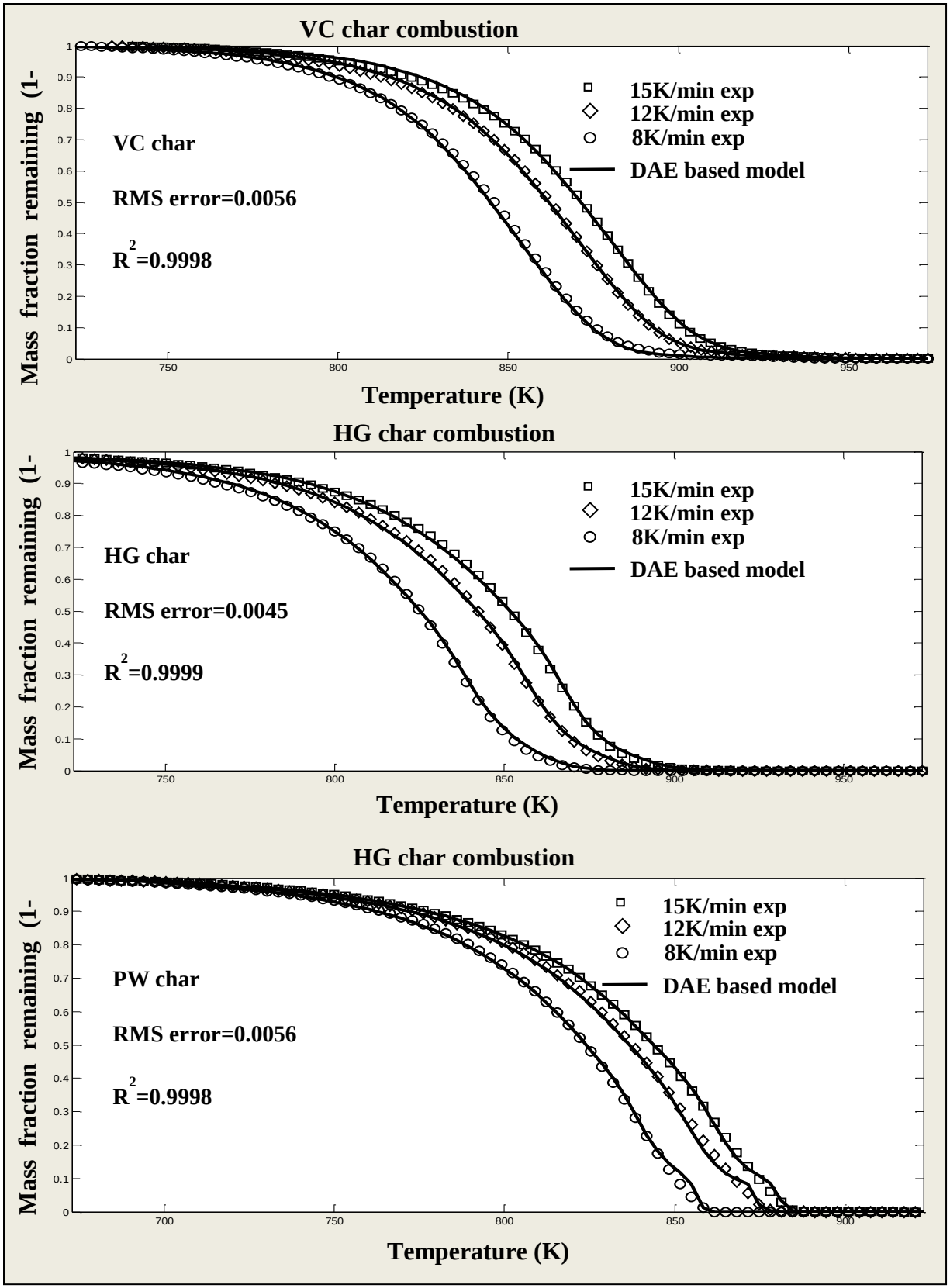

Figure 6-1: Conversion vs. Temperature curves combustion modeling at three heating rates.

Table 6-1: *Kinetic parameters and comparison.*

Sample	**E (kJ/mol)**	**A ($s^{-1}.m^{-1}$)**	f_o	φ	**Coal char equivalent E (kJ/mol)**	**Total weighted % difference**
VC	137.39	2.82E+5	1.00	18.5	137.39	0%
PW	255.48	2.80E+15	0.049	8.29	299.67	-6.0%
	222.28	2.23E+12	0.038		249.25	
	193.68	7.88E+9	0.164		209.36	
	183.30	5.34E+8	0.735		190.34	
HG	127.8	1.60E+5	0.19	10.5	133.26	-4.0%
	130.5	2.17E+5	0.80		135.48	

7. Conclusion

The reaction behaviors of various fuel chars are of great importance in the design and optimisation of combustion systems. From this study, it can be concluded that the DAE based algorithm is a robust and accurate method of kinetics determination. All the materials were successfully modelled using the RPM. The observed accuracies were in the range of 0.0045-0.0056 RMS error values, and 0.9999 and 0.9998 R^2 values. The reactivities of the char samples is presented in the descending order of PW,HG and VC. The reactivity of the biomass materials as compared to coal may be attributed to their high concentration of catalytic metal oxides. The mineralogical assay in this study was able to successfully predict the order of reactivity of the materials. As observed by Dupont et al. [21], the reactivity of the materials under study was found to be directly proportional to the ratio of its potassium vs silicon content. The application of the compensation effect for the comparison of the obtained kinetics was appropriate. It was determined that the activation energies of the PW and HG chars were 6% and 4% lower than that of coal char.

8. References

[1] Scott, S. A., Dennis, J. S., Davidson, J.F., Hayhurst, A. N., 2006. An algorithm for determining the kinetics of devolatilisation of complex solid fuels from thermo-gravimetric experiments. *Chemical Engineering Science,* 61(8), pp.2339-2348.

[2] Irfan, M. F., Usman, M, R., Kusakabe, K., 2011. Coal gasification in CO2 atmosphere and its kinetics since 1948: A brief review. *Energy,* 36(1), pp.12-40.

[3] Henrich, E., Burkle, S., Meza-Renken, Z. I., Rumpel, S., 1999. Combustion and gasification kinetics of pyrolysis chars from waste and biomass. *Journal of Analytical and Applied Pyrolysis* , 49, pp.221–241.

[4] Mani, T., Mahinpey, N., Murugan, P., 2011. Reaction kinetics and mass transfer studies of biomass char gasification with CO_2. *Chemical Engineering Science,* 66(1), pp.36-41.

[5] Vamvuka, D., Karouki, E., Sfakiotakis, S., 2011. Gasification of waste biomass chars by carbon dioxide via thermo-gravimetry. Part I: Effect of mineral matter. *Fuel,* 90(3), pp.1120-1127.

[6] Fermoso, J., Gil, M.V., Pevida, C., Pis, J.J., Rubiera, F., 2010. Kinetic models comparison for non-isothermal steam gasification of coal–biomass blend chars. *Chemical Engineering Journal*, 161(1-2), pp.276-284.

[7] Huang, Z., Zhang, J., Zhao, Y., Zhang, H., Yue, G., Suda, T., Narukawa, M., 2010. Kinetic studies of char gasification by steam and CO2 in the presence of H_2 and CO. *Fuel Processing Technology,* 91(8), pp.843-847.

[8] Gil, M. V., Casal, D.,Pevida, C., Pis, J. J., Rubiera, F., 2010. Thermal behaviour and kinetics of coal/biomass blends during co-combustion. *Bioresource technology,* 101, pp.5601–8.

[9] Kuo-Chao, L., Keng-Tung, W., Chien-Song1, C., Wei-The1, T., 2009. A New Study on Combustion Behavior of Pine Sawdust Characterized by the Weibull Distribution. *Chinese Journal of Chemical Engineering,* 17(5), pp.860-868.

[10] Fermoso, J., Arias, B., Pevida, C., Plaza, M.G., Rubiera, F., Pis, J.J., 2008. Kinetic models comparison for steam gasification of different nature fuel chars. *Journal of Thermal Analysis and Calorimetry*, 91, pp.779-786.

[11] Roberts, D.G., Harris, D.J., 2007. Char gasification in mixtures of CO_2 and H_2O: Competition and inhibition. *Fuel*, 86(17-18), pp.2672-2678.

[12] Ochoa, J., Cassanello, M. C., Bonelli, P, R., Cukierman, A.L., 2001. CO_2 gasification of Argentinean coal chars: a kinetic characterization. *Fuel Processing Technology*, 74(3), pp.161-176.

[13] Dutta, S., Wen, C.Y., Belt, R. J., 1977. Reactivity of Coal and Char. 1. In Carbon Dioxide Atmosphere. *Industrial and Engineering Chemistry Process Design and Development*, 16(1), pp.20-30.

[14] Saloojee, F., 2011. Kinetics of pyrolysis and combustion of a South African coal using the distributed activation energy model. MSc Dissertation. University of Witwatersrand.

[15] Sadhukhan, A. K., Gupta, P., Goyal, T., Saha, R. K., 2008. Modelling of pyrolysis of coal-biomass blends using thermogravimetric analysis. *Bioresource technology*, 99(17), pp.8022–6.

[16] Kastanaki, E., Vamvuka, D., 2006. A comparative reactivity and kinetic study on the combustion of coal–biomass char blends. *Fuel*, 85, pp.1186–1193.

[17] Fermoso, J., Stevanov, C., Moghtaderi, B., Arias, B., Pevida, C., Plaza, M.G., Rubiera, F., Pis, J. J., 2009. High-pressure gasification reactivity of biomass chars produced at different temperatures. *Journal of Analytical and Applied Pyrolysis*, 85(1-2), pp.287-293.

[18] Senneca, O., 2007. Kinetics of pyrolysis, combustion and gasification of three biomass fuels. *Fuel Processing Technology*, 88(1), pp.87-97.

[19] European Commission. 2009. DIRECTIVE 2009/28/EC of the European Parliament and of the Council of 23 April 2009 on the promotion of the use of energy from renewable sources and amending and subsequently repealing Directives 2001/77/EC and 2003/30/EC ., pp.16-62.

[20] Vittee, T., 2012. Determination of Kinetics of Char Reactivity with Carbon Dioxide Using Thermogravimetry and the Distributed Activation Energy Model. MSc Dissertation. University of Witwatersrand.

[21] Dupont, C., Nocquet, T., Da Costa Jr, A. J., Verne-Tournon, C.,2011. Kinetic modelling of steam gasification of various woody biomass chars: Influence of inorganic elements. *Bioresource technology*, 102, pp.9743–8.

[22] Zhang, Y. et al., 2008. Proposal of a semi-empirical kinetic model to reconcile with gasification reactivity profiles of biomass chars. *Fuel*, 87(4-5), pp.475–481.

[23] Zhu, W., Song, W., Lin, W., 2008. Catalytic gasification of char from co-pyrolysis of coal and biomass. *Fuel Processing Technology*, 89(9), pp. 890-896.

[24] Hernandez, J.J., Aranda-Almansa, G., Serrano, C., 2010. Co-Gasification of Biomass Wastes and Coal−Coke Blends in an Entrained Flow Gasifier: An Experimental Study. *Energy & Fuels*, 24(4), pp. 2479-2488.

[25] Wornat, M.J., Hurt, R. H., Davis, K. A., Yang, N. Y. C., 1996. Single-particle combustion of two biomass chars. *Twenty-Sixth Symposium (International) on Combustion/ The Combustion Institute*, pp.3075–3083.

[26] Ahmed, I.I., Gupta, A. K., 2011. Kinetics of woodchips char gasification with steam and carbon dioxide. *Applied Energy*, 88(5), pp.1613–1619.

[27] Liu, G.-S., Niksa, S., 2004. Coal conversion submodels for design applications at elevated pressures. Part II. Char gasification. *Progress in Energy and Combustion Science*, 30(6), pp.679–717.

[28] Zolin A., 2001. Reactivity of solid fuels. PhD dissertation, Department of Chemical Engineering, Technical University of Denmark, Denmark.

[29] Charpenay, S., Serio, M.A. , Solomon, P.R., 1992. The prediction of coal char reactivity under combustion conditions. *Twenty-Fourth Symposium (International) on Combustion/ The Combustion Institute,*, pp.1189–1197.

[30] Vyazovkin, S., 2008. Handbook of Thermal Analysis and Calorimetry, Isoconversional kinetics. Chapter 13, pp. 503-537.